# Design, Synthesis and Catalytic Evaluation of Mono- and Polynuclear Organometallic Materials as Hydroformylation Catalysts

**Nikechukwu Nike Omosun**




**University of Cape Town**

**February 2021**

# Design, Synthesis and Catalytic Evaluation of Mono- and Polynuclear Organometallic Materials as Hydroformylation Catalysts

A thesis submitted to the

**University of Cape Town**

In fulfilment of the requirements for the degree of

**Doctor of Philosophy**

by

Nikechukwu Nike Omosun

Supervisor: Associate Professor Gregory S. Smith


Department of Chemistry
University of Cape Town
South Africa

# Declaration

I declare that "**Design, Synthesis and Catalytic Evaluation of Mono- and Polynuclear Organometallic Materials as Hydroformylation Catalysts**" is my own work and to the best of my knowledge has never been submitted for examination for any degree at any university. All sources of information used are acknowledged, cited and fully referenced at the end of each chapter.

Nikechukwu Nike Omosun

February 2021

# Acknowledgements

I wish to express my heartfelt gratitude to God for bringing me this far in life. My profound appreciation goes to the following people without whose contributions this thesis would not be possible.

My supervisor Associate Professor Gregory Smith for his patience, encouragement, constructive criticism and support throughout the course of this research. To Dr. Siyabonga Ngubane for his helpful inputs and advice. I am indebted to Dr. Shepherd Siangwata for all the suggestions, criticism and most importantly for the invaluable autoclave training. My appreciation extends to the past and present members of the Organometallic Research Group for the priceless time spent together in the lab and in social settings.

I acknowledge the following people for their assistance; Mr. Pete Roberts and Dr. Marwaan Rylands for recording NMR spectra, Mr. Ts'epo Tumeli (University of the Witwatersrand) for Electrospray Ionisation Mass Spectral analyses. To Ms. Deirdre Brooks, I appreciate your warmth and willingness to clarify information. I am also grateful to Dr. Mziyanda Mbaba for his help with proofreading my thesis.

Special thanks to Dr. Bella Owen, Dr. Nadia Baartzes, Mr. Radwan Alnajjar and Mr. Olaolu Fadeyi for their friendship and support that have made my stay in Cape Town a memorable experience. To my brother and sisters, Uzonna, Nkem, Chinonye, and to my sister in-law Ms. Zuma Teschner, thank you for the encouraging words.

I wish to express gratitude to the DST-NRF Centre of Excellence in Catalysis (c*change) and the University of Cape Town for financial support.

This thesis is dedicated to my parents, Michael and Josephine Onyido for giving me the opportunity of an education and to my husband Dr. Garuba Omosun for showing me nothing but unconditional support and encouragement throughout the course of my studies.

# Abstract

The hydroformylation reaction is an important homogeneous rhodium-catalyzed industrial process for the production of linear and branched aldehydes from readily available alkenes. The aldehydes produced serve as major building blocks for valuable chemical and pharmaceutical products. The fast-depleting and expensive, highly-active rhodium metal has triggered an interest in the design and synthesis of new, more efficient, selective and recyclable rhodium-based catalysts. The strategies of introducing hydrophilic substituents, multiple active sites and bulky dendritic ligands are currently explored to enhance catalyst performance and recyclability. This study investigated the synthesis, characterisation and catalytic potential of new water-soluble alpha-diimine Rh(I) complexes, alpha-diimine Rh(I) metallodendrimers and a water-soluble binuclear Rh(I) complex.

New water-soluble disulfonated 1,4-diazabutadiene (DAD) ligands bearing either an ethyl or acenaphthene backbone were prepared. The alpha-diimine *N*,*N*-chelating ligands were synthesised *via* the Schiff base condensation reactions of 4-aminophenol with 1,2-ethanedione or acenapthenequinone, followed by sulfopropylation reactions with 1,3 propanesultone. Complexation of the water-soluble ligands with the rhodium precursor $[Rh(COD)(MeCN)_2]BF_4$ (where COD = 1,5-cyclooctadiene) yielded new water-soluble alpha-diimine Rh(I) complexes. In addition, non-sulfonated 1,4-diazabutadiene (DAD) Rh(I) analogues were synthesised by complexation of the alpha-diimine Schiff base ligands with $[Rh(COD)(MeCN)_2]BF_4$. The complexes were fully characterised using $^{1}H$, $^{13}C\{^{1}H\}$ NMR spectroscopy, IR spectroscopy and electrospray ionisation mass spectrometry.

The complexes were successfully evaluated as catalyst precursors in the hydroformylation of 1-octene. The reaction conditions were optimised at 75 °C, 40 bar syngas pressure for 4 h with 2.87 x $10^{-3}$ mmol catalyst loading. The sulfonated 1,4-diazabutadiene Rh(I) complexes displayed excellent conversion of 1-octene (> 98%) and good chemoselectivity towards aldehydes (> 86%) while the non-sulfonated 1,4-diazabutadiene Rh(I) complexes displayed lower catalyst activity. Recyclability of the disulfonated 1,4-diazabutadiene Rh(I) complexes were successfully conducted over 4 cycles, with a loss in catalytic activity after the third cycle. Inductively coupled plasma optical spectrometry experiments confirmed negligible leaching of the catalyst precursors into the organic layer. Additionally, catalytic experiments in the presence of mercury show unsuppressed catalyst activity, thus suggesting that the hydroformylation reaction is mediated by a molecularly-dispersed homogeneous species.

A series of Fréchet-type dendrons with methyl ester groups at the periphery were subsequently prepared. The α-diimine (DAD) Schiff base ligands were synthesised and coupled to the Fréchet-type dendrons *via* a Williamson ether reaction to yield a new series of alpha-diimine poly(aryl ether) (PAE) dendrimers with methyl ester groups at the periphery. Complexation of the alpha-diimine poly(aryl ether) (PAE) dendrimers with the metal-precursor $[Rh(COD)(MeCN)_2]BF_4$ afforded the three generations of core-functionalised α-diimine Rh(I) metallodendrimers. The dendritic ligands and their corresponding Rh(I) metallodendrimers were fully characterised using standard spectroscopic and analytical techniques.

The core-functionalised alpha-diimine rhodium(I) metallodendrimers were applied as catalyst precursors in the hydroformylation of 1-octene and styrene. For the hydroformylation of 1-octene, the metallodendrimers gave good conversions (> 81%) and good aldehyde chemoselectivity (> 83%) under optimum reaction conditions of 75 °C, 40 bar syngas pressure over 4 h. With respect to regioselectivity, an increase in dendritic generation of the rhodium complexes increased the regioselectivity towards linear aldehydes. For the hydroformylation of aromatic-substituted olefin (styrene), the regioselectivity of the three generations of metallodendrimers were comparable. Therefore, the increased steric crowding around the metal centre had no effect in improving regioselectivity towards linear aldehyde for aromatic-substituted olefinic substrates. Mercury poisoning experiments performed using the three generations of Rh(I) metallodendrimers displayed suppressed activity (< 52%). This is indicative of a catalytic system that follows a combination of homogeneous and heterogeneous pathway.

Lastly, the synthesis and characterization of water-soluble tetrasulfonated tetraimine and disulfonated diimine ligands are described. The ligands were synthesized *via* the Schiff base condensation reactions of 4-hydroxybenzaldehyde with 3,3-diaminobenzidine or *o*-phenylenediamine, followed by nucleophilic reactions with 1,3 propanesultone. Complexation reactions of the water-soluble ligands with $[Rh(COD)(MeCN)_2]BF_4$ afforded water-soluble mononuclear and binuclear Rh(I) complexes. Both complexes displayed excellent water-solubility at room temperature. The compounds were characterised using an array of spectroscopic ($^1H$, $^{13}C\{^1H\}$ NMR, FT-IR spectroscopy) and analytical (mass spectrometry) techniques.

The sulfonated mononuclear and binuclear Rh(I) complexes were evaluated as catalyst precursors in the aqueous biphasic hydroformylation of 1-octene under hydroformylation

conditions of 75 °C, 40 bar syngas pressure for 4 h. Both catalyst precursors gave good catalytic conversion (> 96%) and aldehyde chemoselectivity (> 87%). Notably, the presence of an extra metal centre in the binuclear complex led to an increase in catalyst activity. Recyclability experiments were conducted over 4 cycles, with a significant drop in conversion after each cycle. The drop in catalyst performance may be attributed to catalyst degradation often associated with the reuse of the same catalyst containing phase.

# Publications and Conference Contributions

## Journal Articles

- Hydroformylation of olefins using redox-active rhodium(I) alpha-diimine-cored aryl ether metallodendrimers.
  **Nikechukwu N. Omosun**, Siyabonga Ngubane and Gregory S. Smith. *Applied Catalysis A, General*. 2021, 610, 117950.

- Water-soluble, disulfonated alpha-diimine Rh(I) complexes: synthesis, characterisation and application as catalyst precursors in the hydroformylation of 1-octene.
  **Nikechukwu N. Omosun** and Gregory S. Smith. *European Journal of Inorganic Chemistry*, 2019, 2558-2564.

## Conference Contributions

- Water-soluble, disulfonated alpha-diimine rhodium(I) complexes: synthesis, characterisation and application as catalyst precursors in the hydroformylation of 1-octene. (Poster Presentation). 4th International Conference on Catalysis and Chemical Engineering, Los Angeles, United States. (23 – 26 February 2020).
  **Nikechukwu N. Omosun** and Gregory S. Smith

- Rhodium(I) alpha-diimine-cored aryl ether dendritic macromolecules: controlled synthesis, characterization, and application as catalysts precursors in the hydroformylation of 1-octene. (Poster Presentation). CATSA Conference, Langebaan, South Africa. (10 – 13 November 2019).
  **Nikechukwu N. Omosun** and Gregory S. Smith.

# Abbreviations

| | |
|---|---|
| Acac | Acetylacetone |
| Ar | Aromatic |
| br s | Broad signal |
| $^{13}C\{^{1}H\}$ NMR | Proton-decoupled carbon-13 nuclear magnetic resonance |
| Calcd. | Calculated |
| $CDCl_3$ | Deuterated chloroform |
| $cm^{-1}$ | Reciprocal centimetres |
| COD | 1,5-Cyclooctadiene |
| d | Doublet (NMR) |
| DAD | α-Diimine |
| dd | Doublet of doublets |
| DCM | Dichloromethane |
| DMF | *N*,*N*-Dimethylformamide |
| DMSO | Dimethyl sulfoxide |
| ESI-MS | Electrospray ionisation mass spectrometry |
| eq. | Equivalents |
| EtOH | Ethanol |
| FID | Flame ionization detector |
| FT-IR | Fourier transform infrared spectroscopy |
| GC | Gas chromatography |
| GDP | Gross domestic product |
| h | Hour(s) |
| HR-MS | High resolution mass spectrometry |
| Hz | Hertz |

| | |
|---|---|
| ICP-OES | Inductively coupled optical emission spectrometry |
| IL | Ionic liquid |
| IR | Infrared |
| *J* | Coupling constant |
| m | Multiplet (NMR) |
| MeOH | Methanol |
| mg | Milligram(s) |
| MHz | Megahertz |
| min | Minute(s) |
| mL | Millilitre |
| mmol | Millimole(s) |
| M.P. | Melting point |
| MS | Mass spectrometry |
| m/z | Mass-charge ratio |
| NHCs | *N*-Heterocyclic carbenes |
| NMR | Nuclear Magnetic Resonance |
| p | Pentet (NMR) |
| PAE | Poly(aryl ether) |
| PGMs | Platinum group metals |
| ppm | Parts per million |
| q | Quartet (NMR) |
| r.t. | Room temperature |
| s | Singlet (NMR); strong (IR) |
| $scCO_2$ | Supercritical carbon dioxide |
| Syngas | Synthesis gas |

| | |
|---|---|
| t | Triplet (NMR) |
| $^{t}$Bu | Tertiary butyl |
| TMS | Tetramethylsilane (NMR) |
| TMS | Thermomorphic solvent systems |
| TOF | Turnover frequency |
| TON | Turnover number |
| TPP | Triphenylphosphine |
| TPPMS | Monosulfonated triphenylphosphine |
| TPPTS | Triphenylphosphine trisulfonate |
| μm | Micromolar |
| wt | Weight |

# Table of Contents

**Chapter 5: Summary, conclusions and future outlook**



**Chapter 6: Experimental**

# Chapter 1

## Literature review

### 1.1 Green Chemistry

The Green Chemistry concept was established as a response to the environmental concerns and exploitation of natural resources that emanated from the industrial revolution of the 18th century.[1–3] The U.S. Environmental Protection Agency (EPA) initiated the Green Chemistry holistic approach to sustainable science by declaring policies (Pollution Prevention Act of 1990) that seeks to promote pollution prevention instead of waste treatment and disposal.[4] Green Chemistry can be concisely defined as the design and practice of safe, non-polluting sustainable chemical processes.[5] In 1998, Anastas and Warner published the twelve principles of green chemistry.[6,7] They outlined a clear set of guidelines for further development of environmentally friendly chemical processes (Figure 1.1). In line with this, the demand for industrial processes that follow these principles is a significant impelling cause for the scientific community. In accomplishing these principles, researchers may modify or completely redesign antiquated chemical processes for sustainable/greener alternatives. In this context, various viable alternatives have emerged such as photochemical reactions, catalysis, the use of renewable feedstock (biomass) and greener reaction media (water, ionic liquids and supercritical fluids).[8–12]

### 1.2 Catalysis

The substitution of stoichiometric methods with catalytic alternatives is one of the fundamental pillars of Green Chemistry. Catalysts accelerate reactions by decreasing the activation energy of chemical transformations. It enables industrially important reactions to be carried out efficiently and under practically safe conditions. Additionally, catalytic routes can be designed to maximize the efficient use of raw materials, to be energy efficient and reduced purification steps thus producing little or no waste. Catalysis is central to a myriad of applications; for example, catalytic technologies are used in the production of fine and specialty chemicals, agrochemicals, cosmetics, pharmaceuticals, polymers, pollution abatement technologies and energy production.[13–15]

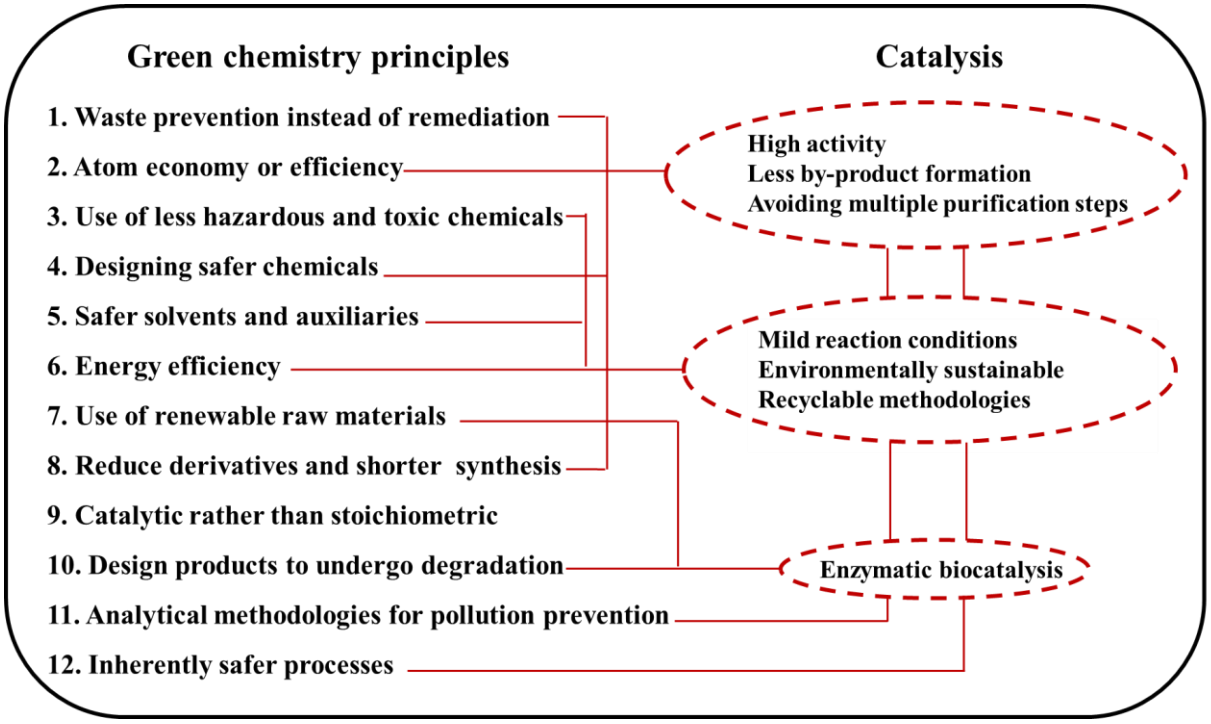


**Figure 1.1** Catalysis as a pillar of Green Chemistry.[6,16]

Roughly 85–90% of all chemical products are made using catalytic processes, and the percentage is increasing steadily.[17] Among the numerous catalysts investigated so far, metal-based catalysts have emerged as effective materials capable of reducing the activation energy in several chemical reactions.[18] Some exemplary industrial use of metal-based catalysts is listed in Table 1.1.

Metal-based catalysts dominate the global catalyst market to the value of 1.5 trillion USD per annum, contributing directly or indirectly to approximately 35% of the world's GDP.[19,20] In particular, transition-metal catalysts are the most studied catalysts due to their inherent properties. Transition-metals have incompletely filled d orbitals and as a result these metals can accelerate chemical reactions by: (a) facilitating coordination with ligands and activation of the reacting species through cleavage or formation of σ or π bonds, (b) attaining different oxidation states and coordination numbers, (c) stabilizing catalytically active intermediates such as carbonyls, metal hydrides and metal alkyls, (d) the ability to orient/assemble reactions within the coordination sphere and promote rearrangements *via* ligand migration.[21,22]

**Table 1.1** Major industrial catalytic processes involving transition metals.[23–25]

| Industrial manufacturing process | Transition-metal catalyst system |
|---|---|
| $NH_3$ synthesis (Haber process) | Fe |
| Water-gas shift reaction | Ni, Fe |
| Catalytic reforming of hydrocarbons | Pt, Re |
| Ethene epoxidation | Ag |
| $HNO_3$ synthesis (Haber-Bosch process) | Pt, Rh |
| Methanation | Ni |
| Fischer-Tropsch synthesis | Fe, Co |
| Hydroformylation | Rh, Co |
| Auto exhaust catalytic converter | Rh, Pt |
| Ziegler-Natta polymerization | Ti, Zr, Hf |
| Ethylene oligomerization | Pd, Co |

### 1.2.1 Heterogeneous catalysis

Catalysis is primarily categorized into two types: homogeneous and heterogeneous catalysis. In a heterogeneous catalytic system, the catalyst is in a different phase from the reactants and products. This phase refers to the physical state of the catalyst in the system.

The ability of solid surfaces to make and break bonds is the basis for the phenomenon of heterogeneous catalysis.[26] Several chemical reactions are catalysed by solid surfaces; for example, the large scale catalytic cracking of petroleum, the conversion of synthesis gas into a mixture of hydrocarbons (Fischer-Tropsch) as well as the oxidation of hydrocarbons.[27,28] An illustrated example is the double-bond hydrogenation mechanism originally proposed by Horiuti and Polanyi for the heterogeneous hydrogenation of ethylene on a Pt catalyst surface (Figure 1.2).[29]

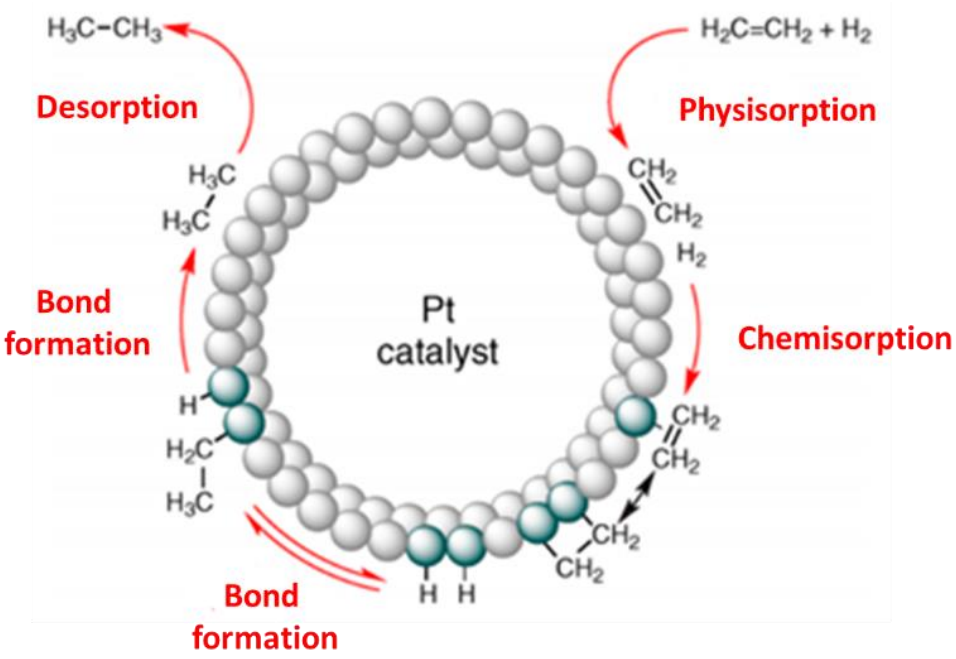


**Figure 1.2** Schematic presentation for the hydrogenation of ethylene mechanism on a platinum catalyst surface.[27]

In a heterogeneous catalytic reaction, the reactants undergo a series of steps on the surface of the catalyst such as physisorption of the reactants on the metal surface which takes place *via* van der Waals forces followed by chemisorption.[30] The chemisorption process is believed to be the crucial step that lowers the activation energy of the reaction. Thereafter, desorption of products from the catalyst sites occurs.[31,32] The chemical industry generally favours the use of the heterogeneous catalytic system, this is because of the nature of heterogeneous catalysts which allows for easy catalyst/product separation.[33] However, factors that have precluded these systems includes the presence of numerous active sites or in some cases the low concentration of active sites resulting to unpredictable activity and non-reproducible results. Also, the harsh operating conditions usually required for heterogeneous systems could lead to unwanted side reactions and decomposition of substrates/products or catalyst.[34,35]

### 1.2.2 Homogeneous catalysis

Homogeneous catalysis refers to a catalytic system in which the substrates and the catalyst are in the same phase, most often the liquid phase. Several important reactions in the bulk and fine chemical industry employ the use of homogeneous catalysts. Examples are the hydroformylation of alkenes, hydrocyanation of olefins, hydrosilylation of ketones and the Pd-

catalysed cross-coupling reactions and the oligomerization of ethylene.[36] The elementary steps in a typical homogeneous catalytic reaction are illustrated in (Scheme 1.1).

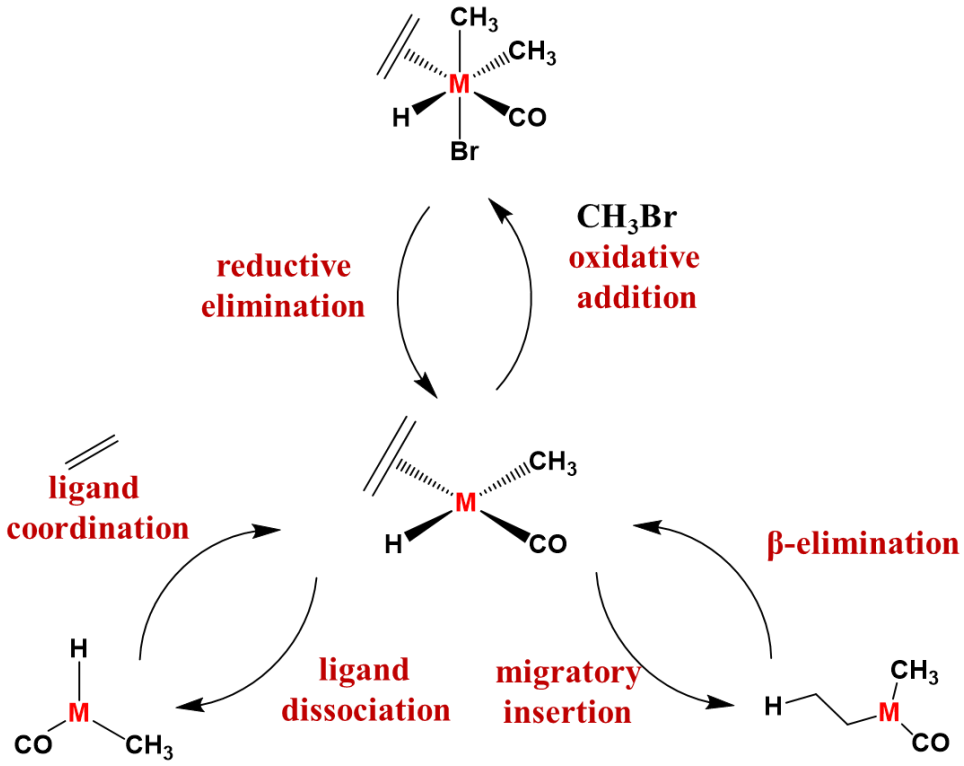


**Scheme 1.1** Schematic illustration of elementary steps in homogeneous catalysis.

The elementary steps are categorised into six main steps: dissociation and coordination, oxidative addition and reductive elimination, insertion and β-elimination.[36–38] These steps are the building blocks which construct the reaction mechanism in a homogeneously catalysed system.

The general sequence in a homogeneous catalytic cycle can be described as: (a) conversion of a catalyst precursor to an active form either by ligand dissociation or interaction with a co-catalyst or promoter, (b) activation of reactants by the active complex, (c) intramolecular reaction in the coordination sphere of the active complex followed by reductive elimination to form the product and, (d) the regeneration of the catalyst to its original active form.[22] The feasibility and the frequency of these steps would depend on the transition metal, ligands coordinated to the metal centre, reaction conditions, and the thermodynamics of the system. Homogeneous catalysts have the leverage of solubility over heterogeneous catalysts. The high degree of interaction between the catalyst and the reactants results to higher activity at mild reaction conditions.[39] The comparative features of homogeneous and heterogeneous catalysis are presented in Table 1.2.

**Table 1.2** Major differences between homogeneous and heterogeneous catalysis.[40]

| Aspect | Homogeneous | Heterogeneous |
|---|---|---|
| Form | Soluble | Usually supported |
| Active site | Molecular active sites, very well-defined, uniform | Poorly defined, limited accessibility |
| Reaction conditions | Lower temperature (< 250 $^{o}$C), lower pressure, low thermal stability | High temperature and pressure, better thermal stability |
| Selectivity | Relatively higher selectivity, easy to optimize | Heterogeneous sites, difficult to control selectivity |
| Reproducibility | Reproducible results | Results are difficult to reproduce |
| Reaction kinetics and mechanism | Easy to establish | Complex kinetics and mechanism, difficult to establish |
| Catalyst recovery | Difficult catalyst recovery | Easy catalyst recovery |

The advantages and limitations of homogeneous and heterogeneous catalytic systems are inherent to the phase of the catalyst in a reaction system. Primarily, catalysis is a molecular phenomenon since it entails the chemical transformation of molecules into other molecules.[23,33] The well-defined molecular level active site of a homogeneous catalyst and its high accessibility to substrates renders a homogeneous catalyst more active and selective compared to a heterogeneous catalyst. However, the benefits of homogeneous catalysis systems are often compromised by the cumbersome and multistep separation of the catalyst from the product.[33,41] Hence, scientists continuously seek to develop new strategies to circumvent this issue.

## 1.3 Hydroformylation

The hydroformylation reaction is the transition-metal catalysed transformation of olefins to aldehydes in the presence of syngas (CO and $H_2$). This results in the addition of a formyl group (H–C=O) and a hydrogen atom to the carbon double bond of the alkene to produce either linear or branched aldehydes.[42] Otto Roelen discovered the hydroformylation reaction in 1938 during an attempt to redirect the ethylene generated from a Fischer–Tropsch synthesis back into the process.[43] This reaction constituted the basics for bulk homogeneous catalysis on an industrial scale.[44,45] The primary industrial use of hydroformylation reaction is in the preparation of butyraldehydes and their hydrogenated downstream products from propylene (Scheme 1.2).[47] Over 12 million tonnes of hydroformylation products are produced each year.[46]

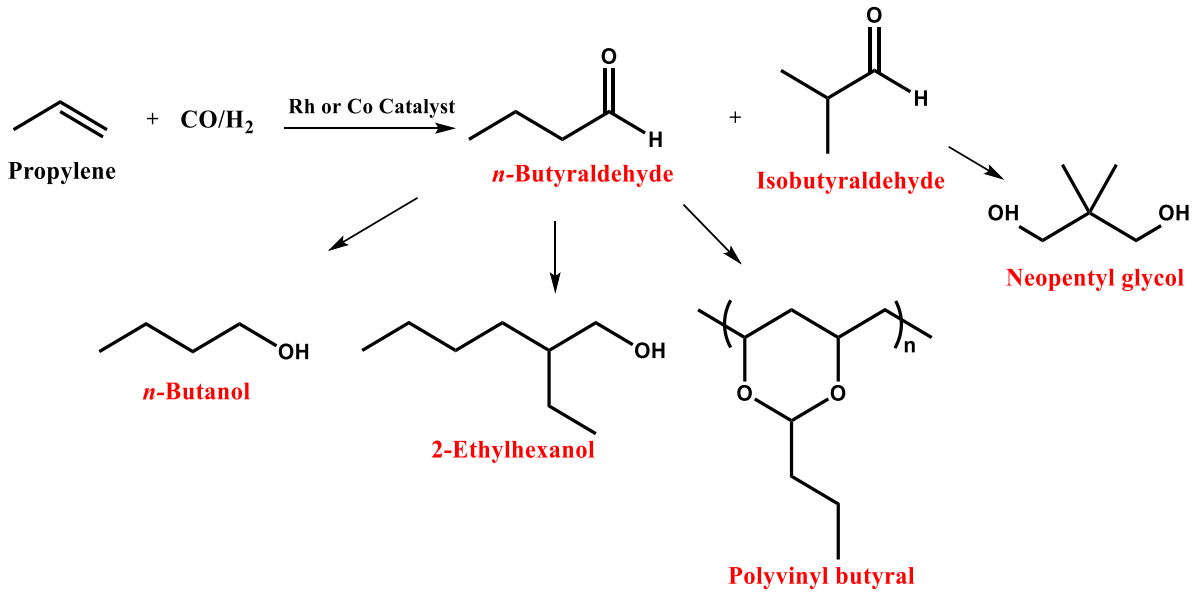


**Scheme 1.2** Downstream products from the hydroformylation of propylene.[47]

The hydroformylation reaction has continuously been developing since its inception and many scientific achievements have resulted. In the earliest advancement of the hydroformylation reaction, unmodified Co catalysts typically of Co-salts or Co–carbonyl complex ($Co_2(CO)_8$) were used as catalyst precursors to form the active $HCo(CO)_4$ intermediate species *in situ*.[22] Several drawbacks with the use of Co-based catalysts includes the oxidation of the Co catalyst to give $Co^{2+}$ salts, fast hydrogenation of the formed aldehydes to alcohols, the use of very high CO pressure in the range of 200 to 450 bar and temperatures as high as 140 to 180 °C.[48] Additionally, the catalyst has to be decomposed by chemical decobaltation before the reaction products can be recovered.[49]

A modification of the classic cobalt catalyst; hydridocarbonyl trialkylphosphine ($HCo(CO)_3PR_3$) was introduced in the 1960s which operates under high temperature (> 140) and lower pressure (50 bar) than the unmodified Co catalysts.[49] The modified catalyst gives improved activity that is partly offset by the unavoidable production of alcohols (side-products). Hydroformylation of olefins using Rh-based catalyst is considered a major breakthrough in homogeneous catalysis. The rhodium system is 1000 times more active than the Co-based catalysts, operating efficiently under milder reaction conditions.[50] As a result, research in the hydroformylation reaction is mainly focused on improving the rhodium-based hydroformylation catalysts.

### 1.3.1 Mechanism of the rhodium-catalysed hydroformylation

Wilkinson *et al.* examined the coordination chemistry and possible intermediates of the ligand-modified rhodium complexes using FT-IR technique and proposed a reaction mechanism that is generally accepted (Scheme 1.3).[51,52] More advanced high pressure *in situ* spectroscopic mechanistic studies have helped tremendously in identifying different catalytic intermediates generated *in situ* during the hydroformylation reaction, thus providing further evidence to support the proposed mechanism by Wilkinson.[53–55]

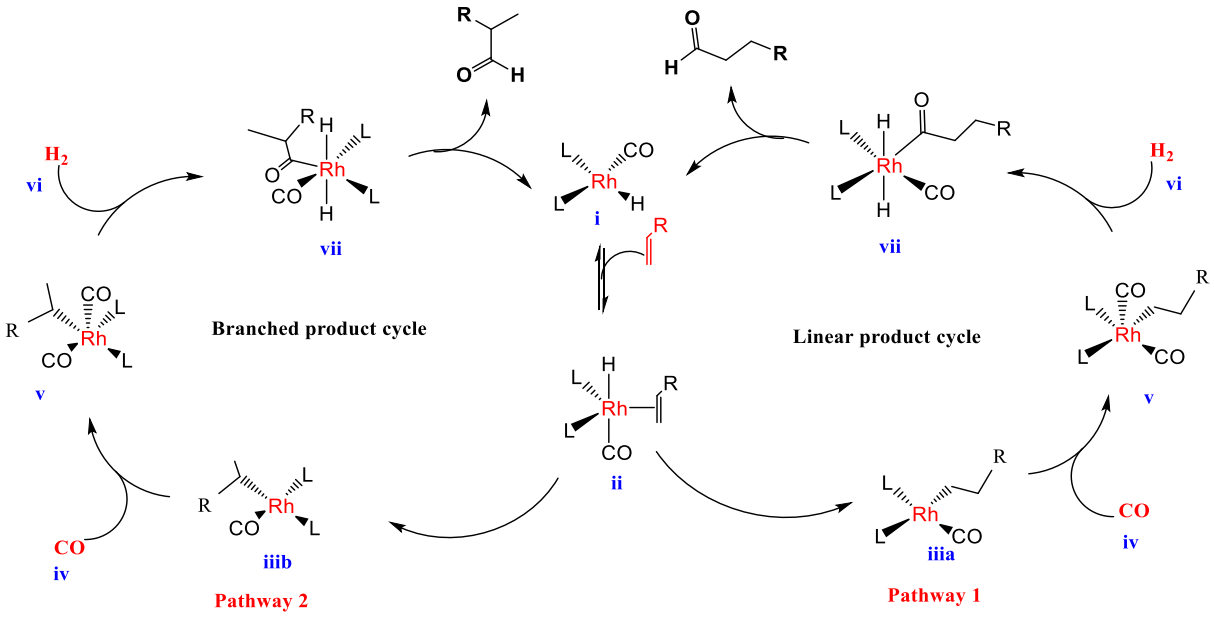


**Scheme 1.3** Mechanism for the hydroformylation reaction.[51,52]

The hydroformylation reaction mechanism begins with the formation of the catalytically active unsaturated 16-electron rhodium hydrido-complex (i) from the loss of a labile ligand. The olefinic substrate coordinates to the rhodium hydrido-complex to form a five-coordinate

intermediate (ii). The migratory insertion of the olefin yields two regio-isomeric (linear or branched) Rh-alkyl intermediates (iiia) or (iiib). The linear intermediate is formed *via* the anti-Markovnikov addition of the hydride moiety (pathway 1), while the branched intermediate is formed *via* Markovnikov addition (pathway 2).[48] Further addition of CO in step (iv) to the unsaturated four coordinate intermediate complex yields rhodium species (v). The oxidative addition of hydrogen (vi) to the rhodium species (v) allows for the formation of the intermediate (vii) complex which undergoes reductive elimination yielding either the linear or branched aldehyde product. The catalytically active unsaturated 16-electron rhodium hydrido-complex (i) is regenerated and the cycle continues. The isomerization (shifts of the olefinic double bond of the substrate) can be mediated by the catalyst intermediate (iiib) through ß-hydride elimination when higher alkenes are used. Therefore, this makes the isomerization and the hydroformylation reactions competing processes.[56]

The selective control of these competing mechanisms and intermediate formation determines the chemoselectivity and the ratio of regio-isomeric aldehydes produced. There are multiple and complex equilibria which influence the hydroformylation steps in very often an unpredictable manner.[56] As a result, the selective steering towards one regio-isomeric aldehyde remains a huge challenge. On the other hand, the nature of the substrate, reaction parameters, steric and electronic properties of the ligand coordinated to the metal centre have been reported to influence the selectivity of the hydroformylation catalyst to a considerable extent.[57]

### 1.3.2 Ligand effects

#### 1.3.2.1 Electronic effects

The electronic effect of ligands, especially phosphorus containing ligands have been thoroughly studied.[58] Infrared data analysis showing changes in the carbonyl stretching frequencies of metal–carbonyl complexes is a reliable yardstick to capture the net electronic effects of ligands.[59] The σ-basicity and π-acidity of ligands is simply characterized or experimentally observed through differences in the IR stretching frequencies of characteristic absorption bands. An example is the study by Strohmeier and Horrock,[59,60] in which carbonyl stretching frequencies of various ligand-coordinated carbonyl complexes were used to explain the overall σ-basicity and π-acidity of ligands. Figure 1.3 illustrates the electronic effects of ligands.

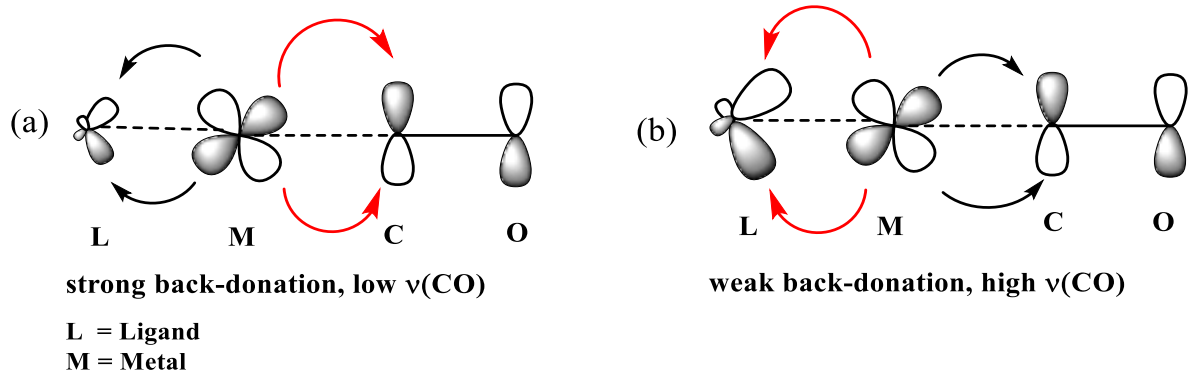


**Figure 1.3** Electronic effects of ligands (a) strong σ-donor ligand (b) strong π-acceptor ligand.[36]

If the employed ligand is a strong σ-donor ligand, the electron density on the metal is increased and a back donation to the CO ligand occurs. This effect shortens the C–O bond length resulting in lowered IR frequencies. In the case of a poor σ-donor or a strong π-acceptor ligand, it competes with CO for the electron back donation and the CO stretching frequencies increases. However, the electronic effect of a ligand may differ from one metal to another. With respect to rhodium-catalysed hydroformylation of alkenes, the influence of electronic ligand properties on catalyst performance has been investigated. It is suggested that the strong metal-to-ligand interaction depends greatly on π-back bonding and this has a direct effect on the rate of hydroformylation. According to the dissociative mechanism, π-acidic ligands lead to stronger metal-to-ligand bond and this results in the facile dissociation of labile ligands to readily form unsaturated catalytically active rhodium hydrido-complex.[61,62] As such, olefin binding becomes thermodynamically more favourable, resulting in higher hydroformylation rates.

### 1.3.2.2 Steric effects

Catalysts often interconvert between various geometries depending on the bulkiness and rigidity of the ligand coordinated to the metal centre. Significant efforts have been made to rationalize or predict ligand steric effects on metal complexes. For example, steric parameters such as the Tolman's cone angle (θ) for monodentate ligands, natural bite angle ($\beta_n$) and pocket angle for bidentate ligands derived from molecular mechanics were proposed (Figure 1.4).[63,64]

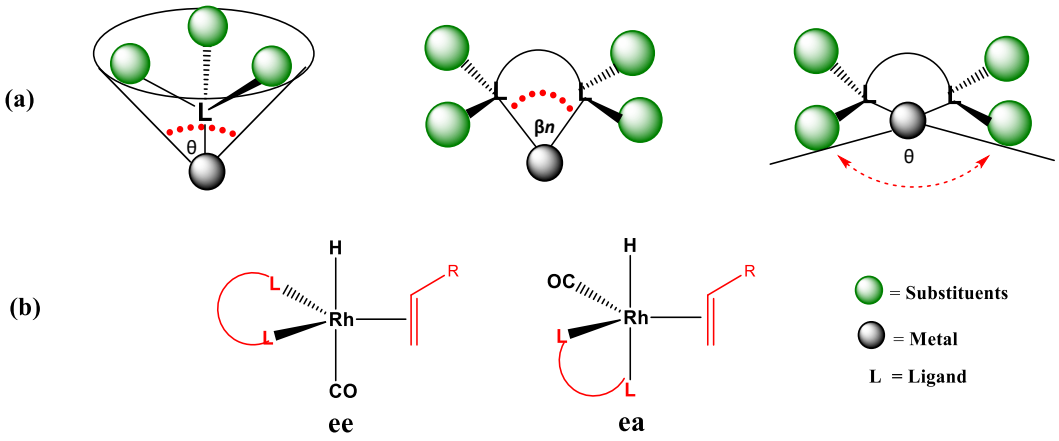


**Figure 1.4** (a) The concept of cone angle, natural bite angle and pocket angle respectively. (b) Bis-equatorial (ee) and equatorial-axial (ea) coordination modes of (Rh(CO)(H)(alkene)L) intermediate.

Bidentate ligands offer better stability, regio- and stereocontrol in catalytic reactions compared to monodentate ligands. The chelating effect of bidentate ligands reduces the plausibility of metal dissociation during catalytic reactions and as a result, the number of species formed are reduced.[65] Barron *et al.* described the concept of pocket angle to portray the steric effect of bidentate ligands using space-filling models derived from crystallographic data.[66] The pocket angle is the interior cone angle or space available for the free rotation of substituents and substrate–metal interaction in a bidentate ligand.[65] The concept of natural bite angle based on molecular mechanics was established by Casey *et al.*[67] It is defined as the preferred chelation angle determined only by the ligand backbone. They suggested that ligands would require an angle of about 120$^{o}$ (wide bite angle) to be capable of forming the equatorial-equatorial (ee) coordination geometry at the metal centre. In the context of hydroformylation, the structure of the alkene complex (Rh(CO)(H)(alkene)L) in a bis-equatorial (ee) fashion is understood to play a crucial role in controlling regioselectivity towards linear aldehyde.[67,68]

Further insights into the ligand steric modulation on the Rh-catalyst using theoretical studies have been performed and studied in detail.[69–72] In particular, Kumar *et al.* examined a variety of substrate and different ligand structures (monodentate and bidentate $PPh_3$ ligands) using quantum density functional theory calculations.[69] Their findings suggested that steric crowding induced by ligand−ligand and ligand−substrate nonbonding interactions stabilizes the transition states leading to the Rh-alkyl intermediates along the pathway to linear aldehydes. Therefore, the design of sterically encumbered ligands is important in improving the regioselectivity of a hydroformylation catalyst towards the much valuable linear aldehyde.

The use of phosphine ligands in homogeneous catalysis has been known for more than half a century. One of the earliest reports involving the use of triphenylphosphine in catalysis is in the "Reppe" chemistry for the synthesis of acrylate esters from alkynes.[73,74] The use of phosphine ligands in catalysis was further popularized by Wilkinson through the revolutionary hydroformylation reaction. However, phosphine ligands are generally difficult to synthesize, very prone to oxidation and P–C bond activation.[48,75–78] Therefore, the investigation and potential use of other classes of ligands such as *N*-Heterocyclic carbenes (NHCs),[62,79] Fischer carbenes[80] and Schiff base ligands for the hydroformylation reaction are been touted. Scholarly contributions of Smith and co-workers on the use of Schiff base ligands have shown promising leads with good activity and high selectivity towards aldehyde.[81–86] Notably, Schiff base ligands are easily obtainable in high yields through a one-step synthesis *via* the quantitative condensation reaction of amines with aldehydes.[87]

Based on the understanding of the hydroformylation reaction and the role ligands play, fine-tuning of metal catalysts through ligand modification is a powerful tool to influence the properties and performance of a catalyst. Rhodium belongs to the rare platinum group metals (PGMs) family. It is the most expensive transition metal used in many homogeneous catalytic reactions.[88] Therefore, the unmitigated usage and efficient recycling of the rhodium-based catalyst is very important. The challenges associated with catalyst separation from post-homogeneously catalysed reaction mixtures can be solved through the use of biphasic (liquid/liquid) catalysis system or by anchoring/immobilizing the Rh-catalyst on a support. However, to enable a recycling approach to be successful, this requires the design of highly active, recyclable and economically viable rhodium-based catalysts.

## 1.4 Biphasic (liquid/liquid) catalyst recovery

The liquid-liquid biphasic catalyst recovery approach employs the immiscible liquid separation strategy. It purports that the catalyst is immobilized in one of the liquid phases and the products/substrate is in the other phase. At elevated temperatures, the reaction is carried out under monophasic conditions or at the interface of the two phases. Post reaction, the reaction mixture is cooled to room temperature and phase separation occurs forming two immiscible liquid layers with the product and catalyst residing in different phases as depicted in Figure 1.5. The product phase is easily separated by decantation, thus enabling the recycling of the catalyst phase.[89]

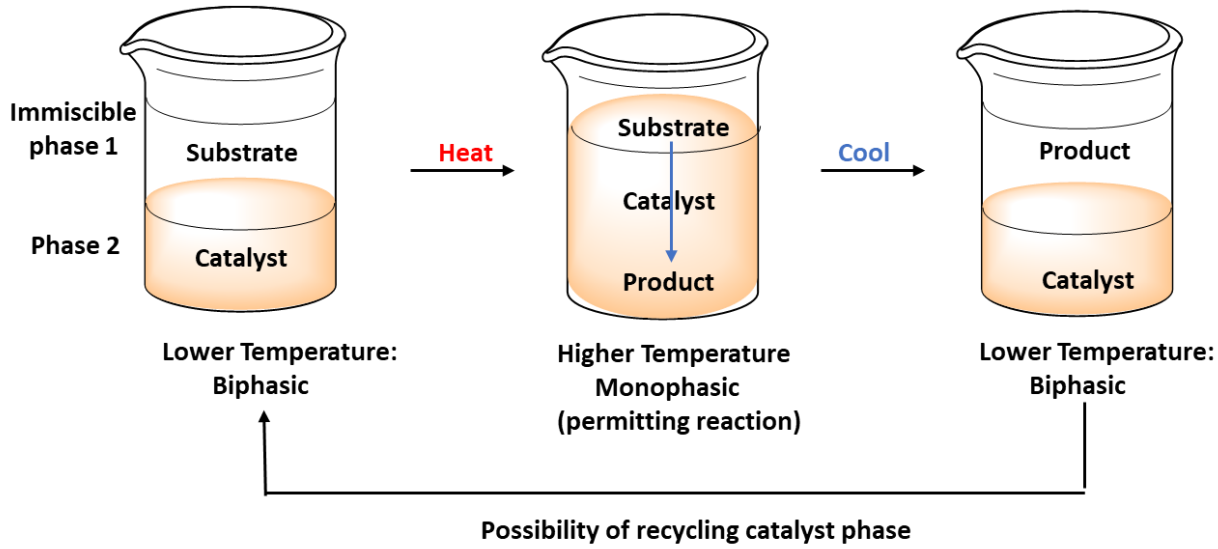


**Figure 1.5** Illustration of the liquid-liquid biphasic catalyst recovery approach.

This temperature dependent phase splitting system is crucial to the success of the biphasic catalysis separation strategy. This strategy has been applied in industry for a variety of reactions, examples are listed in Table 1.3. Various biphasic systems have been touted for the hydroformylation reaction. Examples are the use of ionic liquids, fluorinated solvents, supercritical $CO_2$, thermomorphic solvent systems (TMS) and aqueous biphasic systems.

**Table 1.3** Biphasic catalysis used in industry.[90]

| Process | Company | Metal | Solvent |
|---|---|---|---|
| Oligomerization of ethylene (SHOP) | Shell | Ni | Butane-1,4-diol |
| Hydroformylation of propylene/butylene | RuhrChemie/Rhone-Poluenc | Rh | Water |
| Hydrogenation of unsaturated aldehydes | Rhône-Poluenc | Ru | Water |
| Telomerization of butadiene | Kuraray | Pd | Water/Sulfolane |
| Dimerization of propylene | Institut Francais du Pétrole | Ni | Ionic liquids |
| Oligomerization of ethylene | Universal Oil Products | Ni | Sulfolane |

### 1.4.1 Ionic liquid biphasic catalysis

Ionic liquids (ILs) are salts in their liquid state with low melting points, no vapour pressure, good thermal stability and high ionic conductivity.[91] Ionic liquids can solubilize both organic and inorganic species. As a result, they can be used as solvents for synthesis and catalysis. The non-flammability and non-toxicity characteristics of ILs have made them emerge as environmentally friendly alternatives to volatile organic solvents. Ionic liquids are typically composed of bulky organic cations paired with inorganic anions.[92] These salts can be prepared from a wide variety of ions, enabling their physicochemical properties to be tailored to fit a specific need of a reaction.[93–95]

Chauvin *et al.* published the first investigation of ionic liquid salt (1-butyl-3-methylimidazolium ($BMI^+$)) for the hydroformylation reaction of 1-pentene using $Rh(acac)(CO)_2$ and triarylphosphine.[96] The overall results obtained were poor as a result of the poor solubility and poor affinity of the phosphine ligand in the IL ($BMI^+$). The idea to immobilize the rhodium catalyst in the ionic liquid phase was contrived by Faver *et al.*[97] They reported that the affinity of the rhodium catalyst to the ionic liquid can be enhanced by fine tuning the ligands to fit the nature of the anions and cations of the ionic liquid. Examples of ligands containing ionic tags used in the hydroformylation reactions are shown in Figure 1.6.

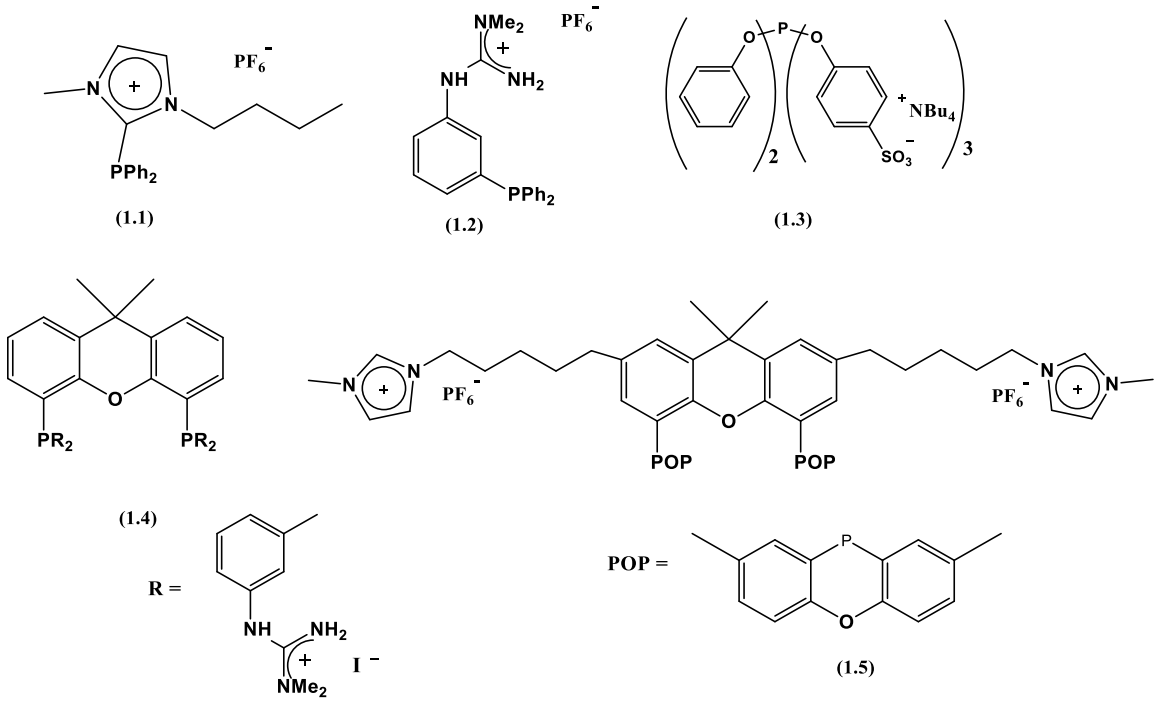


**Figure 1.6** Phosphine and phosphite ligands containing ionic tags.[97,98]

Faver *et al*. reported the synthesis and application of phosphine-functionalized ionic liquids (P-FILs) **1.1**, **1.2** and **1.3** for the hydroformylation of 1-hexene in [BMIM][$BF_4$] and [BMIM][$PF_6$].[97] The good solubility of the ligands in the ionic liquids led to improved activity with excellent Rh retention in the first cycle. However, the activity decreased after two recycling experiments as a result of the partial decomposition of the Rh catalyst. Wasserscheid synthesized phenylguanidinium modified xantphos ligands **1.4** and **1.5**.[98] The ionic ligands were applied in the hydroformylation of 1-octene using Rh(acac)$(CO)_2$ metal precursor in [BMIM][$PF_6$] ionic liquid. Good activities with Rh leaching below the detection limit (ICP < 0.07%) were reported. Additionally, the ionic liquid containing the catalyst were recycled up to four catalytic runs.

The downside of the ionic liquid biphasic catalysis is that large quantities of ionic liquids are often used to dissolve the catalyst. Also, the copious use of highly viscous IL solvent may exacerbate substrate diffusion resistance, thus decreasing the catalyst efficiency.[99,100]

More recently, Jin and co-workers reported the integration of phosphine ligands into ionic liquids (functionalized ionic liquid) to eliminates the need for excessive IL solvent.[100,101] They described the synthesis of phosphine-functionalized polyether guanidinium ionic liquids (RTP-PolyGILs) that possesses the characteristics of room temperature ionic liquids (Figure 1.7).[100] In this way, the catalytic system will require a catalytic amount of the RTP-PolyGILs that plays the dual role of a ligand/carrier of the catalyst and the IL solvent simultaneously.

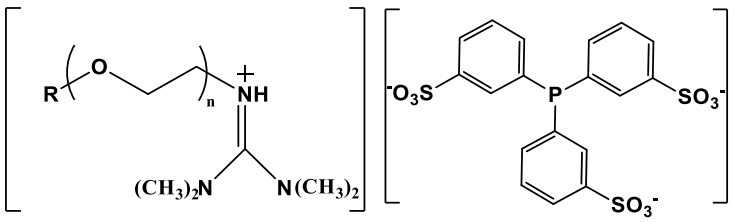


(1.6)

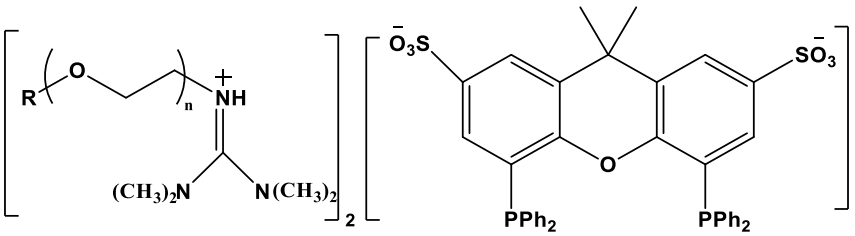


R = $CH_3$, Ph
n = 4, 16

(1.7)

**Figure 1.7** Structures of phosphine-functionalized polyether guanidinium ionic liquids (RTP-PolyGILs).[100]

The RTP-PolyGILs **1.6** and **1.7** were effective for the Rh-catalyzed hydroformylation of 1-octene. The authors reported good recyclability over eleven consecutive runs under neat conditions with low Rh leaching and invariable selectivity for the normal aldehyde. They ascribed the long service life of RTP-PolyGILs and low Rh leaching to the integrated structural design and electrostatic shielding of the surrounding polyether guanidine cations. This stabilises the Rh catalytic active species and thus prevents the formation of inactive Rh clusters. Depending on the product and IL, liquid–liquid (or solvent) extraction is often used to separate the product from the IL/catalyst, this may undermine the green credentials of the process.[99]

### 1.4.2 Fluorous biphasic catalysis

Fluorous solvents, sometimes refer to as fluorocarbons or perfluorocarbons are highly fluorinated liquids. Their extreme hydrophobicity and lack of hydrogen bonding renders them immiscible in aqueous and organic solvents. These features have led to the development of fluorous solvents as switchable solvents for biphasic catalysis. The fluorous biphasic catalysis approach was first demonstrated in 1994 by Horvath and Rabai in the biphasic hydroformylation of primary alkenes using fluorous-derivatised trialkylphosphine in a perfluoromethylcyclohexane solvent system.[102]

In a fluorous biphasic system, two distinct layers are formed in a mixture of a fluorous solvent and an organic solvent at room temperature. The bilayer becomes a one-phase system at elevated temperatures enabling good homogeneous reaction rates that are unimpeded by poor solubility of substrates. Facile phase separation is achieved post-reaction at lower temperatures. The reaction product is extracted from the hydrocarbon phase and the catalyst in the fluorocarbon phase is recycled.[102]

It is important to note that for the fluorous biphasic catalysis to be successful, the homogeneous precatalyst should be preferentially soluble in the f1uorous phase. Therefore, long-chain fluorocarbon tethers or fluoroponytails are appended to the ligand as shown in Figure 1.8.[103] Also, to approximate the reactivity observed in a typical non-fluorinated traditional single-phase system, several spacer methylene groups between the heteroatom of the ligand and the first $CF_2$ group of the fluoroponytails is crucial. This is necessary to shield or decrease the strong electronegative effect of the $CF_2$ group away from the metal centre.[103]

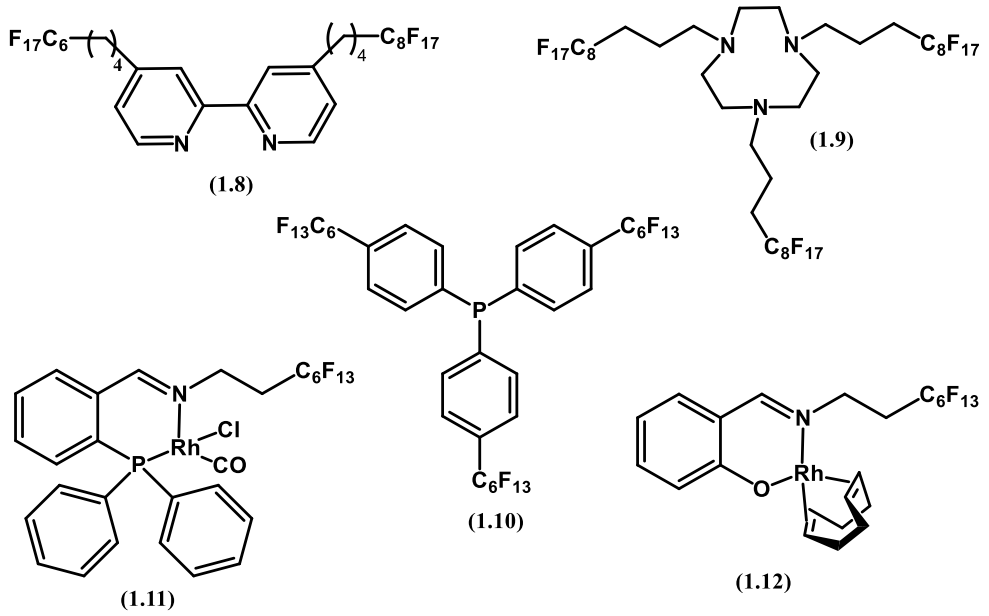


**Figure 1.8** Examples of fluorinated and fluoroponytailed ligands and complexes.[81,103,104]

Foster *et al.* reported the use of fluoroponytailed modified triarylphosphine compound **1.10**.[104] They reported high reaction rates with low leaching of the rhodium and phosphorus into the product. Maqeda *et al.* synthesized fluorous version of salicylaldimine and iminophosphine Schiff base Rh(I) complexes (**1.11** and **1.12**).[81] The catalyst precursors were active in the hydroformylation of 1-octene and gave comparable activity to their non-fluorinated analogue. However, a drastic decline in activity was reported in the second run upon recycling as a result of 93% leaching of the rhodium metal to the organic layer.

Although the fluorous biphasic system is described as an excellent separation approach, the main objection is the high cost and the environmental/toxicological impact of perfluorinated materials.[105,106]

### 1.4.3 Supercritical fluid biphasic approach

Supercritical fluids are compressed gases, having gas-like diffusivities and densities with liquid-like dissolving power and heat capacity. Commonly used supercritical fluids in catalysis is the supercritical carbon dioxide ($scCO_2$).[107] The liquid-like properties of $scCO_2$ with its low cost, availability, non-toxicity and non-flammability makes it an attractive green media alternative for chemical reactions, thus circumventing the use of organic solvents.[108] Several catalytic reactions have been successfully performed in supercritical fluids. These include hydrogenation of esters to alcohols, partial oxidation of hydrocarbons, and hydroformylation.[107,109,110]

The initial study on the use of $scCO_2$ in hydroformylation reaction was by Rathke *et al.* during an attempt to solve liquid/gas mixing problems that occur in conventional solvents.[111] The efficiency of $scCO_2$ as a solvent was studied by comparing the reaction rate of hydrocarbon solvents (methylcyclohexane and heptane) and $scCO_2$ in the hydroformylation of propene. The reaction performed comparably well in $scCO_2$ with higher selectivity towards the linear aldehyde than in the hydrocarbon solvents. Kinetic studies of the reaction indicated that the activation energy obtained in the $scCO_2$ system is 23 ±1.4 kcal $mol^{-1}$, lower than those measured in organic solvents (27-35 kcal $mol^{-1}$). The higher selectivity observed in $scCO_2$ was assumed to be as a result of steric effect exerted by the $CO_2$ molecule coordinated to the central metal. Also, studies by Bach *et al.* on the use of $scCO_2$ in the hydroformylation of 1-hexene reported similar increases in reaction rates with slightly improved *n:i* ratio to those obtained in toluene.[112]

The supercritical solvent can easily be removed from the reaction mixture by decompressing the liquified $CO_2$ to its gaseous state. However, this approach does not address the main problem of catalyst/product separation.[110]

### 1.4.4 Ionic liquid/supercritical carbon dioxide (IL/$scCO_2$) biphasic approach

The limitations of the $scCO_2$ system led to the combination of the favourable properties of ionic liquids with those of supercritical fluids described by Brennecke and co-workers.[113–115] They reported that the ionic liquid improves the solubility of the catalyst while the $scCO_2$ pressure reduces the viscosity of the ionic liquids leading to increased diffusivity and mass transfer. Due to its quadrupole moment, supercritical carbon dioxide is highly soluble in several ionic liquids. Surprisingly, the solubility of ionic liquids in supercritical carbon dioxide is relatively low.[116–118] Therefore, many organic solutes can be extracted from the ionic liquid phase using supercritical carbon dioxide.[116] This allows for a biphasic recyclable process to be developed. Cole-Hamilton demonstrated the feasibility of the IL/$scCO_2$ biphasic approach for hydroformylation reactions in a continuous-flow reactor, as illustrated in Figure 1.9.[117] In the IL/$scCO_2$ biphasic system, ligands or metal precatalysts with ionic appendages are used. The ionic metal precatalyst is dissolved in the ionic liquid tank reactor while the substrate, syngas, and $scCO_2$ are passed into the reactor. Post reaction, the products are extracted with flowing $scCO_2$. The $scCO_2$ is decompressed to release the products while the catalyst and ionic liquid is left behind in the reactor for future recycling.

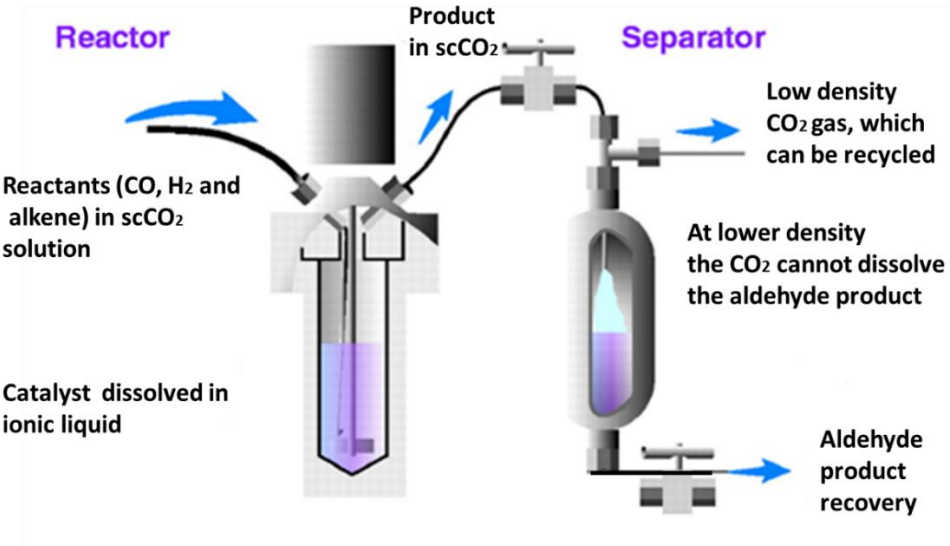


**Figure 1.9** Schematic diagram of Cole-Hamilton's continuous-flow IL/$scCO_2$ biphasic system.[117]

This system has been applied in various homogeneously catalysed reactions such as the Wacker oxidation reactions,[119,120] asymmetric hydrogenation,[121] hydrovinylation[122] and most recently in the synthesis of cyclic carbonates.[123] Alternative systems with $scCO_2$ have also been touted such as the PEG/$scCO_2$ and fluorous/$scCO_2$ biphasic system.[124,125]

### 1.4.5 Thermomorphic solvent system

The thermomorphic solvent system (TMS) proffers the advantage of a true homogeneous single phase system and a catalyst recovery strategy *via* phase separation. TMS are composed of at least two solvents with varying degrees of polarity and high temperature-dependent miscibility gap.[126] In this system, the catalyst is soluble in the polar solvent, while the substrate and product is soluble in the nonpolar solvent. A semi-polar third solvent can also be used as a solubility mediator for the nonpolar and polar components.[127] The concept of the tuneable TMS systems is based on the idea that the mutual solubility of binary solvent mixtures increases with increasing temperature. The system becomes completely monophasic above a certain temperature threshold (T1) (Figure 1.10). Therefore, the reaction takes place under "actual" homogeneous conditions at the operating point without any mass transport limitations.[128–130]

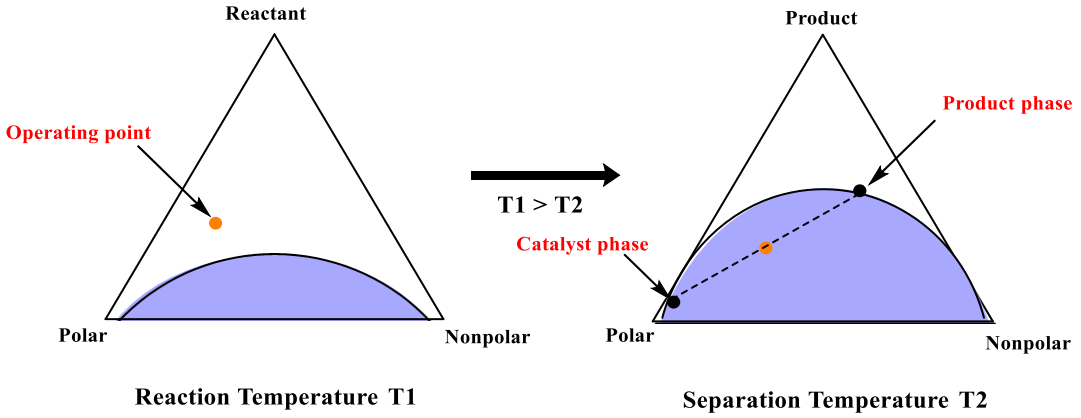


**Figure 1.10** Ternary diagram of a thermomorphic solvent system.[131,132]

The formation of two liquid phases (nonpolar (containing product) and polar (containing catalyst)) is obtained upon cooling to the separation temperature (T2).

The first report of hydroformylation reactions in TMS was by Behr *et al.* in 2005 using propylene carbonate (1,3-dioxolanone), *p*-xylene, and *n*-dodecane.[131] Therein, the rhodium–biphephos catalysed hydroformylation of trans-4-octene gave high yields for the desired linear aldehyde at full conversion. However, leaching of the catalyst into the non-polar phase was ca. 50%. Thus, no recycling experiments were reported.

An extensive TMS solvent screening investigations for the hydroformylation reaction using 1-dodecene and rhodium-biphephos as a model substrate and catalyst respectively was reported by Sundmacher *et al.*[132] They developed a relative solubility method (COSMO-RS) based on DFT calculations. The authors proposed that solvent decisions can be made by comparing solvents having a high relative solubility (HRSC) performance for the catalyst/ligand with a solvent having a low relative solubility for the catalyst/ligand (LRSC). *n*-Decane was chosen as the fixed LRSC solvents due to its extensive use in ongoing research in hydroformylation reactions. The solvents were ranked according to their relative solubilities starting with a maximum value of 0 (referring to maximum solubility). Therein, acetaldehyde gave the most promising TMS system having the lowest relative solubility value over other HRSC solvents such as *N*,*N*-dimethylacetamide, acetone, dimethylformamide and *N*-formylpiperidine. However, Acetaldehyde was not considered as a suitable solvent for hydroformylation reactions due to its low boiling temperature of 20 °C, making experimental validation and analysis difficult. Therefore, DMF was chosen as the solvent of choice for hydroformylation reactions.

Recently, Vorholt and co-workers demonstrated the total integration of the TMS (DMF/*n*-decane) system in a continuous mini-plant process for the hydroformylation of 1-dodecene.[133] The mini-plant vacuum distillation technique offers the advantage of observing factors such as the long-term stability of the catalyst, recycling process performance and parameters. Excellent conversions with an average yield of 55% was achieved at continuous operation of 120 h and distillate temperature of 58 °C.

The collaborative work of Behr and Vorholt led to the investigation of a slightly different approach from the DMF/alkane TMS system.[130] They reported the hydroformylation of methyl 10-undecenoate with a [Rh(acac)$(CO)_2$]/water-soluble 4,5-bis(diphenylphosphino)-9,9-dimethyl-2,7-disulfoxanthene disodium salt system in an aqueous TMS mixture of water and 1-butanol. The water-soluble catalyst was recycled in the aqueous phase, while the products were quantitatively extracted from the 1-butanol phase. High TOF values were reported with regioselectivity of 73% linear aldehyde and catalyst leaching of 15 ppm into the product phase.

The advantages of the thermomorphic solvent systems compared to other recycling strategies is the convenient use of untailored homogeneous catalyst in the case of DMF/alkane TMS system. In addition, the reaction takes place under true homogeneous conditions (without mass transfer limitations between the substrate and the catalyst). The downsides of this system include: (a) the limited number of solvent combinations with a proper miscibility gap to form a TMS system[132] (b) the distortion of the temperature dependency miscibility gap if semi-polar substrates are used thus making it a single phase at low temperature, this effect leads to undesirable catalyst leaching[126] (c) the dependency on organic solvents considerably demeans the green credentials of the process.

### 1.4.6 Aqueous biphasic catalysis

The increasing demand for environmentally sustainable processes has propelled the continual use of water as a solvent for chemical transformations. Its abundancy, availability and immiscibility with most organic substrates and products easily makes water a solvent of choice for biphasic catalysis.[134] Typically, metal catalysts/ligands used in catalytic reactions are insoluble in water. Therefore, for the aqueous biphasic approach to be effective, the catalyst should be soluble in the aqueous phase and insoluble in the organic phase. This requirement brings with it the design of new water-soluble catalyst precursors or the chemical modification of known catalysts by introducing hydrophilic polar groups such as sulfonate, carboxylate or ammonium functionalities.[135,136]

Phosphines ligands have been widely used since the advent of organometallic homogeneous catalysis; therefore, it is not surprising that the initial attempt to synthesise/design water-soluble catalyst were based on phosphine. The first synthesis of sulfonated phosphines (triphenylphosphine mono-sulfonate (TPPMS)) **1.13** (Figure 1.11) was reported in 1958.[137,138] TPPMS are synthesised *via* the direct sulfonation of phosphines. The development of parallel approaches to completely solubilise phosphine in water led to the discovery of the well-known triphenylphosphine trisulfonate (TPPTS) ligand (**1.14)** by Kuntz in 1975.[139,140]

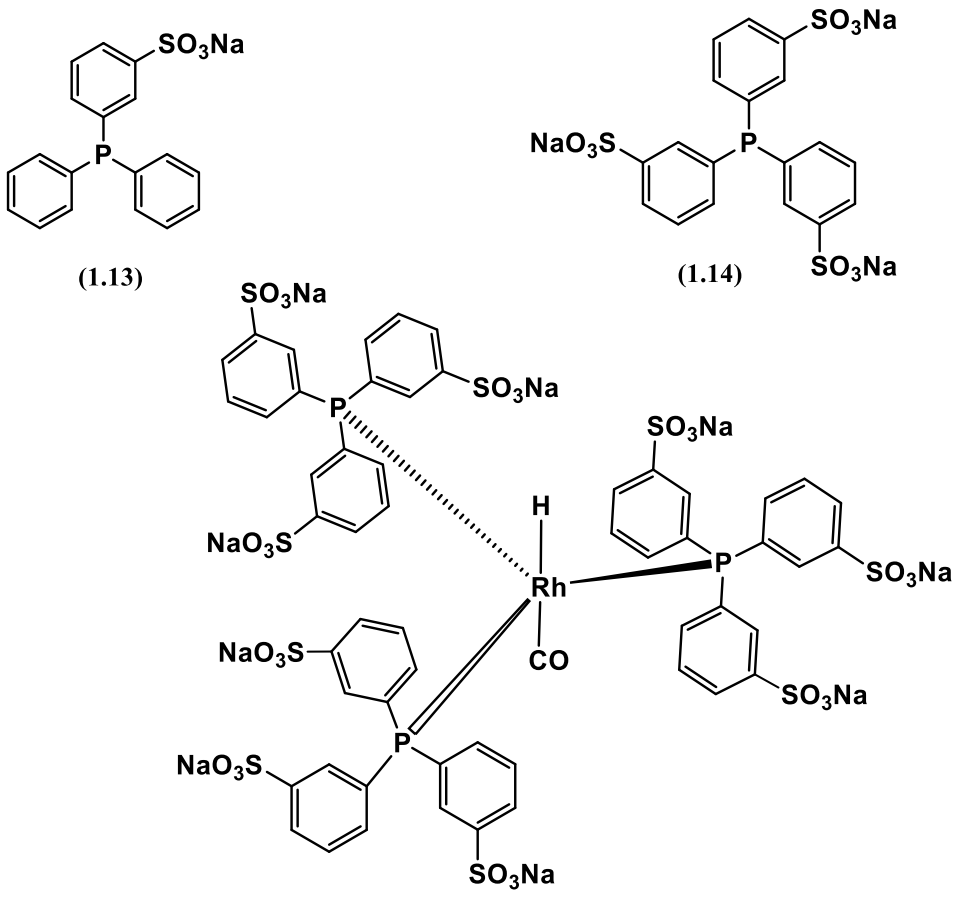


**Figure 1.11** Structure of triphenylphosphine mono-sulfonate (**1.13**), triphenylphosphine tri-sulfonate (**1.14**) and the proposed structure of the *in situ* formed active catalyst from TPPTS (**1.15**).[141]

An important example of an industrial application of aqueous biphasic catalysis is the Rhône Poulenc/Ruhrchemie process developed in 1984 for the hydroformylation of propylene.[142] This process uses a combination of the Rh metal and the TPPTS ligand to generate the active catalyst **1.15**, this process produces about 600,000 tonnes of *n*-butyraldehyde per year.[141]

A simplified flow process of the Rhône Poulenc/Ruhrchemie aqueous biphasic system is illustrated in Figure 1.12. Therein, the reactor contains the precatalyst (TPPTS and metal precursor), the gaseous reactants (CO, $H_2$), and propylene. After the reaction, the reaction mixture is transferred to a gas-liquid separator which separates the gases from the liquid product. The crude product is separated and the aqueous phase containing the catalyst is transported back into the reactor.[135,143]

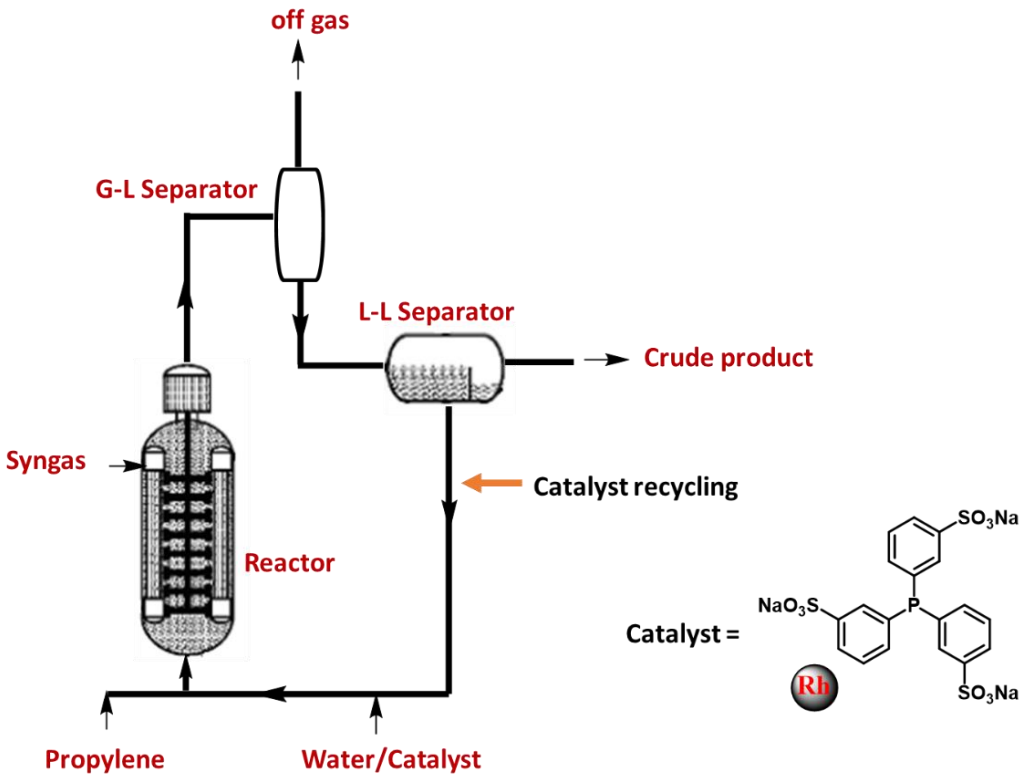


**Figure 1.12** Simplified flow process of the Rhône Poulenc/Ruhrchemie aqueous biphasic system.[135,141,143]

The limitation of this process is that the Rh-TPPTS catalyst biphasic system is not effective for long chain substrates (> C5). This is because, the increasing number of carbon atoms in long chain alkenes results to decreased solubility in water thus leading to mass-transfer problems.[144,145] Strategies that have been employed to overcome this is the use of co-solvents, discrete water-soluble metal catalysts and mass transfer agents such as surfactants and cyclodextrins.

### 1.4.6.1 Co-solvents in aqueous biphasic catalysis

The addition of a co-solvent to a biphasic system can facilitate the migration of higher olefins from the organic phase to the aqueous phase. Monteil *et al.* studied the effect of various co-

solvents with TPPTS in the hydroformylation of 1-octene.[146] Alcohols such as ethanol and methanol were found to increase the concentration of 1-octene in water by two orders of magnitude. However, a significant amount of the catalyst was reported to have leached into the organic phase. More recently, Herrmann *et al.* reported the hydroformylation of methyl oleate using Rh/NaTPPTS catalyst in aqueous-media in the presence of 2-propanol as a co-solvent.[147] They reported quantitative yields (> 98%) for the branched aldehyde, with < 2% of 2-propanol and < 0.5% of the catalyst leaching into the nonpolar product phase. Over ten recycling runs with an accumulative turnover number of 20 000 were reported.

### 1.4.6.2 Surfactants in aqueous biphasic catalysis (micellar catalysis)

Surfactants are amphiphilic compounds containing hydrophilic head and hydrophobic tail. Due to their amphiphilic properties, they can mediate between the confines of two immiscible liquids by forming unique self-assembly features resulting to micelle-like aggregates. (Figure 1.13).[148]

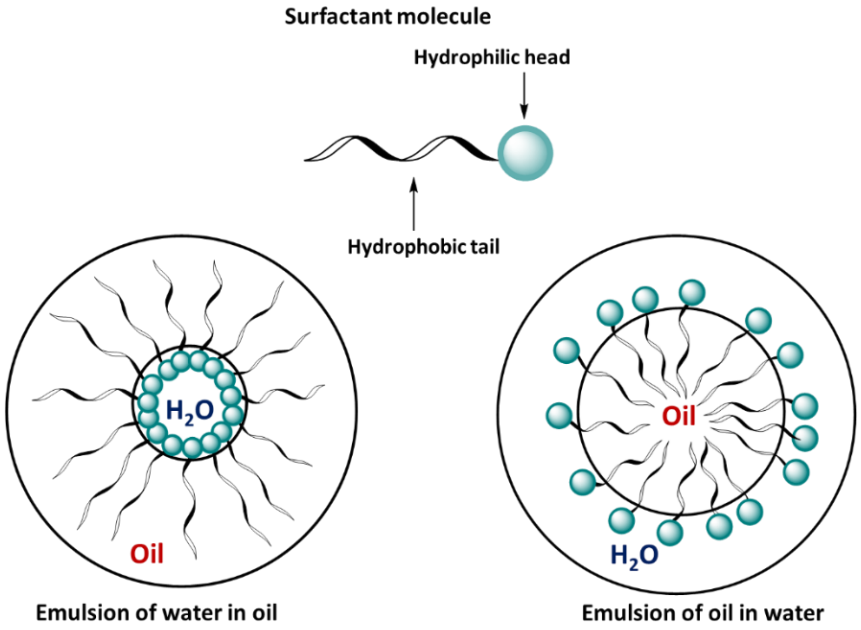


**Figure 1.13** Schematic structure of a surfactant and self-orientation of surfactants in water/oil microemulsion.[148,149]

In a biphasic mixture, surfactants arrange themselves with their heads pointing outwards into the aqueous phase shielding the inner hydrophobic domain of the micelle, thus lowering the interfacial tension between the two liquids.[149,150]

Surfactants are classified based on their polar head group charge. For example, anionic surfactants are surfactants possessing a negatively charged head group, cationic surfactants have a positively charged polar head group, zwitterionic surfactants have a zwitterionic head group (positive and negative charge) while non-ionic surfactants have an uncharged polar head group.[151]

Surfactant-ligands sometimes referred to as amphiphilic ligands are functionalized ligands with a alkyl chain and a hydrophilic head group (figure 1.14).[152]

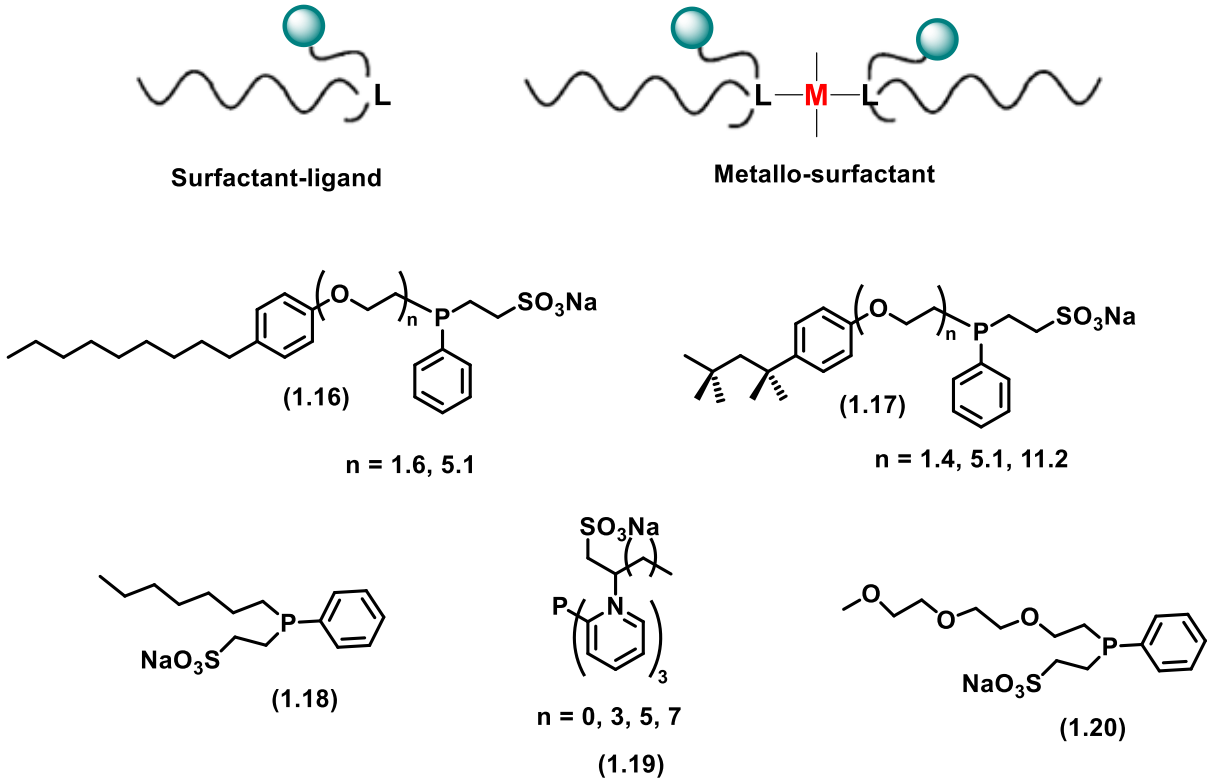


**Figure 1.14** Illustration of surfactant-ligand, metallo-surfactant and examples of surfactant containing phosphine ligand.[152]

The design of amphiphilic ligands and their ability to form molecular micellar arrangement in water/organic solvent media has been reported in the literature. For example, Valls *et al.* reported the synthesis of surfactant containing phosphine ligands **1.16**–**1.20** with the aim of anchoring a metal centre to obtain metallo-surfactants.[152] Therein, the surfactant containing ligands and their metal complexes with varying degree of ethoxylation were synthesised by reacting phenylphosphido-ethanesulfonate with the appropriate alkyl chloride and $PdCl_2$(COD). Aggregation properties of these complexes in water to yield supramolecular arrangements were studied using surface tension measurements. At critical micelle

concentration (CMC), a linear decrease in the surface tension was observed as the concentration of the amphiphilic ligand is increased. Unfortunately, the low solubility of the sulfonated Pd(II) complexes in water hindered investigations into their surfactant properties.

More recently, Pogrzeba *et al.* investigated the phase behaviour of non-ionic surfactants in a microemulsion system for the rhodium-catalysed hydroformylation of 1-dodecane.[153] They reported that the degree of ethoxylation of the surfactants determines the stability and boundary conditions for reactions to occur. They also suggested that the organic−water interface (interfacial area) is where the reaction takes place as illustrated in Figure 1.15. In the case where no surfactant was applied, no reaction progress was observed, thus confirming that the surfactant is needed to enable the hydroformylation reaction to take place in a biphasic system.

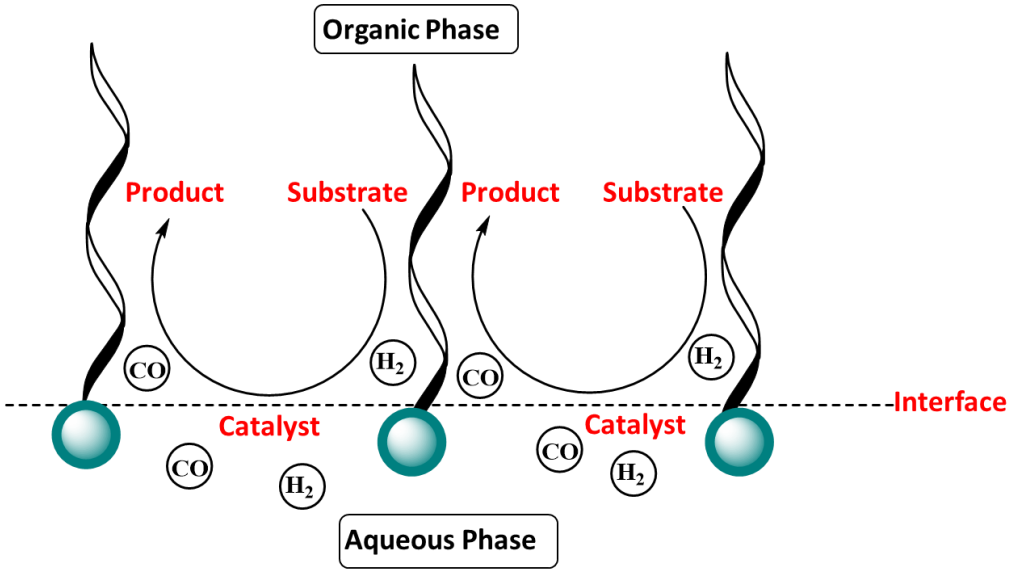


**Figure 1.15** Illustration for the hydroformylation of long chain olefins in microemulsions.[150]

They recommended that when considering easy product separation/catalyst recycling, high concentrations of the surfactant (not exceed 12 wt % of the entire solvent system) in microemulsions should be avoided in order to maintain good and fast switchability of the water/solvent mixture.

This described concept of micellar approach using metallo-surfactant in microemulsion systems has been explored for various catalytic reactions.[154–156] With respect to the hydroformylation, research in the use of metallo-surfactants (surfactants that are catalytically active by themselves) stands at its beginning.

### 1.4.6.3 Cyclodextrins in aqueous biphasic catalysis

Cyclodextrins are cyclic oligosaccharides with an inner hydrophobic surface and outer hydrophilic surface (Figure 1.16a).[157] The application of cyclodextrins in aqueous biphasic hydroformylation reaction was first pioneered and extensively studied by Monflier and co-workers.[158–161] It is hypothesized that the cyclodextrins operate as an inverse phase-transfer agent through host–guest complexing with hydrophobic substrates in biphasic reactions as illustrated in Figure 1.16b. The inner cavity of cyclodextrins allows for the formation of an inclusion complex when it binds to a hydrophobic substrate thereby increasing the hydrophilicity of the substrate. This facilitates substrate migration into the aqueous phase, thus improving substrate-catalyst interaction and the overall rate of the reaction.[157,162]

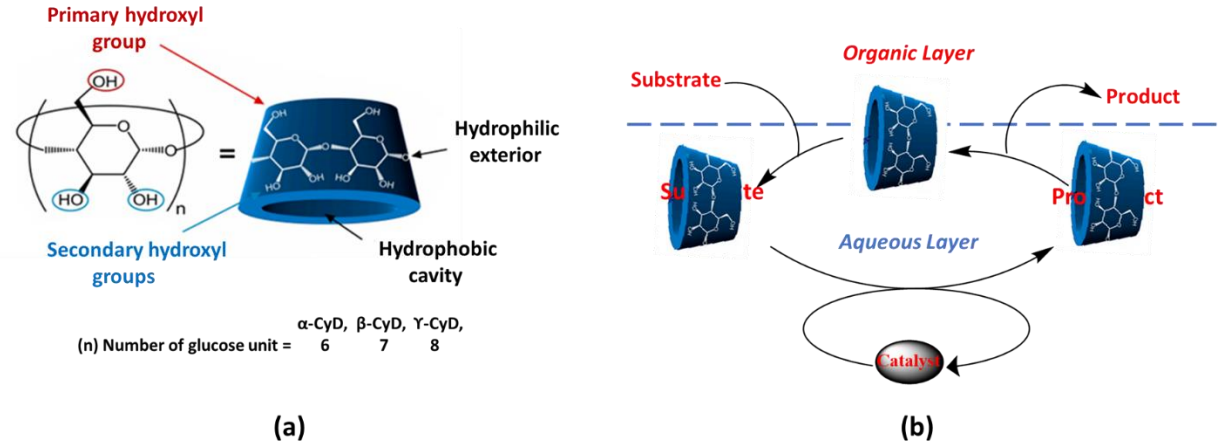


**Figure 1.16** (a) The chemical and 3D structure of cyclodextrin and (b) Illustration of cyclodextrin assisted aqueous biphasic catalysis.[157,162]

Dauchy *et al*. investigated salicylaldimine and salicylhydrazone ligands based on β-cyclodextrin scaffold in the hydroformylation of 1-decene (Figure 1.17).[163] The water-soluble salicylaldimine and salicylhydrazone monosubstituted cyclodextrin were synthesised *via* condensation reactions between sulfonated salicylaldehyde or sulfonated $^{t}$Bu-salicylaldehyde with β-cyclodextrin. The reaction of $[Rh(COD)_2BF_4]$ with ligand **1.21** or **1.22** in an alkaline solution formed the corresponding rhodium complexes *in situ*. Both complexes gave high conversions with good regioselectivity towards linear aldehydes. However, no recyclability studies were reported as a result of high catalyst leaching observed by the coloration of the organic phase, thus insinuating catalyst instability or the partial hydrolysis of the persubstituted cyclodextrin under catalytic conditions.

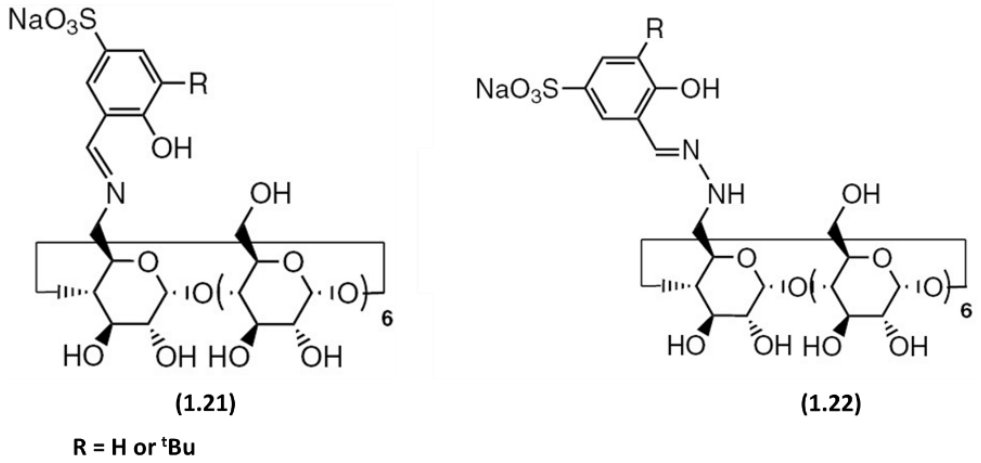


**Figure 1.17** Structures of persubstituted salicylaldimine and salicylhydrazone cyclodextrin.[163]

Generally, cyclodextrin-based catalysts display good hydroformylation activities for olefins possessing carbon atoms lower than twelve (< 12) in biphasic systems.[162] Also, improved regioselectivity for the linear product is often observed as a result of the confinement of reacting species within the cavity.[164] However, for larger olefins (> 12 carbons) the efficiency of cyclodextrin is drastically reduced because of the restricted binding of larger olefins into the cyclodextrin interior, leading to low catalytic activity.[160,165]

### 1.4.6.4 Water-soluble Rh (I) catalyst precursors

An elegant alternative to the classical triphenylphosphine tri-sulfonate (TPPTS) water-soluble ligands, is the use of discrete water-soluble Rh(I) catalyst precursors. The seminal work of Smith and co-workers designed various water-soluble monomeric and multimeric Schiff base metal complexes.[82–84,166] These water-soluble metal complexes have been studied as hydroformylation catalyst for various olefinic substrates. The high polarity of the water-soluble complexes and their consequent insolubility in the organic phase could enable multiphasic reactions to be carried out with little or no leaching of the metal catalyst into the product phase.

Recently, Siangwata *et al.* reported the synthesis of sulfonated salicylaldimine aryl ether Rh(I) mononuclear and trinuclear complexes **1.23** and **1.24** (Figure 1.18).[166] The complexes were successfully evaluated in aqueous biphasic hydroformylation of 1-octene. Both catalyst precursors were highly active as hydroformylation catalysts giving near quantitative conversions and good aldehyde chemoselectivity at reaction conditions of 85 °C and 50 bar. The catalysts were recycled five times in water/toluene mixtures. A decrease in catalyst performance was reported after each run, this was ascribed to the leaching of the catalyst into

the organic layer alongside catalyst degradation. To circumvent leaching issues and adhere to the green chemistry integrity of the aqueous approach, the catalyst precursors were evaluated under neat conditions (in the absence of an organic solvent). Improved catalysts performance in the aqueous biphasic experiments was reported for the trinuclear analogue (**1.24**). This was ascribed to the stabilizing dendritic environment.

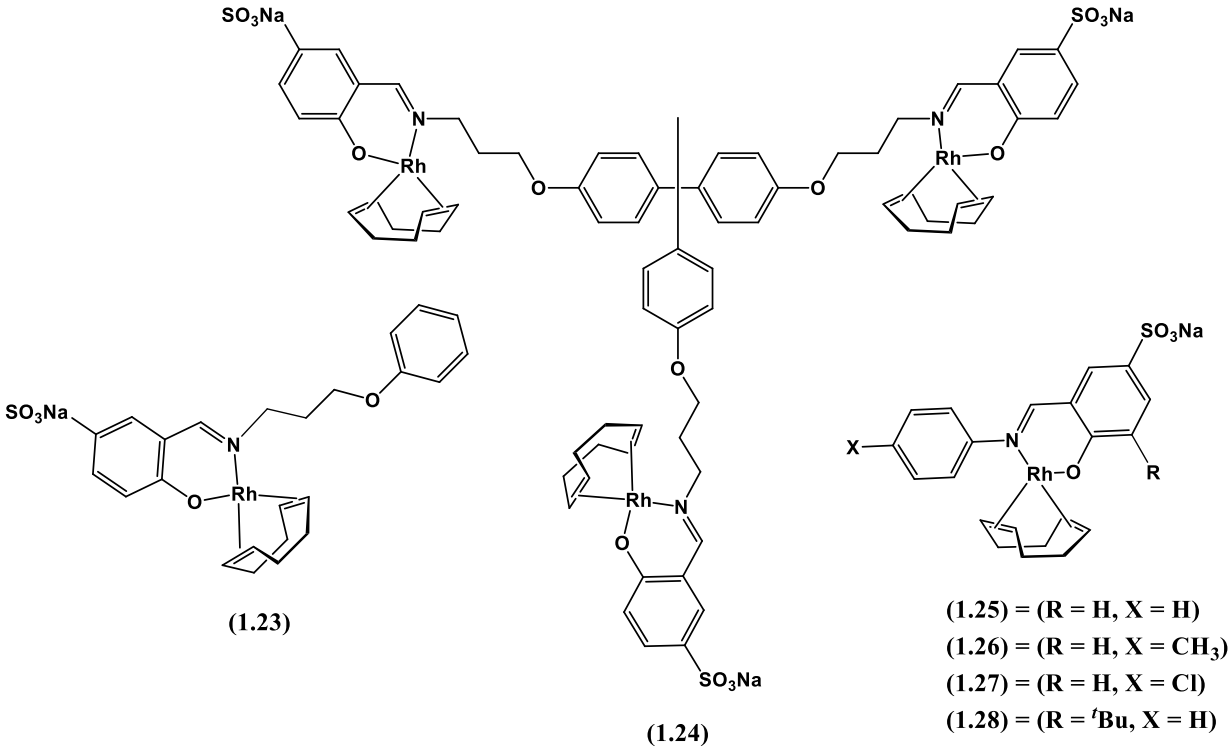


**Figure 1.18** Sulphonated salicylaldimine Rh(I) complexes.[83,166]

Water-soluble sulfonated mononuclear salicylaldimine Rh(I) complexes with varying substituents were reported by Matsinha *et al.*[83] The catalysts display good activity and chemoselectivity at 50 bar syngas pressure and 95 °C temperature. Significant electronic influence was noted with the substituted derivatives. Comparing the catalyst precursor, excellent aldehyde chemoselectivity was maintained with complex **1.26** in all 5 cycles. This was suggested to be as a result of the electron-donating effect of the methyl group. A decline in chemoselectivity was observed for the catalyst possessing the halogenated substituent (**1.27**), while an overall increase in linear aldehyde was observed for the catalyst bearing the bulky *tert*-butyl substituent (**1.28**). In all cases, ICP-OES analysis revealed no detectable levels of Rh present in the organic layer. However black particles in the aqueous layer were observed, this was suggested to be as a result of catalyst decomposition.

A water-soluble non-sulfonated strategy was reported by Ramarou *et al*. based on 1,3,5-triaza-7-phosphaadamantane (PTA).[167,168] A series of water-soluble mono- and multivalent Rh(I) complexes **1.29** – **1.31** (Figure 1.19) were synthesised by the lower rim benzylation of 1,3,5-triaza-7-phosphaadamantane followed by complexation reaction with $[RhCl(COD)]_2$.

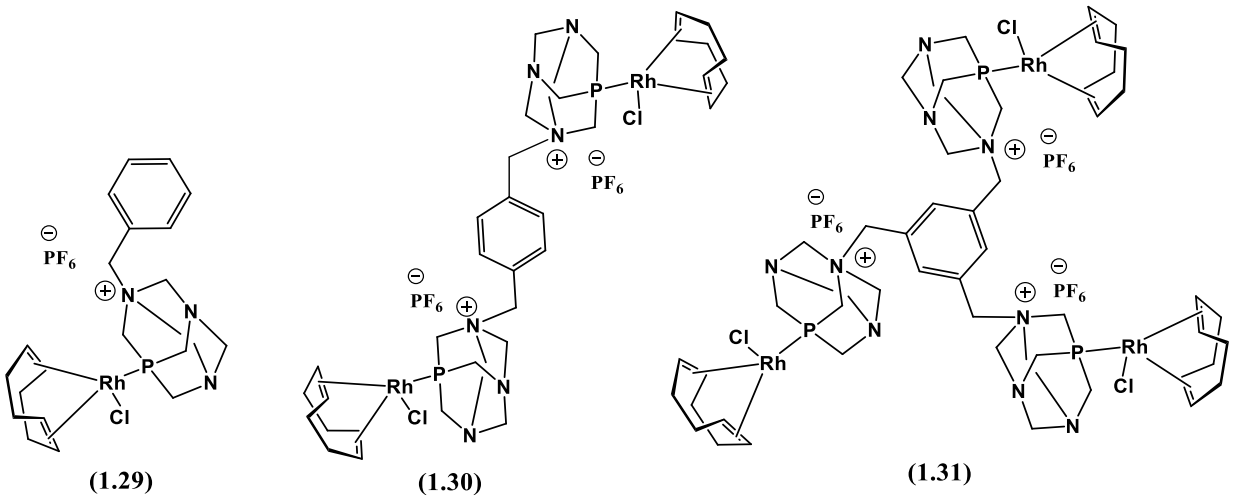


**Figure 1.19** Structure of the Rh(I)-PTA catalyst precursors.[168]

The catalytic efficiency and recyclability of complexes **1.29**–**1.31** were evaluated for hydroformylation of 1-octene in a water/toluene biphasic mixture at optimized conditions of 75 °C and 40 bar syngas pressures. Increased catalytic activity was reported for catalyst precursor **1.30** and **1.31** compared to **1.29**. However, the complexes exhibited poor activity upon recycling as a result of decreased concentration of Rh metal in the system. This was evident from the ICP-OES studies giving ca. 90% of metal leaching to the toluene layer.

## 1.5 Supported catalysts

### 1.5.1 Insoluble supports

A non-biphasic strategy in addressing the difficulties associated with the separation of homogeneous catalysts from the reaction media is the anchoring of the homogeneous catalyst onto a support. The anchoring or immobilization of a catalyst could be *via* covalent or noncovalent interactions such as hydrogen bond, coordination, electrostatic interactions or incorporation by ion exchange reactions.[57,169–171] The support can either be insoluble or soluble in the reaction media. For insoluble support systems, the catalyst can easily be separated by simple filtration of the material. This combines the advantages associated with heterogeneous and homogeneous catalysis. Well-known insoluble supports used in anchoring homogeneous catalyst are the silica mesostructured material (MCM-41) and chitosan.[172–175] Rhodium

complexes are tethered to MCM-41 or chitosan *via* donor ligands as shown in Scheme 1.4. A number of organic–inorganic hybrid materials have been explored for the hydroformylation reaction. Some examples are silica polyamine composite,[176,177] alumina,[178] zeolite,[179] polystyrene beads,[180,181] porous vinyl-polymers,[182,183] and magnetically separable nanocatalysts.[184]

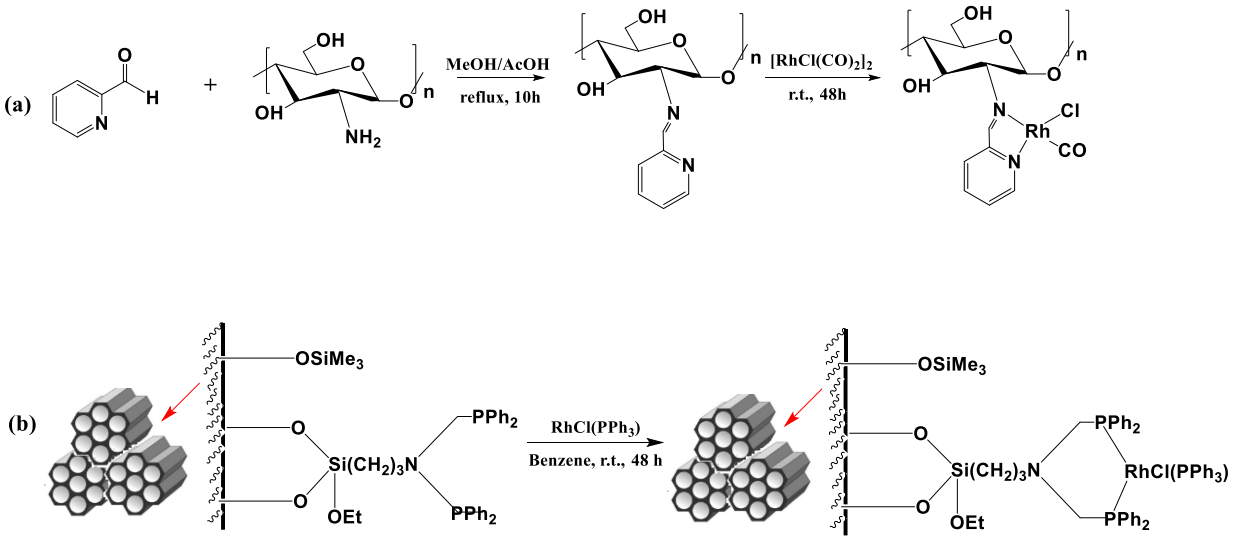


**Scheme 1.4** Rh-catalyst on (a) chitosan and (b) mesoporous material (MCM-41).[174,175]

Problems that are often encountered in the use of insoluble supports include the non-linear kinetic behaviour (irreproducible results), unpredictable selectivity, mass transport limitations and metal leaching.[57,171,185]

### 1.5.2 Soluble support

The problems often encountered with the use of insoluble support can be addressed by anchoring the homogeneous catalyst to soluble supports. The high activity of the homogeneous catalysts is maintained as a result of the uniform dispersity of the catalyst throughout the reaction mixture. Examples of soluble supports that have been explored as recoverable catalysts include the use of soluble polymers such as polyethylene/polyethylene glycol (PEG),[186–191] and highly branched polymeric macromolecules such as dendrimers.[192,193]

### 1.5.2.1 Highly branched macromolecules

Highly branched polymers are a special type of dendritic polymers possessing branching units with the potential of further branching into high density repeating units.[194] Highly branched macromolecules are sub-classed into categories based on their architectural construct, these are: (a) branched-dendritic hybrids (b) hyperbranched polymers (c) dendrigrafts (d) dendrons and (e) dendrimers. As illustrated in Figure 1.20, the first three subclasses exhibits randomly branched structures while the latter three exhibit structures with a uniform degree of branching (DB).[195,196]

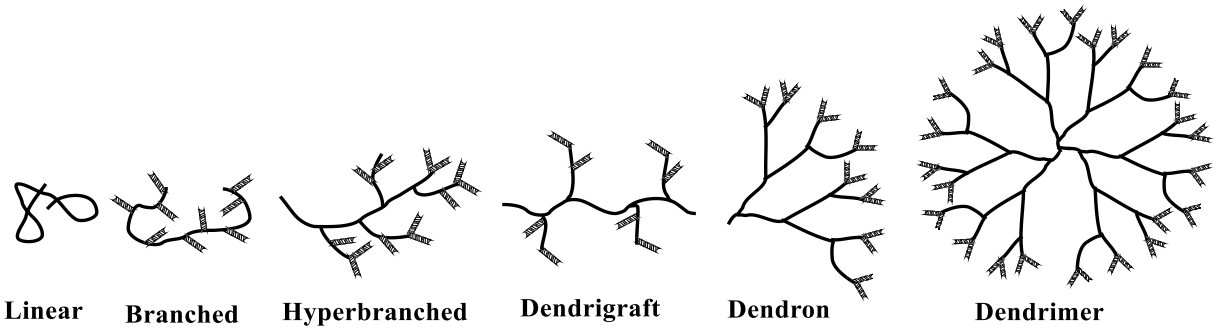


**Figure 1.20** Evolution of linear polymers to dendrimers.[195,196]

Dendrimers are highly branched monodispersed globular macromolecules.[197] Dendrimers emerged from polymer science in the early 1980's and the first archival paper on branched polymers described the synthesis of low molecular weight cascade polyamines published by Fritz Vögtle and coworkers.[198] Years later, Tomalia published the synthesis of poly-amidoamines (PAMAM) up to the 10th generation and named this novel class of polymer 'dendrimer'.[199] The architectural structure of a dendrimer consists of three micro-environments; these are the core, the interior and the peripheral terminal groups.

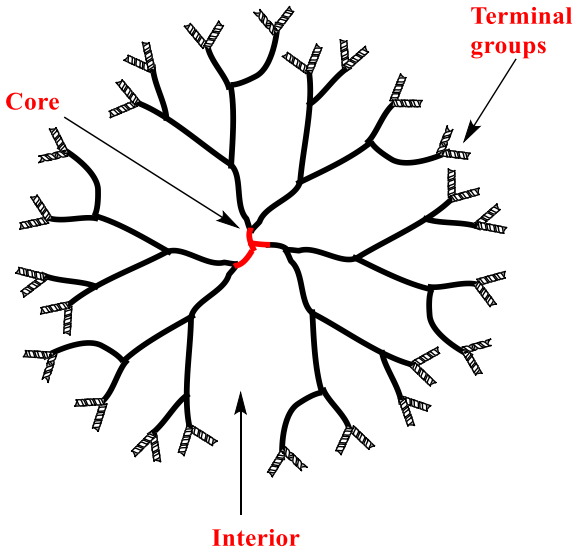


**Figure 1.21** Architectural component of a dendrimer.

Dendrimers can be synthesised by various strategies; the two main routes are the divergent dendritic growth method which emanates from the core to the periphery and the convergent dendritic growth method, a stepwise growth from the periphery to the core.[199,200] Figure 1.22 schematically shows these synthetic strategies.

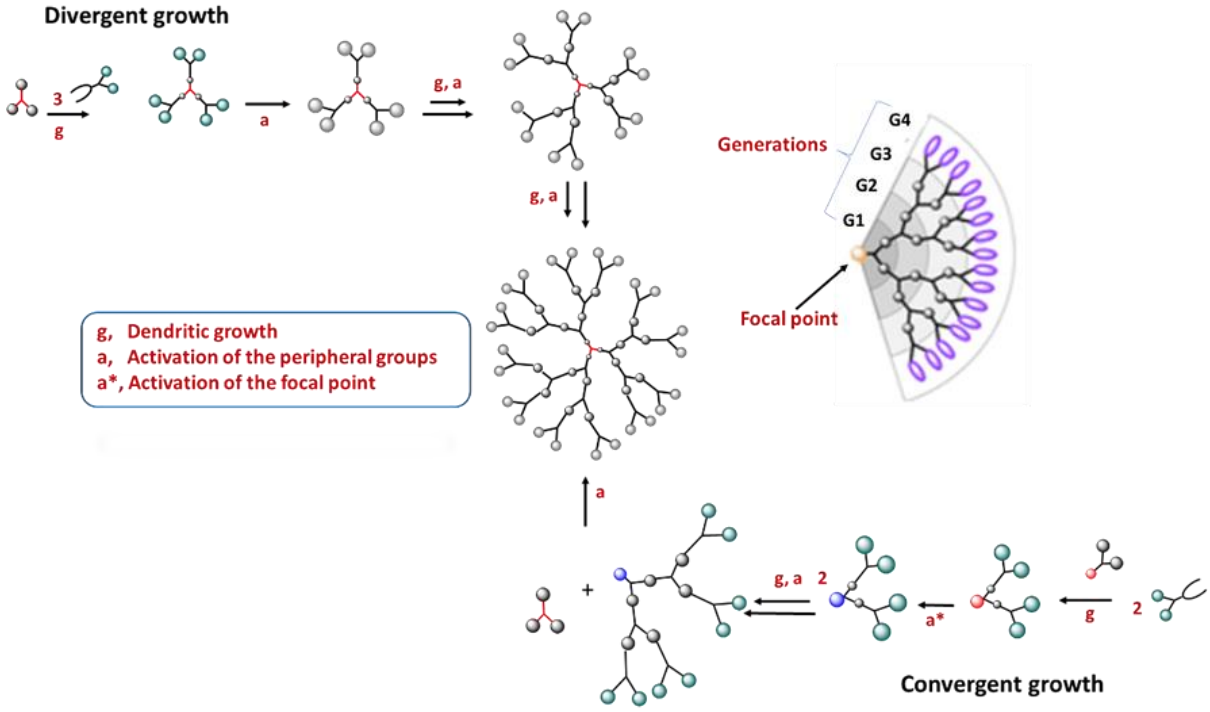


**Figure 1.22** Schematic overview for the synthesis of dendrimers.[199,200]

The convergent growth (outside-in) method to construct dendrimers was introduced by Hawker and Fréchet (Scheme 1.5).[201] In the convergent growth route, the monomers are first synthesised in a controlled manner to generate a well-defined dendron or wedge. The functional group at the focal point of the dendron is activated and coupled to a multi functionalized core moiety. This process is repeated until the desired dendrimer growth is reached. The convergent growth allows for easy monitoring and control of the dendrimer growth because the dendrons are structurally less complicated and much easier to purify.[202]

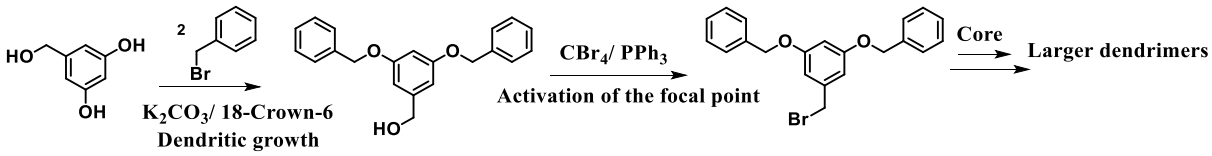


**Scheme 1.5** Hawker and Fréchet's convergent growth strategy.

For the divergent growth approach (inside-out), the strategy entails the use of a core which possesses two or more accessible functionalities and a monomer or wedge with only one activated functional group and dormant/protected functionalities. This allows for controlled covalent attachment to the active group present in the core. Also, an excess of the monomer or wedge is crucial for complete reaction with the core. The generation of the dendrimer is further increased by activating/deprotecting the external functionalities of the dendritic compound and reacting it with an activated monomer. An important example of this route is the poly-amidoamine (PAMAM) dendrimers by Tomalia (Scheme 1.6).[197]

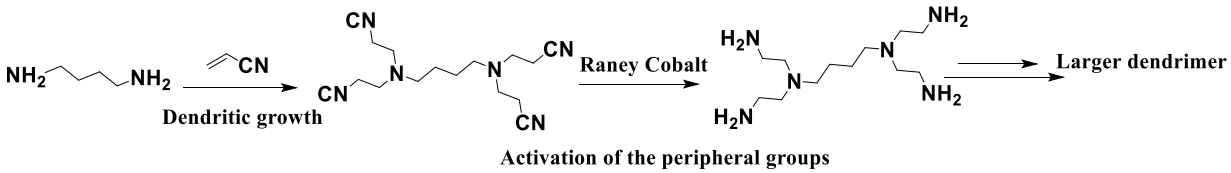


**Scheme 1.6** Divergent growth route to poly-amidoamine dendrimers.

These reaction routes are repeated to achieve higher generation dendrimers with multiple end groups. The dendrimer can be post-functionalized with the desired motifs such as metals to afford metallodendrimers.

The combination of dendritic moieties with the special properties of transition metals, unique hybrid materials with catalytic, optical, magnetic, electro- and photochemical properties can be created.[203] This is a promising area of research with vast possible applications. This also combines the fields of organic, inorganic, supramolecular, and polymer chemistry into a highly interdisciplinary field of research. In catalysis, large dendrimers have been proposed to combine the advantages of both the homogeneous catalysis and heterogeneous catalysis. Their size enables the separation of catalysts while their molecular nature ensures uniform dispersity in solution. In a dendritic framework, catalytic moieties can be placed at the core, peripheral end, interior or at the focal point of a dendron, thus allowing spatial control of the microenvironment around the metal centre.[204,205] Examples of metallodendrimers used in catalytic reactions include; the core functionalised *N*-heterocyclic carbene dendritic complex crafted by Tsuji for hydrosilylation reactions (**1.32**),[206] Kimura's phthalocyanine-centered metallodendrimer catalyst for the oxidation of mercaptoethanol (**1.33**),[207] porphyrin containing terminal ferrocene moieties (**1.34**)[208] and Smith's focal point functionalised polyether dendrons for the hydroformylation of 1-octene (**1.35**) (Figure 1.23).[85]

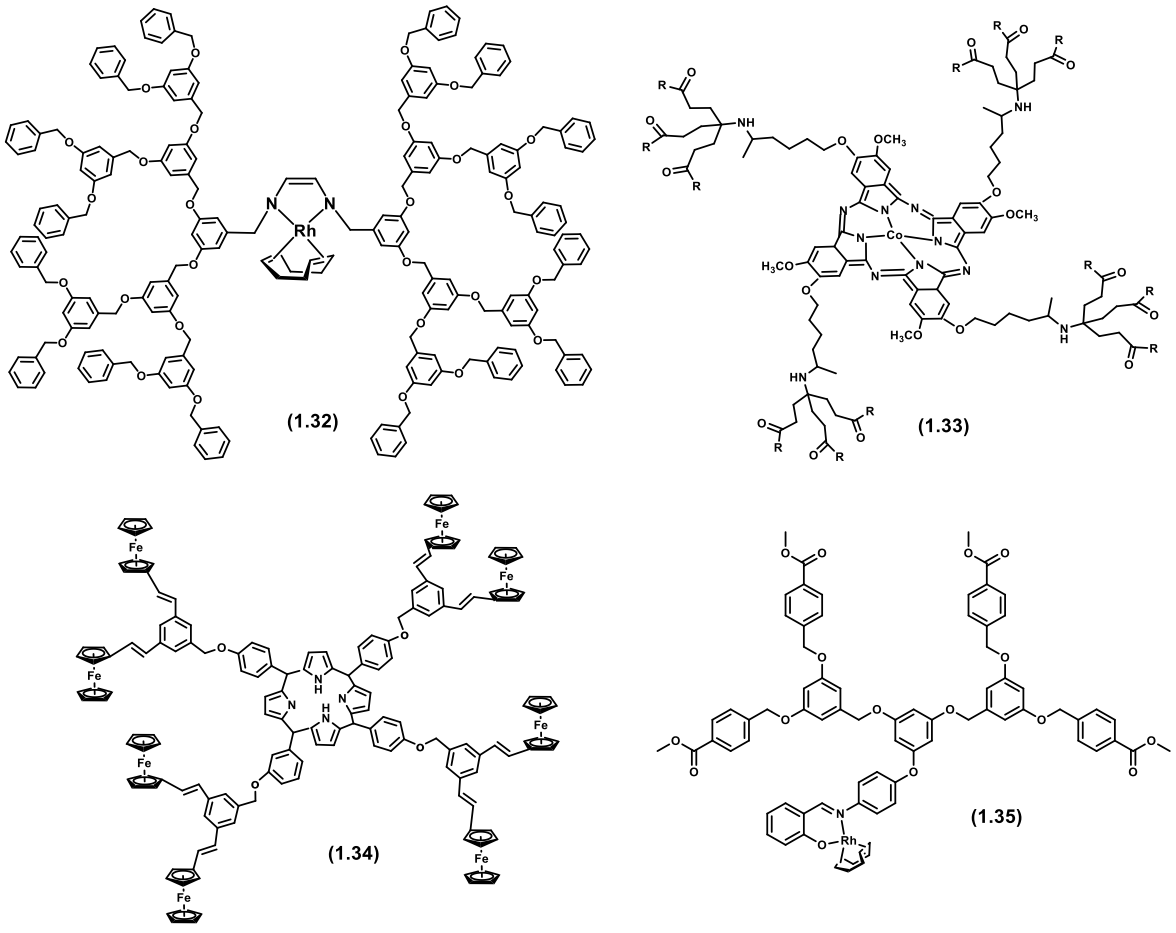


**Figure 1.23** Examples of functionalised dendritic structures at the core, periphery and focal point.

The constructive placement of catalytic groups on a dendritic framework also plays an important role in the activity, selectivity and stability of a catalyst. For example, placing the catalytic site on the periphery of a dendrimer allows for improved activity because of the multi-site catalytic centre that is easily assessable for substrate interaction. On the other hand, placing the catalytic site within the confinement of a dendrimer, the catalyst may benefit from the steric and electronic interactions created by the microenvironment of the dendrimer. This improves the stability and selectivity of a catalyst in cases where steric constraints are believed to influence regioselectivity.

The seminal work of van Koten and co-workers in 1994 on the first application of metallodendrimers in catalytic reactions was based on polycarbosilane nickel(II) complexes for the Kharasch addition of polyhaloalkenes.[209] Their promising results led the way into subsequent investigations of metal containing dendrimers for the hydroformylation reaction. Notable examples are; van Leeuwen's carbosilane dendrimers,[210] Cole-Hamilton's silsesquioxanes-cored dendrimers (POSS)[211] and Smith's Rh(I)-metallodendrimers based on Schiff based ligands.[85,86,212]

#### 1.5.2.2 Metallodendrimers as recyclable catalyst precursors

The use of dendrimers as soluble supports in catalysis provides ways to separate and recycle catalysts. Dendrimers can be precipitated from the reaction media depending on the properties of the dendrimers.[203] The functional groups on the periphery of a dendrimer can be altered to induce solubility in a specific reaction media. As such, catalysts can be recovered by one of the biphasic strategies previously discussed in this chapter. Metallodendrimers can also be separated from the reaction media using nanofiltration techniques. This relies on the difference in molecular weight between a simple organic molecule and a dendritic compound. With this, sufficiently high molecular weight dendrimers can be separated from low molecular weight products with the possibility of reusing the dendritic metal catalyst as depicted in Figure 1.24.[192,213]

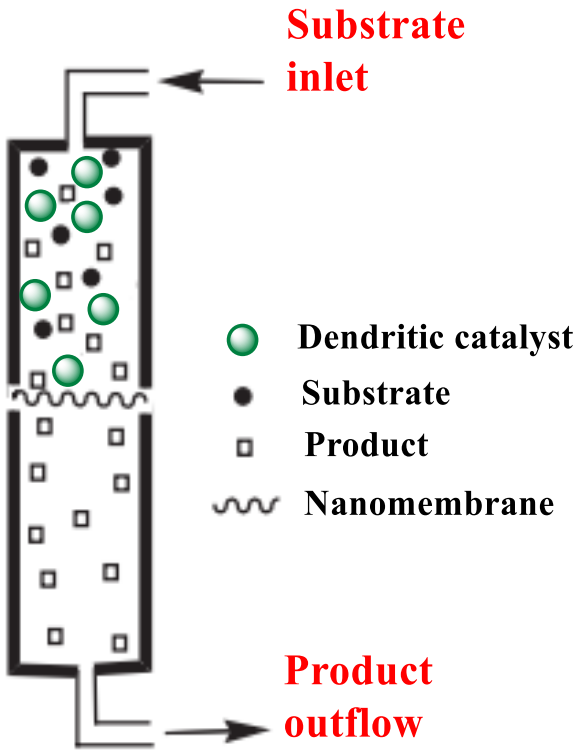


**Figure 1.24** A schematic representation of a nanomembrane reactor system.[203]

Membrane filtration can be performed batch wise or in a continuous-flow membrane reactor (CFMR).[191] The latter offers accurate control of the reactant concentration and reaction time, especially in situations where the product can react further with the catalytically active species to produce unwanted side products.[203]

Examples of dendrimers, their use in hydroformylation, and separation *via* nano or membrane filtration has been described in the literature.[192,214,215] More recently, Siangwata *et al.* corroborated the feasibility of recovering and reusing dendritic metal complexes *via* nanofiltration technique.[216] Therein, the catalytic activity and recyclability of Rh(I)-salicylaldimine-triazole-based trinuclear and mononuclear complexes were studied in detail. The complexes were applied as precatalysts in the hydroformylation of 1-octene, 7-tetradecene and 4-octene. In general, the multinuclear complex gave better activity and could be recycled for at least 5 times with sustained catalytic activity throughout the cycles. The amounts of metal leaching into the permeate were determined by ICP-AES analysis and no detectable levels of rhodium was observed, thus indicating sufficiently strong ligand–metal interaction.

## 1.6 Research justification

The demand for greener chemical processes has led to an increase in the research and development of novel recyclable homogeneous catalytic systems. The use of water for catalytic reactions is an excellent sustainable solvent alternative. However, the high polarity of water restricts the solubility of a typical metal-based catalyst in an aqueous media, this results to low catalytic activity. Therefore, designing suitable electron-rich donor ligands with sufficient hydrophilic functionalities that represses the catalytically active metal species in the aqueous phase is pivotal in enabling the aqueous biphasic recovery approach to be effective. This could combat the challenge of mass transfer limitations encountered in the aqueous hydroformylation of long-chain olefins (1-octene) due to their poor water-solubility. Also, the presences of more than one metal centre in a hydrophilic catalyst may lead to improved catalyst performance.

The unique features of dendrimers such as the high concentration of peripheral end-groups, well-defined architecture, monodispersity and high molecular weight makes dendrimers well-suited as sterically demanding innovative scaffolds for the development of selective and potentially recoverable (environmentally viable) hydroformylation catalysts for long chain olefins and vinylarenes (1-octene and styrene). Longer chain carbons (>C8, Flory-Schulz carbon chain spectrum) and vinylarenes are highly desired as these are predominantly used in cosmetic, plasticiser and detergent streams. This study is in line with the Green Chemistry principles and forms part of the foci of the RSA Olefins Thrust of the Centre of Excellence in Catalysis.

## 1.7 Aim and specific objectives

### 1.7.1 Overall aim

In view of the above, the overall aim of this project is to synthesise and characterize water-soluble mononuclear complexes, binuclear Rh(I) complex, dendrimer-supported Rh(I) complexes and to evaluate their efficiency as catalyst precursors in the hydroformylation of olefins.

### 1.7.2 Specific objectives

The specific objectives of this thesis were:

1. To synthesise and characterize water-soluble and non-water-soluble alpha-diimine ligands.

2. To synthesise and characterize water-soluble and non-water-soluble alpha-diimine Rh(I) complexes.

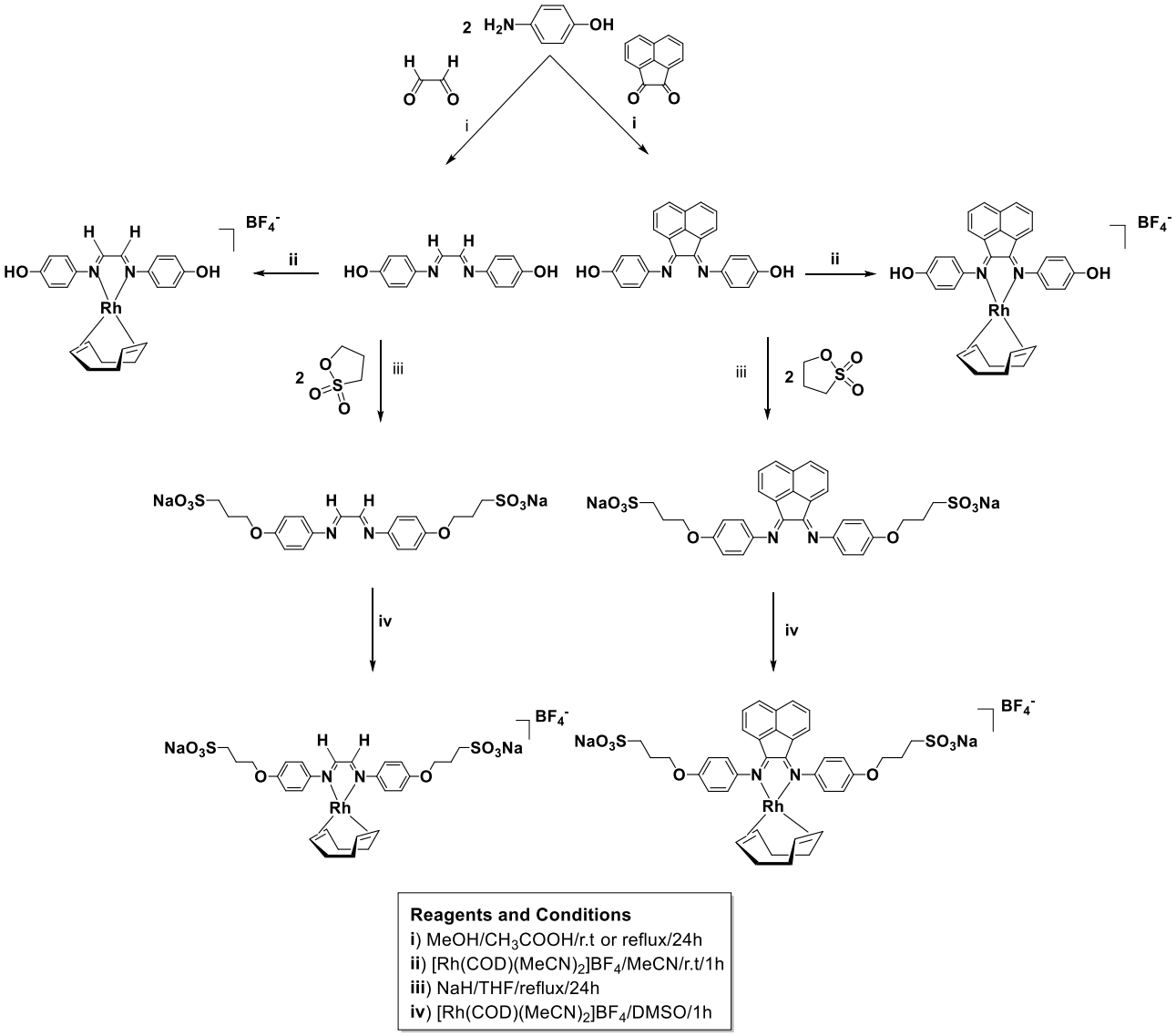


3. To evaluate and compare the water-soluble and non-water-soluble alpha-diimine Rh(I) complexes in the aqueous biphasic hydroformylation of 1-octene.

4. To synthesise and characterize first and second generation Frechet-type dendrons and alpha-diimine-cored aryl ether dendrimers.

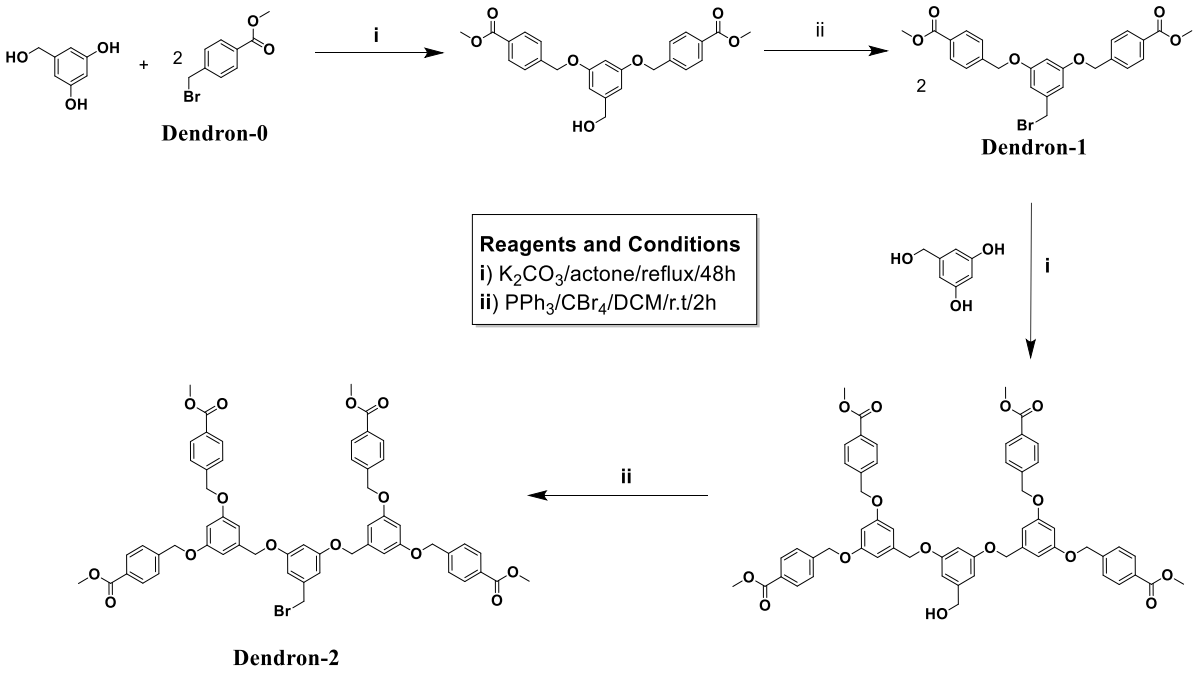


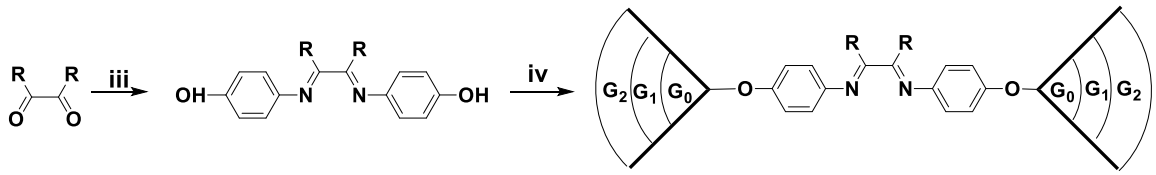


**Reagents and Conditions**
**iii**) 4-aminophenol/MeOH/$CH_3COOH$/reflux/24h
**iv**) Dendron-n/$K_2CO_3$/Acetone/reflux/48h

**R = H or $C_{10}H_8$**

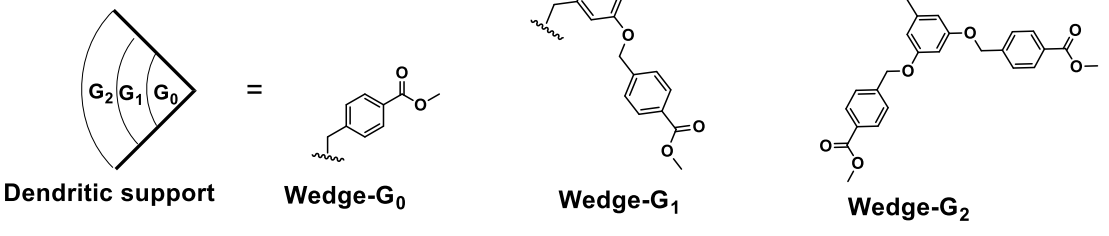

5. To synthesise and characterize Rh(I) alpha-diimine-cored aryl ether metallodendrimers.

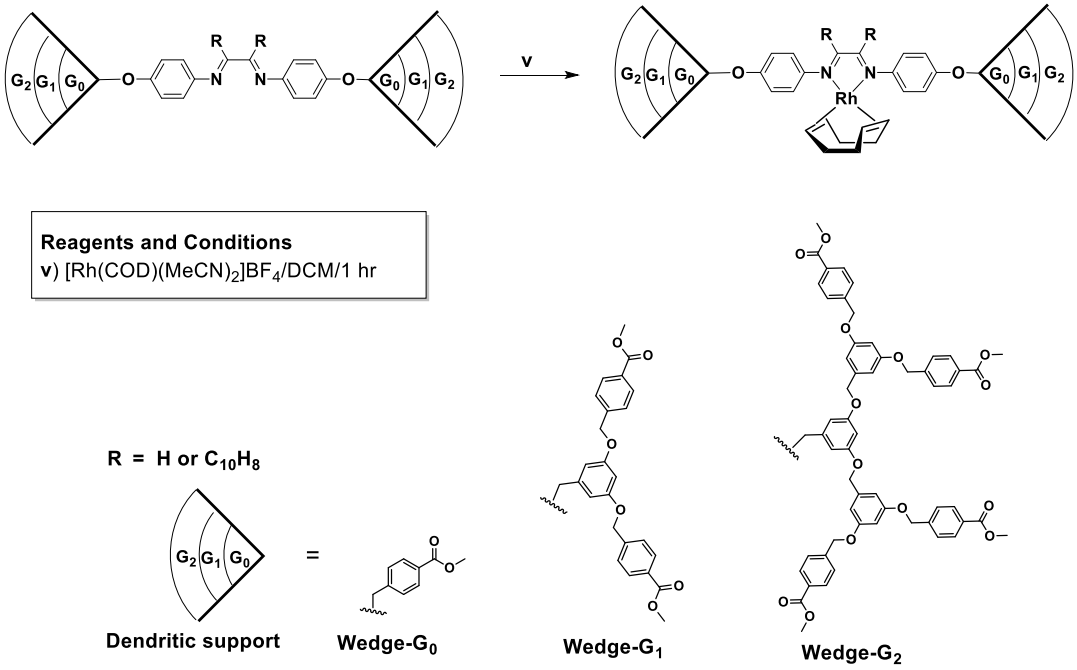


6. To evaluate the metallodendrimers as precatalysts in the hydroformylation of 1-octene and styrene.

7. To synthesise and characterize a water-soluble binuclear tetrasulfonated tetraimine Rh(I) complex.

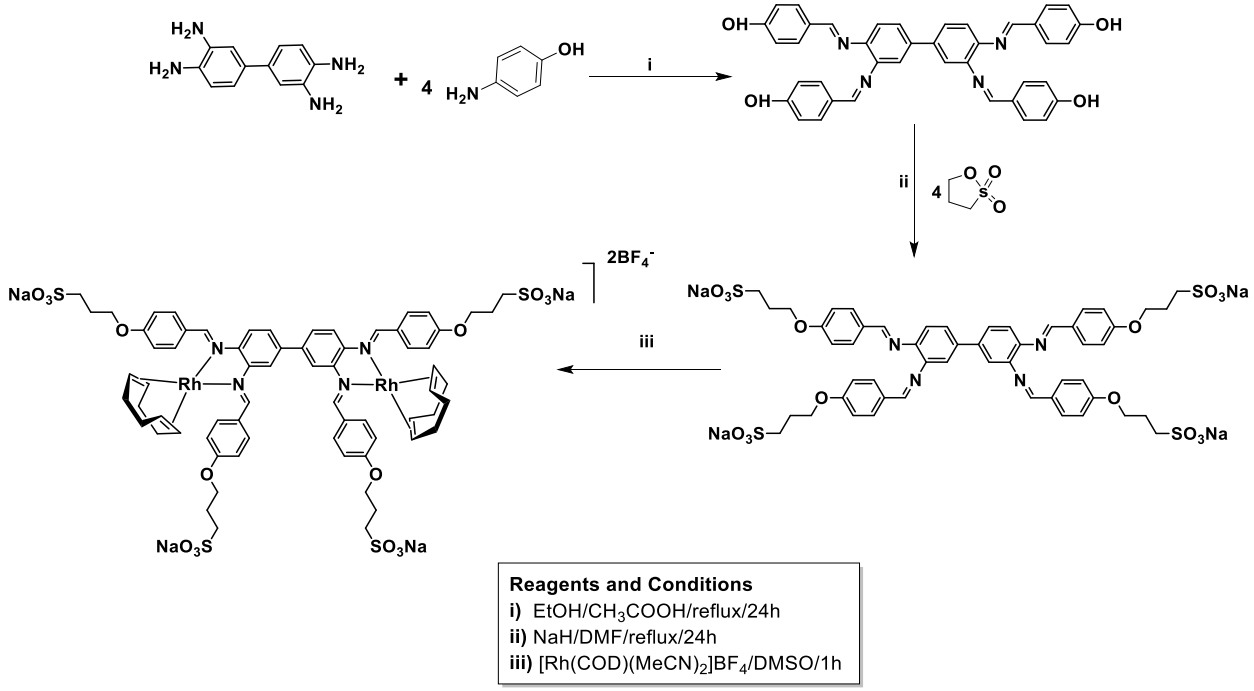

8. To synthesise and characterize a water-soluble mononuclear disulfonated diimine Rh(I) complex.

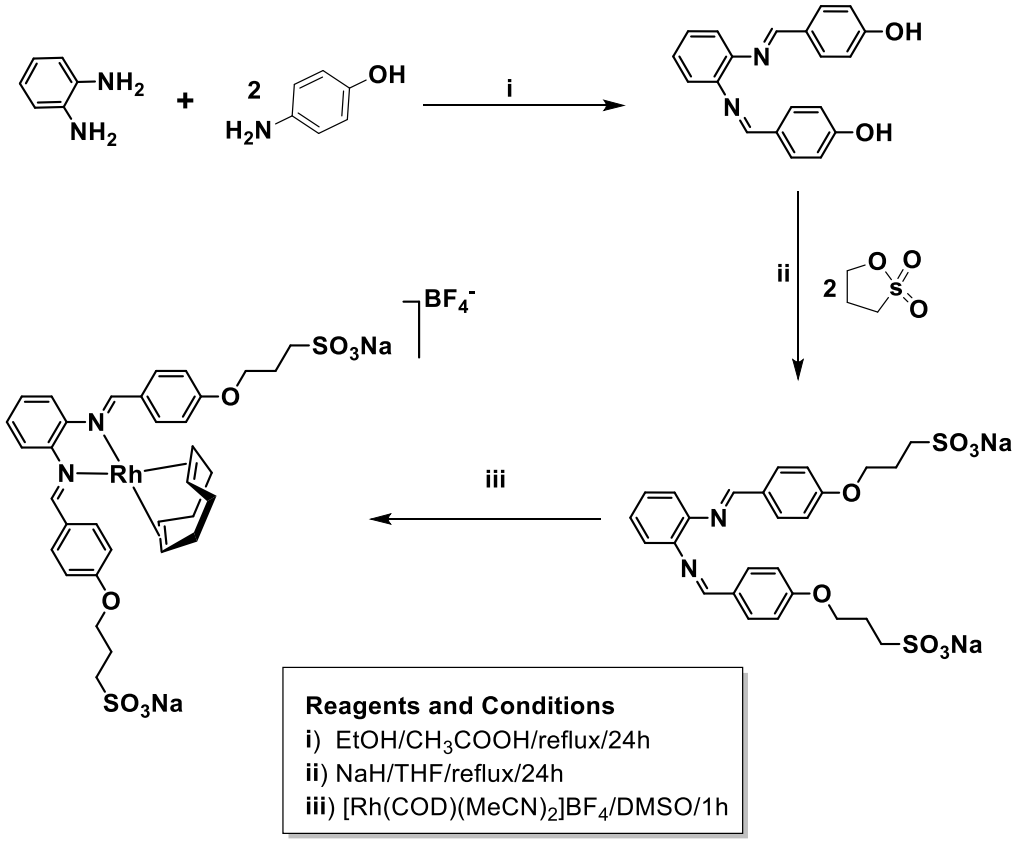


9. To evaluate and compare the efficiency of the water-soluble mono- and binuclear Rh(I) complexes in the aqueous biphasic hydroformylation of 1-octene.

## 1.8 References


1 H. Mohajan, *J. Soc. Sci. Humanit.*, 2019, **5**, 377–387.

2 M. Fasciotti, *Sustain. Chem. Pharm.*, 2017, **6**, 682–689.

3 R. Luque, *Green chemistry*, Nova Science Publishers Inc, 2012.

4 B. A. de Marco, B. S. Rechelo, E. G. Tótoli, A. C. Kogawa and H. R. N. Salgado, *Saudi Pharm. J.*, 2019, **27**, 1–8.

5 S. E. Manahan, *Green Chemistry and the ten Commandments of Sustainability*, ChemChar Research, Columbia, Missouri U.S.A., 2nd edn., 2006.

6 P. T. Anastas and J. C. Warner, *Green Chemistry: Theory and Practice*, Oxford University Press, New York, 1998.

7 R. A. Sheldon, *Chem. Soc. Rev.*, 2012, **41**, 1437–1451.

8 R. A. Sheldon, *J. R. Soc. interface*, 2016, **13**, 1–7.

9 S. K. Sharma and H. Demir, in *Green Chemistry in Scientific Literature: A Bibliometric Study and Research Trends*, CRC Press, Boca Raton, 2019.

10 S. Armenta, S. Garrigues, F. A. Esteve-Turrillas and M. de la Guardia, *TrAC - Trends Anal. Chem.*, 2019, **116**, 248–253.

11 J. García-Serna, L. Pérez-Barrigón and M. J. Cocero, *Chem. Eng. J.*, 2007, **133**, 7–30.

12 J. H. Clark, R. Luque and A. S. Matharu, *Annu. Rev. Chem. Biomol. Eng.*, 2012, **3**, 183–207.

13 C. Hu, C. Lv, S. Liu, Y. Shi, J. Song, Z. Zhang, J. Cai and A. Watanabe, *Catalysts*, 2020, **10**, 188.

14 M. Zhang, X. Xiao, Y. Wu, Y. An, L. Xu and C. Wan, *Catalysts*, 2019, **9**, 1009.

15 S. Wacławek, V. V. T. Padil and M. Černík, *Ecol. Chem. Eng. S*, 2018, **25**, 9–34.

16 P. T. Anastas, M. M. Kirchhoff and T. C. Williamson, *Appl. Catal. A Gen.*, 2001, **221**, 3–13.

17 I. Chorkendorff and J. W. Niemantsverdriet, *Concepts of Modern Catalysis and Kinetics*, Wiley-VCH Verlag GmbH & Co. KGaA, Weinheim, 2nd edn., 2007.

18 J. R. Ludwig, C. S. Schindler and J. R. Ludwig, *Chem*, 2017, **2**, 313–316.

19 Catalyst Market Size, Share and Trends Analysis Report by Raw Material, https://www.grandviewresearch.com/industry-analysis/catalyst-market, (accessed 21 September 2020).

20 Z. Ma and F. Zaera, *Heterogeneous Catalysis by Metals*, John Wiley & Sons, Ltd., 2006.

21 Q. L. Zhou, *Angew. Chem. Int. Ed.*, 2016, **55**, 5352–5353.

22 R. V. Chaudhari, in *Industrial Catalytic Processes for Fine and Specialty Chemicals*,

Elsevier Inc., 2016, pp. 17–39.

23 E. Farnetti, R. Di Monte and J. Kašpar, in *Inorganic and Bio-inorganic Chemistry: Homogeneous and Heterogeneous Catalysis*, EOLSS Publishers, Paris, 2009, vol. 2.

24 J. N. Armor, *Catal. Today*, 2011, **163**, 3–9.

25 D. Sanfilippo, in *Catalytic Industrial Processes*, EOLSS Publishers, Paris, 2009.

26 O. Deutschmann, H. Knözinger, K. Kochloefl and T. Turek, in *Heterogeneous Catalysis and Solid Catalysts*, Wiley-VCH Verlag GmbH & Co. KGaA, 2011, pp. 54–59.

27 J. Heveling, *J. Chem. Educ.*, 2012, **89**, 1530–1536.

28 J. C. Védrine, *Catalysts*, 2017, **7**, 341–366.

29 I. Horiuti and M. Polanyi, *Trans. Faraday Soc.*, 1934, **30**, 1164–1172.

30 J. A. Dumesic, G. W. Huber and M. Boudart, in *Principles of Heterogeneous Catalysis*, Wiley-VCH Verlag GmbH & Co., 2008, pp. 1–7.

31 J. K. Norsko, *Reports Prog. Phys.*, 1990, **53**, 1–10.

32 W. M. H. S. and N. H. de Boer, *J. Phys. Chem.*, 1960, **64**, 1579–1580.

33 C. Copéret, M. Chabanas, R. Petroff Saint-Arroman and J. M. Basset, *Angew. Chem. Int. Ed.*, 2003, **42**, 156–181.

34 P. Munnik, P. E. De Jongh and K. P. De Jong, *Chem. Rev.*, 2015, **115**, 6687–6718.

35 J. Pritchard, G. A. Filonenko, R. Van Putten, E. J. M. Hensen and E. A. Pidko, *Chem. Soc. Rev.*, 2015, **44**, 3808–3833.

36 P. W. N. M. van Leeuwen, *Homogeneous catalysis: understanding the art*, Kluwer Academic Publishers, Dordrecht, 2004.

37 C. J. Paul Kamer, N. H. Joost Reek and P. W. N. M. van Leeuwen, in *Mechanisms in Homogeneous Catalysis*, ed. B. Heaton, Wiley-VCH Verlag GmbH & Co. KGaA, 2005.

38 R. V. Chaudhari, *Curr. Opin. Drug Discov. Dev.*, 2008, **11**, 820–828.

39 X. Li, L. Zhang, S. Wang and Y. Wu, *Front. Chem.*, 2020, **7**, 948–1015.

40 S. Ranga, *Int. J. Eng. Technol. Sci. Res.*, 2017, **4**, 1496–1500.

41 X. Cui, W. Li, P. Ryabchuk, K. Junge and M. Beller, *Nat. Catal.*, 2018, **1**, 385–397.

42 R. Franke, D. Selent and A. Börner, *Chem. Rev.*, 2012, **112**, 5675–5732.

43 B. Cornils, W. A. Herrmann and M. Rasch, *Angew. Chem. Int. Ed.*, 1994, **33**, 2144–2163.

44 G. D. Frey, *J. Organomet. Chem.*, 2014, **754**, 5–7.

45 K. Dong, X. Fang, R. Jackstell and M. Beller, *Chem. Commun.*, 2015, **51**, 2015.

46 Y. li Liu, J. gui Zhao, Y. jiang Zhao, H. M. Liu, H. yan Fu, X. li Zheng, M. lin Yuan, R. xiang Li and H. Chen, *RSC Adv.*, 2019, **9**, 7382–7387.

47 S. K. Ritter, *Chem. Eng. News Arch.*, 2013, 91, 38–40.

48 A. Börner and R. Franke, *Hydroformylations: Fundamentals, Processes and Applications in Organic Synthesis*, Wiley-VCH, Weinheim, 2016.

49 R. Tudor and M. Ashley, *Platin. Met. Rev.*, 2007, **51**, 115–162.

50 J. Hagen, in *Industrial catalysis: A practical approach*, Wiley-VCH, Weinheim, 2015, pp. 59–67.

51 D. Evans, J. A. Osborn and G. Wilkinson, *J. Chem. Soc. A Inorganic, Phys. Theor.*, 1968, 3133–3142.

52 W. R. Moser, C. J. Papile, D. A. Brannon, R. A. Duwell and S. J. Weininger, *J. Mol. Catal.*, 1987, **41**, 271–292.

53 S. Shylesh, D. Hanna, A. Mlinar, X. Q. Kŏng, J. A. Reimer and A. T. Bell, *ACS Catal.*, 2013, **3**, 348–357.

54 A. Jörke, T. Gaide, A. Behr, A. Vorholt, A. Seidel-Morgenstern and C. Hamel, *Chem. Eng. J.*, 2017, **313**, 382–397.

55 J. M. Dreimann, E. Kohls, H. F. W. Warmeling, M. Stein, L. F. Guo, M. Garland, T. N. Dinh and A. J. Vorholt, *ACS Catal.*, 2019, **9**, 4308–4319.

56 M. Vilches-Herrera, L. Domke and A. Börner, *ACS Catal.*, 2014, **4**, 1706–1724.

57 S. Hanf, L. A. Rupflin, R. Gläser and S. A. Schunk, *Catalysts*, 2020, **10**, 510–546.

58 N. Fey, A. G. Orpen and J. N. Harvey, *Coord. Chem. Rev.*, 2009, **253**, 704–722.

59 W. Strohmeier and F. J. Müller, *Chem. Ber.*, 1967, **100**, 2812–2821.

60 W. D. Horrocks and R. C. Taylor, *Inorg. Chem.*, 1963, **2**, 732–737.

61 S. C. Van der Slot, J. Duran, J. Luten, P. C. J. Kamer and P. W. N. M. Van Leeuwen, *Organometallics*, 2002, **21**, 3873–3883.

62 M. Sparta, K. J. Børve and V. R. Jensen, *J. Am. Chem. Soc.*, 2007, **129**, 8487–8499.

63 T. L. Brown and K. J. Lee, *Coord. Chem. Rev.*, 1993, **128**, 89–116.

64 L. Gonsalvi, A. Guerriero, E. Monflier, F. Hapiot and M. Peruzzini, *Top. Curr. Chem.*, 2013, **342**, 1–48.

65 P. W. N. M. Van Leeuwen, P. C. J. Kamer, J. N. H. Reek and P. Dierkes, *Chem. Rev.*, 2000, **100**, 2741–2769.

66 Y. Koide, S. G. Bott and A. R. Barron, *Organometallics*, 1996, **15**, 2213–2226.

67 J. A. Casey, C. P. Whiteker, G. T. Melville, M. G. Petrovich, L. M. Gavey and D. R. Powell, *J. Am. Chem. Soc*, 1992, **114**, 5535.

68 P. D. Achord, P. Kiprof and B. Barker, *J. Mol. Struct. Theochem*, 2008, **849**, 103–111.

69 M. Kumar, R. V. Chaudhari, B. Subramaniam and T. A. Jackson, *Organometallics*, 2014, **33**, 4183–4191.

70 R. P. Dias, M. S. L. Prates, W. B. De Almeida and W. R. Rocha, *Int. J. Quantum Chem.*, 2011, **111**, 1280–1292.

71 S. A. Decker and T. R. Cundari, *New J. Chem.*, 2002, **26**, 129–135.

72 E. Daura-Oller, J. M. Poblet and C. Bo, *Dalton. Trans.*, 2003, **1**, 92–98.

73 W. J. Reppe, W. Schweckendiek, *Justus Liebigs Ann. Chem.*, 1948, **560**, 140–116.

74 Triphenylphosphine, https://en.wikipedia.org/wiki/Triphenylphosphine, (accessed 10 October 2020).

75 B. Zhang, H. Jiao, D. Michalik, S. Kloß, L. M. Deter, D. Selent, A. Spannenberg, R. Franke and A. Börner, *ACS Catal.*, 2016, **6**, 7554–7565.

76 L. C. Matsinha, S. Siangwata, G. S. Smith and B. C. E. Makhubela, *Catal. Rev. Sci.*

*Eng.*, 2019, **61**, 111–133.

77 F. Zhou, L. Zhang, Q. Wu, F. Guo, S. Tang, B. Xu, M. Yuan, H. Fu, R. Li, X. Zheng and H. Chen, *Appl. Organomet. Chem.*, 2018, **33**, 4646.

78 B. Stewart, A. Harriman and L. J. Higham, *Organometallics*, 2011, **30**, 5338–5343.

79 W. Gil and A. M. Trzeciak, *Coord. Chem. Rev.*, 2011, **255**, 473–483.

80 T. Mashabane, G. K. Ramollo, G. Kleinhans, S. De Doncker, S. Siangwata, M. A. Fernandes, A. Lemmerer, G. S. Smith and D. I. Bezuidenhout, *J. Organomet. Chem.*, 2020, **920**, 121341.

81 L. Maqeda, B. C. E. Makhubela and G. S. Smith, *Polyhedron*, 2015, **91**, 128–135.

82 S. Siangwata, N. Baartzes, B. C. E. Makhubela and G. S. Smith, *J. Organomet. Chem.*, 2015, **796**, 26–32.

83 L. C. Matsinha, S. F. Mapolie and G. S. Smith, *Dalton. Trans.*, 2015, **3**, 1240–1248.

84 E. B. Hager, B. C. E. Makhubela and G. S. Smith, *Dalton. Trans.*, 2012, **41**, 13927.

85 C. Williams, M. Ferreira, E. Monflier, S. Mapolie and G. S. Smith, *Dalton. Trans.*, 2018, **47**, 9418–9429.

86 B. C. E. Makhubela, A. M. Jardine, G. Westman and G. S. Smith, *Dalton. Trans.*, 2012, **41**, 10715.

87 D. S. Afrin, A. B. Farhana, H. B. Md Saddam, K. M. Nuruzzaman, B. Kudrat-E-Zahan and A. B. Md Mahasin, *Int. J. Chem. Stud.*, 2018, **6**, 2859–2866.

88 C. R. M. Rao and G. S. Reddi, *TrAC- Trends Anal. Chem.*, 2000, **19**, 565–586.

89 W. Keim, *Green Chem.*, 2003, **5**, 105–111.

90 E. A. Karakhanov and A. L. Maksimov, *Russ. J. Gen. Chem.*, 2009, **52**, 125–135.

91 A. Vioux, L. Viau, S. Volland and J. Le Bideau, *Comptes Rendus Chim.*, 2010, **13**, 242–255.

92 T. Welton, *Biophys. Rev.*, 2018, **10**, 691–706.

93 M. Haumann and A. Riisager, *Chem. Rev.*, 2008, **108**, 1474–1497.

94 V. I. Pârvulescu and C. Hardacre, *Chem. Rev.*, 2007, **107**, 2615−2665.

95 Y. Qiao and A. D. Headley, *Catalysts*, 2013, **3**, 709–725.

96 Y. Chauvin, L. Mussmann and H. Olivier, *Angew. Chem. Int. Ed.*, 1996, **34**, 2698–2700.

97 F. Favre, H. Olivier-Bourbigou, D. Commereuc and L. Saussine, *Chem. Commun.*, 2001, **15**, 1360–1361.

98 P. Wasserscheid, H. Waffenschmidt, P. Machnitzki, K. W. Kottsieper and O. Stelzer, *Chem. Commun.*, 2001, **5**, 451–452.

99 M. J. Muldoon, *Dalton. Trans.*, 2010, **39**, 337–348.

100 X. Jin, J. Feng, H. Song, J. Yao, Q. Ma, M. Zhang, C. Yu, S. Li and S. Yu, *Green Chem.*, 2019, **21**, 3583–3596.

101 X. Jin, J. Feng, Q. Ma, H. Song, Q. Liu, B. Xu, M. Zhang, S. Li and S. Yu, *Green Chem.*, 2019, **21**, 3267–3275.

102 I. T. Horváth and J. Rábai, *Science*, 1994, **266**, 72–75.

103 R. H. Fish, *Chem. Eur. J.*, 1999, **5**, 1677–1680.

104 D. F. Foster, D. Gudmunsen, D. J. Adams, A. M. Stuart, E. G. Hope, D. J. Cole-Hamilton, G. P. Schwarz and P. Pogorzelec, *Tetrahedron*, 2002, **58**, 3901–3910.

105 M. Houde, J. W. Martin, R. J. Letcher, K. R. Solomon and D. C. G. Muir, *Environ. Sci. Technol.*, 2006, **40**, 3463–3473.

106 A. P. Dobbs and M. R. Kimberley, *J. Fluor. Chem.*, 2002, **118**, 3–17.

107 P. G. Jessop, T. Ikariya and R. Noyori, *Chem. Rev.*, 1999, **99**, 475–494.

108 J. Fang, H. Jin, T. Ruddy, K. Pennybaker, D. Fahey and B. Subramaniam, *Ind. Eng. Chem. Res.*, 2007, **46**, 8687–8692.

109 A. Murielle F. Sellin, A. Ingrid Bach, B. Jeremy M. Webster, C. Francisco Montilla, C. Vitor Rosa, C. Teresa Avilés, M. Poliakoffb and and D. J. Cole-Hamilton, *Dalton. Trans.*, 2002, **24**, 4569–4579.

110 J. D. Grunwaldt, R. Wandeler and A. Baiker, *Catal. Rev. Sci. Eng.*, 2007, **45**, 1–96.

111 T. R. Rathke, J. W. Klingler, R. J. Krause, *Organometallics*, 1991, **10**, 1350–1355.

112 I. Bach and D. J. Cole-Hamilton, *Chem. Commun.*, 1998, **14**, 1463–1464.

113 L. A. Blanchard, D. Hancu, E. J. Beckman and J. F. Brennecke, *Nature*, 1999, **399**, 28–29.

114 L. A. Blanchard, Z. Gu and J. F. Brennecke, *J. Phys. Chem. B*, 2001, **105**, 2437–2444.

115 B. . Mellein and J. . Brennecke, *J. Phys. Chem.*, 2007, **111**, 4837–4843.

116 S. P. Kelley, L. A. Flores, M. S. Shannon, J. E. Bara and R. D. Rogers, *Chem. Eur. J.*, 2017, **23**, 14332–14337.

117 D. J. Cole-Hamilton, *Science*, 2003, **299**, 1702–1706.

118 M. F. Sellin, P. B. Webb and D. J. Cole-Hamilton, *Chem. Commun.*, 2001, **8**, 781–782.

119 Z. Hou, B. Han, L. Gao, T. Jiang, Z. Liu, Y. Chang, X. Zhang and J. He, *New J. Chem.*, 2002, **26**, 1246–1248.

120 R. Liu, P. Zhang, S. Zhang, T. Yan, J. Xin and Z. Xiangping, *Rev. Chem. Eng.*, 2016, **32**, 1–23.

121 R. A. Brown, P. Pollet, E. McKoon, C. A. Eckert, C. L. Liotta and P. G. Jessop, *J. Am. Chem. Soc.*, 2001, **123**, 1254–1255.

122 A. Bösmann, G. Franciò, E. Janssen, M. Solinas, W. Leitner and P. Wasserscheid, *Angew. Chem. Int. Ed.*, 2001, **40**, 2697–2699.

123 A. B. Paninho, A. L. R. Ventura, L. C. Branco, A. J. L. Pombeiro, M. Guedes daSilva, M. F. C. Nunes da Ponte, K. T. Mahmudov and A. V. M. Nunes, *J. Supercrit. Fluids*, 2018, **132**, 71–75.

124 D. J. Heldebrant and P. G. Jessop, *J. Am. Chem. Soc.*, 2003, **125**, 5600–5601.

125 D. Koch and W. Leitner, *J. Am. Chem. Soc.*, 1998, **120**, 13398–13404.

126 J. Bianga, K. U. Künnemann, T. Gaide, A. J. Vorholt, T. Seidensticker, J. M. Dreimann and D. Vogt, *Chem. Eur. J.*, 2019.

127 A. Behr, G. Henze, L. Johnen and C. Awungacha, *J. Mol. Catal. A Chem.*, 2008, **285**, 20–28.

128 Y. Brunsch and A. Behr, *Angew. Chem. Int. Ed.*, 2013, **52**, 1586–1589.

129 A. Behr, L. Johnen and A. J. Vorholt, *ChemCatChem*, 2010, **2**, 1271–1277.

130 T. Gaide, J. M. Dreimann, A. Behr and A. J. Vorholt, *Angew. Chem. Int. Ed.*, 2016, **55**, 2924–2928.

131 A. Behr, G. Henze, O. Dietmar and B. Turkowski, *Green Chem.*, 2005, **7**, 645–649.

132 K. McBride, T. Gaide, A. Vorholt, A. Behr and K. Sundmacher, *Chem. Eng. Process. Process Intensif.*, 2015, **99**, 97–106.

133 J. M. Dreimann, H. Warmeling, J. N. Weimann, K. Künnemann, A. Behr and A. J. Vorholt, *AIChE J.*, 2016, **62**, 4377–4383.

134 J. Herwig and R. Fischer, in *Rhodium Catalyzed Hydroformylation*, Kluwer Academic Publishers, Dordrecht, 2000, pp. 189–202.

135 W. A. Herrmann and C. W. Kohlpaintner, *Angew. Chem. Int. Ed.*, 1993, **32**, 1524–1544.

136 S. Desset and D. J. Cole-Hamilton, *Angew. Chem. Int. Ed.*, 2009, **48**, 1472–1474.

137 S. Ahrland, J. Chatt, N. R. Davies and A. A. Williams, *J. Chem. Soc.*, 1958, **1**, 276–288.

138 P. J. Dyson, D. J. Ellis and T. Welton, *Platin. Met. Rev.*, 1998, **42**, 135–140.

139 R. V. Chaudhari, A. Bhattacharya and B. M. Bhanage, *Catal. Today*, 1995, **24**, 123–133.

140 F. Joó, in *Encyclopedia of Catalysis*, John Wiley & Sons, Inc., 2010, pp. 1–84.

141 C. W. Kohlpaintner, R. W. Fischer and B. Cornils, *Appl. Catal. A Gen.*, 2001, **221**, 219–225.

142 L. Gonsalvi, *Catalysts*, 2018, **8**, 543–552.

143 A. H. G. Cents, D. W. F. Brilman and G. F. Versteeg, *Ind. Eng. Chem. Res.*, 2004, **43**, 7465–7475.

144 R. M. Deshpande, H. Purwanto, R. Delmas and V. Chaudhari, *J. Mol. Catal. A Chem.*, 1997, **126**, 133–140.

145 B. Cornils, *Org. Process Res. Dev.*, 1998, **2**, 121–127.

146 F. Monteil, R. Queau and P. Kalck, *J. Organomet. Chem.*, 1994, **480**, 177–184.

147 N. Herrmann, J. Bianga, T. Gaide, M. Drewing, D. Vogt and T. Seidensticker, *Green Chem.*, 2019, **21**, 6738–6745.

148 D. Nikunj and J. Tejas, *Int. J. Appl. Chem.*, 2017, **13**, 663-672.

149 S. Polarz, M. Kunkel, A. Donner and M. Schlötter, *Chem. Eur. J.*, 2018, **24**, 18842.

150 T. Pogrzeba, M. Illner, M. Schmidt, N. Milojevic, E. Esche, J. U. Repke and R. Schomäcker, *Ind. Eng. Chem. Res.*, 2019, **58**, 4443–4453.

151 D. C. Cullum, in *Introduction to Surfactant Analysis*, Springer, Dordrecht, 1994, pp. 17–41.

152 E. Valls, A. Solsona, J. Suades, R. Mathieu, F. Comelles and C. López-Iglesias, *Organometallics*, 2002, **21**, 2473–2480.

153 T. Pogrzeba, M. Schmidt, N. Milojevic, C. Urban, M. Illner, J. U. Repke and R. Schomäcker, *Ind. Eng. Chem. Res.*, 2017, **56**, 9934–9941.

154 G. La Sorella, G. Strukul and A. Scarso, *Green Chem.*, 2015, **17**, 644–683.

155 T. Lorenzetto, G. Berton, F. Fabris and A. Scarsoa, *Catal. Sci. Technol.*, 2020, **10**, 4492–4502.

156 A. Donner, B. Trepka, S. Theiss, F. Immler, J. Traber and S. Polarz, *Langmuir*, 2019, **35**, 16514–16520.

157 F. Topuz and T. Uyar, *Pharmaceutics*, 2019, **11**, 6–41.

158 L. Leclercq, F. Hapiot, S. Tilloy, K. Ramkisoensing, J. N. H. Reek, P. W. N. M. Van Leeuwen and E. Monflier, *Organometallics*, 2005, **24**, 2070–2075.

159 T. Mathivet, C. Méliet, Y. Castanet, A. Mortreux, L. Caron, S. Tilloy and E. Monflier, *J. Mol. Catal. A Chem.*, 2001, **176**, 105–116.

160 A. Cocq, H. Bricout, F. Djedaïni-Pilard, S. Tilloy and E. Monflier, *Catalysts*, 2020, **10**, 56.

161 F. Hapiot, S. Menuel, M. Ferreira, B. Léger, H. Bricout, S. Tilloy and E. Monflier, *ACS Sustain. Chem. Eng.*, 2017, **5**, 3598–3606.

162 M. Elard, J. Denis, M. Ferreira, H. Bricout, D. Landy, S. Tilloy and E. Monflier, *Catal. Today*, 2015, **247**, 47–54.

163 M. Dauchy, M. Ferreira, J. Leblond, H. Bricout, S. Tilloy, G. S. Smith and E. Monflier, *Pure Appl. Chem.*, 2018, **90**, 845–855.

164 S. S. Nurttila, P. R. Linnebank, T. Krachko and J. N. H. Reek, *ACS Catal.*, 2018, **8**, 3469–3488.

165 E. Monflier, S. Tilloy, G. Fremy, Y. Castanet and A. Mortreux, *Tetrahedron Lett.*, 1995, **36**, 9481–9484.

166 S. Siangwata, N. J. Goosen and G. S. Smith, *Appl. Catal. A Gen.*, 2020, **603**, 117736.

167 D. S. Ramarou, B. C. E. Makhubela and G. S. Smith, *Inorganica Chim. Acta*, 2019, **496**, 119051.

168 D. S. Ramarou, B. C. E. Makhubela and G. S. Smith, *J. Organomet. Chem.*, 2018, **870**, 23–31.

169 M. Raynal, P. Ballester, A. Vidal-Ferran and P. W. N. M. Van Leeuwen, *Chem. Soc. Rev.*, 2014, **43**, 1660–1733.

170 D. Ma, Y. Wang, A. Liu, S. Li, C. Lu and C. Chen, *Catalysts*, 2018, **8**, 404–410.

171 F. Quignard and A. Choplin, in *Comprehensive Coordination Chemistry II*, 2004, pp. 445–467.

172 C. M. Standfest-Hauser, T. Lummerstorfer, R. Schmid, H. Hoffmann, K. Kirchner, M. Puchberger, A. M. Trzeciak, E. Mieczyńska, W. Tylus and J. J. Ziółkowski, *J. Mol. Catal. A Chem.*, 2004, **210**, 179–187.

173 L. Huang, Y. He and S. Kawi, *J. Mol. Catal. A Chem.*, 2004, **265**, 247–257.

174 H. Zhao, J. Peng and M. Cai, *Catal. Letters*, 2012, **142**, 138–142.

175 B. C. E. Makhubela, A. Jardine and G. S. Smith, *Green Chem.*, 2012, **14**, 338–347.

176 D. Gorbunov, D. Safronova, Y. Kardasheva, A. Maximov, E. Rosenberg and E. Karakhanov, *ACS Appl. Mater. Interfaces*, 2018, **10**, 26566–26575.

177 M. A. Goni, E. Rosenberg, S. Meregude and G. Abbott, *J. Organomet. Chem.*, 2016, **807**, 1–10.

178 P. Li, W. Thitsartarn and S. Kawi, *Ind. Eng. Chem. Res.*, 2009, **48**, 1824–1830.

179 J. M. Andersen, *Platin. Met. Rev.*, 1997, **41**, 132–137.

180 R. Den Heeten, B. H. G. Swennenhuis, P. W. N. M. Van Leeuwen, J. G. De Vries and P. C. J. Kamer, *Angew. Chem. Int. Ed.*, 2008, **47**, 6602–6605.

181 S. I. Fujita, S. Akihara, S. Fujisawa and M. Arai, *J. Mol. Catal. A Chem.*, 2007, **268**, 244–250.

182 Q. Sun, Z. Dai, X. Liu, N. Sheng, F. Deng, X. Meng and F. S. Xiao, *J. Am. Chem. Soc.*, 2015, **137**, 5204–5209.

183 D. J. Macquarrie and J. J. E. Hardy, *Ind. Eng. Chem. Res.*, 2005, **44**, 8499–8520.

184 S. Shylesh, V. Schünemann and W. R. Thiel, *Angew. Chem. Int. Ed.*, 2010, **49**, 3428–3459.

185 J. F. Toczko, in *Comprehensive Chirality*, 2012, pp. 209–227.

186 A. G. Panda, P. J. Tambade, Y. P. Patil and B. M. Bhanage, *React. Kinet. Mech. Catal.*, 2010, **93**, 143–148.

187 A. G. Panda, M. D. Bhor, S. S. Ekbote and B. M. Bhanage, *Catal. Letters*, 2009, **131**, 649–655.

188 Z. J. Zheng Sun, Yanhua Wang, Mingming Niu, Huaiqiang Yi, Jingyang Jiang, *Catal. Commun.*, 2012, **27**, 78–82.

189 B. Bibouche, D. Peral, D. Stehl, V. Söderholm, R. Schomäcker, R. Von Klitzing and D. Vogt, *RSC Adv.*, 2018, **8**, 23332–23338.

190 D. Peral, D. Stehl, B. Bibouche, H. Yu, J. Mardoukh, R. Schomäcker, R. von Klitzing and D. Vogt, *J. Colloid Interface Sci.*, 2018, **513**, 638–646.

191 D. E. Bergbreiter, J. Tian and C. Hongfa, *Chem. Rev.*, 2009, **109**, 530–582.

192 R. Van Heerbeek, P. C. J. Kamer, P. W. N. M. van Leeuwen and J. N. H. Reek, *Chem. Rev.*, 2002, **102**, 3717–3756.

193 E. De Jesús and J. C. Flores, *Ind. Eng. Chem. Res.*, 2008, **47**, 7968–7981.

194 B. I. Voit and A. Lederer, *Chem. Rev.*, 2009, **109**, 5924–5973.

195 C. Gao and D. Yan, *Prog. Polym. Sci.*, 2004, **29**, 183–275.

196 S. S. Gillani, M. A. Munawar, K. M. Khan and J. A. Chaudhary, *J. Iran. Chem. Soc.*, 2020, **1**, 823–855.

197 D. A. Tomalia, H. Baker, J. Dewald, M. Hall, G. Kallos, S. Martin, J. Roeck, J. Ryder and P. Smith, *Polym. J.*, 1985, 17, 117–132.

198 E. Buhleier, W. Wehner and F. Vogtle, *Synthesis-stuttgart*, 1978, **1978**, 155–158.

199 M. Sowinska and Z. Urbanczyk-Lipkowska, *New J. Chem.*, 2014, **38**, 2168.

200 M. V. Walter and M. Malkoch, *Chem. Soc. Rev.*, 2012, **41**, 4593–4609.

201 C. J. Hawker and J. M. J. Frechet, *J. Am. Chem. Soc.*, 1990, **112**, 7638–7647.

202 M. M. and S. García-Gallego, in *Monographs in Supramolecular Chemistry*, Royal Society of Chemistry, 2020, pp. 1–20.

203 J. N. H. Reek, S. Arévalo, R. van Heerbeek, P. C. J. Kamer and P. W. N. M. van Leeuwen, *Adv. Catal.*, 2006, **49**, 71–151.

204 L. J. Twyman, A. S. H. King and I. K. Martin, *Chem. Soc. Rev.*, 2002, **31**, 69–82.

205 P. Govender, B. Therrien and G. S. Smith, *Eur. J. Inorg. Chem.*, 2012, 2853–2862.

206 T. Fujihara, Y. Obora, M. Tokunaga, H. Sato and Y. Tsuji, *Chem. Commun.*, 2005, **36**, 4526–4528.

207 M. Kimura, M. Kato, T. Muto, K. Hanabusa and H. Shirai, *Macromolecules*, 2000, **33**, 1117–1119.

208 A. S. Abd-el-aziz and E. A. Strohm, *Polymer (Guildf).*, 2012, **53**, 4879–4921.

209 J. W. J. Knapen, A. W. Van Der Made, J. C. De Wilde, P. W. N. M. Van Leeuwen, P. Wijkens, D. M. Grove and G. Van Koten, *Nature*, 1994, **372**, 659–663.

210 G. E. Oosterom, S. Steffens, J. Reek, P. Kamer and P. van Leeuwen, *Top. Catal.*, 2002, **19**, 61–73.

211 L. Ropartz, R. E. Morris, D. F. Foster and D. J. Cole-Hamilton, *Chem. Commun.*, 2001, **4**, 361–362.

212 N. C. Antonels, J. R. Moss and G. S. Smith, *J. Organomet. Chem.*, 2011, **696**, 2003–

2007.

213 S. Hwang, C. D. Shreiner, C. N. Moorefield and G. R. Newkome, *New J. Chem.*, 2007, **31**, 1192.

214 S. C. Bourque, F. Maltais, W. J. Xiao, O. Tardif, H. Alper, P. Arya and L. E. Manzer, *J. Am. Chem. Soc.*, 1999, **121**, 3035–3038.

215 J. N. H. Reek, D. de Groot, G. E. Oosterom, P. C. J. Kamer and P. W. N. M. van Leeuwen, *Comptes Rendus Chim.*, 2003, **6**, 1061–1077.

216 S. Siangwata, N. C. C. Breckwoldt, N. J. Goosen and G. S. Smith, *Appl. Catal. A Gen.*, 2019, **585**, 117–179

# Chapter 2

## Synthesis, characterization and application of disulfonated alpha-diimine Rh(I) complexes as aqueous biphasic hydroformylation catalyst precursors

This chapter has been published as: Water-soluble, disulfonated alpha-diimine Rh(I) complexes: synthesis, characterisation and application as catalyst precursors in the hydroformylation of 1-octene. **N. N. Omosun** and G. S. Smith. *European Journal of Inorganic Chemistry*, 2019, 2558-2564.

### 2.1 Introduction

Homogeneous catalytic systems exhibits superior performance over heterogeneous catalytic systems with respect to activity and selectivity, and it is known that the rhodium-catalyzed hydroformylation reaction proceeds favourably well in homogeneous systems under mild reaction conditions.[1–4] However, the challenges of the homogeneous catalysis is the difficulty of recovery and reuse of the expensive rhodium catalyst.[5–8]

A strategy that has been developed to address these challenges is the aqueous biphasic catalysis. It allows the feasibility of catalyst recovery and recycling by phase separation.[9,10] Therefore, the design of catalysts that are soluble in water is necessary to enable the aqueous biphasic strategy to be effective. The idea of introducing hydrophilic substituents into electron-rich ligands and their incorporation into organometallic complexes has proven to be a successful approach.[11–16] This strategy is in line with the Green Chemistry principles which promotes the design of environmentally friendly chemical processes.[17–19] An example of a well-established industrial application of the aqueous biphasic catalysis system is the Ruhrchemie/Rhône Poulenc oxo process which makes use of the water-soluble rhodium complex based on the triphenylphosphine trisulfonate (TPPTS) ligand.[20–22]

Despite the successful application of the commercialized TPPTS ligand over the years, major drawbacks of the rhodium-based TPPTS catalyst includes its instability in the presence of air/oxygen and the restricted use to only short chain olefins (<C4) due to mass transfer limitations of higher carbon chain alkenes across the interface.[23–25] These limitations has stimulated the research towards the development of new rhodium complexes based on other

water-soluble ligand systems that are air-stable and capable of being applied as catalyst precursors in the hydroformylation of longer chain olefins (>C5).

The N=C–C=N alpha-diimine (1, 4-diazabutadiene) ligand family are known to stabilize organometallic complexes.[30,31] Alpha-diimine ligands have been applied in catalytic transformations such as olefin polymerization,[32–34] cross-coupling reactions,[35,36] alcohol oxidation,[37] and oxidative carbonylation reactions.[38] However, the use of alpha-diimine ligands for the hydroformylation reaction has not been explored. The two interesting key features of these class of diimine compounds are: (i) the presence of two *exo* imines directly bonded to two alpha carbons which leads to better σ-donating and better π-accepting properties and (ii) the stereoelectronic effect of the substituents attached to the imine which has been reported to positively influence the kinetics and thermodynamics of migratory CO insertion in olefin polymerization reaction.[39–42] In this study, alpha-diimine ligands with *para* hydroxyl groups which allows for substitution with hydrophilic entities such as sulfonates at the focal point were used as ligand precursors in the synthesis of water-soluble rhodium complexes. In addition, introducing bulky substituents on the backbone could impact sterics around the metal centre and the electronic properties of the catalyst.[43–47]

This chapter describes the synthesis and characterization of two new water-soluble rhodium(I) precatalyst bearing sulfonated α-diimine *N,N-bis(arylimino)ethane* or sulfonated *N,N-bis(arylimino)-acenaphthene* (aryl-BIAN) ligand. These compounds were characterized using a range of analytical and spectroscopic techniques, such as $^{1}$H and, $^{13}$C{$^{1}$H} nuclear magnetic resonance (NMR) spectroscopy, Fourier-transform infrared spectroscopy (FTIR) spectroscopy and high-resolution mass spectrometry (HRMS). The sulfonated Rh(I) 1,4-diazabutadiene (DAD) complexes were evaluated as catalyst precursors in the aqueous biphasic hydroformylation of 1-octene (higher olefin) and compared to non-sulfonated Rh(I) 1,4-diazabutadiene (DAD) complexes.

## 2.2 Results and discussion

### 2.2.1 Synthesis of alpha-diimine Schiff base ligands

The alpha-diimine ligands phenol, 4,4′-(1,2-ethanediylidenedinitrilo)bis (**2.1**) and phenol, 4,4′-(1,2-acenaphthenediylidenedinitrilo)bis (**2.2**) were synthesised *via* an acid-catalyzed Schiff base condensation reaction following modified literature procedures (Scheme 2.1).[48,49]

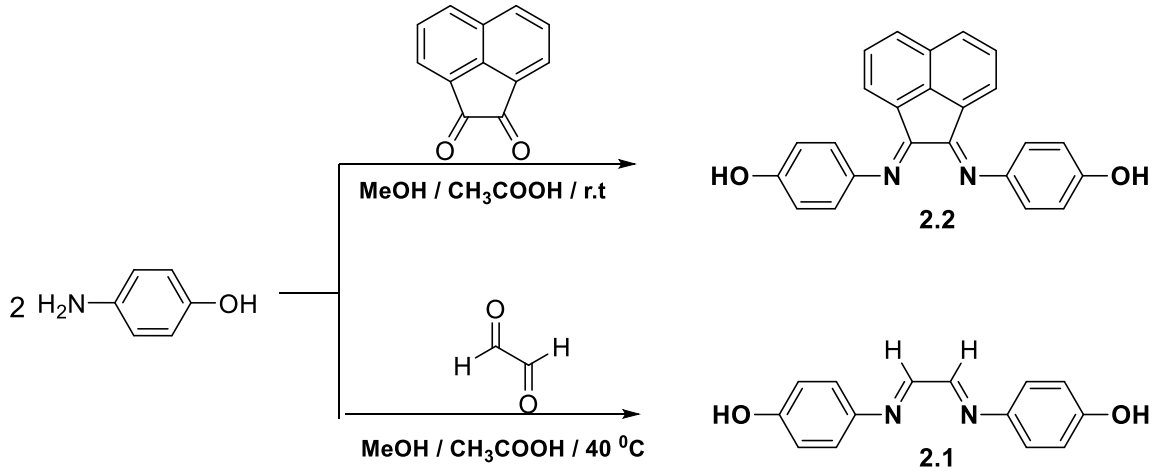


**Scheme 2.1** Synthesis of α-diimine ligands **2.1** and **2.2**.

Mechanistically, the acid-catalyzed Schiff base condensation reaction proceeds *via* nucleophilic attack of a carbonyl electrophile by a primary amine (Step 1). This generates a carbocation which further reacts with the lone pair of electrons on the nitrogen of the amine (Step 2). The unstable product of this step is stabilized by the loss of an equivalent of water from the molecule. Since the carbinolamine is an alcohol, it undergoes an acid-promoted dehydration to yield the final Schiff base imine product (Step 3) (Scheme 2.2).[50,51]

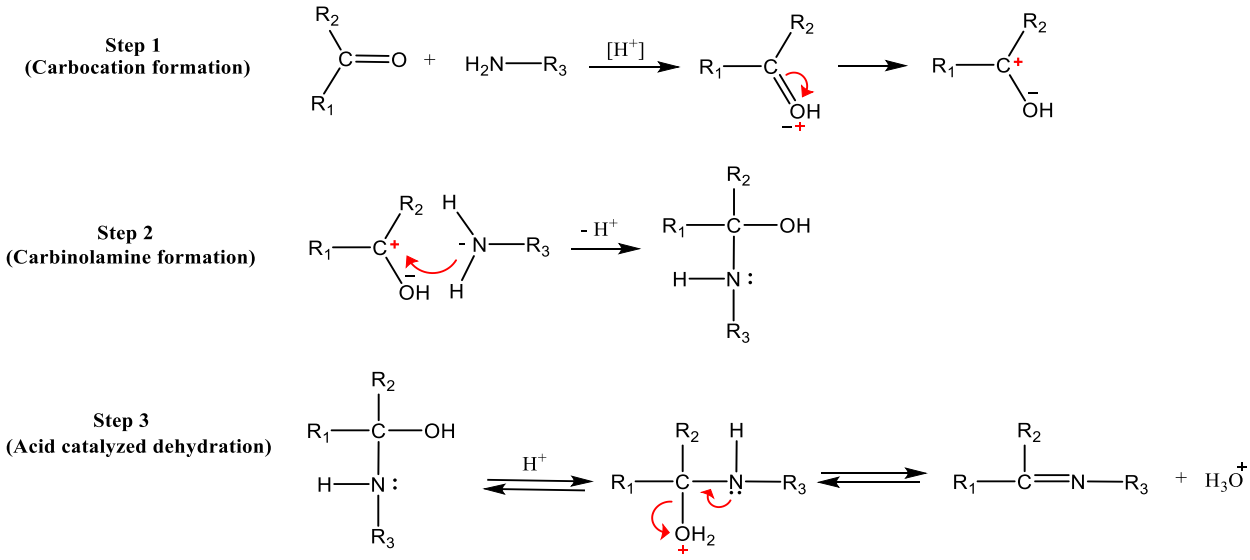


**Scheme 2.2** Schiff-base condensation reaction mechanism.

The carbonyl compounds (1,2-ethanedione and acenapthenequinone) were reacted with two molar equivalents of 4-amino phenol in methanol and a catalytic amount (6 drops) of glacial acetic acid. The products **2.1** and **2.2** were obtained as yellow and orange powders in moderate

yields of 57% and 68 % respectively. Both ligands display excellent solubility in organic solvents such as acetone, dichloromethane, and dimethyl sulfoxide at room temperature.

### 2.2.2 Characterization of alpha-diimine Schiff base ligands

***NMR spectroscopy***

In the $^{1}$H NMR spectrum of **2.1** and **2.2**, the peak associated to the primary amine proton peak of the 4-aminophenol at 4.34 ppm is absent. This confirms a successful Schiff base condensation reaction. The $^{1}$H NMR spectrum of **2.1** (Figure 2.1) displays a distinct imine proton signal H-1 at 8.42 ppm as a singlet and the peak for the phenolic protons of **2.1** appears as a broad signal at 9.78 ppm (H-6) each integrating for 2 protons due to the symmetrical nature of the molecule. The aromatic protons are observed as a pair of doublets in the range of 7.35 – 6.80 ppm. This is a downfield shift in resonance frequency of the aromatic phenyl protons of 4-aminophenol at 6.50 ppm prior to condensation. The observed downfield shift may be attributed to the deshielding of the respective protons as a result of the electron-withdrawing effect of the imine.

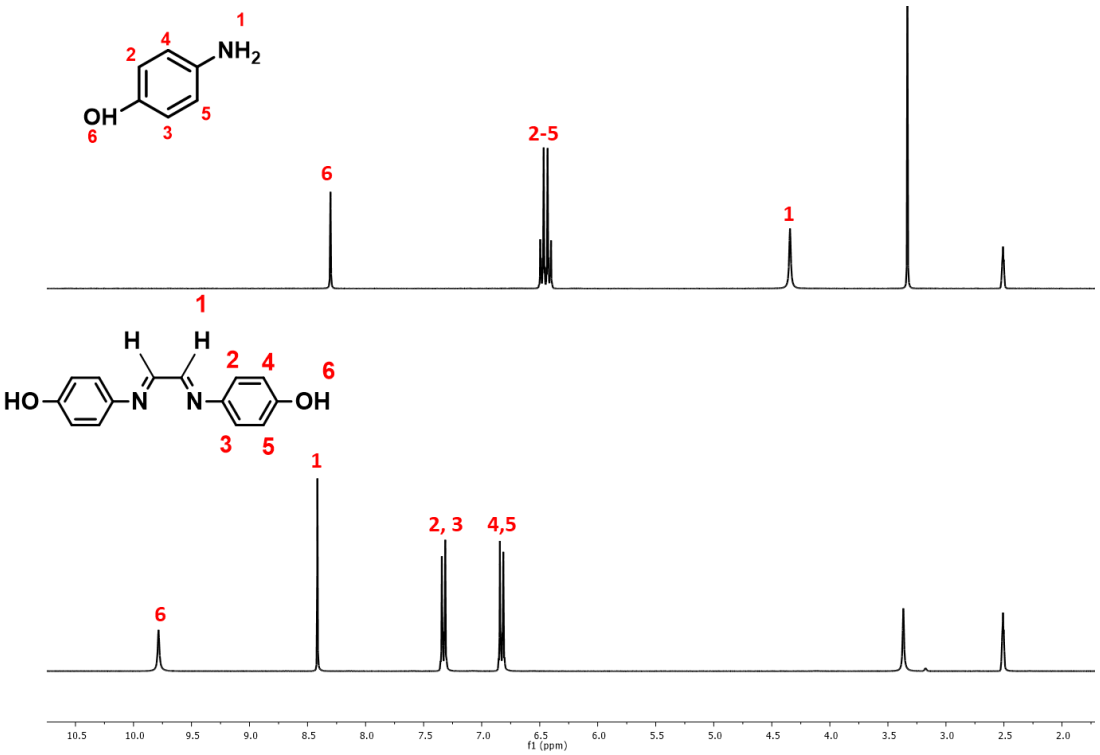


**Figure 2.1** Stacked $^{1}$H NMR spectra (DMSO-$d_6$) of 4-amino phenol and ligand **2.1**.

Successful synthesis of **2.2** is shown in the $^{1}$H NMR spectrum (Figure 2.2). A singlet at 9.41ppm is assigned to the phenolic proton H-8. H-3 which is ortho coupled to H-2 appear as

a doublet at 7.00 ppm with coupling constant of 7.2 Hz. The doublet at 8.06 ppm is assigned to H-1 with a coupling constant of 8.2 Hz which is coupled to H-2. Consequently, H-2 which is ortho coupled to both H-1 and H-3 appears as a triplet at the region of 7.54 – 7.49 ppm. The assignment of the acenaphthene protons to the corresponding signals is in agreement with similar compounds previously reported by Yi-Chen *et al.*[52] and Wang *et al.*[53] The signal for the phenyl protons (H-4 to H-7) appears as a singlet due to the symmetrical nature of the molecule as a result of the rigid acenaphthene backbone which prevents rotation around the imine carbon–carbon bond and forces the imine nitrogen atoms to remain in a fixed orientation. It has been reported that the *bis(N-arylimino)acenaphthene* derivatives of alpha diimine ligands are more rigid and sterically bulky compared to diimine ligands derived from glyoxal or acyclic diketones and this rigidity may impose stable chelation to metal complexes exhibiting a more limited range of bonding modes and impacting high chemical stability with respect to hydrolysis or cleaving of the central C–C bond.[54–57]

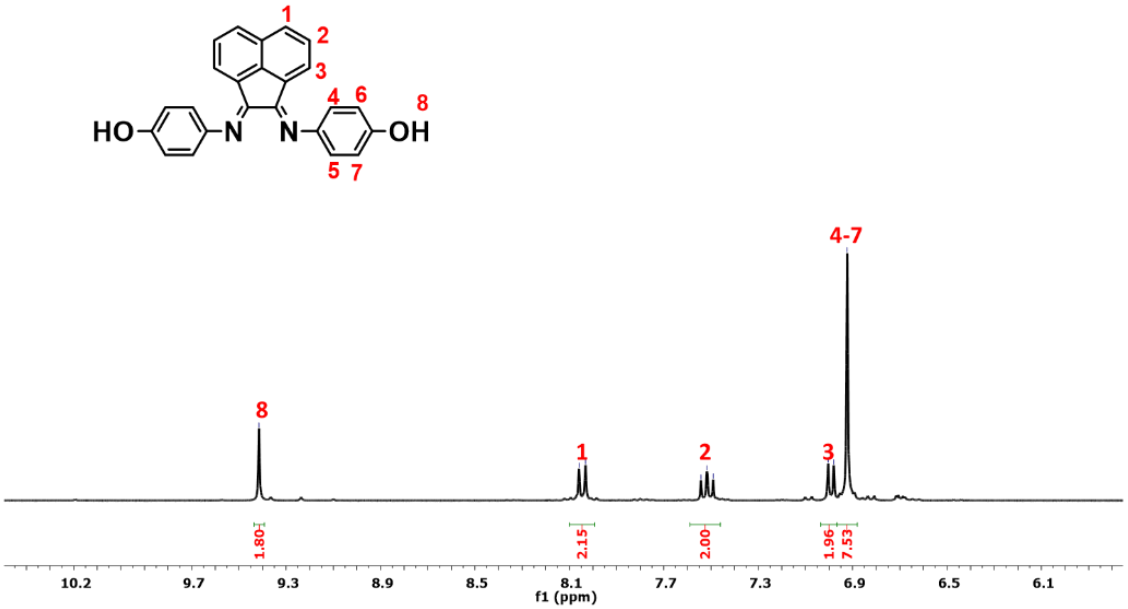


**Figure 2.2** $^{1}$H NMR spectrum for ligand **2.2** in DMSO-$d_6$.

The $^{13}C\{^{1}H\}$ NMR spectra of both ligands gave the expected number of carbon signals for each compound, further confirming the formation of the proposed structures. The signals for the imine carbons were observed as singlets at 158.5 and 160.5 ppm for the α-diimine ligands **2.1** and **2.2** respectively.

***Infrared spectroscopy* and *Mass spectrometry***

FTIR spectral analysis was used to confirm the functional groups indicative of a successful condensation reaction. The absence of the carbonyl stretching vibration of the acenapthenequinone at 1720 $cm^{-1}$ suggests a successful condensation of the carbonyl and the amine. The typical stretching frequencies for the C=N double bond occur as an absorption band of medium intensity at 1632 $cm^{-1}$ and 1659 $cm^{-1}$ while the OH functionality is observed at 3075 $cm^{-1}$ and 3289 $cm^{-1}$ for compounds **2.1** and **2.2** respectively, thus confirming the formation of the proposed compounds.

Mass spectrometry of both compounds were analysed using high-resolution electrospray ionisation mass spectrometry (ESI-MS). The positive ion mode mass spectral data obtained for ligands **2.1** and **2.2** is in agreement with the proposed structures. In both cases, the base peak corresponding to the $[M+H]^+$ protonated molecular ion fragment was observed at 241.0996 (*m/z*) and 365.0854 (*m/z*) for **2.1** and **2.2**, respectively.

### 2.2.3 Synthesis of water-soluble alpha-diimine ligands

Sultones are cyclic esters of hydroxyl sulfonic acids.[58] They have emerged as valuable heterocyclic intermediates in both general organic synthesis and natural product synthesis to introduce alkyl chains carrying negatively charged sulfonate functionality. Sultones are used in the production of dyes, pharmaceuticals, cosmetics, agrochemicals and surfactants to confer hydrophilicity.[58–61] Sultones react readily by undergoing a nucleophilic ring opening reaction which occurs by the cleaving of the C–O bond in the presence of nucleophiles.[62–65] This therefore makes cyclic sultones suitable sulfoalkylating agents for synthesising water soluble compounds (Scheme 2.3).

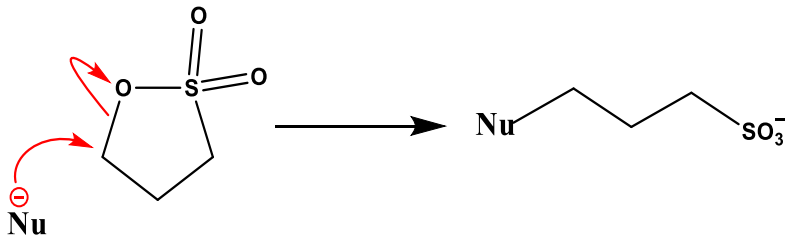


**Scheme 2.3** Reactivity of 1,3-Propanesultone.

1,3-Propanesultone was chosen for the introduction of the alkyl-sulfo group unto the alpha-diimine ligands **2.1** and **2.2** in the presence of sodium hydride (NaH) and dry THF (Scheme

2.4). Herein, the phenoxide is generated with the use of the deprotonating agent (NaH) followed by ring-opening of the cyclic sulfonate by the nucleophilic attack from the phenoxide ion.

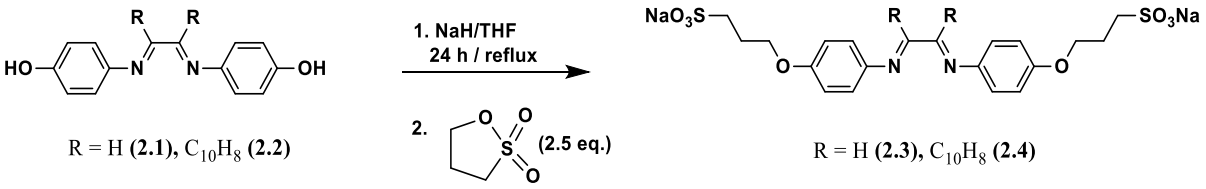


**Scheme 2.4** Synthesis of disulfonated α-diimine ligands **2.3** and **2.4**.

The reaction gave high yields (> 64%) when excess of 1,3-propanesultone (2.5 eq.) is added slowly to the reaction mixture compared to when the exact two molar equivalents of 1,3-propanesultone is added readily (yields < 35%). The disulfonated α-diimine products **2.3** and **2.4** display excellent solubility in water (123 mg/mL and 128 mg/mL respectively) and DMSO at room temperature. The water-soluble compounds were used as ligand precursors in the synthesis of water-soluble rhodium(I) complexes.

### 2.2.4 Characterization of water-soluble alpha-diimine ligands

***NMR spectroscopy***

In the $^{1}$H NMR spectrum of **2.3** shown in Figure 2.3, aliphatic signals were observed and no hydroxyl proton signal was present. This attest to the successful deprotonation and sulfoalkylation of compound **2.1**. The triplet at 4.11 ppm is assigned to the propyl proton H-6 which is coupled with the adjacent methylene proton H-7. Proton H-7 appear as pentet signals in the range 2.14 – 2.05 ppm due to its coupling to the two adjacent methylene protons H-6 and H-8. The triplet at 3.01 – 2.95 ppm is assigned to H-8 propyl proton which is adjacently coupled to H-7.

For ligand **2.4**, the phenyl protons attached to the imine appear as quartets alluding to the fluxionality resulting from a change from a symmetrical to asymmetrical molecule upon sulfonation. Additionally, similar splitting patterns were observed in the $^{1}$H NMR of **2.4** to that of **2.3**. Comparing the $^{13}$C NMR spectra of ligands **2.1** and **2.2** to **2.3** and **2.4,** signals corresponding to the propyl carbon was observed at 67.69, 48.39 and 25.80 ppm for compound **2.3** and 68.35, 49.46 and 29.50 ppm for compound **2.4**.

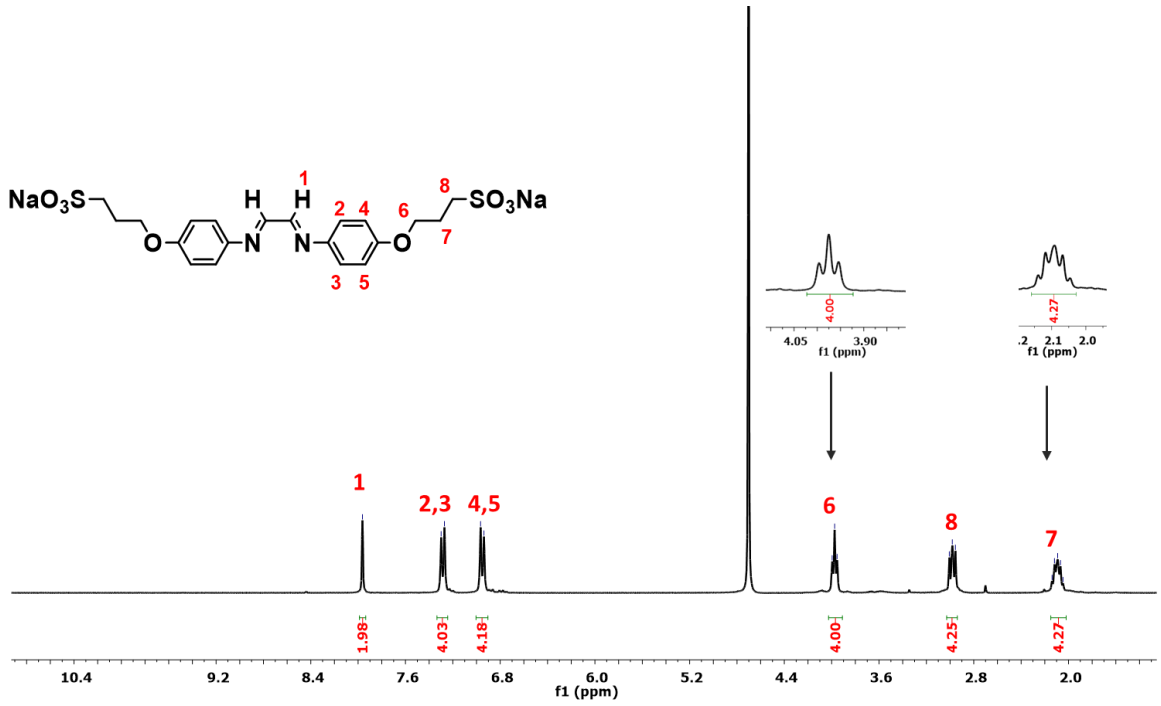


**Figure 2.3** $^{1}$H NMR spectrum of ligand **2.3** in $D_2O$-$d_2$.

### *Infrared spectroscopy* and *Mass spectrometry*

IR spectroscopy was used to confirm the functional groups indicative of a successful alkylation reaction. The absence of a broad hydroxy stretching vibration at the region of 3075 $cm^{-1}$ and 3289 $cm^{-1}$ for compounds **2.3** and **2.4** respectively, confirms a successful sulfopropylation reaction. The typical stretching frequencies for the sulfonic S=O functionality occur as a band of medium intensity at 1185 $cm^{-1}$ and 1181 $cm^{-1}$ for compounds **2.3** and **2.4** respectively. The mass spectral data revealed the molecular weight fragment as 526.9700 $[M+H]^+$ for **2.3** and 653.021 $[M+H]^+$ for **2.4** in the positive-ion mode.

## 2.2.5 Synthesis of alpha-diimine Rh(I) complexes

The non-sulfonated α-diimine rhodium complexes **2.5** and **2.6** containing $BF_4^-$ counter-ions were readily synthesized by reacting ligands **2.1** or **2.2** with $[Rh(COD)(MeCN)_2]BF_4$ in acetonitrile at room temperature for one hour (Scheme 2.5).

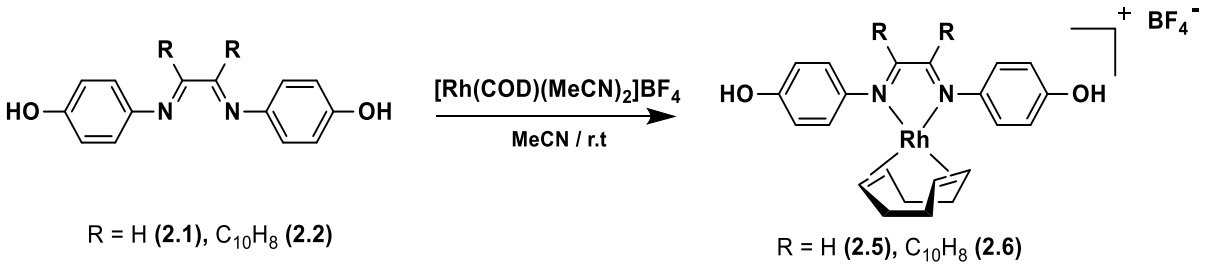


**Scheme 2.5** Synthesis of α-diimine rhodium complexes **2.5** and **2.6**.

The $[Rh(COD)(MeCN)_2]BF_4$ metal precursor was initially prepared by reacting $[(Rh(COD)Cl)_2]$ and $AgBF_4$ in acetonitrile at room temperature. The stoichiometric by-product (AgCl) was separated from the reaction solution using a syringe filter following literature methods.[66] The complexes **2.5** and **2.6** were isolated as dark red powders in good yields of 59% and 61% respectively.

### 2.2.6 Characterization of alpha-diimine Rh(I) Complexes

***NMR spectroscopy***

The $^1$H NMR spectrum of complex **2.5** is shown in Figure 2.4 as a representative example. The protons of the cyclooctadiene moiety are observed at 3.90 ppm, 2.37 ppm and 1.83 ppm and each signal integrates for 4 protons. This is in agreement with the proposed structure. The endo and exo-methylene protons (H-8 and H-9) are observed as two separate signals due to their non-equivalent chemical environment. This observation is similar to earlier reported Rh(COD) complexes.[26,29,67] Metal-ligand coordination was confirmed by A downfield shift of the imine proton signal from 8.24 ppm to 8.62 ppm is observed in the $^1$H NMR spectrum of complex **2.5**. Also, and a change in multiplicity of the phenyl protons attached to the imine from a singlet to a quartet is observed for complex **2.6**.

In the $^{13}C\{^1H\}$ NMR spectra of the complexes **2.5** and **2.6**, a downfield shift of the imine carbon signal is observed upon complexation of ligand **2.1** and **2.2** respectively. This is further evidence of coordination of the imine nitrogen to the Rh metal centre. Broad signals assigned COD signals were also observed at 83.86 and 30.60 ppm.

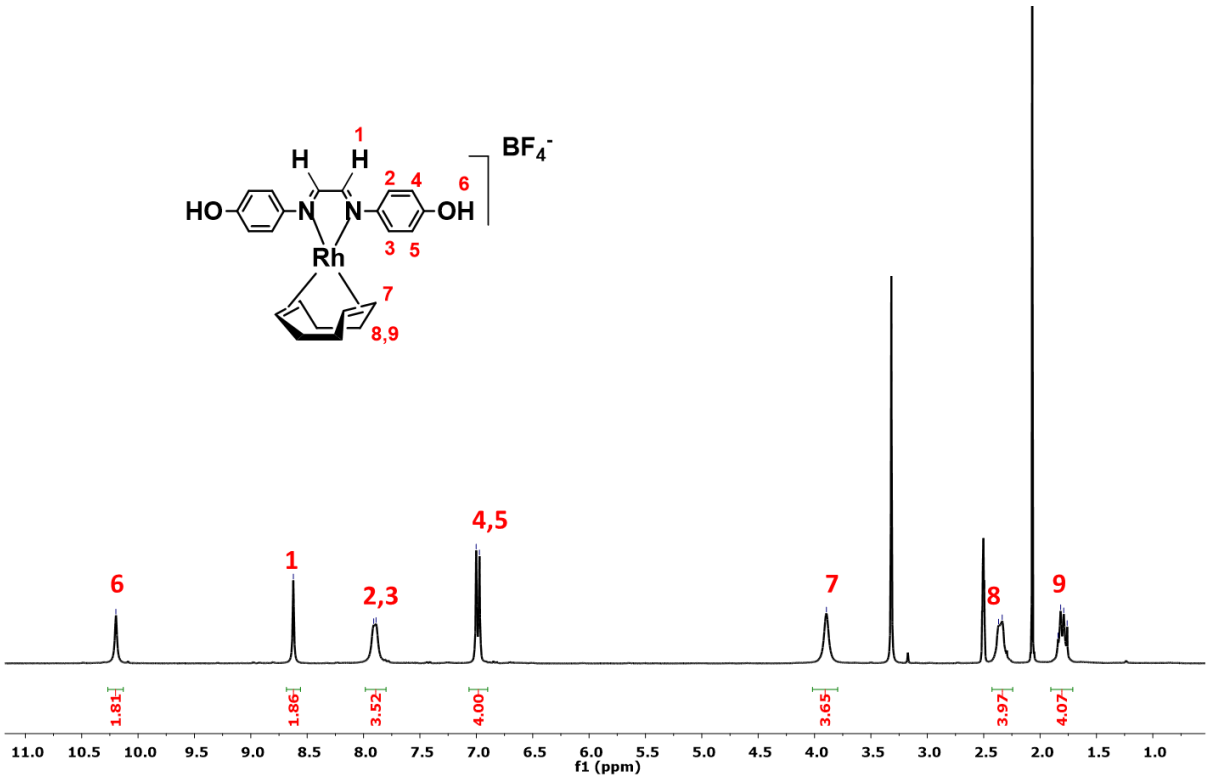


**Figure 2.4** $^{1}$H NMR spectrum of complex **2.5** in DMSO-$d_6$.

### *Infrared spectroscopy* and *Mass spectrometry*

Coordination of the imine nitrogen to the rhodium metal centre was confirmed by a hypsochromic shift of the imine stretching vibration bands to lower wave numbers in the region of $\nu_{(C=N)}$ = 1607 cm$^{-1}$ for complex **2.5** (Figure 2.5) and $\nu_{(C=N)}$ = 1623 cm$^{-1}$ for complex **2.6**. The electrospray ionisation mass spectra were recorded in the positive ion-mode for all complexes. M refers to the complex cation excluding the $BF_4^-$ counter-ion. The molecular ion fragment $[M+MeCN+Na]^+$ for complex **2.5** was observed at *m/z* = 515.1010. The parent ion peak $[M]^+$ was observed at *m/z* = 575.1060 for complex **2.6**.

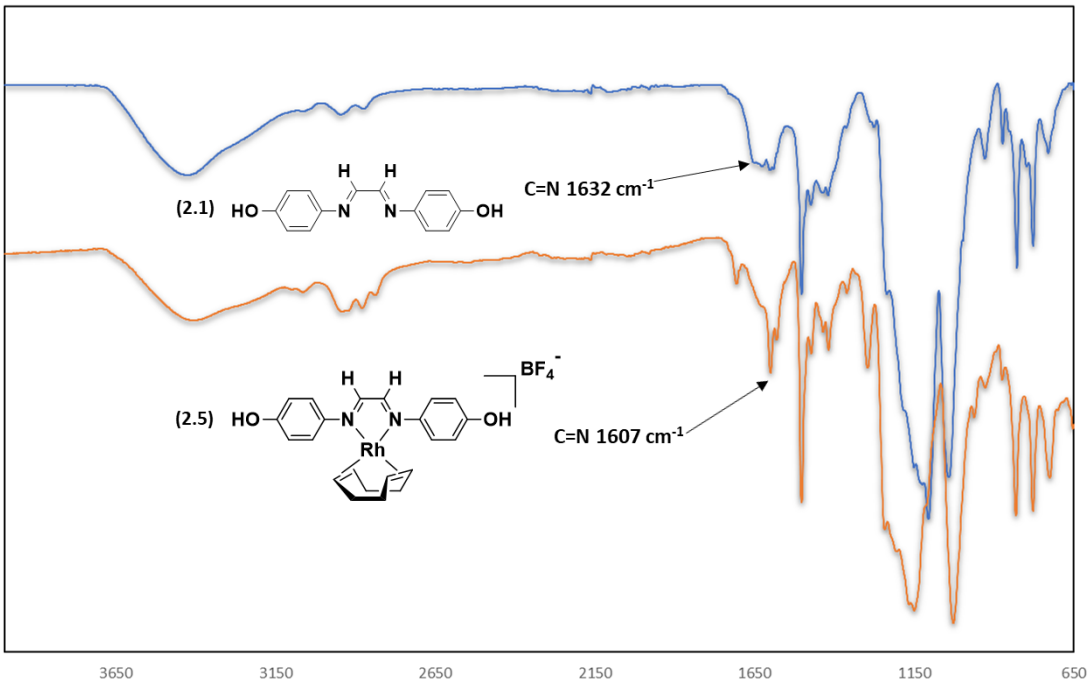


**Figure 2.5** Stacked infrared spectra for ligand **2.1** and complex **2.5**.

### 2.2.7 Synthesis of water-soluble disulfonated alpha-diimine Rhodium(I) Complexes

The synthesis of the disulfonated alpha-diimine Rh(I) complexes **2.7** and **2.8** were achieved using $[Rh(COD)(MeCN)_2]BF_4$ metal precursor previously prepared *in situ* from $[(Rh(COD)Cl)_2$ and $AgBF_4$ in acetonitrile at room temperature. The complexes were obtained in quantitative yield by reacting slight excess of $[Rh(COD)(MeCN)_2]BF_4$ with the appropriate ligand (**2.3** or **2.4**) at room temperature in DMSO (Scheme 2.6).

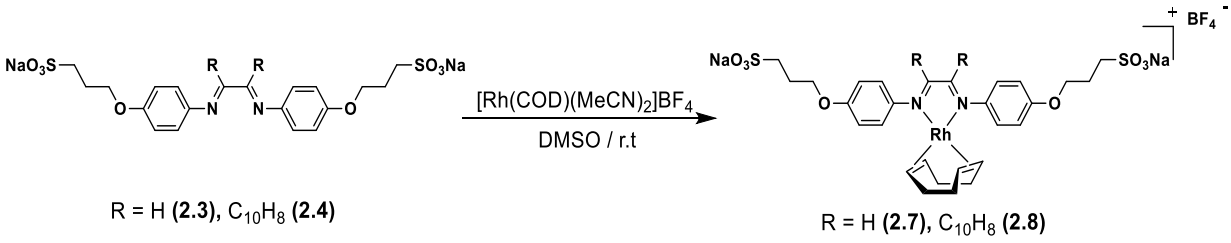


**Scheme 2.6** Synthesis of disulfonated α-diimine rhodium complexes **2.7** and **2.8**.

DMSO proved useful as the solvent of choice as it possesses sufficient polarity to dissolve the salt-like ligands and complexes. The displacement of acetonitrile from $[Rh(COD)(MeCN)_2]BF_4$ was facile, affording new rhodium complexes **2.7** and **2.8** as red solids in 56% and 62% yields respectively. The hydrophilic complexes were simply purified by washing the product with acetone to remove the unreacted $[Rh(COD)(MeCN)_2]BF_4$. The

complexes (**2.7** and **2.8**) display good solubility in water (102 mg/mL and 106 mg/mL respectively) at room temperature.

### 2.2.8 Characterization of water-soluble disulfonated alpha-diimine Rhodium(I) Complexes

***NMR spectroscopy***

The $^{1}$H NMR spectra of the disulfonated metal complexes in deuterated DMSO exhibits signals consistent with the proposed structures. The $^{1}$H NMR spectrum for complex **2.7** (Figure 2.6) displays similar signals to those observed in the $^{1}$H NMR spectrum of **2.8** (Figure 2.7). For instance, for both complexes **2.7** and **2.8**, the signals of the cyclooctadiene moiety are observed as broad signals between δ 3.97 – 3.92, 2.41 – 2.36 and 1.84 – 1.72 ppm with each peak integrating for 4 protons. In addition, coordination-induced down field shift was observed for the imine proton H-1 from 8.44 ppm to 8.68 ppm due to the deshielding effects of the Rh metal (Figure 2.6). Comparing the $^{1}$H NMR spectrum of ligand **2.4** and complex **2.8**, a significant down field shift was observed for the acenaphthene ring. This may be attributed to an increase in electron density induced by metal coordination.

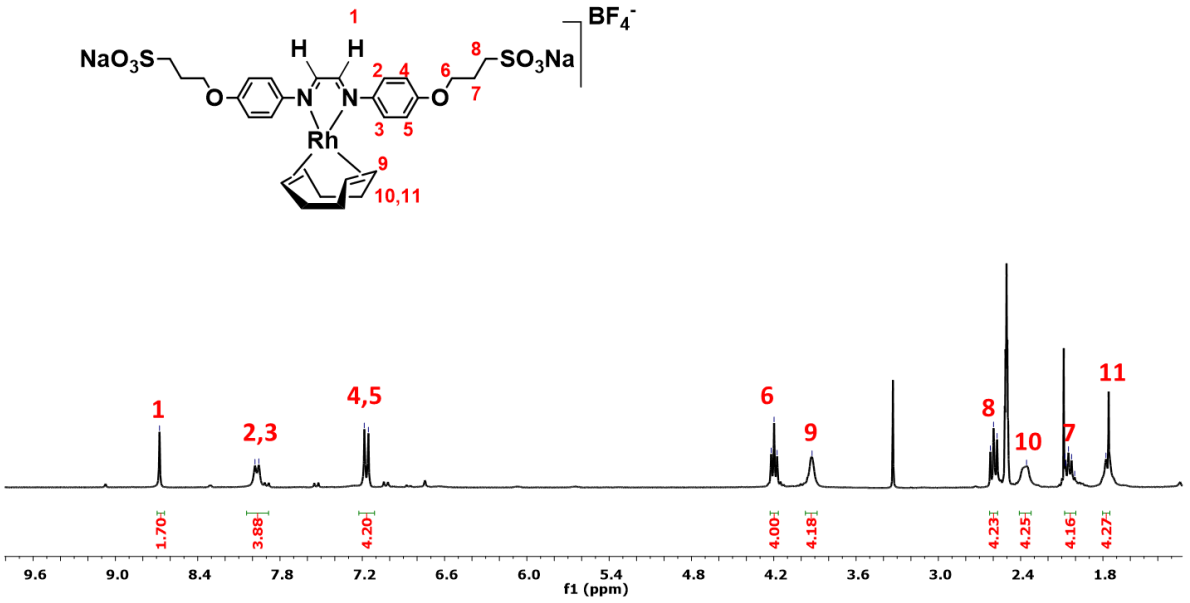


**Figure 2.6** $^{1}$H NMR spectrum of complex **2.7** in DMSO-$d_6$.

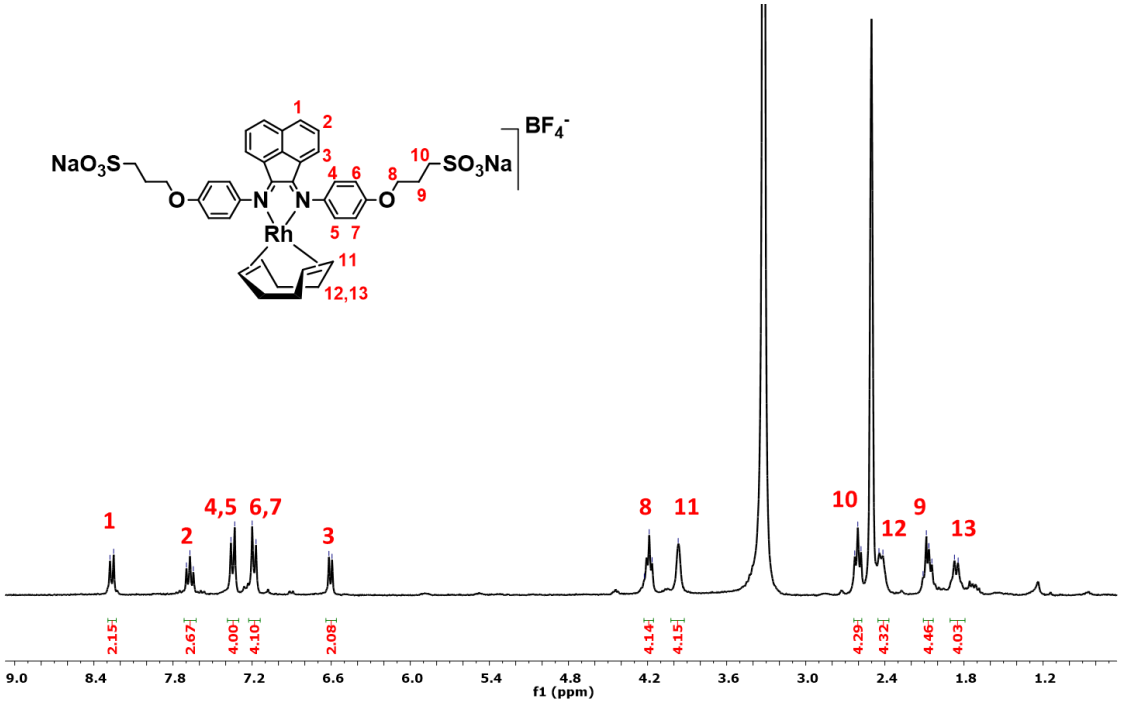


**Figure 2.7** $^{1}$H NMR spectrum of complex **2.8** in DMSO-$d_6$.

### *Infrared spectroscopy* and *Mass spectrometry*

The structural identity of the complexes **2.7** and **2.8** were further confirmed by infrared spectroscopy. Comparing the infrared spectra of the disulfonated rhodium complexes to their corresponding ligands, a decrease to lower wavenumbers of the imine absorption band was observed. This shift in the FT-IR spectra of the complexes is due to the synergic effects between the imine nitrogen and Rh metal centre. This effect could be attributed to the lone pair of electrons of the imine nitrogen being donated to the empty orbitals of the metal. This, together with the back-donation from the metal d-orbitals into the empty $\pi$-anti bonding orbitals of the ligand weakens the imine bonds; consequently, a hypsochromic phenomenon occurs.

The mass spectrum (positive mode) of complex **2.7** is displayed in Figure 2.8. The data revealed the parent ion $[M]^+$ at 739.2161 *m/z* and $[M+H]^+$ molecular fragment at 740.2184 *m/z*, where M refers to the complex cation excluding the $BF_4^-$ counter-ion. For complex **2.8**, the molecular fragment $[M+H]^+$ was observed at 864.0600 *m/z*.

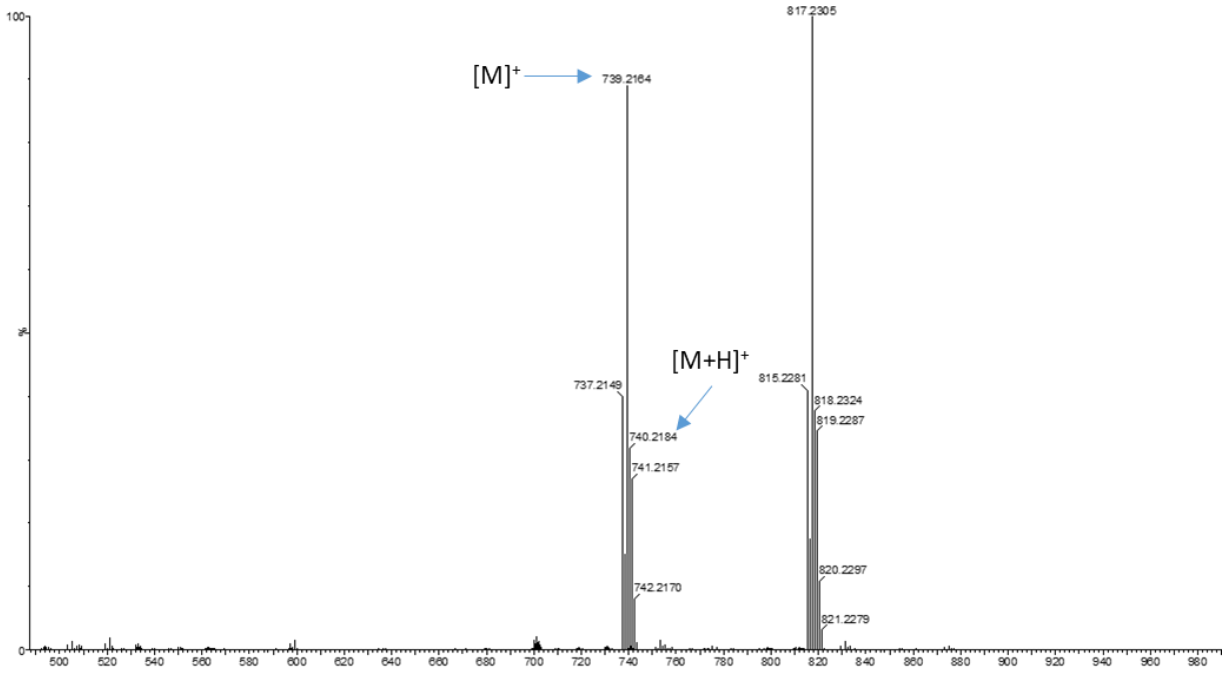


**Figure 2.8** Mass spectrum of complex **2.7**.

### 2.2.9 Hydroformylation studies

The complexes **2.5** – **2.8** were tested as catalyst precursors in the hydroformylation of 1-octene. Scheme 2.7 shows the reaction of 1-octene with syngas (1:1, $CO/H_2$) in the presence a Rh(I) catalyst to form linear and branched aldehydes as well as the isomerised products of 1-octene.

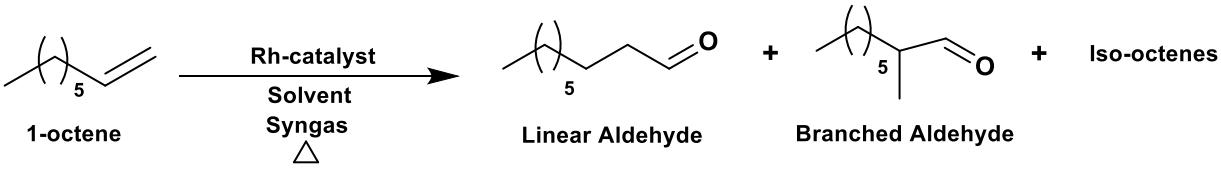


**Scheme 2.7** Hydroformylation of 1-octene to yield linear and branched aldehydes.

#### 2.2.9.1 Preliminary screening using catalyst precursor 2.5

Preliminary screening studies were carried out to identify reaction conditions which gives excellent conversion, chemoselectivity as well as regioselectivity at the mildest conditions possible. Catalyst precursor **2.5** which is the simplest and most representative structure of all the catalysts synthesized in this study was used to identify optimal conditions in the hydroformylation of 1-octene.

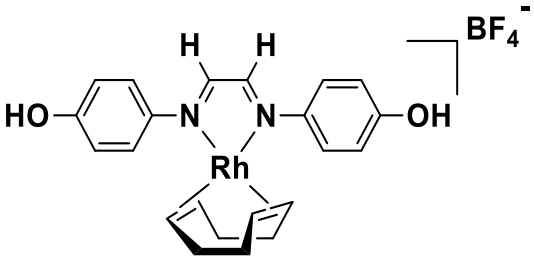


**(2.5)**

Optimisation studies were performed by varying the temperature (55 °C, 75 °C and 95 °C) and syngas pressure (20 bar, 30 bar and 40 bar). The reactions were performed in toluene (5 mL) for 4 h. Samples were analysed by gas chromatography using *n*-decane as the internal standard. The data in Table 2.1 are graphically represented in Figure 2.9 – 2.11.

**Table 2.1** Optimization result of the hydroformylation of 1-octene with respect to temperature and pressure using catalyst precursor **2.5**.

| Entry | Temperature ($^0$C) | Pressure (bar) | Conversion (%) | Aldehydes (%) | Iso-octenes (%) | *n:iso* | TOF ($h^{-1}$) |
|---|---|---|---|---|---|---|---|
| **1** | 55 | 20 | 67 | 44 | 56 | 2.8 | 185 |
| **2** | 55 | 30 | 89 | 70 | 30 | 2.4 | 204 |
| **3** | 55 | 40 | 94 | 75 | 25 | 1.9 | 211 |
| | | | | | | | |
| **4** | 75 | 20 | 81 | 42 | 58 | 2.8 | 213 |
| **5** | 75 | 30 | 90 | 57 | 43 | 1.8 | 321 |
| **6** | 75 | 40 | 95 | 72 | 28 | 2.2 | 329 |
| | | | | | | | |
| **7** | 95 | 20 | 90 | 72 | 28 | 1.5 | 409 |
| **8** | 95 | 30 | >99 | 95 | 5 | 0.7 | 584 |
| **9** | 95 | 40 | >99 | 96 | 4 | 0.6 | 600 |

Reaction conditions: The reactor was loaded with toluene (5 mL), 1-octene (0.805 g, 7.175 mmol), internal standard *n*-decane (0.204 g, 1.435 mmol) and catalyst loading ($2.87 \times 10^{-3}$ mmol). The reactor was purged with nitrogen three times, followed by purging three times with syngas. Catalyst to substrate ratio used was (1:2500). The reactions were carried out for 4 h and the data was analysed using GC-FID. TOF = (mmol of aldehydes/mmol of catalyst)/time. Average error estimate = ± 0.34.

### 2.2.9.2 Effect of temperature and pressure on catalyst activity

Moderate conversion of 1-octene (67%) and turnover frequencies of 185 $h^{-1}$ were observed at lowest conditions of pressure (20 bar) and temperature (55 °C) (Table 2.1, entry 1). Further increases in temperature from 75 °C to 95 °C at constant pressure led to an increase in conversions from 81% to 90% and in turn increased turnover frequencies were observed (Table 2.1, entries 4 and 7). Increasing the pressure to 30 and 40 bar and maintaining the temperature at 95 °C gave an increase in substrate conversion > 99% (Figure 2.9). Generally, an increase in temperature and pressure led to an increase in conversion and turnover frequency. This result suggests more energy (high temperature and pressure) is required for the activation of the alkene and substantial hydroformylation process to take place.

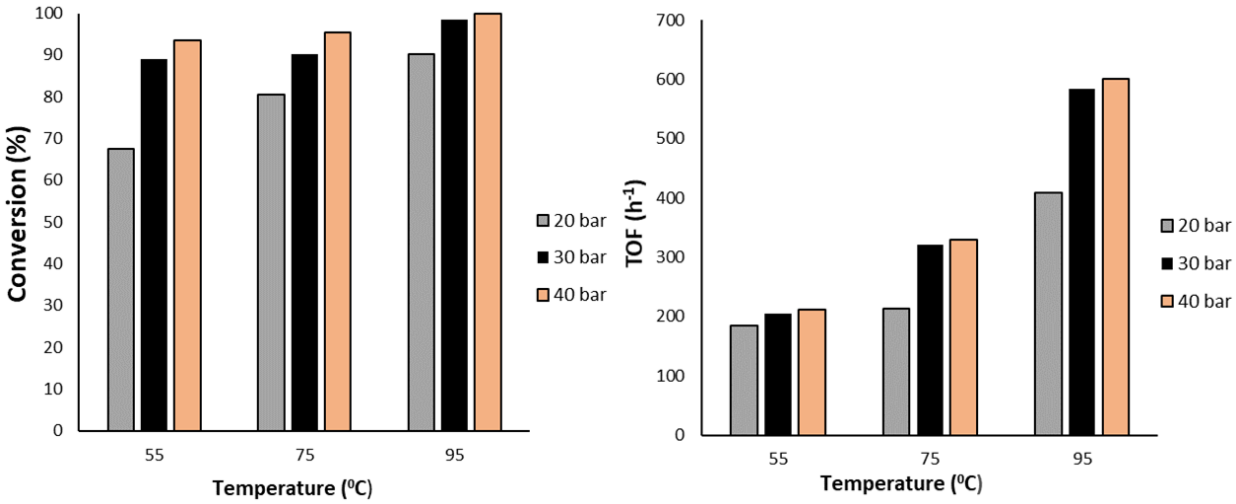


**Figure 2.9** Conversion and activity as a function of temperature for catalyst precursor **2.5**.

### 2.2.9.3 Effect of temperature and pressure on catalyst regio- and chemoselectivity

At temperatures maintained at 55 °C and pressure at 20 bar, transformation of 1-octene to largely iso-octene was observed (56%) (Table 2.1, entry 1). Increasing the pressure to 30 bar and 40 bar resulted in an increase in the hydroformylation of 1-octene to aldehydes 70% and 75% respectively (Table 2.1, entries 2 and 3). Furthermore, it is interesting to note that further increase in temperature to 95 °C and 20 bar syngas pressure led to an increase in the formation of aldehydes of 72% from 44% (55 °C / 20 bar) with reduced formation of iso-octenes (< 27%)

and an *n:iso* ratio of 1.5 was observed (Table 2.1, entries 1 and 7). This is ascribed to high catalyst activity at elevated temperature, an effect that is generally observed in rhodium-catalyzed hydroformylation reactions.[68]

Increasing the pressure to 30 and 40 bar at constant temperature of either 75 °C or 95 °C gave an increase in aldehyde formation and consequently reduced iso-octenes (Figure 2.10). These observations are in agreement with the general trends observed in rhodium-catalyzed hydroformylation,[69,70] wherein an increase in syngas pressures is known to suppress the isomerization of 1-octene and promotes the hydroformylation reaction. It is known that increasing the CO pressure in the hydroformylation reaction results in an increase of CO concentration in the reaction medium. The CO scavenges the vacant site of the 16-electron alkyl rhodium intermediate, this suppresses alkene isomerisation and accelerates the CO migration step.[71,72] This ideally, results to an increase in olefin transformation to aldehydes.

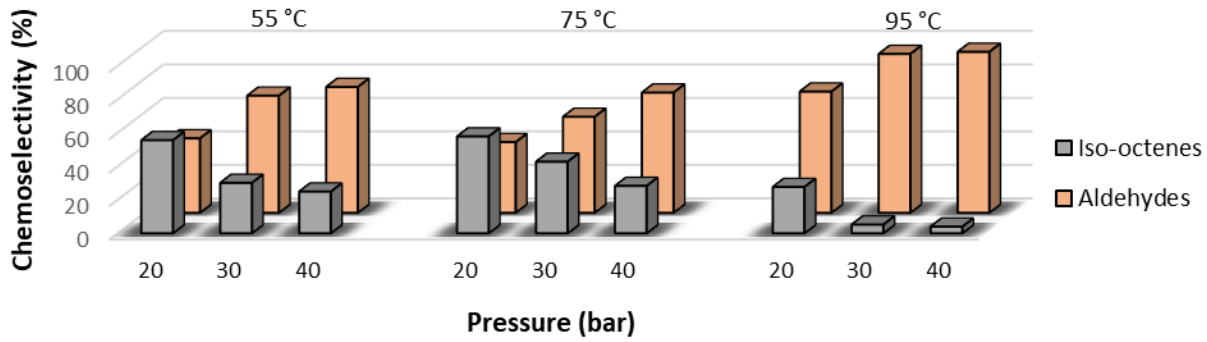


**Figure 2.10** Chemoselectivity as a function of pressure for catalyst precursor **2.5**.

The regioselectivity of catalyst precursor **2.5** towards branched aldehyde was predominant as the temperature is increased to 95 °C (Figure 2.11). This could be attributed to the fast isomerization of the terminal of olefin to internal olefin and subsequent hydroformylation under high temperatures.[73]

In line with Green Chemistry principles, milder condition (Table 2.1, entry 6) was identified to be the suitable condition with respect to substrate conversion (95%), and chemoselectivity for aldehydes (72%).

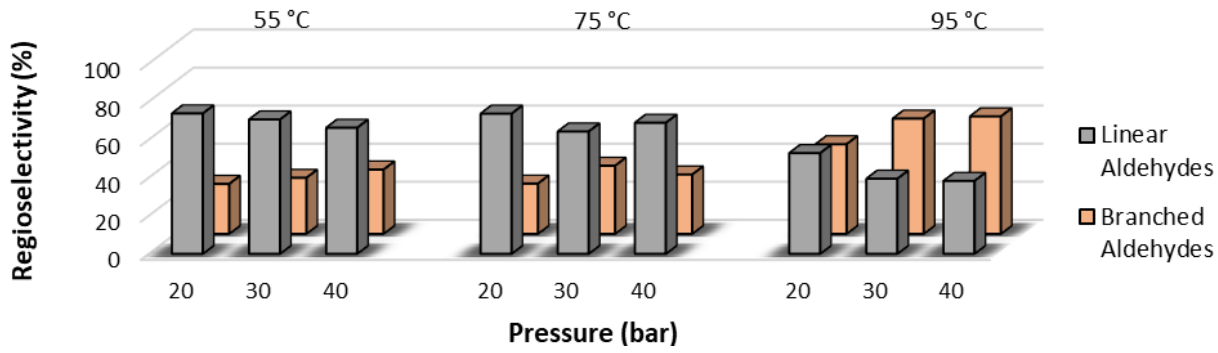


**Figure 2.11** Regioselectivity as a function of pressure for catalyst precursor **2.5.**

### 2.2.9.4 Aqueous biphasic hydroformylation of 1-octene

The limited miscibility of water with commonly used organic solvents as well as its availability and non-hazardous nature makes it a prime candidate for application in biphasic catalysis. In addition, using water-soluble catalyst in an aqueous biphasic process enables the separation of the catalyst from the final reaction mixture. This is essential for efficient catalyst recycling. Several approaches relying on phase manipulations have been developed to overcome mass transfer limitations often observed in biphasic hydroformylation reaction such as the use of surfactants, cosolvent, amphiphilic ligands and cyclodextrins etc., as summarized in the previous chapter. However, catalyst leaching into the organic phase remains a major impediment. In order to circumvent this problem, the use of water as the bulk solution was employed. This may result in minimized catalyst leaching and the isolation of products in sufficiently pure state.

The hydroformylation reaction with catalysts precursor **2.5** – **2.8** were performed under the established optimum conditions 75 °C/40 bar. Aqueous biphasic catalysis was carried out using water-soluble catalyst precursors **2.7** and **2.8** and compared to the non-sulfonated 1,4-diazabutadiene rhodium(I) complexes (**2.5** and **2.6**) which was carried out in monophasic organic solvent system (toluene).

The regio- and chemoselectivity data for **2.5** – **2.8** presented in Table 2.2 are graphically represented in Figure 2.12 and 2.13. All catalyst precursors gave high conversions greater than (> 95 %) and showed good regioselectivity for linear aldehydes (> 65%).

**Table 2.2** Hydroformylation of 1-octene using catalyst precursor **2.5 - 2.8.**

| Precatalyst | Conversion (%) | Aldehydes (%) | Linear Aldehydes (%) | Branched Aldehydes (%) | Iso-octenes (%) | *n:iso* | TOF ($h^{-1}$) |
|---|---|---|---|---|---|---|---|
| **2.5** | 95 | 72 | 69 | 31 | 28 | 2.2 | 329 |
| **2.6** | 97 | 70 | 70 | 30 | 30 | 2.4 | 317 |
| **2.7** | 98 | 86 | 66 | 34 | 14 | 1.9 | 522 |
| **2.8** | 99 | 88 | 73 | 27 | 12 | 2.7 | 539 |

Reaction conditions: The reactor (90 mL) was loaded with toluene (5 mL) for catalyst precursor **2.5** and **2.6**, $H_2O$ (5 mL) for catalyst precursor **2.7** and **2.8**, 1-octene (0.805 g, 7.175 mmol), internal standard *n*-decane (0.204 g, 1.435 mmol) and catalyst loading ($2.87 \times 10^{-3}$ mmol). The reactor was purged with nitrogen three times, followed by purging three times with syngas. Catalyst to substrate ratio used was (1:2500). The reactions were carried out for 4 h at 75 °C/40 bar. TOF = (mmol of aldehydes/mmol of catalyst)/time. Average error estimate: = ± 0.13.

Turnover frequencies of 329 $h^{-1}$ and 317 $h^{-1}$ were observed for catalyst precursors **2.5** and **2.6** while turnover frequencies of 522 $h^{-1}$ and 539 $hr^{-1}$ were observed for **2.7** and **2.8** respectively (Table 2.2). The higher turnover frequencies displayed by catalyst **2.7** and **2.8** could be attributed to the excellent solubility in water as there is more substrate to catalyst interaction. With respect to chemoselectivity and regioselectivity, catalyst precursor **2.7** and **2.8** showed superior performance (Figure 2.13 and 2.14), this is relative to the TOF values in yielding aldehydes (Figure 2.12).

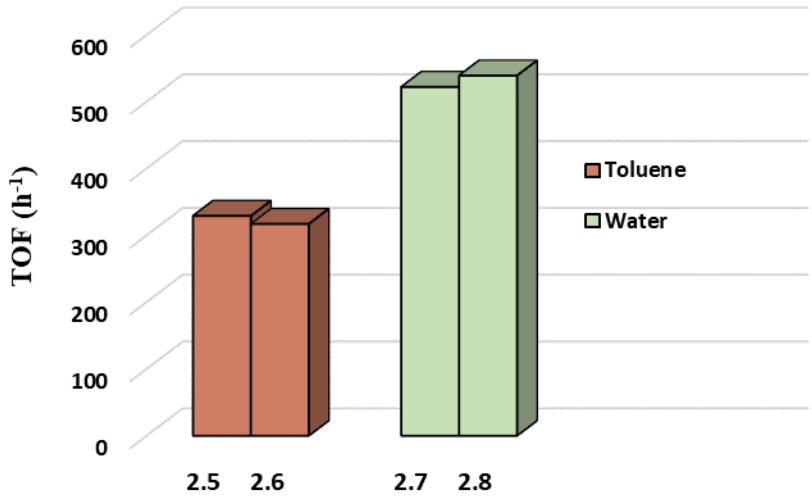


**Figure 2.12** Activity of catalyst precursor **2.5** and **2.6** in water and **2.7** and **2.8** in toluene.

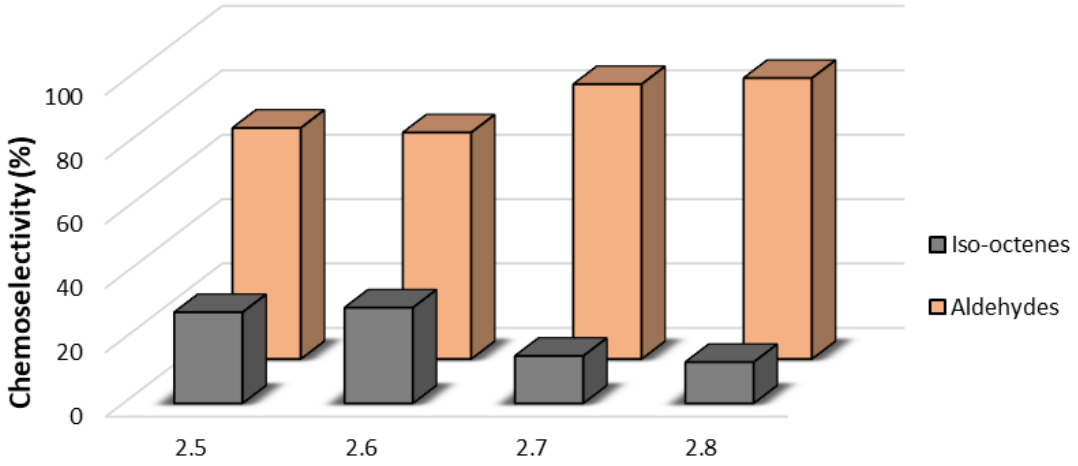


**Figure 2.13** Chemoselectivity of catalyst precursor **2.5 – 2.8**.

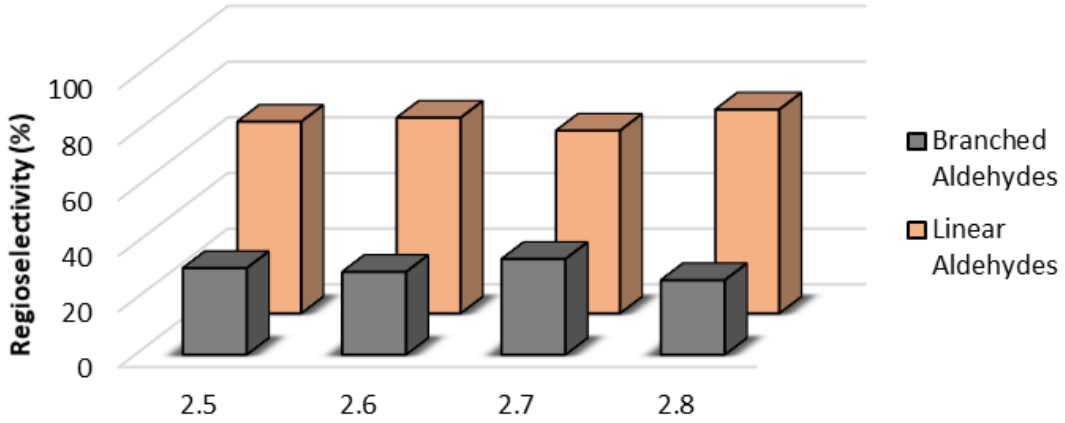


**Figure 2.14** Regioselectivity of catalyst precursor **2.5 – 2.8**.

### 2.2.9.5 Recyclability studies of catalysts 2.7 and 2.8

After a typical hydroformylation reaction, the reaction mixture was cooled to room temperature and the product (contained in the organic phase) was separated by decantation (Figure 2.15).

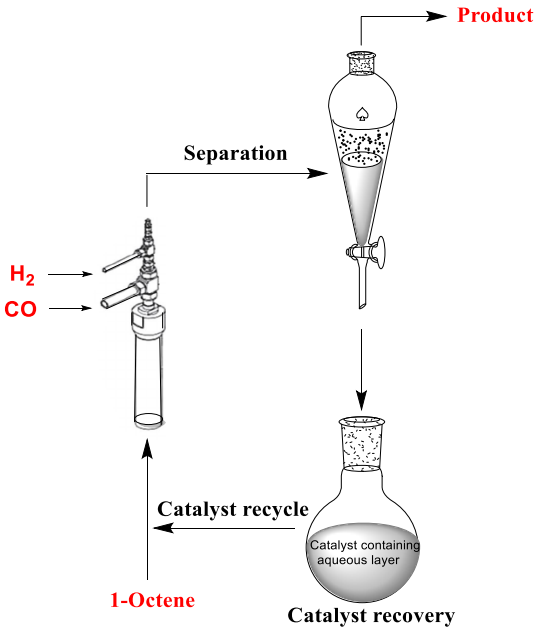


**Figure 2.15** Illustrating aqueous biphasic catalyst recycling strategy.

The catalyst-containing solution (aqueous phase) was successfully reused over four consecutive cycles with overall conversions > 65% (Figure 2.16). The first two cycles gave good conversions (> 90%) with high regioselectivity towards linear aldehydes.

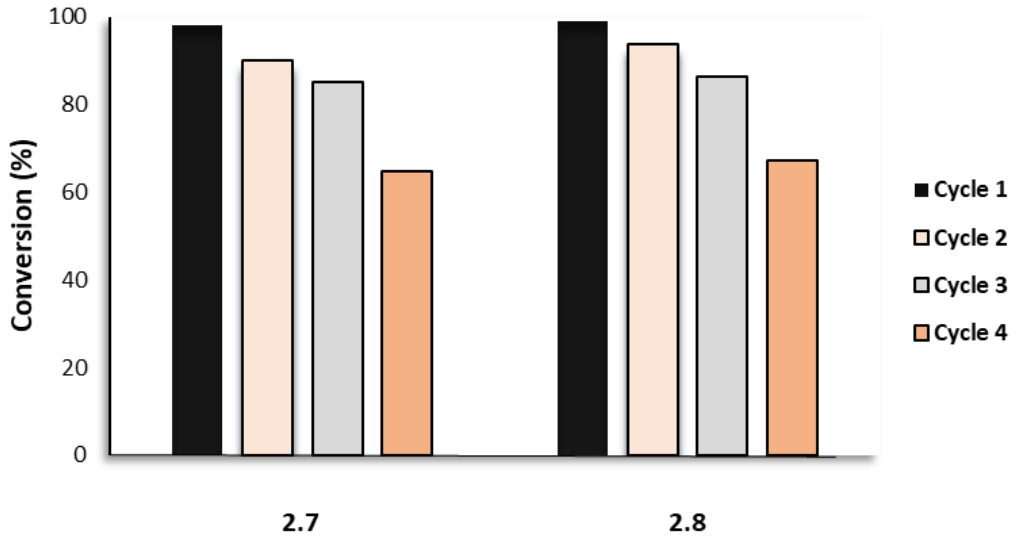


**Figure 2.16** Conversion upon recycling of catalyst precursor **2.7** and **2.8.**

The regioselectivity of each catalyst varied upon recycling as shown in Figure 2.17. This may be attributed to changes in the structure of the active catalyst under hydroformylation conditions as it is recycled. Comparing catalyst precursors **2.7** and **2.8**, increased formation of

linear aldehydes were observed using the latter. This could be attributed to the sterics imposed by the acenaphthene backbone. It is being reported that the steric attributes of the ligand coordinated to the metal centre influences the regioselectivity of a hydroformylation catalyst towards linear aldehydes, this favours the anti-Markovnikov migratory insertion.[75–77]

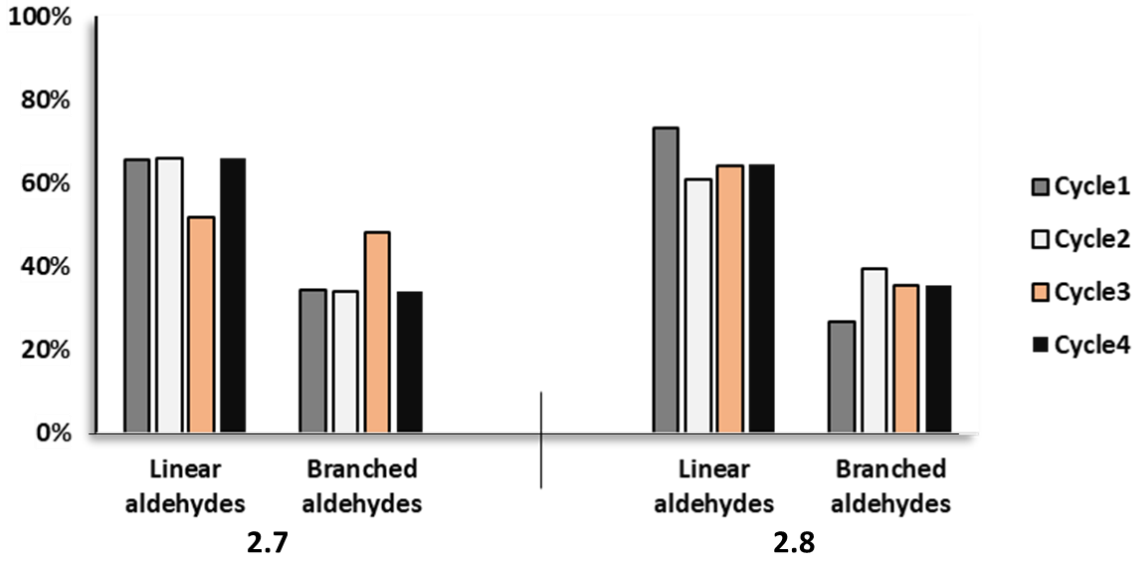


**Figure 2.17** Regioselectivity upon recycling of catalyst precursor **2.7** and **2.8**.

A drop in the formation of aldehyde from 86% to 55% for catalyst precursor **2.7** and 88% to 62% for catalyst precursor **2.8** was observed after the third cycle. Also, an increase in the formation of iso-octenes from 14% to 45% for catalyst precursor **2.7** and 12% to 38% for catalyst precursor **2.8** were observed (Figure 2.18). In the fourth cycle. The efficiency of the catalyst upon recycling drastically decreases with noticeable catalyst decomposition observed by the darkened colouration of the aqueous phase. As shown, conversion of 85% of which the total aldehydes are 51% and iso-octenes are 49% for catalyst precursor **2.7**. For catalyst precursor **2.8**, conversion of 86% was observed giving total aldehydes of 52% and iso-octenes of 48%. This is a significant drop in chemoselectivity of the catalyst precursors upon recycling.

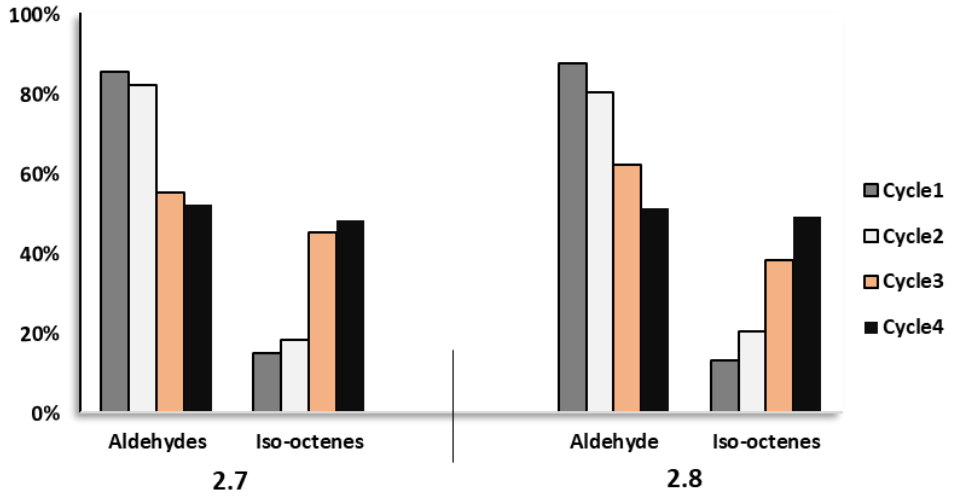


**Figure 2.18** Chemoselectivity upon recycling of catalyst precursor **2.7** and **2.8**.

The conversion of 1-octene using the water-soluble Rh(I) complexes (**2.7** and **2.8**) was evaluated at various times (Figure 2.19). This was conducted under the optimised conditions 75 °C and 40 bar. At 1 hour the conversion ranged between 12% and 18% for both complexes **2.7** and **2.8**. An increase in conversion up to 55% is observed after 2 h and 100% at 8 h. Slight differences in olefin conversion of **2.7** and **2.8** are seen in the first 4 h. After 6 h, similar quantitative conversions of 1-octene (> 99%) were observed for both catalyst precursor **2.7** and **2.8**. Concomitantly, there is an increase in the turnover frequency. In general, the performance of the catalyst increases as reaction time increases.

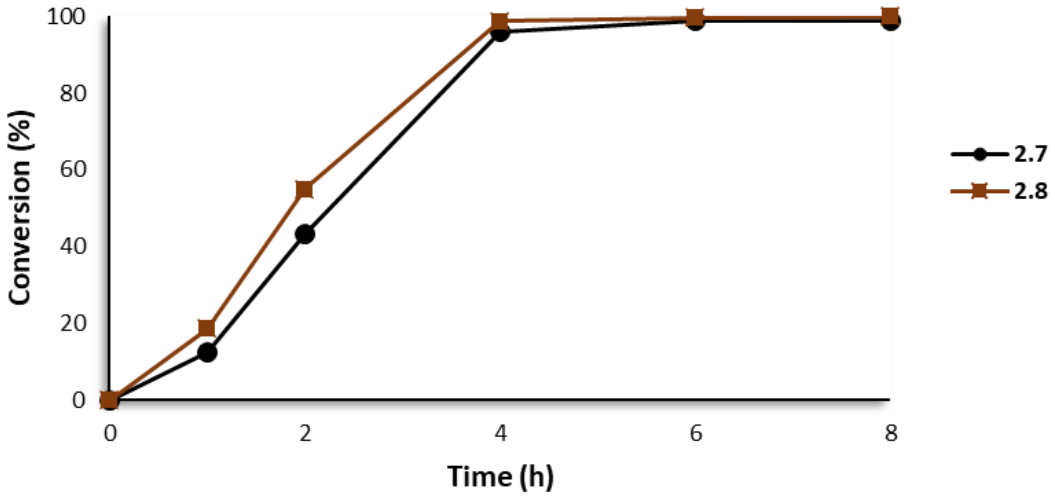


**Figure 2.19** Conversion of 1-octene over 8 h using catalyst precursors **2.7** and **2.8**.

### 2.2.9.6 Catalyst leaching experiments and stability studies

To investigate the origin of the decrease in the catalyst performance, the organic layer was analysed using ICP-MS analysis after each recycling procedure. The results showed low quantities of rhodium concentration in the organic layer in first cycle and negligible leaching was observed in the second cycle (< 0.003%) and no rhodium leaching in the third and fourth cycle suggesting no significant decrease of rhodium concentration in the aqueous phase. Therefore, the decrease in efficiency of the catalyst after the fourth cycle may be due to the degradation of the catalyst upon recycling. This is consistent with previously reported literature on catalyst decomposition.[67,78,79]

Preliminary stability studies of ligand **2.3** and complex **2.7** in solution were investigated using $^{1}$H NMR spectroscopy over a 4 hour period at high temperatures 75 °C and 95 °C in $D_2O$. The complex **2.7** proved to be stable at 75 °C in aqueous medium as no significant change in the spectrum was observed. However, at 95 °C signals corresponding to the cyclooctadiene moieties were no longer observed (Figure 2.20).

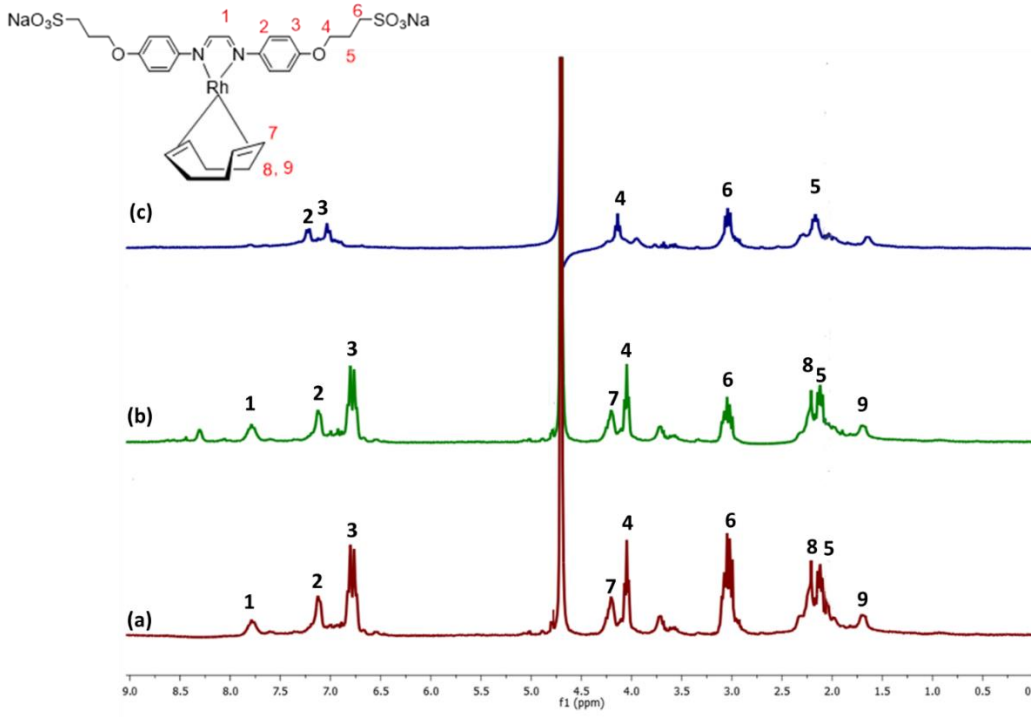


**Figure 2.20** $^{1}$H-NMR spectrum of complex **2.7** in $D_2O$ (a) at room temperature (b) after 4 hrs at 75 °C (c) after 4 hrs at 95 °C.

It also appears that in the $^{1}$H NMR spectrum of the sulfonate ligand **2.3** after 4 hrs at 95 °C, a new signal at 4.72 ppm was observe (Figure 2.21). This may be attributed to catalyst disintegration by hydrolysis at high temperatures. However, to fully establish the stability of these complexes in water, in situ temperature-programmed decomposition (TPD) studies under controlled conditions would be required.

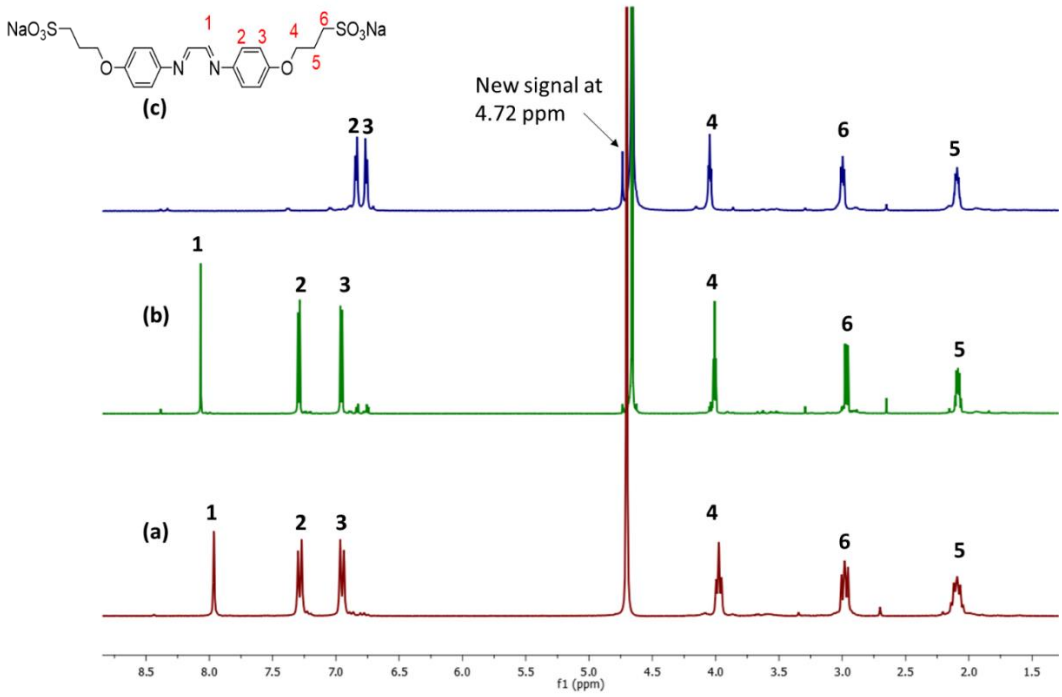


**Figure 2.21** $^{1}$H-NMR spectrum of ligand **2.3** in $D_2O$ (a) at room temperature (b) after 4 hrs at 75 °C (c) after 4 hrs at 95 °C.

### 2.2.9.7 Mercury poisoning experiments

The mercury poisoning (mercury drop) test is a rapid and commonly used method to determine the homogeneity of a catalytic process, it is based on the ability of mercury to supress catalyst reactivity as it amalgamates with the catalyst or get adsorbed onto the surface of heterogeneous catalyst.[80–82] Homogeneous catalysts typically show no change in catalytic performance in the presence of Hg and this therefor establishes if a catalyst is homo- or heterogeneous in nature.

**Table 2.3** Hydroformylation of 1-octene using catalyst precursor **2.5 - 2.8** in the presence of mercury**.**

| Entry | Precatalyst | Conversion (%) | Aldehydes (%) | Iso-octenes (%) | *n:iso* |
|---|---|---|---|---|---|
| **1** | **2.5** | 54 | 41 | 59 | 1.7 |
| **2** | **2.6** | 56 | 38 | 60 | 2.1 |
| **3** | **2.7** | 98 | 86 | 14 | 1.9 |
| **4** | **2.8** | 98 | 88 | 13 | 2.7 |

Reaction conditions: The reactor (90 mL) was loaded with toluene (5 mL) for catalyst precursor **2.5** and **2.6** and $H_2O$ (5 mL) for catalyst precursor **2.7** and **2.8**, 1-octene (0.805 g, 7.175 mmol), internal standard *n*-decane (0.204 g, 1.435 mmol) and catalyst loading ($2.87 \times 10^{-3}$ mmol). A drop of mercury was added, and the reactor was purged with nitrogen three times, followed by purging three times. with syngas. Catalyst to substrate ratio used was (1:2500). The reactions were carried out for 4 h at $75^0$C/40 bar and the data was analysed using GC-FID. Average error estimate: = ± 0.51.

The Mercury poisoning test was done by adding a drop of mercury into each reactor containing catalyst precursor at optimized conditions of 75 °C/40 bar for 4 h. A substantial drop in conversion from 95% to 54% was observed for catalyst precursor **2.5** and from 97% to 56% for catalyst precursor **2.6** (Table 2.3, entries 1 and 2), this suggests a combination of homogeneous and heterogeneous catalysis. However, no significant changes in conversion were observed with the water-soluble analogues **2.7** and **2.8** in the presence of mercury thereby suggesting a homogeneous catalytic system.

## 2.3 Summary

In this chapter, alpha-diimine ligands (**2.1** and **2.2**) and disulfonated α-diimine ligands (**2.3** and **2.4**) were successfully synthesized and isolated in good yields. The compounds (**2.1** – **2.4**) were characterised using an array of spectroscopic and analytical techniques. The ligands (**2.1** – **2.4**) were complexed with the suitable rhodium precursor ($[Rh(COD)(MeCN)_2]BF_4$) to give the respective Rh(I) Schiff-base complexes (**2.5** – **2.8**). The disulfonated α-diimine Rh(I) complexes **2.7** and **2.8** are highly soluble in water and stable at room temperature. $^1$H, $^{13}C\{^1H\}$ NMR spectroscopy, infrared spectroscopy and mass spectrometry (positive-ion mode) were used to confirm the integrity of the compounds synthesised (**2.1** – **2.8**). The efficiency of the water-soluble complexes was evaluated as catalyst precursors in the aqueous hydroformylation of 1-octene and compared to those of their non-water-soluble analogues. Excellent conversion of 1-octene to aldehydes with higher turnover frequencies and good chemo- and regioselectivities were observed using catalyst precursors **2.7** and **2.8**. The recyclability tests revealed that the water-soluble catalyst precursors can be reused up to four times with a loss in catalytic activity observed after the third run. In addition, the mercury drop test using catalyst

precursors **2.7** and **2.8** confirmed the absence of any nanoparticles and that the active catalytic species are molecularly distributed in the reaction medium (homogeneously catalysis).

## 2.4 References


1 C. Van Leeuwen, Piet W.N.M., Claver, *Rhodium Catalyzed Hydroformylation: Introduction to hydroformylation*, Kluwer Academic Publishers, Dordrecht, 2000.

2 B. Breit, in *Recent Advances in Alkene Hydroformylation*, ed. M. J. Krische, Springer Berlin Heidelberg, 2007, pp. 139–172.

3 H. U. Blaser, A. Indolese and A. Schnyder, *Curr. Sci.*, 2000, **78**, 1336–1344.

4 M. Schmidt, B. Blom, T. Szilvási, R. Schomäcker and M. Driess, *Eur. J. Inorg. Chem.*, 2017, **2017**, 1284–1291.

5 I. Vural Gürsel, T. Noël, Q. Wang and V. Hessel, *Green Chem.*, 2015, **17**, 2012–2026.

6 S. G. Manjunatha, P. Rangappa, S. Sythana, S. M. Babu, K. Tadiparthi and C. Gundala, *Green Chem. Lett. Rev.*, 2013, **6**, 77–87.

7 S. M. Nobre, S. I. Wolke, R. G. da Rosa and A. L. Monteiro, *Tetrahedron Lett.*, 2004, **45**, 6527–6530.

8 X. Cui, W. Li, P. Ryabchuk, K. Junge and M. Beller, *Nat. Catal.*, 2018, **1**, 385–397.

9 O. Wachsen, K. Himmler and B. Cornils, *Catal. Today*, 1998, **42**, 373–379.

10 P. J. Dyson, D. J. Ellis and T. Welton, *Platin. Met. Rev.*, 1998, **42**, 135–140.

11 J. Zhou, X. Guo, C. Tu, X. Li and H. Sun, *J. Organomet. Chem.*, 2009, **694**, 697–702.

12 M. Benatmane, K. Cousin, N. Laggoune, S. Menuel, E. Monflier, P. Woisel, F. Hapiot and J. Potier, *ChemCatChem*, 2018, **10**, 5306–5313.

13 G. Fremy, R. Grzybek, E. Monflier, A. Mortreux, A. M. Trzeciak and J. Ziolkowski, *J. Organomet. Chem.*, 1995, **505**, 11–16.

14 E. Monflier, S. Tilloy, G. Fremy, Y. Barbaux and A. Mortreux, *Tetrahedron Lett.*, 1995, **36**, 387–388.

15 A. Cocq, H. Bricout, F. Djedaïni-Pilard, S. Tilloy and E. Monflier, *Catalysts*, 2020, **10**, 56.

16 M. Dauchy, M. Ferreira, J. Leblond, H. Bricout, S. Tilloy, G. S. Smith and E. Monflier, *Pure Appl. Chem.*, 2018, **90**, 845–855.

17 R. A. Sheldon, *J. R. Soc. interface*, 2016, **13**, 1–7.

18 V. Ravichandran, *J. Young Pharm.*, 2018, **10**, 131.

19 U. Chanshetti, *Int. J. Adv. Res. Chem. Sci.*, 2014, **1**, 110–115.

20 J. N. H. Reek, S. Arévalo, R. van Heerbeek, P. C. J. Kamer and P. W. N. M. van Leeuwen, *Adv. Catal.*, 2006, **49**, 71–151.

21 K. V Katti, H. Gali, C. J. Smith and D. E. Berning, *Am. Chem. Soc.*, 1999, **32**, 9–17.

22 S. Siangwata, N. Baartzes, B. C. E. Makhubela and G. S. Smith, *J. Organomet. Chem.*, 2015, **796**, 26–32.

23 S. K. Sharma and R. V. Jasra, *Catal. Today*, 2015, **247**, 70–81.

24 L. Obrecht, P. C. J. Kamer and W. Laan, *Catal. Sci. Technol.*, 2013, **3**, 541–551.

25 B. Cornils, *Org. Process Res. Dev.*, 1998, **2**, 121–127.

26 L. Maqeda, B. C. E. Makhubela and G. S. Smith, *Polyhedron*, 2015, **91**, 128–135.

27 E. B. Hager, B. C. E. Makhubela and G. S. Smith, *Dalton Trans.*, 2012, **41**, 13927.

28 S. Siangwata, N. C. C. Breckwoldt, N. J. Goosen and G. S. Smith, *Appl. Catal. A Gen.*, 2019, **585**, 117–179.

29 C. Williams, M. Ferreira, E. Monflier, S. Mapolie and G. S. Smith, *Dalton Trans.*, 2018, **47**, 9418–9429.

30 T. A. es Vitor Rosa, Carla I. M. Santos, Richard Welter, Gabriel Aullon, Carlos Lodeiro, *Inorg. Chem.*, 2010, **49**, 8699–8708.

31 Y. Zhao, Y. Liu, Q. S. Li and J. H. Su, *Dalton Trans.*, 2016, **45**, 246–252.

32 S. Dai, S. Zhou, W. Zhang and C. Chen, *Macromolecules*, 2016, **49**, 8855–8862.

33 X. Sui, C. Hong, W. Pang and C. Chen, *Mater. Chem. Front.*, 2017, **1**, 967–972.

34 F. Z. Wang, S. S. Tian, R. P. Li, W. M. Li and C. Le Chen, *Chinese J. Polym. Sci.*, 2017, **36**, 157–162.

35 G. A. Grasa, A. C. Hillier and S. P. Nolan, *Org. Lett.*, 2001, **3**, 1077–1080.

36 M. E. Hanhan, *Appl. Organomet. Chem.*, 2008, **22**, 270–275.

37 J. Zhou, X. Li and H. Sun, *Can. J. Chem.*, 2011, **8**, 782–790.

38 F. Fini, M. Beltrani, R. Mancuso, B. Gabriele and C. Carfagna, *Adv. Synth. Catal.*, 2015, **357**, 177–184.

39 L. Gonsalvi, J. A. Gaunt, H. Adams, A. Castro, G. J. Sunley and A. Haynes, *Organometallics*, 2003, **22**, 1047–1054.

40 S. A. Svejda and M. S. Brookhart, *Organometallics*, 1999, **18**, 65–74.

41 S. Ernst and W. Kaim, *J. Am. Chem. Soc.*, 1986, **108**, 3578–3586.

42 C. O. Brien, M. Y. Wong, D. B. Cordes, A. M. Z. Slawin and E. Zysman-colman, *Organometallics*, 2015, **34**, 13–22.

43 W. C. Anderson, S. H. Park, L. A. Brown, J. M. Kaiser and B. K. Long, *Inorg. Chem.*

*Front.*, 2017, **4**, 1108–1112.

44 F. Y. Zhang, X. B. Lan, C. Xu, H. G. Yao, T. Li and F. S. Liu, *Org. Chem. Front.*, 2019, **6**, 3292–3299.

45 L. Zhu, D. Zang, Y. Wang, Y. Guo, B. Jiang, F. He, Z. Fu, Z. Fan, M. A. Hickner, Z. K. Liu and L. Q. Chen, *Organometallics*, 2017, **36**, 1196–1203.

46 L. K. Johnson, C. M. Killian and M. Brookhart, *J. Am. Chem. Soc.*, 1995, **117**, 6414–6415.

47 D. P. Gates, S. A. Svejda, E. Onate, C. M. Killian, L. K. Johnson, P. S. White and M. Brookhart, *Macromolecules*, 2000, **33**, 2320–2334.

48 L. Biancalana, L. K. Batchelor, T. Funaioli, S. Zacchini, M. Bortoluzzi, G. Pampaloni, P. J. Dyson and F. Marchetti, *Inorg. Chem.*, 2018, **57**, 6669–6685.

49 E. C. I. Matei, T. Lixandru, *Bul. Institutului Politeh. din Iasi*, 1960, **6**, 171–176.

50 S. Hossain, P. Kanti Roy, K. Zahan and C. Zakaria, *Int. J. Chem. Stud.*, 2018, **6**, 19–31.

51 E. H. Cordes and W. P. Jencks, *J. Am. Chem. Soc.*, 1962, **84**, 832–837.

52 Y. C. Chan, A. Salhin, M. K. Mohamed Ali and B. Salleh, *J. Cryst. Process Technol.*, 2013, **3**, 69–73.

53 J. Wang, R. Ganguly, L. Yongxin and H. Sen Soo, *Inorg. Chem.*, 2017, **56**, 7811–7820.

54 S. Anga, T. Pal, R. K. Kottalanka, M. Paul and T. K. Panda, *canchemtrans*, 2013, **1**, 105–115.

55 M. Gasperini, F. Ragaini and S. Cenini, *Organometallics*, 2002, **12**, 2950–2957.

56 X. Yu, F. Zhu, D. Bu and H. Lei, *RSC Adv.*, 2017, **7**, 15321–15329.

57 V. Rosa, T. Avile, G. Aullon, B. Covelo and C. Lodeiro, *Inorg Chem.*, 2008, **47**, 7734–7744.

58 O. O. B. Soile, *Int. J. Adv. Res. Technol.*, 2014, **3**, 81–98.

59 T. Rawner, M. Knorn, E. Lutsker, A. Hossain and O. Reiser, *J. Org. Chem.*, 2016, **81**, 7139−7147.

60 J. H. Flanagan, S. H. Khan, S. Menchen, S. A. Soper and R. P. Hammer, *Bioconjug. Chem.*, 1997, **8**, 751–756.

61 D. Wieczorek, A. Dobrowolski, K. Staszak, D. Kwaśniewska and P. Dubyk, *J. Surfactants Deterg.*, 2017, **20**, 151–158.

62 G. M. T. Smith, P. M. Burton and C. D. Bray, *Angew. Chem. Int. Ed.*, 2015, **54**, 15236–15240.

63 V. Sikervar, *e-EROS Encycl. Reagents Org. Synth.*, 2014, **3**, 1–4.

64 Shovan Mondal, *Chem. Rev.*, 2012, **112**, 5339–5355.

65 B. Li, W. Yan, C. Zhang, Y. Zhang, M. Liang, F. Chu, Y. Gong, B. Xu, P. Wang and H. Lei, *Molecules*, 2015, **20**, 4307–4318.

66 B. Oelkers and J. Sundermeyer, *Dalton Trans.*, 2011, **40**, 12727–12741.

67 L. C. Matsinha, S. F. Mapolie and G. S. Smith, *Dalton Trans.*, 2015, **3**, 1240–1248.

68 M. Hashemihezaveh, K. Mahanpoor and D. Soudbar, *Pet. Sci. Technol.*, 2015, **33**, 473–480.

69 A. M. Kluwer, M. J. Krafft, I. Hartenbach, B. de Bruin and W. Kaim, *Top. Catal.*, 2016, **59**, 1787–1792.

70 C. Van Leeuwen, Piet W.N.M., Claver, in *Rhodium catalyzed hydroformylation*, Kluwer Academic Publishers, Dordrecht, 2000.

71 A. Stefani, G. Consiglio, C. Botteghi and P. Pino, *J. Am. Chem. Soc.*, 1973, **95**, 6504–6505.

72 P. Dingwall, J. A. Fuentes, L. Crawford, A. M. Z. Slawin, M. Bühl and M. L. Clarke, *J. Am. Chem. Soc.*, 2017, **139**, 15921–15932.

73 G. G. Stanley, in *Kirk-Othmer Encyclopedia of Chemical Technology*, John Wiley & Sons, Inc., 2017, p. 8.

74 L. C. Matsinha, S. Siangwata, G. S. Smith and B. C. E. Makhubela, *Catal. Rev. Sci. Eng.*, 2019, **61**, 111–133.

75 M. Kumar, R. V. Chaudhari, B. Subramaniam and T. A. Jackson, *Organometallics*, 2014, **33**, 4183–4191.

76 J. Hjortkjaer, *Mol. Catal.*, 1979, **5**, 377–384.

77 S. S. Nurttila, P. R. Linnebank, T. Krachko and J. N. H. Reek, *ACS Catal.*, 2018, **8**, 3469–3488.

78 Y. li Liu, J. gui Zhao, Y. jiang Zhao, H. M. Liu, H. yan Fu, X. li Zheng, M. lin Yuan, R. xiang Li and H. Chen, *RSC Adv.*, 2019, **9**, 7382–7387.

79 S. Paganelli, O. Piccolo, F. Baldi, M. Gallo, R. Tassini, M. Rancan and L. Armelao, *Catal. Commun.*, 2015, **71**, 32–36.

80 J. K. Dunleavy, *Platin. Met. Rev.*, 2006, **50**, 156.

81 V. M. Chernyshev, A. V. Astakhov, I. E. Chikunov, R. V. Tyurin, D. B. Eremin, G. S. Ranny, V. N. Khrustalev and V. P. Ananikov, *ACS Catal.*, 2019, **9**, 2984–2995.

82 P. Forzatti and L. Lietti, *Catal. Today*, 1999, **52**, 165–181.

# Chapter 3

## Synthesis, characterization and application of Rh(I) alpha-diimine-cored aryl ether metallodendrimers as catalyst precursors in the hydroformylation of olefins

This chapter has been published as: Hydroformylation of olefins using redox-active rhodium(I) alpha-diimine-cored aryl ether metallodendrimers. **N. N. Omosun**, S. Ngubane and G. S. Smith. *Applied Catalysis A, General.* 2021, 610, 117950.

### 3.1 Introduction

The formation of isomeric product mixtures (linear/branched aldehydes and isomerised alkenes) in the hydroformylation reaction has stimulated the research towards highly active and selective catalysts. The design of catalysts which are regioselective towards linear aldehydes is desirable due to their plethora of applications.[1–5] Over the past few decades, research aimed at improving the hydroformylation reaction has focussed on ligand modification,[6,7] reaction kinetics,[8–10] varying ligand-to-catalyst mole ratio and the use of two-phase solvent systems.[11–13] It has been established that the steric and electronic attributes of the ligand coordinated to the rhodium centre influences the regio-discriminating ability of a hydroformylation catalyst to a considerable extent.[14–18] Bulky donor ligands induce steric constraints that favour the anti-Markovnikov addition pathway and thus makes the catalyst more selective towards the formation of linear aldehydes.

Dendrimers are hyperbranched radially symmetric class of polymers. Their chemistry is one of the most rapidly emerging areas of modern chemistry.[19–21] Since the first report of the synthesis of dendritic molecules by Fritz Vogtle in 1978, there has been increased attention and exigent demand for dendrimers with unique properties.[22] As a result of their distinct structural topology and polyfunctionality, dendrimers have been successfully applied as catalysts,[23–26] as novel materials,[27–29] light harvesting systems,[30–32] and as drug delivery agents in nanomedicine.[33–36] Dendrimers display hierarchical conformational ordering at various stages of their growth, eventually reaching globular conformations at higher generations.[37–39] An increase in the degree of branching of dendrimers exponentially increases the functionalities at the periphery, this impacts on their physical and chemical properties. Therefore, important differences exist

between the overall shape of low and high generation dendrimers. In catalysis, dendrimers offer precise locations for catalytic sites, i.e. at the dendron focal point, at the core, at the interior framework/intersections or at the branch termini (periphery).[40] Core-functionalized dendrimers are of interest in catalysis because the encapsulation of the catalytic site at the core may impose certain properties such as enhanced stability through dielectric effects, increased selectivity through steric restrictions and proximal confinement of reacting species.[27,41–44] Metal-encapsulated dendrimers has been applied in a broad range of catalytic reactions such as metal-catalyzed C–C bond formation and allylic oxidation, and the concept of sterics controlling selectivity has been investigated in these catalytic reactions.[45–50] However, the use of core-functionalize dendrimers in the hydroformylation reaction is often less explored due to the difficulty in encapsulating a single catalyst into a dendritic structure. There are few reports in the literature on the use of core-functionalized dendrimers for the hydroformylation reaction. An example is the Van Leeuwen's three generations of carbosilane dendrimers with different branching multiplicities possessing a rigid xanthene backbone at the core (Figure 3.1).

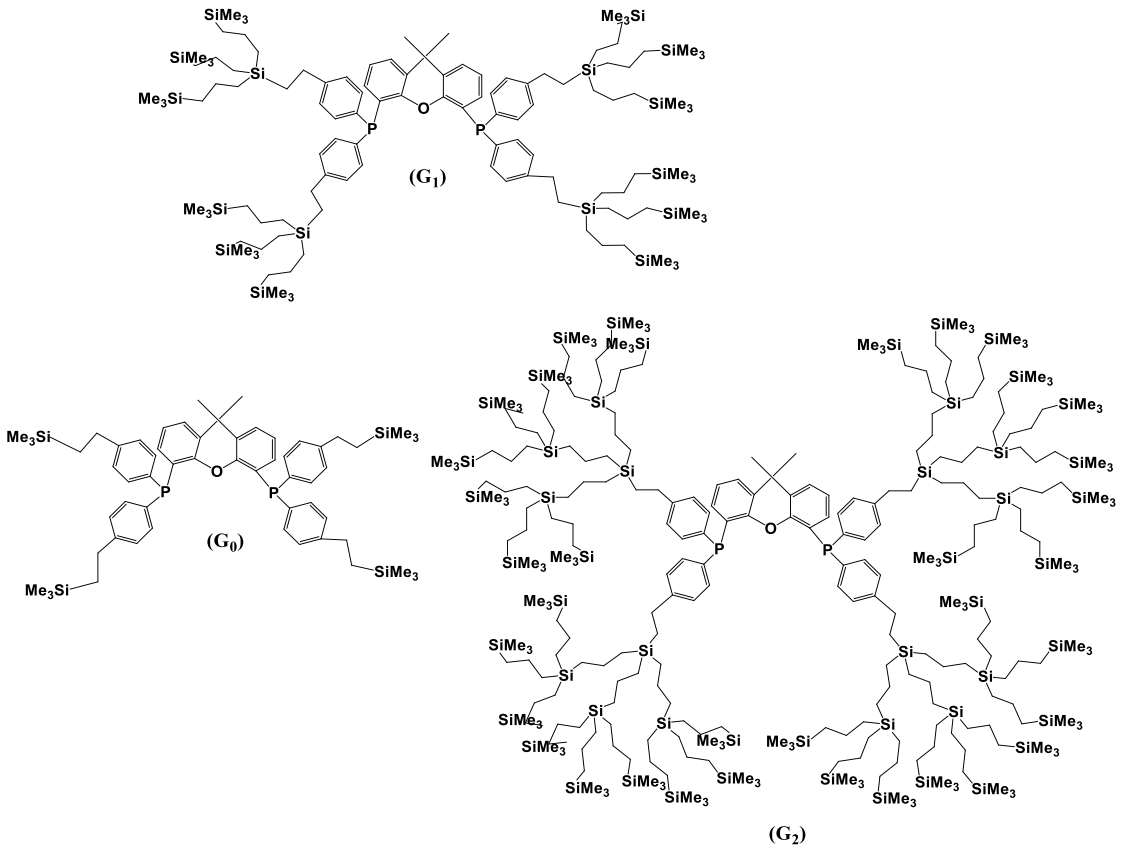


**Figure 3.1** Three generations of Van Leeuwen's core-functionalized carbosilane dendrimers with xantphos type ligands used for the hydroformylation of 1-octene.[51]

Despite the preferential application of the phosphine/diphosphine-based ligand system in the hydroformylation reaction, there has been great interest in investigating alternative ligand systems.[52–55] The α-diimine Schiff base ligand family are of interest due to their facile synthesis,[56] low cost and versatile coordination behaviour together with their strong δ-donor/π-acceptor properties.[57,58] The incorporation of dendritic wedges on the para hydroxy aryl site of the α-diimine ligand structure may enable the tuning of the intrinsic properties of the catalyst, as well as enhance the stability and selectivity of the catalyst.[59] In addition, the possibility of introducing substituents on the backbone of the α-diimine core provides more design options which may restrict the flexibility of the N=C–C=N skeleton and may impose some degree of stereocontrol around the metal centre.

This chapter expands the scope of complementary strategy in improving catalyst selectivity and in the synthesis of potential recyclable hydroformylation catalysts through ligand modification. Building up on the previous study from Chapter two on α-diimine Schiff-base Rh(I) complexes, the synthesis and characterization of three generations of core-functionalised α-diimine dendrimers and their corresponding Rh(I) complexes is described herein. The metallodendrimers were characterized using a range of spectroscopic techniques, such as $^{1}H$ and, $^{13}C\{^{1}H\}$ nuclear magnetic resonance (NMR) spectroscopy, Fourier-transform infrared (FTIR) spectroscopy and high-resolution mass spectrometry (HRMS). The metallodendrimers were evaluated as catalyst precursors in the hydroformylation reaction, using 1-octene and styrene as model substrates.

## 3.2 Results and discussion

### 3.2.1 Synthesis of first generation ($G_1$) Fréchet-type dendron wedge

The Fréchet-type dendron (**3.1**) was synthesised *via* the Williamson ether reaction following literature procedures (Scheme 3.1).[60] 3,5-Dihydroxybenzyl alcohol was reacted with two molar equivalents of methyl 4-(bromomethyl) benzoate in the presences of potassium carbonate and a catalytic amount of 18-crown-6 in acetone as illustrated in Scheme 3.1. The product (**3.1**) was isolated in good yields (78%).

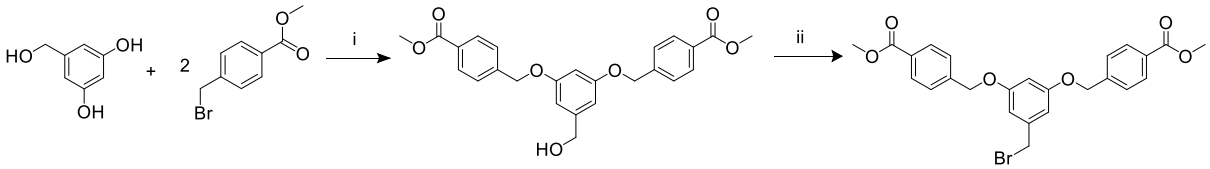


**Reagents and Conditions**
**(i)** $K_2CO_3$ / Acetone / 18-crown-6 / reflux / 24 h.
**(ii)** $CBr_4$ / $PPh_3$ /THF / r.t / 4 h.

**Scheme 3.2** Synthesis of Fréchet-type dendrons **3.1** and **3.2**.

Mechanistically, the Williamson ether reaction involves the formation of an alkoxide ion by the deprotonation of the alcohol by a base. This is followed by the nucleophilic attack on the alkyl halide, forming an ether. In this step, the bond cleavage and bond formation takes place simultaneously.[61–63] Notably, the Williamson ether synthesis is inefficient if the halides are sterically impeded.[64] Additionally, catalytic amount a phase-transfer agent (18-crown-6 ether) is usually added to enhance the solubility of the reagents or nucleophile in the organic solvent, consequently resulting in improved yields.[65,66]

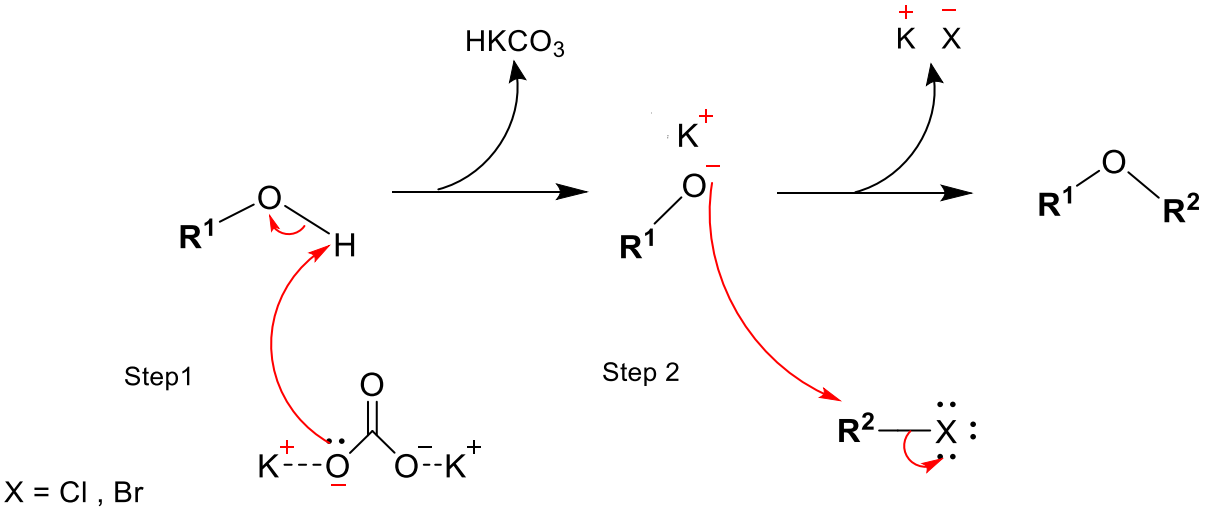


**Scheme 3.2** Proposed mechanism of the Williamson ether reaction.[67]

The benzylic alcohol product (**3.1**) was converted to the corresponding bromide compound **3.2** by reaction with carbon tetrabromide and triphenylphosphine *via* the Appel reaction in which alcohols are transformed into alkyl halides.

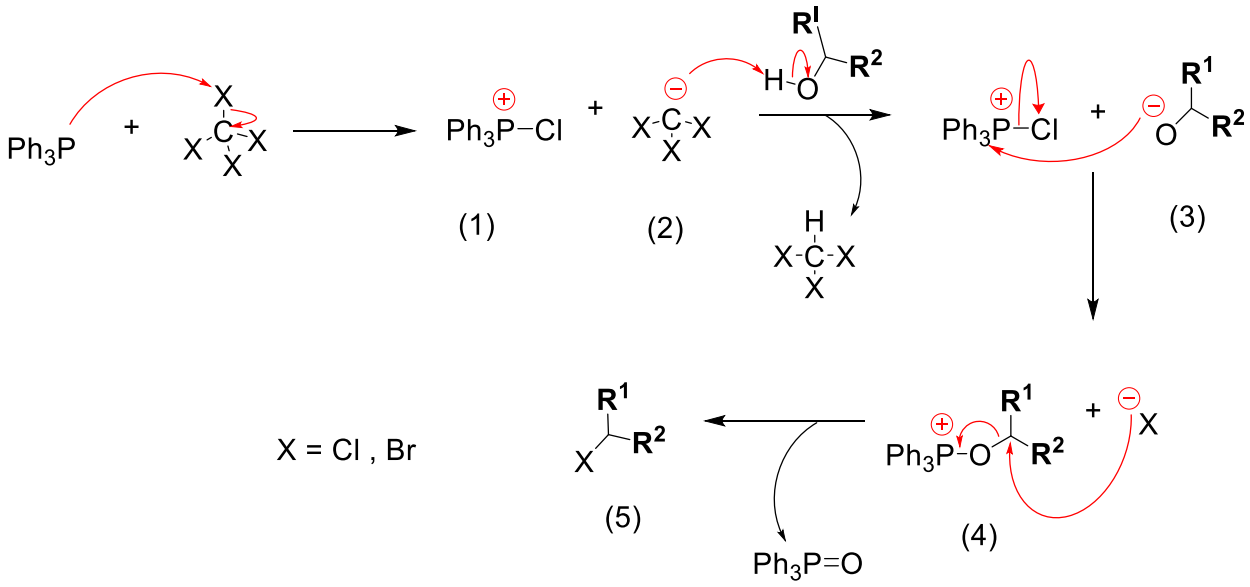


**Scheme 3.3** Proposed mechanism of the Appel reaction.[75]

The Appel reaction proceeds with the halogenation of triphenyl phosphine in the presence of a tetrahalomethane to form the phosphonium salt (1) followed by the proton abstraction of the alcohol by the trihalide-methyl anion (2) to form the alkoxide (3). The nucleophilic displacement of the halide by the alkoxide generates the oxyphosphonium intermediate (4). In a nucleophilic substitution reaction ($S_N2$), the halide (nucleophile) attacks the carbon stereocenter resulting in the alkyl halide product (5) and the triphenylphosphine oxide by-product.[68]

### 3.2.2 Characterization of first generation Fréchet-type dendron wedges ($G_1$)

***NMR spectroscopy***

The $^1$H NMR spectrum of compound **3.1**, shown in Figure 3.2, displays the typical AA'BB' quartet signal for external 1,4-disubstituted aryl ring in the range 7.98 – 7.38 ppm. The internal 1,3,5-trisubstituted aryl proton signals are observed in the range 6.54 – 6.43 ppm. These protons appear as a doublet (H-3) and triplet (H-4) which is often observed for 1,3,5-trisubstituted aryl systems ($AB_2$ long-range coupling) with a coupling constant of 2.2 Hz. The methylene proton *para* to the external aryl rings appears as a singlet at 5.01 ppm, integrating for four protons, while the methylene protons adjacent to the hydroxy group are observed at 4.55 ppm as a singlet, integrating for two protons. The methyl proton was observed at the expected chemical shift of 3.84 ppm as a distinct singlet, integrating for six protons. The $^1$H NMR spectrum of compound **3.2** (the halogenated product) displays similar signals to compound **3.1**. As

expected, there is an upfield shift of the methylene proton signal H-2 from 4.55 ppm to 4.32 ppm. This shift is attributed to the less electron-withdrawing character of the bromide functional group in comparison to the oxygen of the hydroxy group that is directly bonded to the methylene carbon.

The $^{13}C\{^{1}H\}$ NMR spectra of compounds **3.1** and **3.2** displays the expected number of carbon signals, consistent with the proposed structures. The methylene carbon and methoxy carbon signals are observed between 52.09 – 69.92 ppm. Signals corresponding to the external 1,4-disubstituted aryl rings are observed as two distinct signals at 130.02 ppm and 127.17 ppm respectively. Additionally, the signal for the of the ester group (C=O) resonates at 166.76 ppm.

***Infrared spectroscopy***

Infrared spectra of compounds **3.1** and **3.2** were recorded in the solid state using the ATR sampling technique. The characteristic phenolic *v*(ArO-H) vibrations at 3150 $cm^{-1}$ of 3,5-dihydroxybenzyl alcohol was not observed in the IR spectrum of compound **3.1**. The presence of characteristic ester *v*(C=O) absorption band at 1720 $cm^{-1}$ attest to successful dialkylation of 3,5-dihydroxybenzyl alcohol to afford compound **3.1**. Additionally, the presence of a broad band at 3520 $cm^{-1}$ is indicative of the benzylic *v*(O-H). Comparing the IR spectra of compounds **3.1** and **3.2**, the absence of the benzylic *v*(O-H) broad band at 3520 $cm^{-1}$ in the IR spectrum of **3.2** confirms the bromination of compound **3.1**.

### 3.2.3 Synthesis of second generation($G_2$) Fréchet-type dendron wedge

The Fréchet-type dendron (**3.3**) with four ester groups at the periphery was synthesised by reacting 3,5-dihydroxybenzylic alcohol with two molar equivalents of compound **3.2** *via* the Williamson ether reaction in the presence of potassium carbonate and a catalytic amount of 18-crown-6 in acetone. Subsequent halogenation of compound **3.3** *via* the Appel reaction resulted in the corresponding brominated compound (**3.4)** (Scheme 3.4).

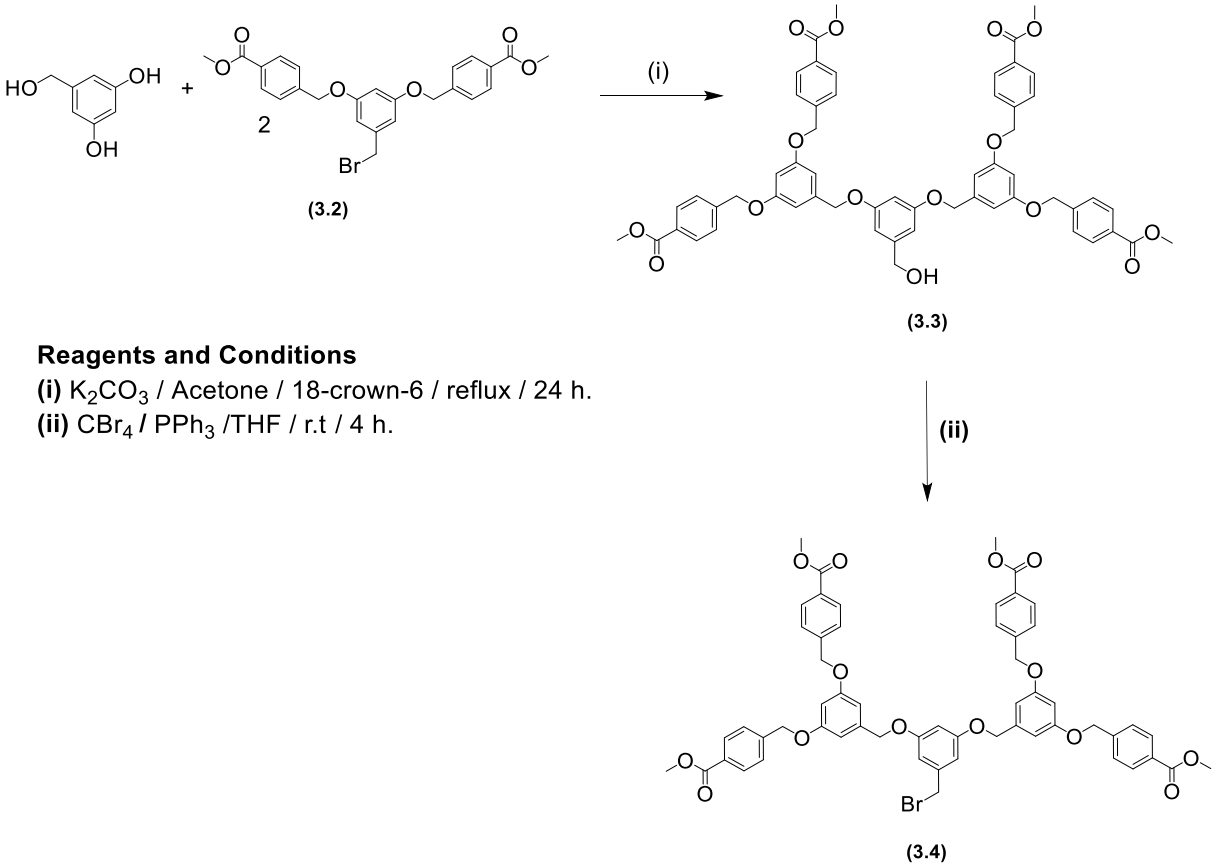


**Scheme 3.4** Synthesis of Fréchet-type dendrons **3.3** and **3.4**.

### 3.2.4 Characterization of second generation ($G_2$) Fréchet-type dendron wedges

***NMR spectroscopy***

The $^1$H NMR spectra of the second generation Fréchet-type dendron **3.3** and **3.4** display distinctive signals when compared to the first generation Fréchet-type dendron **3.1** and **3.2** (Figure 3.2). Two additional signals assigned to the new aryl ether moieties are observed in the region of 6.57 – 6.45 ppm and an additional methylene proton peak is observed at 4.89 ppm. The methylene proton signal of the brominated product (**3.4**) displays similar upfield shift to that of **3.2**. This is ascribed to the less electron-withdrawing character of the bromide moiety. The signal of the methoxy proton was used as a diagnostic signal to elucidate the spectra of the $G_2$ dendrons. The methoxy signal integrates for six protons for the first generation Fréchet-type dendron and twelve protons for the second generation Fréchet-type dendron. Also, the signal at 6.42 ppm (H-4) for $G_1$ and 6.37 ppm (H-3) for $G_2$ integrates for one proton across the dendron series.

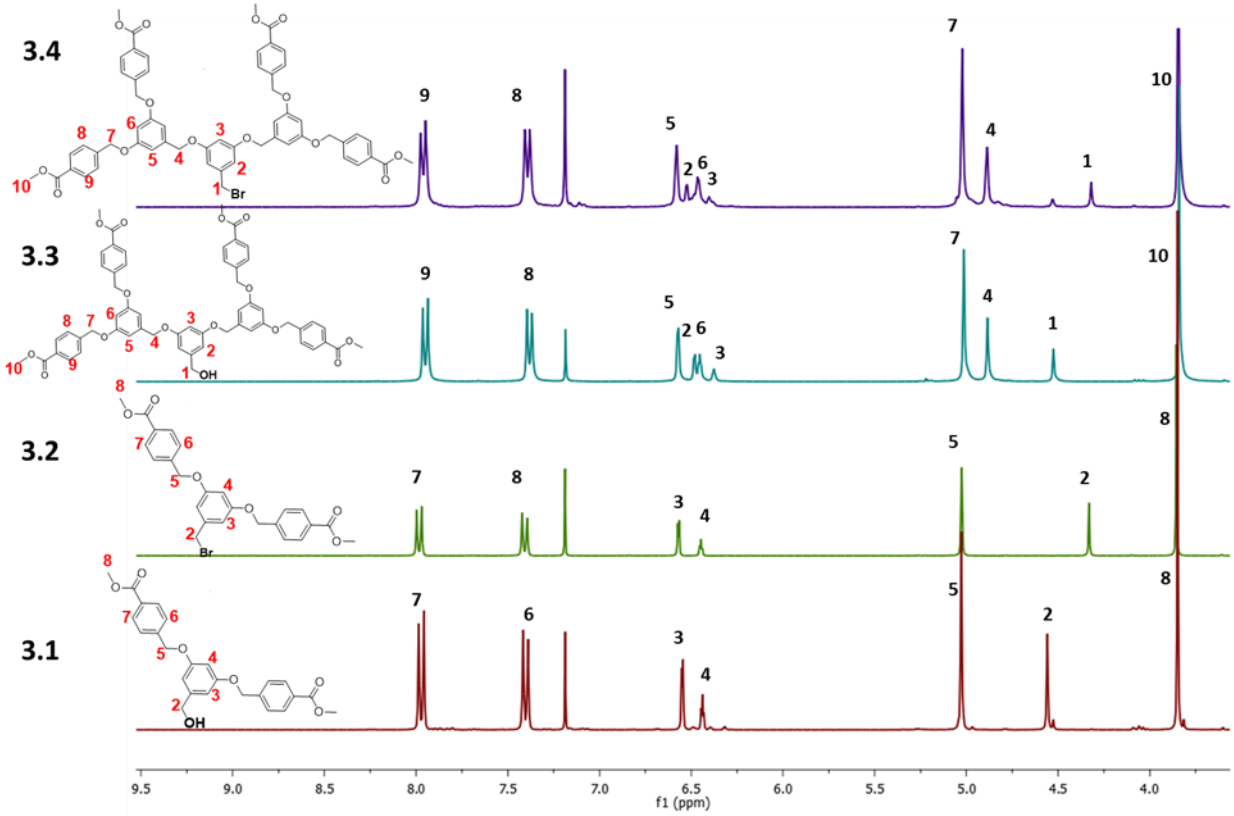


**Figure 3.2** $^{1}$H NMR spectra ($CDCl_3$) of Fréchet-type dendron series **3.1** – **3.4**.

***Infrared spectroscopy***

Similar to compounds **3.1** and **3.2**, the signal at 1720 $cm^{-1}$ corresponds to the characteristic ester *ν*(C=O) absorption band. The absence of the *ν*(O-H) vibration at 3511 $cm^{-1}$ indicates the successful functional group conversion of compound **3.3**. The spectroscopic data for these dendrons are in agreement with those reported in the literature.[69,70]

### 3.2.5 Synthesis of alpha-diimine poly(aryl ether) dendrimers

Three generations of poly(aryl ether) α-diimine dendrimers were synthesised using a convergent-growth strategy (Scheme 3.5). The α-diimine precursor ligands **2.1** and **2.2** were synthesised *via* a Schiff base condensation reaction as earlier reported in Chapter two (Section 2.2.1).

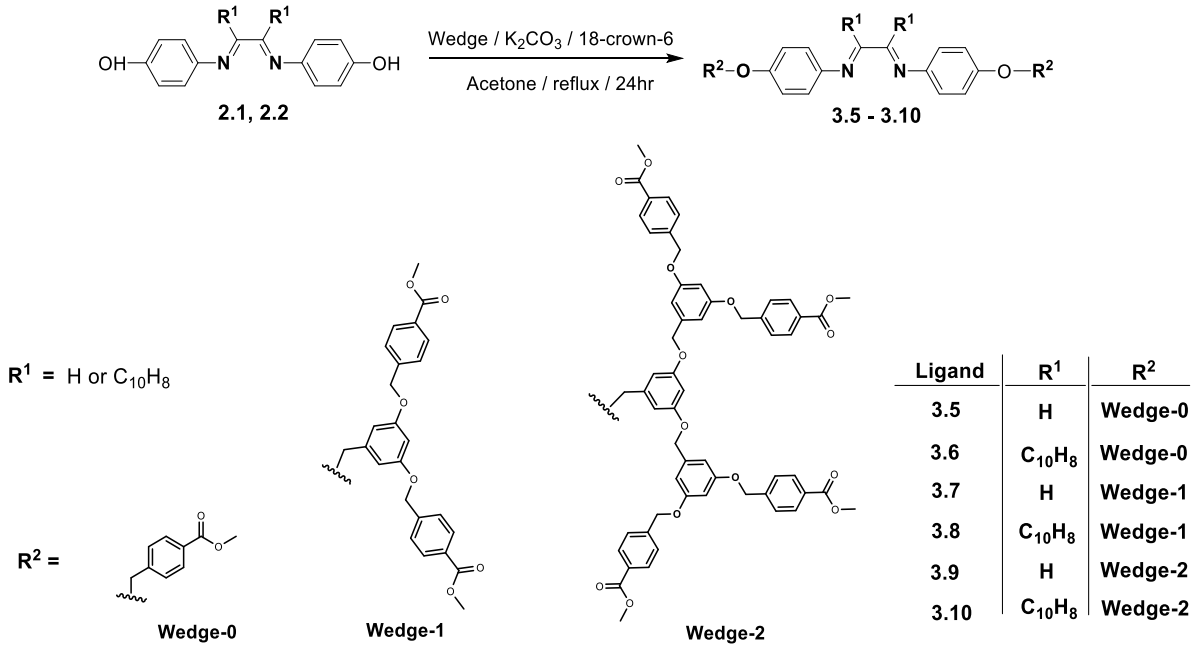


**Scheme 3.5** Synthesis of three generations of α-diimine poly(aryl ether) dendrimers **3.5** – **3.10**.

The reaction of the α-diimine precursor ligands **2.1** or **2.2** with methyl 4-(bromomethyl) benzoate in a Williamson ether reaction synthesis led to the formation of the $G_0$ α-diimine dendrimers **3.5** and **3.6**, with two ester groups at the periphery. The $G_1$ α-diimine dendrimers **3.7** and **3.8** were synthesised by reacting the precursor ligand **2.1 or 2.2** with the first generation Fréchet-type dendron **3.2** *via* the Williamson ether synthesis. Similarly, $G_2$ α-diimine dendrimers (**3.9** and **3.10**) were synthesised by reacting the ligand precursor **2.1** or **2.2** with the second generation Fréchet-type dendron **3.4,** as illustrated in Scheme 3.5. The dendrimers bearing ethyl backbone were isolated as yellow powders, while the dendrimers bearing the acenaphthene backbone were isolated as red powders.

### 3.2.6 Characterization of alpha-diimine poly(aryl ether) dendrimers

***NMR spectroscopy***

In the $^1$H NMR spectra of **3.5 – 3.10** (Figure 3.3 and 3.4), no phenolic signals at 9.78 ppm (**2.1)** and 9.41 ppm (**2.2)** were observed, this is indicative a successful deprotonation and the accompanying nucleophilic substitution with the respective dendrons, resulting in the formation of the poly aryl ether products **3.5** – **3.10**. The signal for the imine proton (H-C=N) was observed as a singlet at 8.33 ppm for compound **3.5** The signals representing the acenaphthene backbone protons for compound **3.6** were observed at 7.82 ppm, 7.38 ppm and 6.93 ppm. The signals for the internal phenyl protons in compound **3.6** appear as a singlet at

7.02 ppm due to the symmetrical nature of the molecule. Proton signals corresponding to the external aryl rings resonates as doublets at 8.00 ppm and 7.44 ppm for compound **3.5** and at 8.02 ppm and 7.50 ppm for compound **3.6**. The methylene and methoxy proton signals are observed as singlets at 5.09 and 3.86 ppm for compound **3.5** and at 5.13 and 3.86 ppm for compound **3.6**, respectively. The signals for the imine/acenaphthene core and the methoxy terminal group integrate in a 1:2 ratio. This further affirms the successful synthesis of the low generation dendrimers **3.5** and **3.6**.

Successful synthesis of first-generation ($G_1$) dendrimers **3.7** and **3.8** is evident by the presence of signals corresponding to the extended wedges. All the expected aromatic signals were observed in the appropriate region between 8.38 ppm and 6.48 ppm for compound **3.7** and between 7.99 ppm and 7.43 ppm for compound **3.8**. The methylene and methoxy protons were observed at 5.04 ppm and 3.84 ppm for compound **3.7**, and at 5.07 ppm and 3.85 ppm for compound **3.8**. The signals for the diagnostic imine/acenaphthene proton core and the methoxy terminal groups integrate in a 1:4 ratio.

Similar trends in splitting pattern and coupling constants were observed in the $^1$H NMR spectra of second-generation dendrimers **3.9** and **3.10** as that of the first-generation dendrimers**.** The diagnostic imine/acenaphthene proton core and the methoxy terminal signals integrate in a 1:8 ratio. In addition, as the generation of the dendrimer increases, a decrease in intensity of the signal corresponding to the α-diimine core is observed.

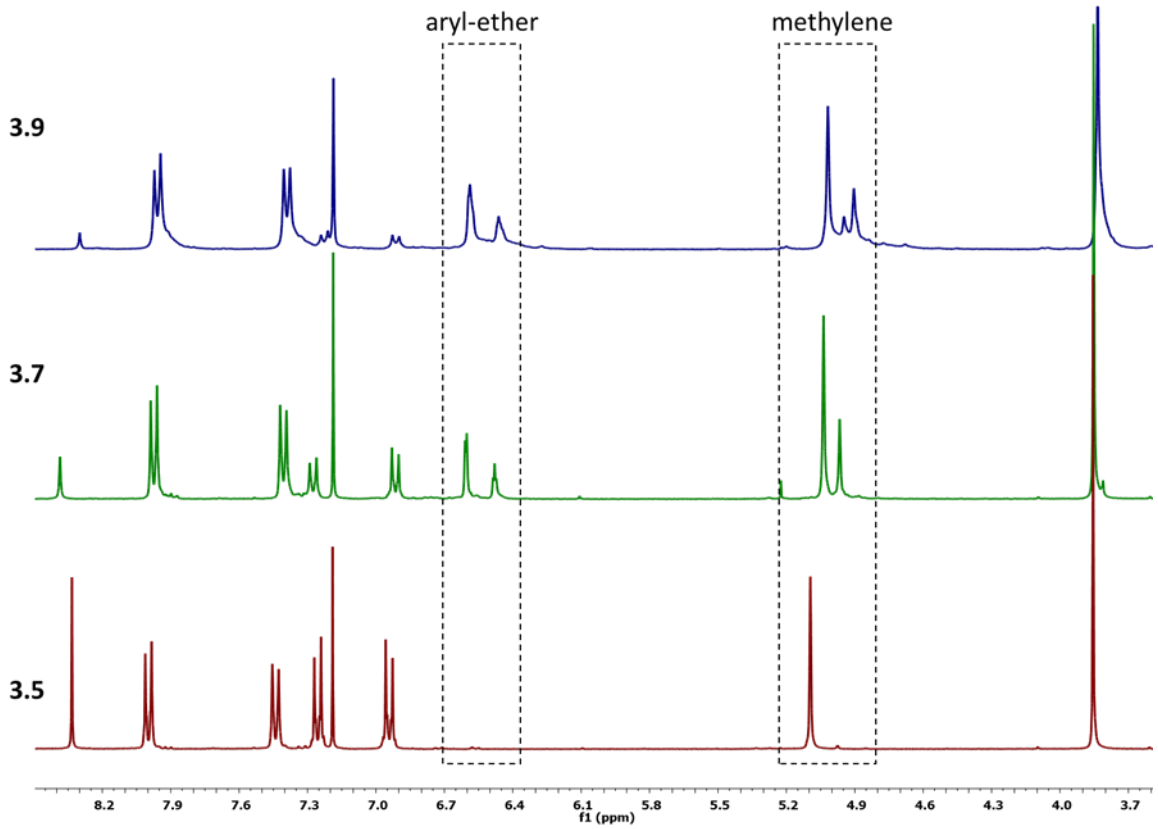


**Figure 3.3** Stacked $^{1}H$ NMR spectra ($CDCl_3$) of compound **3.5**, **3.7** and **3.9**.

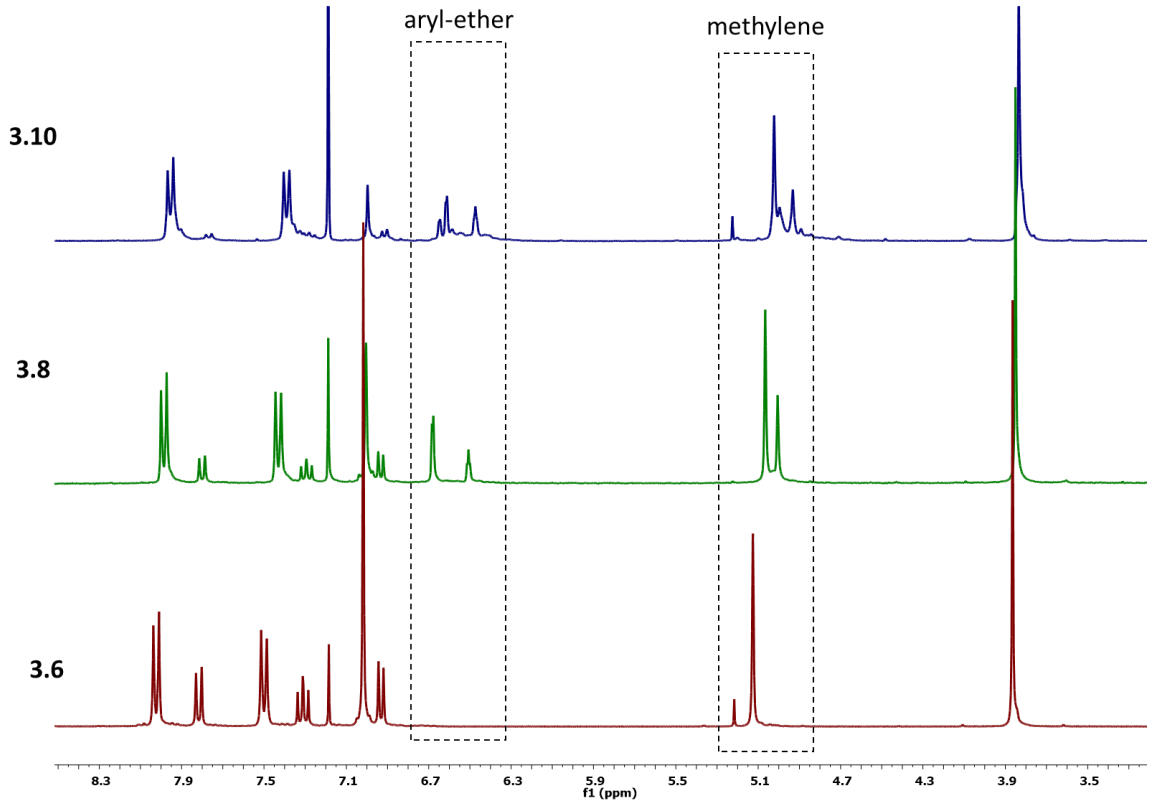


**Figure 3.4** Stacked $^{1}H$ NMR spectra ($CDCl_3$) of compound **3.6**, **3.8** and **3.10.**

The $^{13}C\{^{1}H\}$ NMR spectra of compounds **3.5** – **3.10** gave the expected number of carbon resonances, confirming the formation of the proposed structures. The signals for the imine carbons were observed in the range 154.93 – 159.95 ppm across the dendritic series.

***Infrared spectroscopy* and *Mass spectrometry***

FTIR spectral analysis was used to confirm the functional groups indicative of the formation of the desired compounds and the absorption bands are summarised in Table 3.1. The absorption band for the imine moieties are observed in the IR spectra for compounds **3.5** – **3.10**. The *ν*(C=N) vibration appears as a band of medium intensity in the region of 1611 – 1691 $cm^{-1}$. No phenolic *ν*(O-H) band at 3075 $cm^{-1}$ and 3289 $cm^{-1}$ were observed. This correlates with the $^{1}H$ NMR spectroscopic elucidation.

**Table 3.1** Infrared absorbances for compounds **3.5 – 3.10**.

| Compound | Wavenumber ($cm^{-1}$) | | |
|---|---|---|---|
| | C=O | C=N | C=C |
| **3.5** | 1768.59 | 1691.54 | 1573.78 |
| **3.6** | 1726.43 | 1661.10 | 1589.64 |
| **3.7** | 1714.53 | 1611.45 | 1588.54 |
| **3.8** | 1715.14 | 1651.10 | 1595.76 |
| **3.9** | 1716.51 | 1657.58 | 1597.57 |
| **3.10** | 1715.11 | 1662.99 | 1593.61 |

The masses of the alpha-diimine dendrimers were determined using ESI-MS. The mass spectra of compounds **3.5 – 3.8** and **3.10** reveal peaks corresponding to the protonated molecular ions $[M+H]^{+}$ as the base peak, while the spectrum of compounds **3.9** display peaks for the $[M+2H]^{2+}$ fragment. These results further confirm the structures of the desired compounds. The experimental and calculated *m/z* values are summarised in Table 3.2.

**Table 3.2** Determined *m/z* values and their corresponding calculated values for **3.5 – 3.10**.

| Compound | Found (*m/z*) | Calculated (*m/z*) |
|---|---|---|
| **3.5** | 537.2008 $[M+H]^+$ | 537.2025 |
| **3.6** | 661.2320 $[M+H]^+$ | 661.2338 |
| **3.7** | 1077.3798 $[M+H]^+$ | 1077.3809 |
| **3.8** | 1201.4121 $[M+H]^+$ | 1201.4122 |
| **3.9** | 1079.3376 $[M+2H]^{2+}$ | 1079.3722 |
| **3.10** | 2281.6196 $[M+H]^+$ | 2281.7691 |

### 3.2.7 Synthesis of Rh(I) alpha-diimine poly(aryl ether) metallodendrimers

The synthesis of the rhodium(I) 1,5-cyclooctadiene (COD) *N*,*N*-alpha-diimine aryl ether dendrimers involved two reactions. First, the preparation of the $[Rh(COD)(MeCN)_2]BF_4$ metal precursor, followed by the reaction of the metal precursor with the α-diimine dendritic ligands (**3.5 – 3.10**) to afford the core-functionalised rhodium(I) metallodendrimers (**3.11 – 3.16**), as depicted in Scheme 3.6. The complexes were isolated as stable red powders in yields of 52 – 67%.

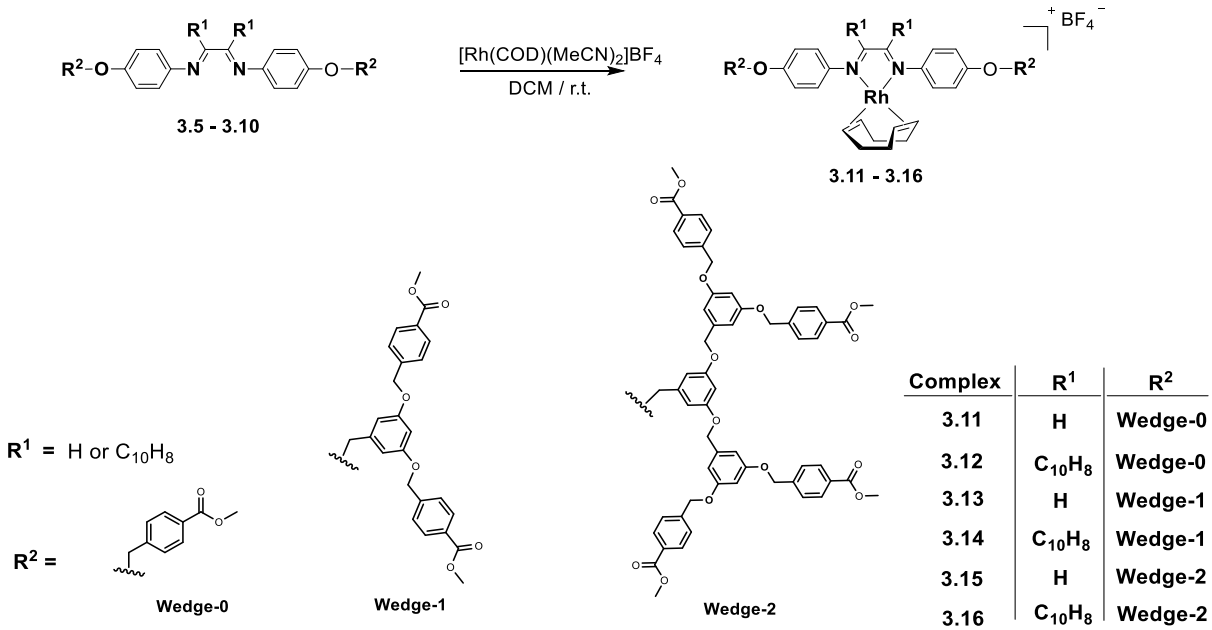


**Scheme 3.6** Synthesis of α-diimine-cored rhodium(I) metallodendrimers (**3.11** – **3.16**).

### 3.2.8 Characterization of Rh(I) alpha-diimine poly(aryl ether) metallodendrimers

***NMR spectroscopy***

All signals in the $^{1}$H NMR spectra of the metallodendrimers were assigned unambiguously by considering chemical shifts, integral ratios and data obtained from 2D NMR experiments. Evidence of successful complexation of the α-diimine dendrimer **3.5** were indicated by the upfield shift of the imine proton resonance from 8.33 ppm for compound **3.5** to 8.14 ppm in the $^{1}$H NMR spectrum of the complex **3.11** (Figure 3.5). This significant upfield shift is attributed to the increased electron density from the Rh metal to the imine nitrogen. Notably, four new signals ( H-8, H-10, H-9 and H-11) are observed in the $^{1}$H NMR spectrum of complex **3.11**. This corresponds to the chemically non-equivalent methylene protons (2.39 ppm, 1.82 ppm) and olefinic protons (4.32 ppm, 4.02 ppm) of the cyclooctadiene moiety. The splitting pattern of the olefinic signals is attributed to the *trans effect* induced by the chelating *N,N*-diimine moiety. This phenomenon has been observed with structurally similar bidentate Rh(COD) complexes.[71,72]

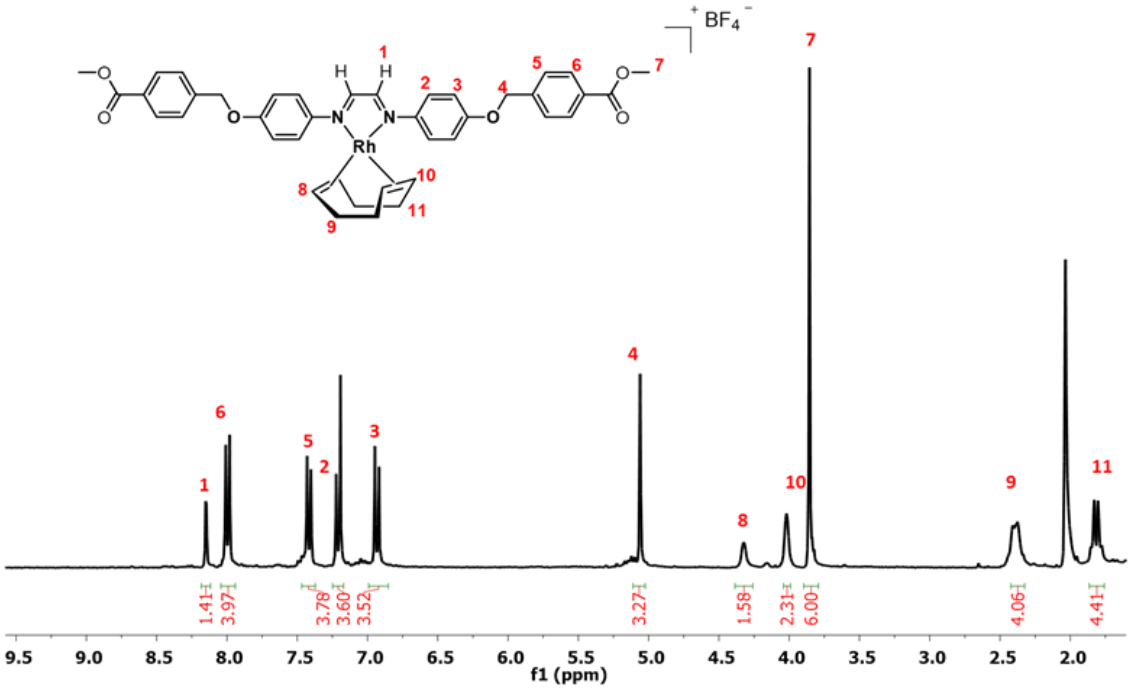


**Figure 3.5** $^{1}$H NMR spectrum of complex **3.11** in $CDCl_3$.

Comparing the $^{1}$H NMR spectra of ligand **3.6** and complex **3.12** (Figure 3.6), resonance shifts of the acenaphthene proton signals are observed, indicating successful metal coordination. There is a downfield shift in the signal of H-1 proton from 7.82 ppm to 7.95 ppm. An upfield shift was observed for acenaphthene proton H-3 from 6.93 ppm to 6.52 ppm. These shifts are attributed to the electronic influences upon coordination of the metal to the ligand. Trends in chemical shifts of the acenaphthene protons upon coordination are consistent with structurally similar complexes in literature.[73] Additionally, the protons H-4 and H-5 of the phenyl ring directly bonded to the imine nitrogen appear as quartet signals, alluding to the fluxionality resulting from the change from a symmetrical molecule to an asymmetrical molecule. Evidence of successful coordination is the presence of the olefinic (H-10) and methylene (H-11 and H-12) proton signals of the COD moiety (1.79 ppm – 4.00 ppm), each integrating for four protons.

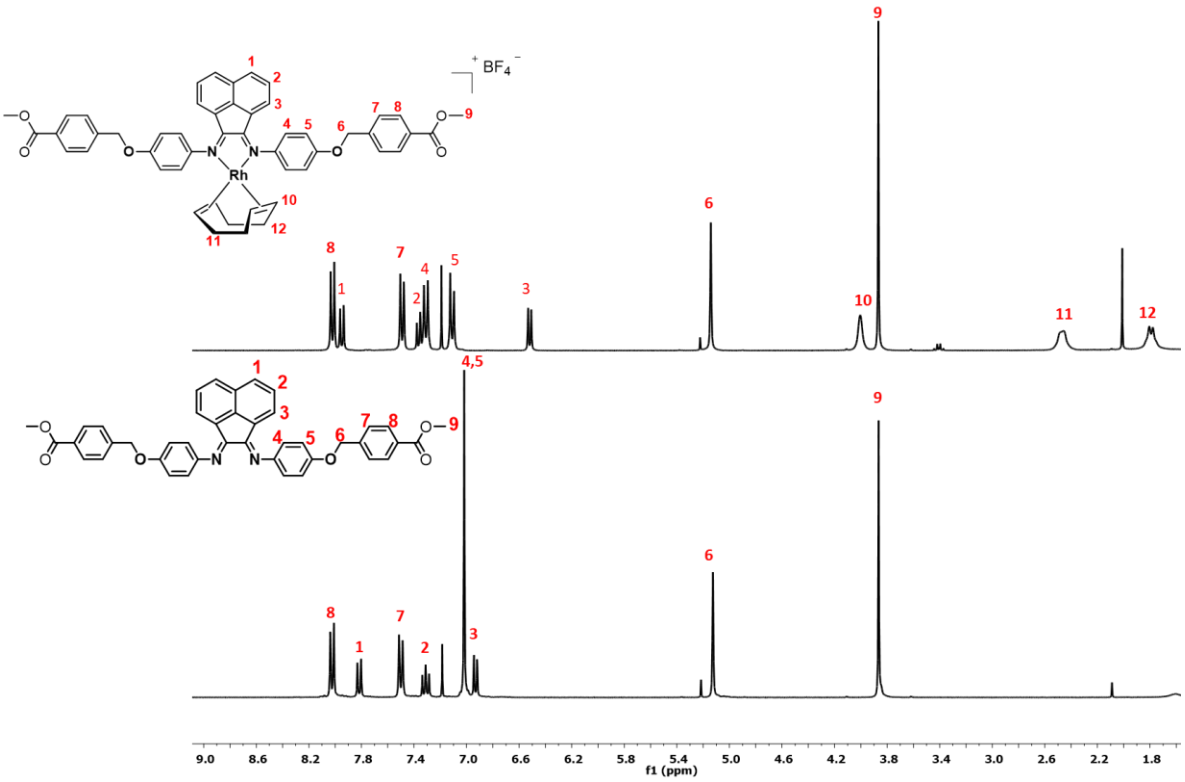


**Figure 3.6** Stacked $^{1}$H NMR spectra ($CDCl_3$) of ligand **3.6** and complex **3.12**.

For complex **3.13,** an upfield shift of the imine proton signal is observed from 8.42 ppm (for compound **3.7**) to 8.39 ppm and the signals for the olefinic and methylene COD moiety are observed at the expected region. Comparing the $^{1}$H NMR spectra of ligand **3.8** and complex **3.14** (Figure 3.7), a downfield resonance shift for the acenaphthene proton (H-1) from 7.80 ppm (for compound **3.8**) to 7.91 ppm, and an upfield shift for proton H-3 from 6.93 ppm to 6.48, are observed for complex **3.14**. Additionally, proton signals for the olefinic and

methylene COD moiety are observed at 1.79 – 4.01 ppm, for complex **3.13** and at 1.78 – 4.01 ppm for complex **3.14**.

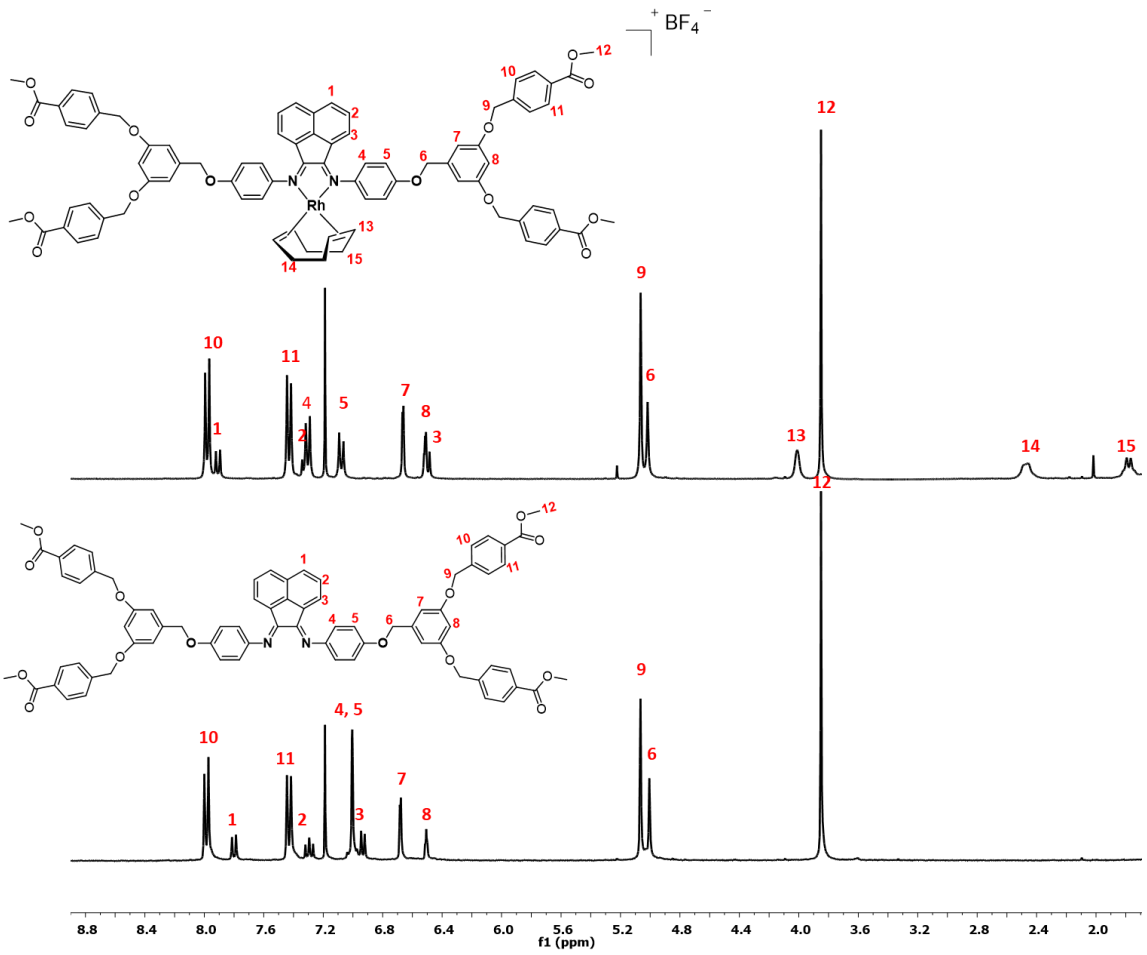


**Figure 3.7** Stacked $^{1}$H NMR spectra ($CDCl_3$) of ligand **3.8** and complex **3.14**.

Similar trends in imine and acenaphthene resonance shifts are observed upon coordination in the $^{1}$H NMR spectra of compounds **3.15** and **3.16** (Figure 3.8 and 3.9). Notably, resonance overlap, and broadened signals are observed for the higher generation metallodendrimers ($G_2$). This is attributed to the slow tumbling of larger macromolecules in solution resulting in faster relaxation of transverse magnetization (short *T2*).[74] The integration of these signals correlates with the number of protons in the proposed structures. Additionally, the olefinic and methylene COD signals, in the region of 1.69 – 4.15 ppm for compound **3.15** and 1.67 – 4.14 ppm for compound **3.16** provides further evidence of successful coordination.

The $^{13}$C{$^{1}$H} NMR spectra of the complexes display the expected number of carbon signals for each compound, further confirming the formation of the proposed structures. Additionally, the carbon signals corresponding to the COD moiety is observed in the region of 26.14 – 28.17

ppm for methylene COD protons and in the region of 82.55 – 85.97 ppm for the olefinic COD protons across the three generations metallodendrimers.

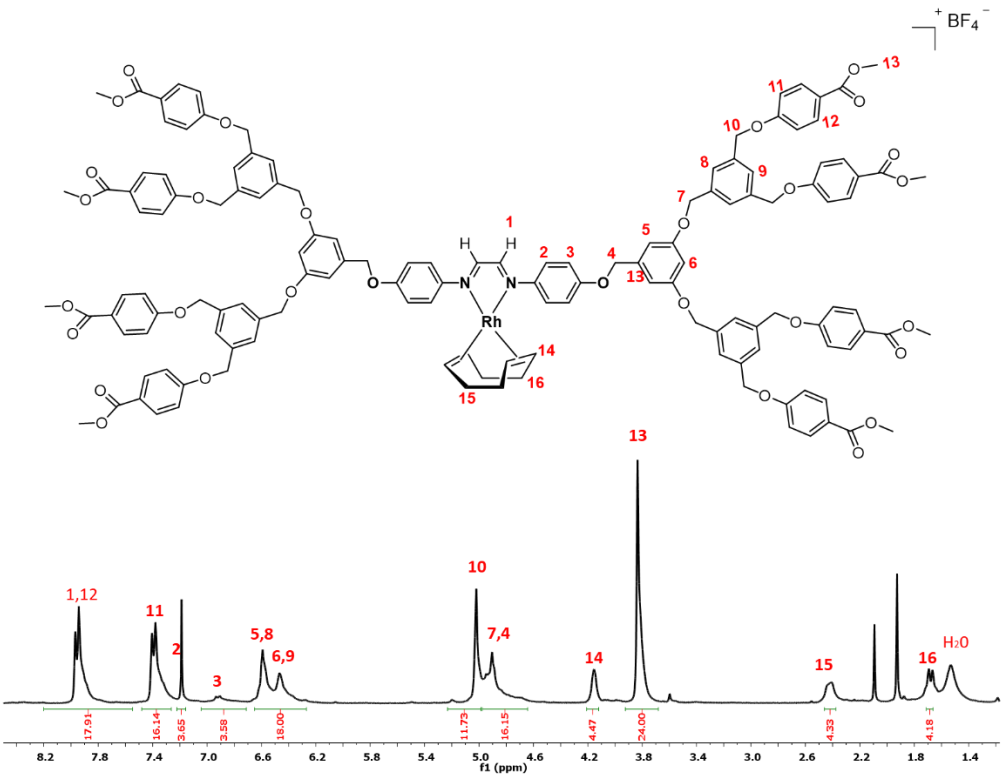


**Figure 3.8** $^{1}H$ NMR spectrum of complex **3.15** in $CDCl_3$.

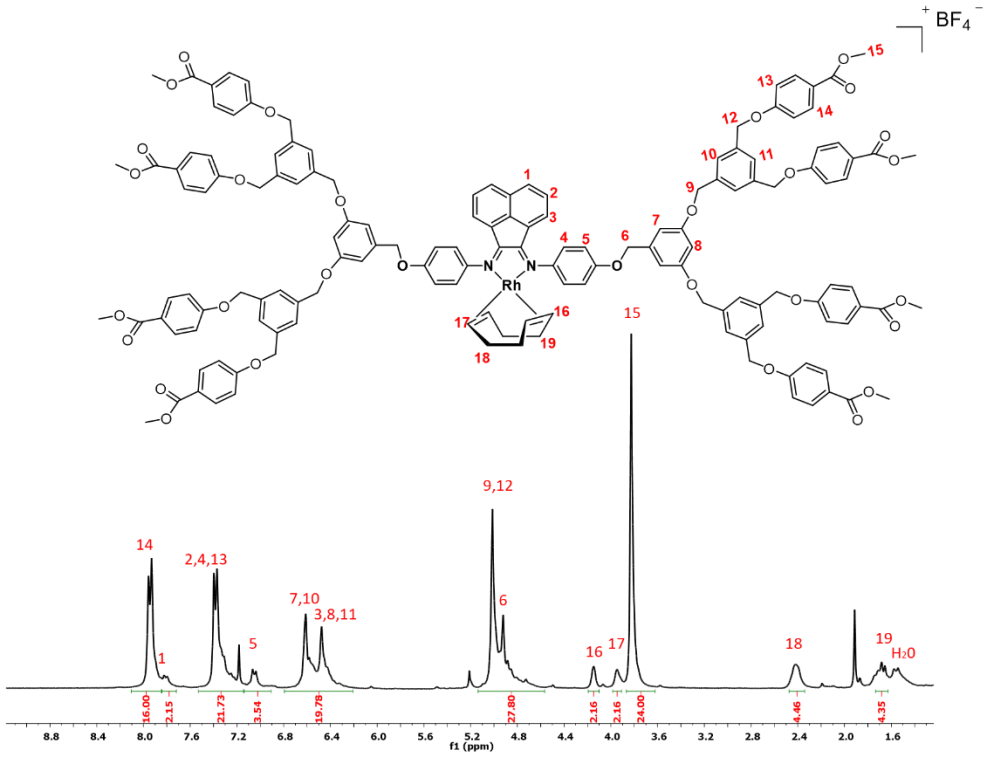


**Figure 3.9** $^{1}H$ NMR spectrum of complex **3.16** in $CDCl_3$.

***Infrared spectroscopy* and *Mass spectrometry***

The cooperation between the metal and the coordinating Schiff base ligands is unequivocally identified by shifts in vibrational frequencies of the *ν*(C=N) stretching bands. A decrease to lower wavenumbers of the imine bands is observed upon complexation. This is because of the synergistic effect involving ligand-to-metal sigma donation and metal-to-ligand pi backdonation which results in weakening of the imine bonds. Consequently, this lowers the imine stretching frequency. This observation further corroborates the coordination of the metal to the imine nitrogen atoms.

The mass spectra of compounds **3.11** and **3.13** reveal peaks corresponding to the ionized ammonium adduct $[M+NH_4]^+$ of the proposed structures, where M refers to the complex cation excluding the $BF_4^-$ counter-ion. The $[M+H]^+$ adduct was observed as the base peak for complex **3.12** (Figure 3.10). The mass spectrum of compound **3.14** reveals a peak corresponding to the molecular $[M+K]^+$ adduct, while the spectra of compounds **3.15** and **3.16** display peaks for the molecular adduct $[M+MeCN+Na]^{2+}$ and $[M+H+NH_4]^{2+}$adducts, respectively. These results further confirm the structures of the desired compounds. The experimental and calculated *m/z* values are summarised in Table 3.3.

**Table 3.3** Determined *m/z* values for **3.11 – 3.16** and Imine infrared absorptions bands ($cm^{-1}$) For (ligands) and complexes.

| Compound | ESI-MS Found (*m/z*) | IR imine ($cm^{-1}$) |
|---|---|---|
| **3.11** | 765.1935 $[M+NH_4]^+$ | 1675.77 (1691.54) |
| **3.12** | 871.2234 $[M+H]^+$ | 1643.21 (1661.10) |
| **3.13** | 1305.3751 $[M+NH_4]^+$ | 1611.45 (1601.14) |
| **3.14** | 1450.3705 $[M+K]^+$, | 1651.10 (1624.18) |
| **3.15** | 1216.4147 $[M+MeCN+Na]^{2+}$ | 1657.58 (1644.42) |
| **3.16** | 1255.3978 $[M+H+NH_4]^{2+}$ | 1662.99 (1632.15) |

IR ***ν*(C=N)** for the ligands are shown in brackets.

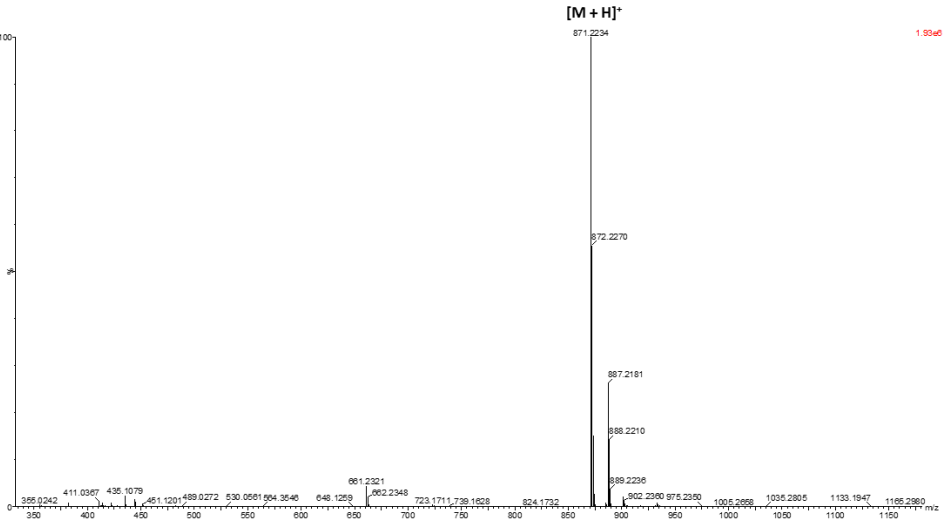


**Figure 3.10** Mass spectrum (positive mode) of complex **3.12**.

### 3.2.9 Cyclic voltammetric studies of the redox behaviour of Rh(I) alpha-diimine poly(aryl ether) metallodendrimers

In order to probe the electronic environment around the Rh(I) metal centre in this metallodendrimer series, cyclic voltammetry (CV) experiments were performed. Measurements were carried out on all complexes in a non-coordinating solvent ($CH_2Cl_2$) containing 0.10 M [$NBu_4$][$BF_4$] as a supporting electrolyte. Cyclic voltammetry on the dendritic ligands was also carried out in order to ascertain the metal-centred electron transfer reactions of the Rh(I) complexes from those associated with the conjugation of the ligands. The pertinent electrochemical data of the complexes are presented in Table 3.4, with selected voltammograms of complexes **3.11**, **3.13, 3.15** and **3.16** shown in Figure 3.11.

**Table 3.4** Redox Potentials of complexes **3.11** – **3.16**[a].

| | Potential (V) | | | | | |
|---|---|---|---|---|---|---|
| | **3.11** | **3.12** | **3.13** | **3.14** | **3.15** | **3.16** |
| **Ligand** | -0.53[b] | -1.43 | -1.42[b] | -0.41 | -0.45[b] | -0.31 |
| $E_{pa}$[c] | 1.41 | 1.39 | 1.36 | 1.23 | 1.11 | 1.05 |

[a]All potentials are referred against a Ag/AgCl reference electrode and taken at a scan rate of 100 mV $s^{-1}$. [b]Quasireversible process, $E_{pc}$, [c] $Rh^{I/III}$ oxidation process.

All complexes show distinct redox processes associated with a well-defined one-electron ligand-based reductions and metal-centred Rh(I)/(III) oxidations. The ligand-based reductions

correspond to the radical anion formation in which the diimine that is reduced to a diamine. This phenomenon correlates well with structurally related α-diimine complexes.[73] A quasi-reversible reduction peak potential was observed for complexes **3.11**, **3.13** and **3.15** at $E_{pc}$ values of -0.53 V, -1.42 V and -0.45 V respectively, whereas reversibility of this process is observed for complexes **3.12**, **3.14** and **3.16**. This can be attributed to the extended aromaticity of the acenaphthene backbone on the α-diimine ligands. The irreversible anodic peak potentials ($E_{pa}$) of the $Rh^{I}/Rh^{III}$ oxidation process at 1.41 V for complex **3.11** is shifted cathodically upon introduction of higher generation dendritic wedges, suggesting electronic energy transfer from the electron-rich polyether dendritic fragments to the Rh centre thus making it easier to oxidize. This trend was observed for all complexes **3.12 – 3.16**. When comparing the acenaphthyl-containing complexes (**3.12**, **3.14** and **3.16)** to those of the glyoxal derivatives (**3.11**, **3.13** and **3.15**), the former oxidizes at lower potentials. This could be attributed to the induction effect exerted by the acenaphthyl backbone in addition to the extension of the wedges accordingly. Generally, the acenaphthyl backbone has more electron donating ability than the hydrogen atoms on the diimine ligands of complexes **3.11**, **3.13** and **3.15**.[75,76] Overall, the irreversibility of the metal-centred oxidations of the complexes suggest an EC redox mechanism as a result of the dissociation of the COD ligand. This labile moiety generates a 16-electron complex which is essential for the hydroformylation catalytic activity reported herein.

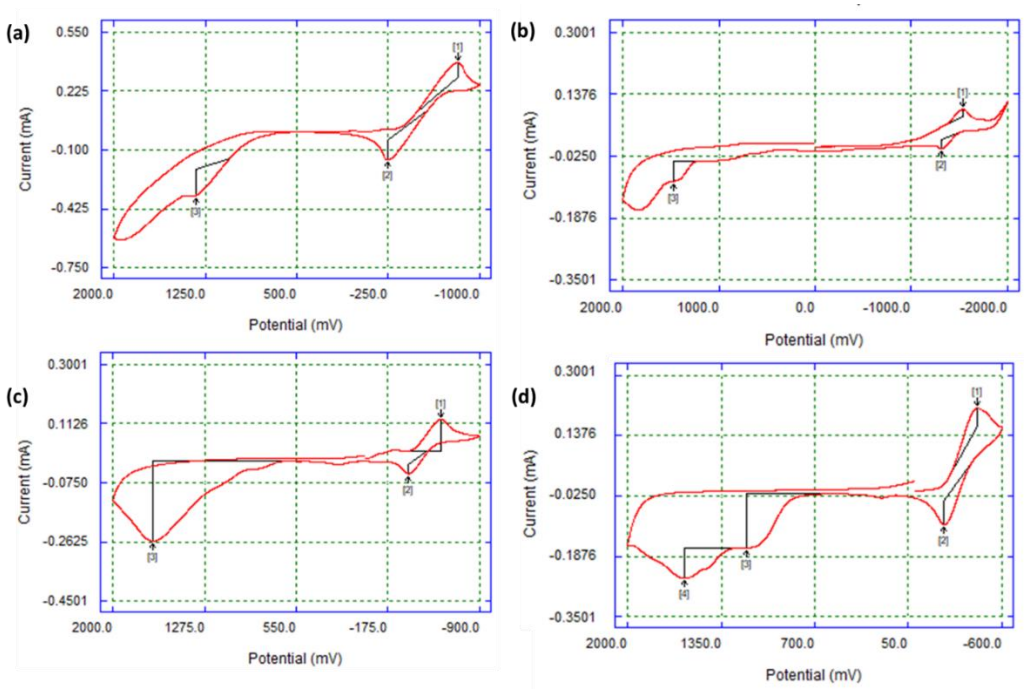


**Figure 3.11** Cyclic voltammograms of (a) **3.11** (b) **3.13** (c) **3.15** and (d) **3.16** in dichloromethane containing 0.10 M $[NBu_4][BF_4]$ at ambient temperature.

### 3.2.10 Hydroformylation studies

The poly(aryl ether) α-diimine metallodendrimers **3.11** – **3.16** were assessed as catalyst precursors in the hydroformylation reaction using previously optimized conditions of temperature and pressure (75 °C and 40 bar). The substrates 1-octene and styrene were used as representative substrates for higher olefins and vinylic aromatics respectively. The reactions were carried out in toluene (5 mL) for 4 h and product samples were analysed using gas chromatography.

#### 3.2.10.1 Hydroformylation of 1-octene

All the catalyst precursors **3.11** – **3.16** gave good conversions (> 82%) and TOF values in the range of 427 – 613 $h^{-1}$ (Table 3.5). No hydrogenation side-products were observed, and small amounts (<18%) of isomerised substrate were detected. This is indicative of the good chemoselectivity of the catalysts towards aldehydes under the chosen hydroformylation conditions.

**Table 3.5** Hydroformylation of 1-octene using catalyst precursors **3.11 – 3.16**[a]

| Entry | Pre-catalyst | Conversion (%) | Aldehydes (%) | Linear Aldehydes (%) | Branched Aldehydes (%) | Iso-octenes (%) | TOF ($h^{-1}$) | TON |
|---|---|---|---|---|---|---|---|---|
| 1 | **3.11** | 99 | 99 | 51 | 49 | 1 | 613 | 2479 |
| 2 | **3.12** | 99 | 98 | 49 | 51 | 1 | 612 | 2475 |
| 3 | **3.13** | 92 | 95 | 54 | 46 | 5 | 546 | 2307 |
| 4 | **3.14** | 90 | 95 | 59 | 41 | 5 | 534 | 2254 |
| 5 | **3.15** | 81 | 85 | 67 | 33 | 15 | 434 | 2031 |
| 6 | **3.16** | 82 | 83 | 67 | 33 | 17 | 427 | 2051 |
| 7 | **3.11**[b] | 52 | 58 | 52 | 48 | 42 | 291 | 1193 |
| 8 | **3.13**[b] | 45 | 55 | 53 | 47 | 45 | 239 | 979 |
| 9 | **3.16**[b] | 42 | 41 | 57 | 43 | 59 | 198 | 831 |

[a] Reaction conditions: The reactor (90 mL) was loaded with toluene (5 mL), 1-octene (0.805 g, 7.175 mmol), internal standard *n*-decane (0.204 g, 1.435 mmol) and catalyst loading ($2.87 \times 10^{-3}$ mmol). The reactor was purged with nitrogen three times, followed by purging three times with syngas. Catalyst to substrate ratio used was (1:2500). The reactions were carried out for 4 h at 75 $^{0}$C/40 bar. TOF = (mmol of aldehydes/mmol of catalyst)/time and TON = (mmol of substrate converted/mmol of catalyst). [b] The reaction was conducted in the presence of mercury. Average error estimate = ± 0.55.

### 3.2.10.2 Influence of the increasing dendritic scaffold on catalyst activity

Catalyst precursors **3.11** and **3.12** ($G_0$ metallodendrimers) gave good activities of 613 and 612 $h^{-1}$ respectively (Table 3.5, entries 1 and 2). It is noteworthy to recognize that a good turnover frequency value is a reflection of the rate of active catalysts formation and the stability of these active species under hydroformylation conditions. Although the dendritic scaffold may play a stabilizing role under hydroformylation conditions, a decrease in catalytic activity is observed using catalyst precursors **3.13** and **3.14** ($G_1$ metallodendrimers) with an activity of 546 $h^{-1}$ and 534 $h^{-1}$ respectively. A further decrease in activity is observed going from the first-generation ($G_1$) metallodendrimers to the second-generation ($G_2$) metallodendrimers (**3.15** and **3.16**) (Table 3.5, entries 5 and 6). With respect to total substrate converted (iso-octenes and aldehydes), the catalyst precursors gave TON values in the range of 2031 – 2479. In general, a decrease in activity was observed as the generation of the catalyst increases.

This decrease in catalyst performance could be attributed to a more difficult mass transport due to steric constraints imposed by the bulky dendritic framework which hinders the approach of the substrate. In spite of the observed cathodic shift in the oxidation ($Rh^{I/III}$) of complex **3.15** and **3.16**, the greater steric bulk of the higher generation metallodendrimers can also suggests a decrease in kinetics towards the formation of a CO-coordinated Rh-species. These findings correlate well with the earlier work of Van Leeuwen *et al*. in the hydroformylation of 1-octene using core-functionalized mono- and diphosphines rhodium dendrimers.[51]

### 3.2.10.3 Influence of the increasing dendritic scaffold on catalyst selectivity

Catalyst selectivity is one of the most important parameters in identifying a successful hydroformylation catalyst. A highly selective catalyst towards the desired product aligns the process with the Green Chemistry principles, such as (i) the reduction of waste (side-products) and (ii) enhancing the atom economic nature of the reaction. In this work, the small amount of isomerization products (internal alkenes) obtained under these conditions using catalyst precursor **3.11** – **3.16** (<17%) suggests a lower β-hydride elimination process (Scheme 3.7).

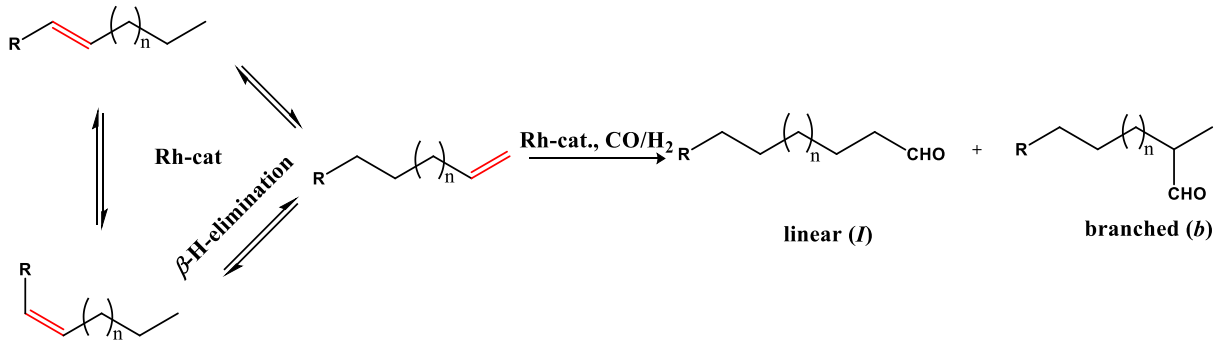


**Scheme 3.7** Relationship between isomerization and the final hydroformylation of a terminal olefin.[77]

The migration of the double bond of the terminal olefins through β-hydride elimination usually generates the thermodynamically favoured isomer. However, the isomerization cycle can be interrupted by the formation of the corresponding metal−acyl complexes.[77–79] It is known that metal−acyl complexes, which are derived from the insertion of CO into the metal−alkyl bond are mostly irreversibly converted into aldehydes. Therefore, all effects (including but not limited to the stereoelectronic properties of the ligand) that support this step favour the hydroformylation over isomerization.[77,80,81] Catalyst precursors **3.11** and **3.12** ($G_0$ metallodendrimers) gave excellent chemoselectivity towards aldehydes (> 99%) (Scheme 3.11). A slight decrease in aldehyde formation was observed using $G_2$ metallodendrimers (**3.13** – **3.16**) from 95% (**3.13** and **3.14**) to 83%. In general, a decrease in chemoselectivity is observed as the generation of the catalyst increases (Figure 3.12). This decrease in chemoselectivity could be as a result of the reduced hydroformylation rates of the lager metallodendrimers or by the presence of nanoparticles which may be responsible for the isomerisation of olefins.[4,72]

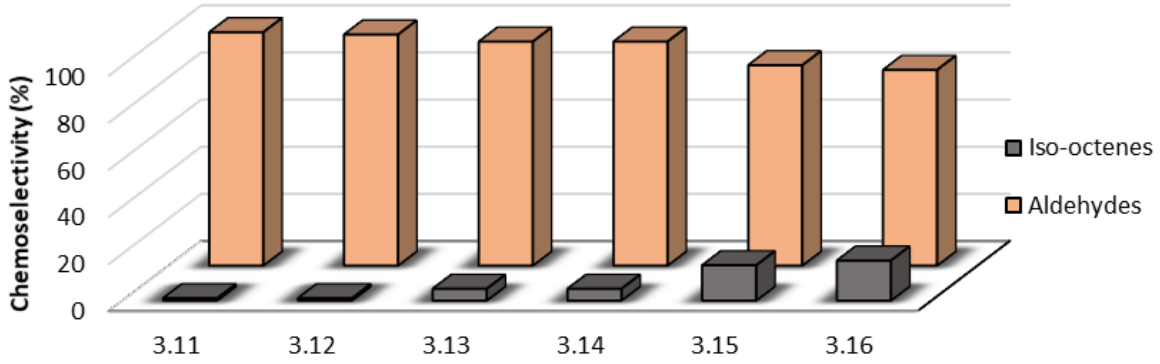


**Figure 3.12** Chemoselectivity of catalyst precursor **3.11 – 3.16** in the hydroformylation of 1-octene.

The lower generations $G_0$ metallodendrimers (**3.11** and **3.12**) gave moderate regioselectivity for linear aldehydes (51 – 49%) (Figure 3.13). The quantity of linear aldehydes increased to 54% and 59% when slightly higher dendritic structures were evaluated (**3.13** and **3.14**, respectively). This attests to the positive influence of the sterics of the dendritic scaffold on the regioselectivity towards linear aldehydes. The highest linear selectivity was obtained with the $G_2$ metallodendrimers **3.15** and **3.16**, which gave 67% of linear aldehydes with an *n:iso* ratio of 2.0 respectively. Generally, as the generation of the catalyst increases the regioselectivity for the linear aldehyde increases and the formation of isomeric branched aldehyde is suppressed. This increase in regioselectivity with each generation depicts well the effect of increased sterics exerted by the dendrimeric environment. In addition, the dendrimer may provide a favourable microenvironment for the catalytically active rhodium species that influence selectivity towards linear aldehydes. This observation is similar to rhodium-based systems where steric constraints permit increased regioselectivity and this phenomena is referred to as a 'positive dendritic effect'.[49,82–85] Additionally, the regioselectivity of these catalysts can attest to a lower β-hydride elimination process and the possibility of reverse isomerization of internal olefins to α-olefins, which would subsequently lead to hydroformylation to the linear products.

Additionally, the incorporation of a bulky substituent on the backbone of the α-diimine-core of the rhodium(I) complexes do not seem to influence the activity and selectivity of these catalysts as each dendrimeric catalyst set show comparable performance for the hydroformylation reaction.

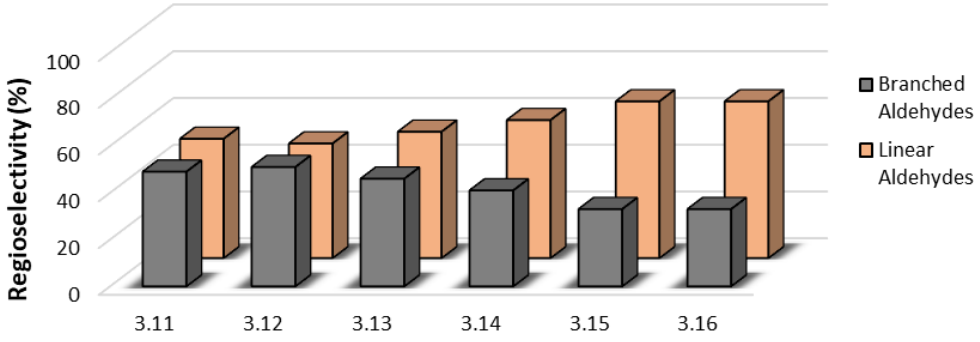


**Figure 3.13** Regioselectivity of catalyst precursors **3.11 – 3.16** in the hydroformylation of 1-octene.

### 3.2.10.4 Selectivity as a function of time

The inferior hydroformylation activity of the catalyst precursors **3.15** and **3.16** ($G_2$ metallodendrimers) to the lower generation catalyst precursors could indicate an incomplete or slow rate of active catalyst formation. This implies that stopping the reaction at 4 h, effectually interrupts the hydroformylation performance of the metallodendrimers.

In an effort to optimize the catalytic efficiency of the least performing catalyst precursor of all the metallodendrimers synthesised in this study, a time-dependent reaction profile for the hydroformylation of 1-octene was carried out using the $G_2$ metallodendrimer (**3.16**). The conversion and regioselectivity of the catalyst precursor were evaluated at various time intervals using the optimized conditions of 75 °C and 40 bar (at intervals of 1 h, 2 h, 4 h, 6 h, 8 h and 10 h). The product distribution profile is shown in Figure 3.14.

The substrate and product-distribution-time profile show a gradual decline of 1-octene over time, with *ca*. 40 mol% of 1-octene present after 1 h of the reaction. Further decrease in 1-octene is observed over time reaching 100% depletion after 8 h. The accumulation of iso-octenes is observed in the system after 1 h. As the reaction time increases a gradual decrease in the isomerization of 1-octene occurs, this decreases abruptly after 8 h. With respect to regioselectivity, the *n/iso* ratio of aldehydes gradually increases as the reaction time is increased. This implies that the anti-Markovnikov addition pathway is the major reaction route for the hydroformylation of 1-octene in this study. Additionally, the hydroformylation of iso-octene contributes to the rest of aldehyde yield. This hypothesis is well supported by the change in iso-octene from 18.36 mol% in 1 h to 6.72 mol% in 6 h, with an increase in branched aldehyde formation. However, the formation of linear aldehyde remains predominant as the *n/iso* ratio of aldehydes is greater than 1.0 at all stages of the reaction. Notably, subsequent linear aldehyde in theory may be produced by the hydroformylation of newly formed 1-octene from the reverse isomerization of iso-octene.[77] Extending the reaction time to 10 h, no increase in regioselectivity is observed, this is as a result of the complete depletion of the 1-octene and isomerised octene in the reaction system. This is in agreement with results in the literature, wherein the chemoselectivity towards aldehydes is reported to increase at extended reaction time.[72,86,87] The 100% quantitative conversion of 1-octene attest to the stability of the active catalyst under hydroformylation conditions.

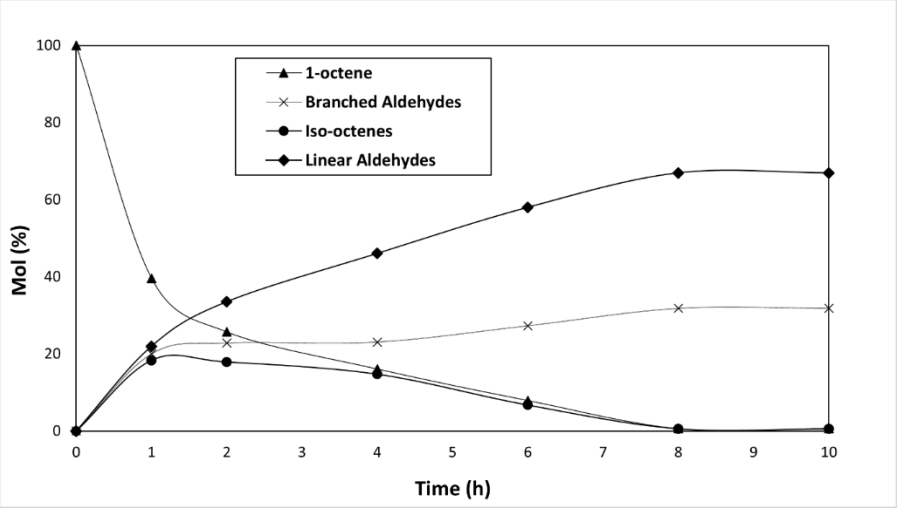


**Figure 3.14**. Substrate and product-distribution as function of time for catalyst precursor **3.16**.

### 3.2.10.5 Hydroformylation of styrene

The promising results with respect to activity and regioselectivity in the hydroformylation of 1-octene prompted investigations into the hydroformylation of vinyl aromatic substrate (styrene). All catalyst precursors gave high conversions (> 84%) with good activity of 525 – 625 $h^{-1}$ (Table 3.6). The hydroformylation of styrene produced more of the branched product as depicted in Figure 3.15.

The selectivity towards branched aldehydes suggests that steric hindrance around the metal centre had no effect on the regioselectivity in the hydroformylation of styrene and that the formation of a stabilizing allyl intermediate induced by the electron donation from the benzene ring is predominant in this case. This directs the hydroformylation of styrene to the position adjacent to the aryl ring and precedence for this is given in the literature.[88] In addition, the thermodynamics of the reaction system and steric hindrance induced by bulky substrate have been reported to influence the regioselectivity of vinylarenes.[89–92]

**Table 3.6** Hydroformylation of styrene using catalyst precursors **3.11 – 3.16**[a]

| Entry | Pre-catalyst | Conversion (%) | Linear Aldehydes (%) | Branched Aldehydes (%) | TOF ($h^{-1}$) | TON |
|---|---|---|---|---|---|---|
| **1** | **3.11** | >99 | 11 | 89 | 622 | 2487 |
| **2** | **3.12** | 98 | 11 | 89 | 614 | 2455 |
| **3** | **3.13** | 100 | 15 | 85 | 625 | 2500 |
| **4** | **3.14** | 97 | 16 | 84 | 607 | 2428 |
| **5** | **3.15** | 84 | 12 | 88 | 527 | 2108 |
| **6** | **3.16** | 84 | 12 | 88 | 525 | 2099 |
| **7** | **3.16**[b] | >99 | 8 | 92 | 311 | 2491 |
| **8** | **3.16**[c] | 52 | 11 | 89 | 232 | 997 |

[a] Reaction conditions: The reactor (90 mL) was loaded with toluene (5 mL), Styrene (0.747 g, 7.17 mmol) and catalyst loading (2.87 $\times 10^{-3}$ mmol). The reactor was purged with nitrogen three times, followed by purging three times with syngas. Catalyst to substrate ratio used was (1:2500). The reactions were carried out for 4 h at $75^0$C/40bar and the data was analysed using GC-FID. TOF = (mmol of aldehydes/mmol of Rh)/time and TON = (mmol of substrate converted/mmol of catalyst). [b] The reactions were carried out for 8 h. [c] The reaction was performed in the presence of mercury. Average error estimate = ± 0.46.

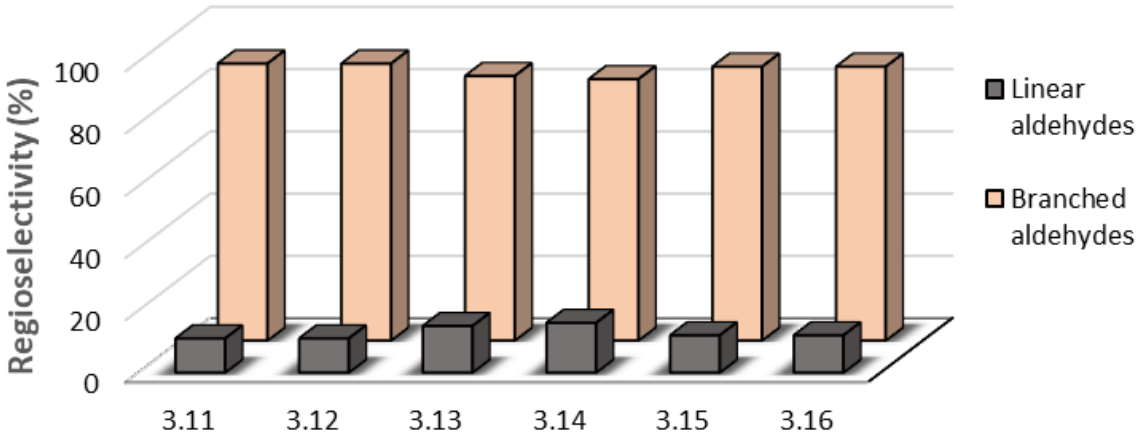


**Figure 3.15** Regioselectivity of catalyst precursors **3.11 – 3.16** in the hydroformylation of styrene.

### 3.2.10.6 Mercury poisoning experiments

Mercury drop poisoning test was conducted to determine if the system is homogeneously (molecular) or heterogeneously-catalysed (mediated by metal nanoparticles). This approach is based on the ability of mercury to interact with heterogeneous catalysts forming an amalgam which renders the catalyst inactive (catalyst poisoning), thus a decline in catalytic activity occurs. The mercury poisoning test was performed by adding a drop of mercury into each reactor containing the catalyst precursor using optimised conditions (75 °C, 40 bar) for 4 h. Metallodendrimers **3.11, 3.13** and **3.16** were used as representative catalyst precursors for each dendritic series. As shown in Figure 3.16, a drop in conversion was observed in the presence of mercury in the hydroformylation of 1-octene. This suggests that the conversion is attributed to a combination of homogeneous and heterogeneous catalysis. This is consistent with results (catalyst poisoning) for catalyst precursor **3.16** (Table 3.6, Entry 8) in the hydroformylation of styrene.

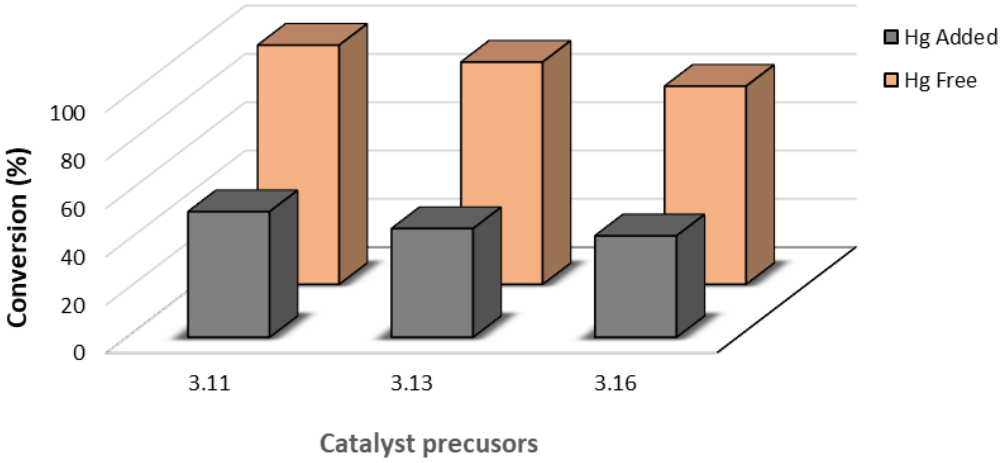


**Figure 3.16** Conversion of catalyst precursors **3.11**, **3.13** and **3.16** in the presence of mercury.

### 3.2.10.7 High pressure NMR experiments

To confirm the *in situ* generation of the catalytically active rhodium hydride complex, high pressure NMR (HP-NMR) spectroscopy experiments were carried out. Metal hydride moieties are easily detectable in $^{1}$H NMR as they appear high field of the TMS region where no other resonance appear. The position of the hydride resonance varies depending on the electronic

properties of the ligands coordinated to the rhodium atom.[93] Catalyst precursors **3.12** and **3.14** were dissolved in $CDCl_3$ and pressurized with 30 bar of syngas ($CO/H_2$ (1:1)) and incubated at ambient temperature for about 10 minutes to allow formation of the hydride species. An evidence of Rh-hydride specie formation is the appearance of an upfield hydride resonance observed at -7.13 and -7.14 ppm for **3.12** and **3.14** respectively (Figure 3.17). A single hydride resonance in the $^1H$ NMR spectra suggests that one rhodium-hydride specie is present in solution.

These metal-hydride signals appear in the range (-5 to -25 ppm) with electron-donating ligands reported in the literature.[94,95] The new singlet observed at 4.58 ppm is assigned to hydrogen gas in solution as denoted by the asterisk.[96,97]

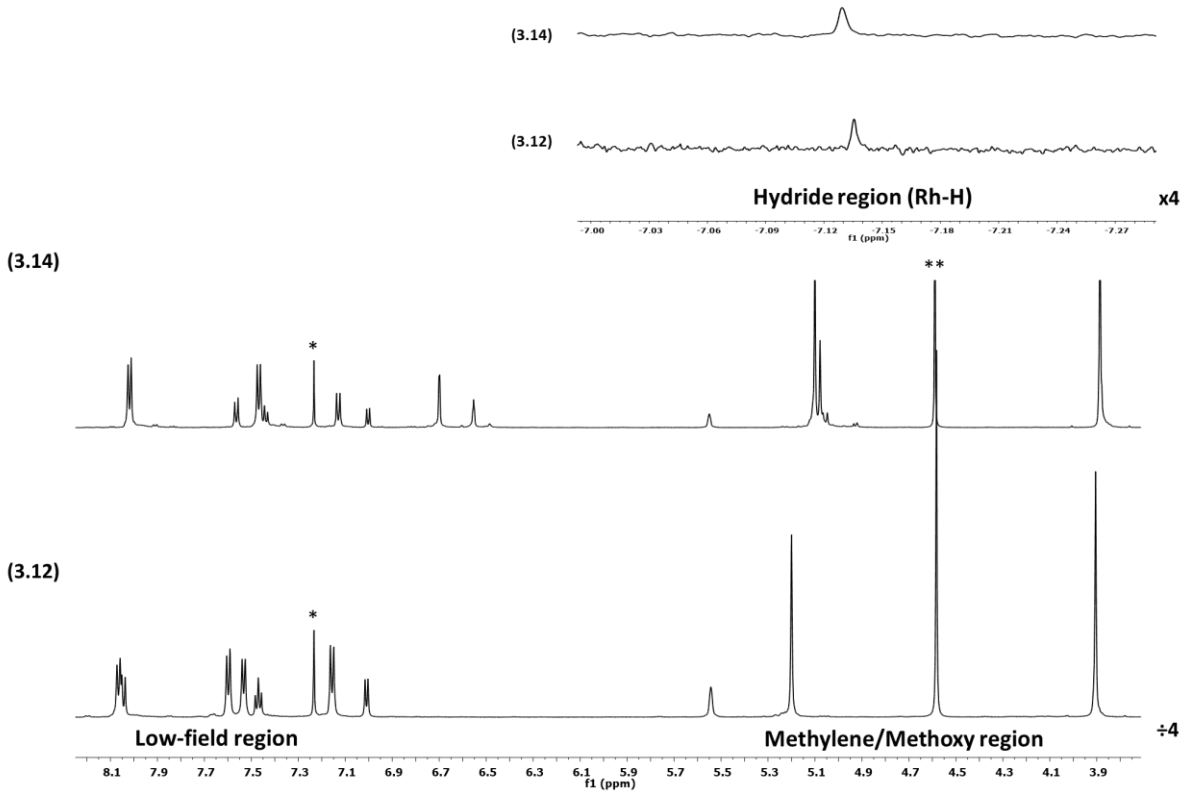


**Figure 3.17** Stacked $^1H$ NMR spectra ($CDCl_3$) of **3.12** and **3.14** showing the formation of rhodium-hydride specie (*$CDCl_3$, **Hydrogen gas in solution).

## 3.3 Summary

A series of Fréchet-type dendrons (**3.1** – **3.4**) were prepared by template procedures (Williamson ether synthesis and the Appel reaction). The dendrons were isolated in good yields and characterised accordingly. The alpha-diimine Schiff base ligands **2.1** and **2.2** were once

more prepared by Schiff-base condensation reactions and were isolated in high yields. The alpha-diimine Schiff base ligands were reacted with methyl 4-(bromomethyl) benzoate or immobilised to the appropriate Fréchet dendron (**3.2** and **3.5**) *via* the Williamson ether synthesis to yield a series of poly(aryl ether) dendrimers with alpha-diimine Schiff-bases at the core (**3.5** – **3.10**). These classes of dendrimers are new and have been fully characterised using various analytical and spectroscopic techniques. The coordination of these dendrimers to $[Rh(COD)(MeCN)_2]BF_4$ metal precursor afforded new α-diimine-cored rhodium(I) metallodendrimers (**3.11** – **3.16**).

The electron-donating character of the α-diimine-cored rhodium(I) metallodendrimers was ascertained by means of cyclic voltammetry. The electrochemical studies of the complexes show an irreversible oxidation suggesting the formation of new species that does not revert to the starting complex upon reduction. The catalytic studies of the rhodium-catalysed hydroformylation of 1-octene using the dendritic catalyst precursors (**3.11** – **3.16**) revealed that an increase in the dendritic generation of the α-diimine-cored rhodium complexes increased the regioselectivity towards linear aldehydes. On the other hand, a reduction in substrate conversion was observed. This suggest that the decrease in conversion is attributed to the reduced accessibility of the substrate to the catalytic site. Extending the hydroformylation reaction time from 4 h to 8 h using the larger α-diimine-cored rhodium(I) metallodendrimers (**3.16)** catalyst precursor led to near quantitative conversion of 1-octene with good regioselectivity towards aldehyde. The regioselectivity of the low generation metallodendrimers is comparable to that of the larger dendritic analogues for the hydroformylation of styrene. This suggest that steric constrain at the catalytic site of the α-diimine-cored rhodium(I) metallodendrimers had no impact in influencing the regioselectivity towards linear aldehydes for the hydroformylation of vinyl arenes.

## 3.4 References

1 R. Franke, D. Selent and A. Börner, *Chem. Rev.*, 2012, **112**, 5675–5732.

2 S. S. Joshi, A. Bhatnagar and V. V. Ranade, in *Industrial Catalytic Processes for Fine and Specialty Chemicals*, Elsevier, 2016, pp. 317–392.

3 H. U. Blaser, A. Indolese and A. Schnyder, *Curr. Sci.*, 2000, **78**, 1336–1344.

4 L. Le Goanvic, J. Ternel, J. L. Couturier, J. L. Dubois and J. F. Carpentier, *Catalysts*,

2018, **8**, 21–26.

5 M. Kumar, R. V. Chaudhari, B. Subramaniam and T. A. Jackson, *Organometallics*, 2014, **33**, 4183–4191.

6 C. J. Cobley, K. Gardner, J. Klosin, C. Praquin, C. Hill, G. T. Whiteker, A. Zanotti-Gerosa, J. L. Petersen and K. A. Abboud, *J. Org. Chem.*, 2004, **69**, 4031–4040.

7 S. Siangwata, N. Baartzes, B. C. E. Makhubela and G. S. Smith, *J. Organomet. Chem.*, 2015, **796**, 26–32.

8 D. Y. Murzin, A. Bernas and T. Salmi, *J. Mol. Catal. A Chem.*, 2010, **315**, 148–154.

9 N. C. C. Breckwoldt, N. J. Goosen, H. C. M. Vosloo and P. Van Der Gryp, *React. Chem. Eng.*, 2019, **4**, 695–704.

10 S. Siangwata, N. C. C. Breckwoldt, N. J. Goosen and G. S. Smith, *Appl. Catal. A Gen.*, 2019, **585**, 117–179.

11 J. M. Dreimann, H. Warmeling, J. N. Weimann, K. Künnemann, A. Behr and A. J. Vorholt, *AIChE J.*, 2016, **62**, 4377–4383.

12 Y. Brunsch and A. Behr, *Angew. Chem. Int. Ed.*, 2013, **52**, 1586–1589.

13 M. S. Shaharun, B. K. Dutta and H. Mukhtar, *J. Appl. Sci.*, 2011, **11**, 1157–1163.

14 J. B. Claridge, R. E. Douthwaite, M. L. H. Green, R. M. Lago, S. C. Tsang and A. P. E. York, *J. Mol. Catal.*, 1994, **89**, 113–120.

15 S. S. Nurttila, P. R. Linnebank, T. Krachko and J. N. H. Reek, *ACS Catal.*, 2018, **8**, 3469–3488.

16 L. A. Van der Veen, P. H. Keeven, G. C. Schoemaker, J. N. H. Reek, P. C. J. Kamer, P. W. N. M. van Leeuwen, M. Lutz and A. L. Spek, *Organometallics*, 2000, **19**, 872–883.

17 D. Evans, J. A. Osborn and G. Wilkinson, *J. Chem. Soc. A Inorganic, Phys. Theor.*, 1968, 3133–3142.

18 D. Evans, G. Yagupsky and G. Wilkinson, *J. Chem. Soc. A Inorganic, Phys. Theor.*, 1968, 2660–2665.

19 G. R. Newkome and X. Lin, *Macromolecules*, 1991, **24**, 1443–1444.

20 E. Buhleier, W. Wehner and F. Vogtle, *Synthesis-stuttgart*, 1978, **1978**, 155–158.

21 T. Baig, J. Nayak, V. Dwivedi, A. Singh and P. K. Tripathi, *Int. J. Adv. Pharmacy, Biol. Chem.*, 2015, **4**, 44–59.

22 G. M. Dykes, *J. Chem. Technol. Biotechnol.*, 2001, **76**, 903–918.

23 P. Li, W. Thitsartarn and S. Kawi, *Ind. Eng. Chem. Res.*, 2009, **48**, 1824–1830.

24 J. N. H. Reek, S. Arévalo, R. van Heerbeek, P. C. J. Kamer and P. W. N. M. van Leeuwen, *Adv. Catal.*, 2006, **49**, 71–151.

25 D. Astruc and F. Chardac, *Chem. Rev.*, 2001, **101**, 2991–3023.

26 D. Astruc, D. Wang, C. Deraedt, L. Liang, R. Ciganda and J. Ruiz, *Synth.*, 2015, **47**, 2017–2031.

27 A. Alam, A. Jahan and W. Khan, *Adv. Mater.*, 2017, **6**, 52–56.

28 G. R. Newkome, E. He and C. N. Moorefield, *Chem. Rev.*, 1999, **99**, 1689–1746.

29 S. Hwang, C. D. Shreiner, C. N. Moorefield and G. R. Newkome, *New J. Chem.*, 2007, **31**, 1192.

30 Y. Zeng, Y. Li, J. Chen, G. Yang and Y. Li, *Asian J. Chem.*, 2010, **3**, 992–1005.

31 A. Adronov and J. M. J. Fréchet, *Chem. Commun.*, 2000, **18**, 1701–1710.

32 G. M. Stewart and M. A. Fox, *J. Am. Chem. Soc.*, 1996, **7863**, 4354–4360.

33 S. Michlewska, M. Ionov, D. Shcharbin, M. Maroto-díaz, R. Gomez, F. Javier, D. Mata and M. Bryszewska, *Eur. Polym. J.*, 2017, **87**, 39–47.

34 M. Maroto-díaz, B. T. Elie, P. Gómez-sal, J. Pérez-serrano, R. Gómez, M. Contel and F. J. De Mata, *Dalton Trans.*, 2016, 7049–7066.

35 Y. Yan, J. Zhang, L. Ren and C. Tang, *Chem. Soc. Rev.*, 2016, **45**, 5232–5263.

36 P. Govender, T. Riedel, P. J. Dyson and G. S. Smith, *J. Organomet. Chem.*, 2015, **799**–**800**, 38–44.

37 F. Vögtle, *Dendrimers*, Springer-Verlag Berlin Heidelberg, 1998.

38 E. Abbasi, S. F. Aval, A. Akbarzadeh, M. Milani, H. T. Nasrabadi, S. W. Joo, Y. Hanifehpour, K. Nejati-Koshki and R. Pashaei-Asl, *Nanoscale Res. Lett.*, 2014, **9**, 1–10.

39 A. Gupta, S. Dubey and M. Mishra, *J. Drug Deliv. Ther.*, 2018, **8**, 328–339.

40 Y. Niu and R. M. Crooks, *Comptes Rendus Chim.*, 2003, **6**, 1049–1059.

41 B. Helms and J. M. J. Fréchet, *Adv. Synth. Catal.*, 2006, **348**, 1125–1148.

42 G. E. Oosterom, R. J. Van Haaren, J. N. H. Reek, P. C. J. Kamer and P. W. N. M. Van Leeuwen, *Chem. Commun.*, 1999, **1**, 1119–1120.

43 M. Ooe, M. Murata, T. Mizugaki, K. Ebitani and K. Kaneda, *Nano Lett.*, 2002, **2**, 999–1002.

44 S. Hecht, *J. Polym. Sci.*, 2003, **41**, 1047–1058.

45 A. Ouali and A. M. Caminade, *Catalytic Sites inside the Dendrimeric Structure for Homogeneous Catalysis*, 2011.

46 M. Ooe, M. Murata, T. Mizugaki, K. Ebitani and K. Kaneda, *J. Am. Chem. Soc.*, 2004, **126**, 1604–1605.

47 R. Ye, A. V. Zhukhovitskiy, C. V. Deraedt, F. D. Toste and G. A. Somorjai, *Acc. Chem. Res.*, 2017, **50**, 1894–1901.

48 T. Mizugaki, M. Ooe, K. Ebitani and K. Kaneda, *J. Mol. Catal. A Chem.*, 1999, **145**, 329–333.

49 L. Ropartz, R. E. Morris, D. F. Foster and D. J. Cole-Hamilton, *Chem. Commun.*, 2001, **4**, 361–362.

50 Y. Niu, L. K. Yeung and R. M. Crooks, *J. Am. Chem. Soc.*, 2001, **123**, 6840–6846.

51 G. E. Oosterom, S. Steffens, J. Reek, P. Kamer and P. van Leeuwen, *Top. Catal.*, 2002, **19**, 61–73.

52 A. Börner and R. Franke, *Hydroformylations: Fundamentals, Processes and Applications in Organic Synthesis*, Wiley-VCH, Weinheim, 2016.

53 L. C. Matsinha, S. Siangwata, G. S. Smith and B. C. E. Makhubela, *Catal. Rev. Sci. Eng.*, 2019, **61**, 111–133.

54 T. Mashabane, G. K. Ramollo, G. Kleinhans, S. De Doncker, S. Siangwata, M. A. Fernandes, A. Lemmerer, G. S. Smith and D. I. Bezuidenhout, *J. Organomet. Chem.*, 2020, **920**, 121341.

55 B. Breit and W. Seiche, *Pure Appl. Chem.*, 2006, **78**, 249–256.

56 S. T. Tsantis, D. I. Tzimopoulos, M. Holyńska and S. P. Perlepes, *Int. J. Mol. Sci.*, 2020, **4**, 119–133.

57 G. Koten and K. Vrieze, *Advances in Organometallic Chemistry*, Academic Press. Inc., Amsterdam, 1982, vol. 21.

58 S. Kumar, *J. Heterocycl. Chem.*, 2019, **56**, 1168–1230.

59 A. Caminade, A. Ouali, R. Laurent and J. Majoral, *Catalysis Within Dendrimers*, Springer International Publishing, 2017.

60 P. E. Berget, J. M. Teixeira, J. L. Jacobsen and N. E. Schore, *Tetrahedron Lett.*, 2007, **48**, 8101–8103.

61 E. Fuhrmann and J. Talbiersky, *Org. Process Res. Dev.*, 2005, **9**, 206−211.

62 A. Williamson, *Justus Liebigs Ann. Chem.*, 1851, **77**, 37–49.

63 A. Williamson, *RSC Adv.*, 1852, **4**, 229–239.

64 A. K. Mosstafa Kazemia, Zahra Noorib, Homa Kohzadia, Mohsen Sayadia, *Iran. Chem. Commun.*, 2013, **1**, 43–50.

65 S. D. Naik and L. K. Doraiswamy, *AIChE J.*, 1998, **44**, 612–646.

66 H. H. Freedman and R. A. Dubois, *Tetrahedron Lett.*, 1975, **16**, 3251–3254.

67 R. J. Ouellette and J. D. Rawn, in *Organic Chemistry*, Elsevier Inc., 2018, pp. 507–536.

68 R. Appel, *Angew. Chem. Int. Ed.*, 1975, **14**, 801–811.

69 M. Nishida, A. Momotake, Y. Shinohara, Y. Nishimura and T. Arai, *J. Porphyr.*

*Phthalocyanines*, 2007, **11**, 448–454.

70 Y. Tang, Gang; Hu, Minqi; Ma, Yongcui; You, Dan; Bi, *RSC Adv.*, 2016, **6**, 42786–42793.

71 L. C. Matsinha, S. F. Mapolie and G. S. Smith, *Dalton Trans.*, 2015, **3**, 1240–1248.

72 C. Williams, M. Ferreira, E. Monflier, S. Mapolie and G. S. Smith, *Dalton Trans.*, 2018, **47**, 9418–9429.

73 N. F. Romashev, A. L. Gushchin, I. S. Fomenko, P. A. Abramov, I. V. Mirzaeva, N. B. Kompan'kov, D. B. Kal'nyi and M. N. Sokolov, *Polyhedron*, 2019, **173**, 114110.

74 M. P. Foster, C. A. McElroy and C. D. Amero, *Biochemistry*, 2007, **46**, 331–340.

75 W. C. Anderson, S. H. Park, L. A. Brown, J. M. Kaiser and B. K. Long, *Inorg. Chem. Front.*, 2017, **4**, 1108–1112.

76 F. Y. Zhang, X. B. Lan, C. Xu, H. G. Yao, T. Li and F. S. Liu, *Org. Chem. Front.*, 2019, **6**, 3292–3299.

77 M. Vilches-Herrera, L. Domke and A. Börner, *ACS Catal.*, 2014, **4**, 1706–1724.

78 H. M. Colquhoun, J. Holton, D. J. Thompson and M. V. Twigg, in *In: New Pathways for Organic Synthesis*, Springer, Boston, MA, 1984, p. 173.

79 T. C. Morrill and C. A. D'Souza, *Organometallics*, 2003, **22**, 1626–1629.

80 J. M. Birbeck, A. Haynes, H. Adams, L. Damoense and S. Otto, *ACS Catal.*, 2012, **2**, 2512–2523.

81 S. C. Van der Slot, P. C. J. Kamer, P. W. N. M. Van Leeuwen, J. A. Iggo and B. T. Heaton, *Organometallics*, 2001, **20**, 430–440.

82 L. Ropartz, K. J. Haxton, D. F. Foster, R. E. Morris, A. M. Z. Slawin and D. J. Cole-Hamilton, *J. Chem. Soc. Dalton. Trans.*, 2002, **23**, 4323–4334.

83 A. S. Abd-El-Aziz and I. Manners, *Frontiers in Transition Metal-Containing Polymers*, John Wiley & Sons, 2006.

84 A. Dahan and M. Portnoy, *J. Polym. Sci. Part A Polym. Chem.*, 2005, **43**, 235–262.

85 D. J. Cole-Hamilton and Robert P. Tooze, *Catalyst Separation, Recovery, and Recycling: chemistry and process design*, Springer Science & Business Media, 2006.

86 A. Oukhrib, L. Bonnafoux, A. Panossian, S. Waifang, D. H. Nguyen, M. Urrutigoity, F. Colobert, M. Gouygou and F. R. Leroux, *Tetrahedron*, 2014, **2014**, 1431–1436.

87 J. October and S. F. Mapolie, *J. Organomet. Chem.*, 2017, **840**, 1–10.

88 R. P. Dias, M. S. L. Prates, W. B. De Almeida and W. R. Rocha, *Int. J. Quantum Chem.*, 2011, **111**, 1280–1292.

89 C. Bergounhou, D. Neibecker and R. Mathieu, *J. Mol. Catal. A Chem.*, 2004, **220**, 167–

182.

90 R. Lazzaroni, A. Raffaelli, R. Settambolo, S. Bertozzi and G. Vitulli, *J. Mol. Catal.*, 1989, **50**, 1–9.

91 T. Fuchikami and I. Ojima, *J. Am. Chem. Soc.*, 1982, **104**, 3527–3529.

92 S. Yu, Y. M. Chie, Z. H. Guan, Y. Zou, W. Li and X. Zhang, *Org. Lett.*, 2009, **11**, 241–244.

93 C. J. Paul Kamer, N. H. Joost Reek and P. W. N. M. van Leeuwen, in *Mechanisms in Homogeneous Catalysis*, ed. B. Heaton, Wiley-VCH Verlag GmbH & Co. KGaA, 2005.

94 Z. Liu, R. J. Deeth, J. S. Butler, A. Habtemariam, M. E. Newton and P. J. Sadler, *Angew. Chem. Int. Ed.*, 2013, **52**, 4194–4197.

95 W. Xu, A. j. Lough and R. H. Morris, *Can. J. Chem.*, 1997, **75**, 475–482.

96 H. Fujiwara, J. Yamabe and S. Nishimura, *Chem. Phys. Lett.*, 2010, 42–44.

97 M. Matsumoto and J. H. Espenson, *J. Am. Chem. Soc.*, 2005, **127**, 11447–11453.

# Chapter 4

## Synthesis, characterization and application of water-soluble mononuclear diimine and binuclear tetraimine Rh(I) complexes as catalyst precursors in the aqueous biphasic hydroformylation of 1-octene

### 4.1 Introduction

Metal catalysts bearing multiple active sites have become the subject of extensive investigations in catalysis.[1–7] The ascendancy of metalloenzymes possessing multinuclear active metal sites inspired the interest in the development of multinuclear catalysts.[8–10] Research in catalysis using multinuclear complexes is primarily focused on the rational design of catalysts containing either metal–metal bonds[11–13] or conformationally favourable metal centres connected by multidentate ligands.[14–16] From a structural perspective, bimetallic catalysts may be classified into several types such as dimeric catalysts (bridged systems), tethered bimetallic systems and dinucleating catalysts.[17–20] The catalytic performance of a bimetallic catalyst may be linked to the type of metal–substrate interaction of the two metal centres. However, the type of interaction between the substrate and the two metal centres of a binuclear catalyst in a catalytic process is often difficult to identify.[17,21,22] Various metal-substrate interactive patterns have been described in the literature.[17,23–25] Selected examples are illustrated in Figure 4.1.

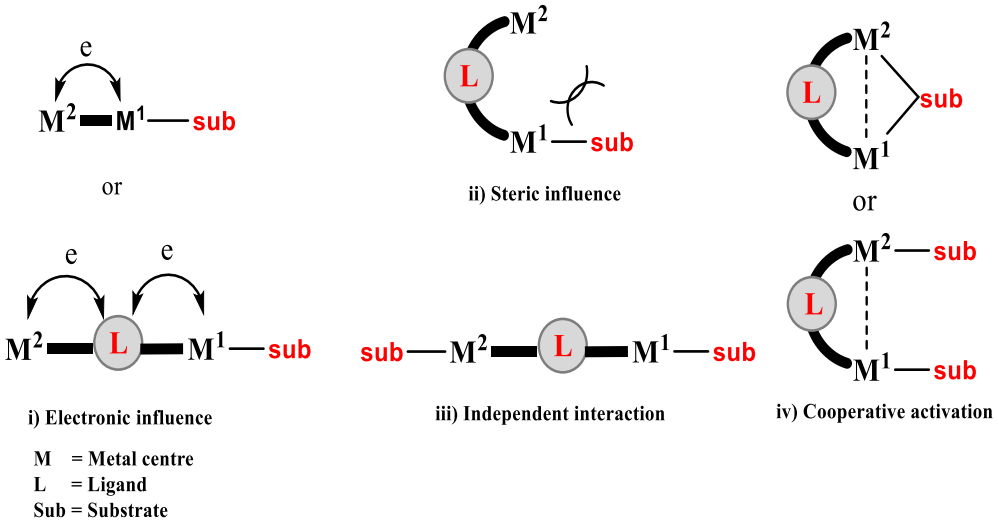


**Figure 4.1** Examples of metal-substrate interactive patterns of bimetallic catalysts.[17,23]

Plausible bimetallic–substrate interactions could occur wherein: (i) one of the metal centres may interact with the substrate to catalyse the reaction while the second metal centre provides electronic stability through a shared ligand or metal–metal redox cooperation, (ii) one of the metal centres interacts with the substrate while the second metal centre as well as the binding ligands imparts steric-hindrance and thus directing the substrate to a favourable alignment, (iii) each of the metal centres bound to the same ligand architecture can act independently (no intramolecular metal–metal interaction) and (iv), the two metal species are involved in the dual activation of the substrate and/or ligand–exchange processes (synergistic metal–metal cooperativity), providing bimetallic reaction pathways.[17,23] Additionally, it has been proposed that the close proximity of the two metal centres in a bimetallic system may improve the stability and performance of the catalyst.[6,23,26,27]

Superior activity and selectivity with bimetallic complexes over their monometallic congeners have been reported in the literature.[28–30] The catalytic multi-step processes of the hydroformylation transformation reaction such as the migratory insertion, oxidative addition, reductive elimination, or β-elimination transformations mainly rely on the inherent properties of the single-site metal centre of a typical monometallic catalyst.[22,31,32] Therefore, introducing a second catalytic site into a single-frame ligand may offer improvements towards favourable catalytic activity. As a result, the design of catalyst systems containing two metals centres is an attractive approach for optimizing the single-site hydroformylation catalysts.

In this perspective, the facile synthesis of new water-soluble homobimetallic Rh(I) bearing *N*-donor ligand system is reported. The bidentate ancillary ligand in this study is designed to chelate two discrete metal centres *via* the tetraimine nitrogen donor atoms that are supported by a conformationally rigid biphenyl spacer. Additionally, the introduction of hydrophilic substituents such as the sulfonate moiety enables easy and convenient catalyst recovery *via* the aqueous biphasic strategy. The ligands and their corresponding complexes were characterized using a range of spectroscopic and analytical techniques, such as $^{1}H$, $^{13}C\{^{1}H\}$ nuclear magnetic resonance (NMR) spectroscopy, Fourier-transform infrared (FT-IR) spectroscopy, Mass spectrometry and melting points. The water-soluble bimetallic complex was evaluated as a catalyst precursor in the aqueous biphasic hydroformylation of 1-octene. The efficiency of the bimetallic complex was rationalized *post hoc* by performance comparison with its monometallic analogue.

## 4.2 Results and discussion

### 4.2.1 Synthesis and characterization of tetraimine and diimine Schiff base ligands

Tetraylnitrilomethylidyne−hexaphenyl compound (**4.1**) was synthesised *via* an acid-catalyzed Schiff base condensation reaction following a literature procedure (Scheme 4.1).[33]

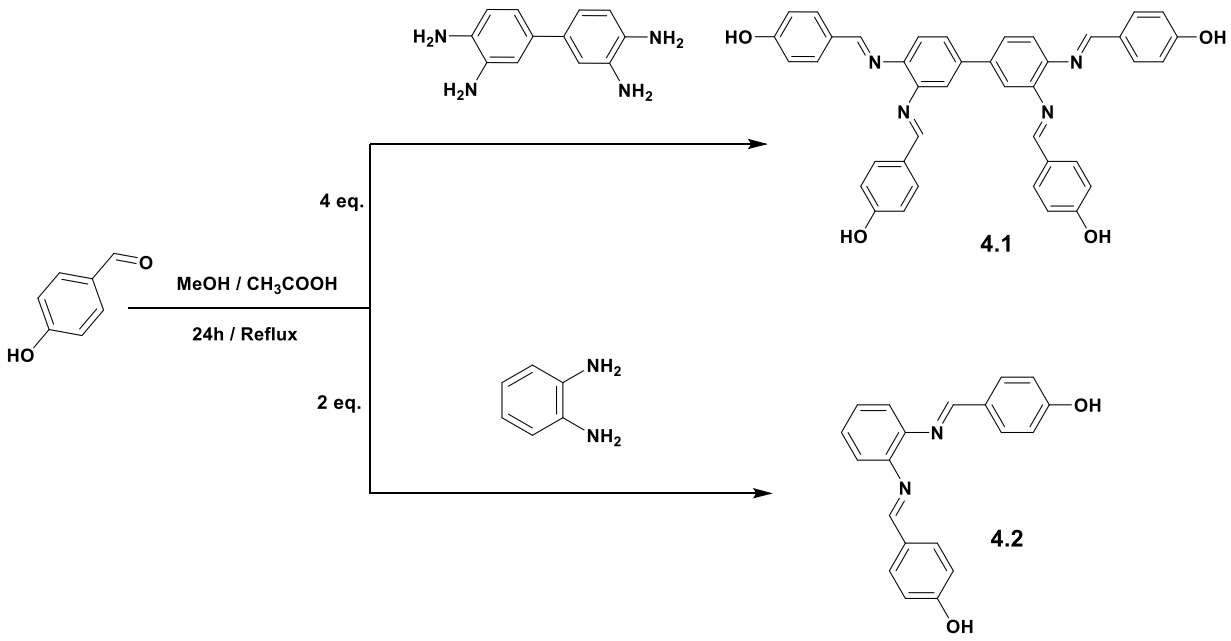


**Scheme 4.3** Synthesis of tetraamine and diimine compound **4.1** and **4.2**.

The tetraamine compound (3,3'-diaminobenzidine) was reacted with four molar equivalents of 4-hydroxybenzaldehyde and catalytic amounts of glacial acetic acid under reflux conditions in anhydrous methanol. Compound **4.1** was obtained as an off-white powder in good yield of 83%. Following similar procedure, 4,4′-(1,2-Phenylenebis(nitrilomethylidene))bisphenol[34] (**4.2**) was synthesised by reacting *O*-phenylenediamine with two molar equivalents of 4-hydroxybenzaldehyde in anhydrous methanol in the presence of catalytic amounts of acetic acid under reflux conditions. The compound (**4.2)** was obtained as a white powder in good yield (80%).

***NMR spectroscopy***

The $^{1}$H NMR spectrum of **4.1** (Figure 4.2) correlates with literature[33] and accounts for all the expected protons in the structure of **4.1**. The $^{1}$H NMR spectrum of **4.1** displays a distinct imine proton signal (H-7) at 5.50 ppm as a singlet. The resonance for the phenolic hydroxyl protons (H-1 and H-2) appears as two separate broad signals at 9.96 and 9.40 ppm respectively each

integrating for 2 protons. The biphenyl protons are observed as overlapping signals between 7.72 – 7.58 ppm while the signals for the aromatic phenolic protons are overlapping between 7.55 and 6.66 ppm.

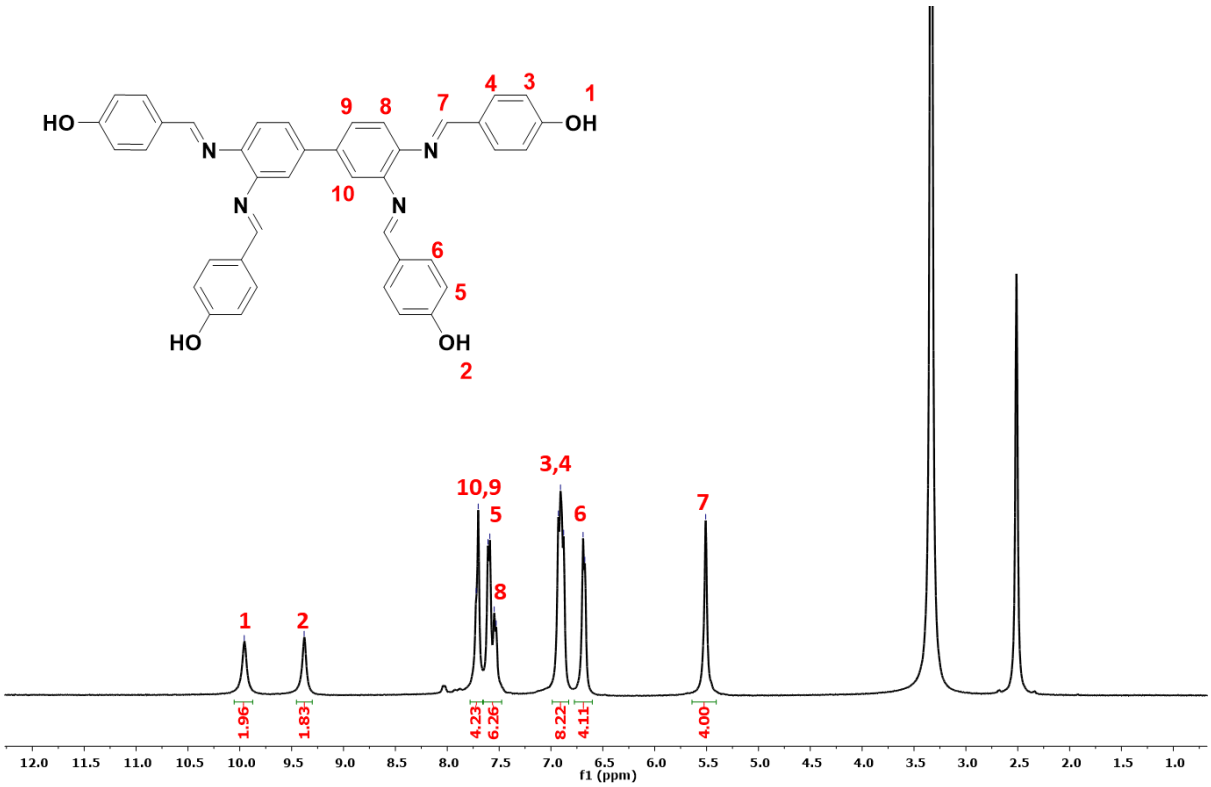


**Figure 4.2** $^{1}$H NMR spectrum for compound **4.1** in DMSO-$d_6$.

The $^{1}$H NMR spectrum of **4.2** (Figure 4.3) accounts for all the expected protons in the structure of **4.2**. The signals for the hydroxyl protons H-8 and H-9 in Figure **4.3** are observed as broad signals at 9.97 and 9.51 ppm respectively. Successful condensation reaction is evidenced by diagnostic signal for the imine protons at 5.42 ppm (H-5). Additionally, signals for the aromatic protons resonate as doublets and multiplets between 7.66 and 6.65 ppm due to coupling with neighbouring protons.

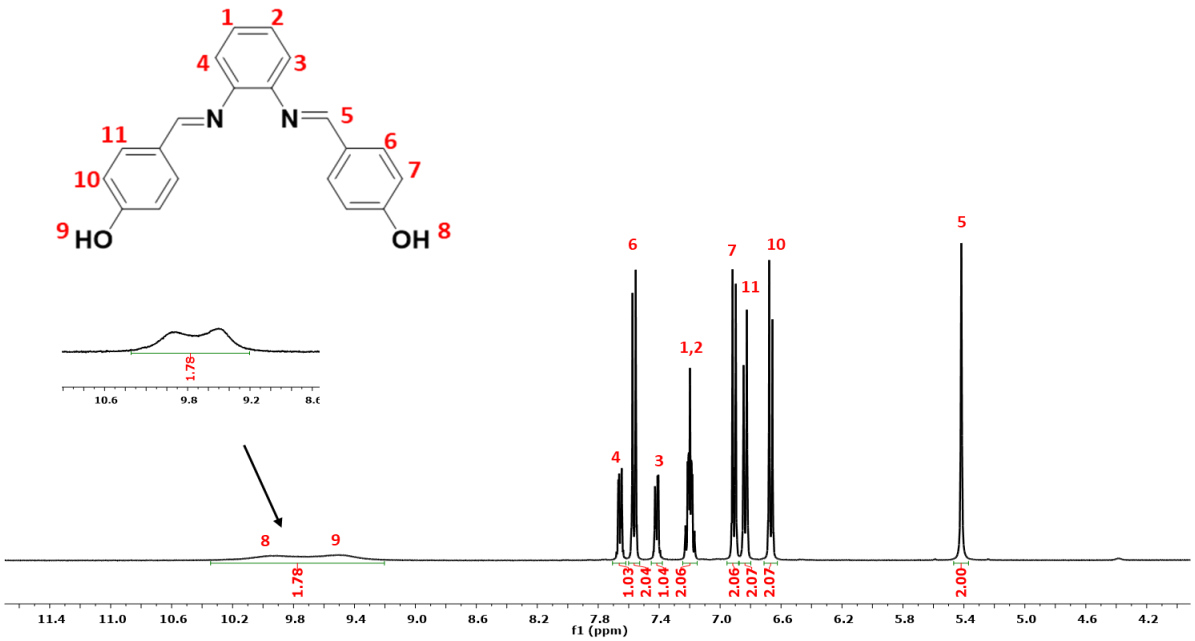


**Figure 4.3** $^{1}$H NMR spectrum for compound **4.2** in DMSO-$d_6$.

The $^{13}C\{^{1}H\}$ NMR spectra of compounds **4.1** and **4.2** display all signals in the expected regions. All aromatic carbon atoms resonate between 159.35 and 119.30 ppm, while the imine carbon gives rise to a signal at 154.64 and 154.06 ppm for compounds **4.1** and **4.2** respectively.

***Infrared spectroscopy***

The FT-IR spectrum of compound **4.1** shows a characteristic ν(C=N) stretching vibration at 1619 $cm^{-1}$ and an ν(O–H) absorption band at 3022 $cm^{-1}$. Additionally, the C=C stretching vibration of the phenyl rings give rise to signals in the region of 1517 − 1241 $cm^{-1}$. The spectroscopic data for compound **4.1** are in agreement with those reported in the literature.[33] The infrared spectrum of **4.2** shows the presence of a characteristic strong imine ν(C=N) absorption band at 1628 $cm^{-1}$, and an absorption band at 2936 $cm^{-1}$ corresponding to the ν(O–H) stretching frequency.

### 4.2.2 Synthesis and characterization of water-soluble tetraimine and diimine ligands

The introduction of the alkyl-sulfonate group to the tetraimine compound **4.1** and the diimine compound **4.2** was carried out using the appropriate equivalents of 1,3-propanesultone as illustrated in Scheme 4.2.

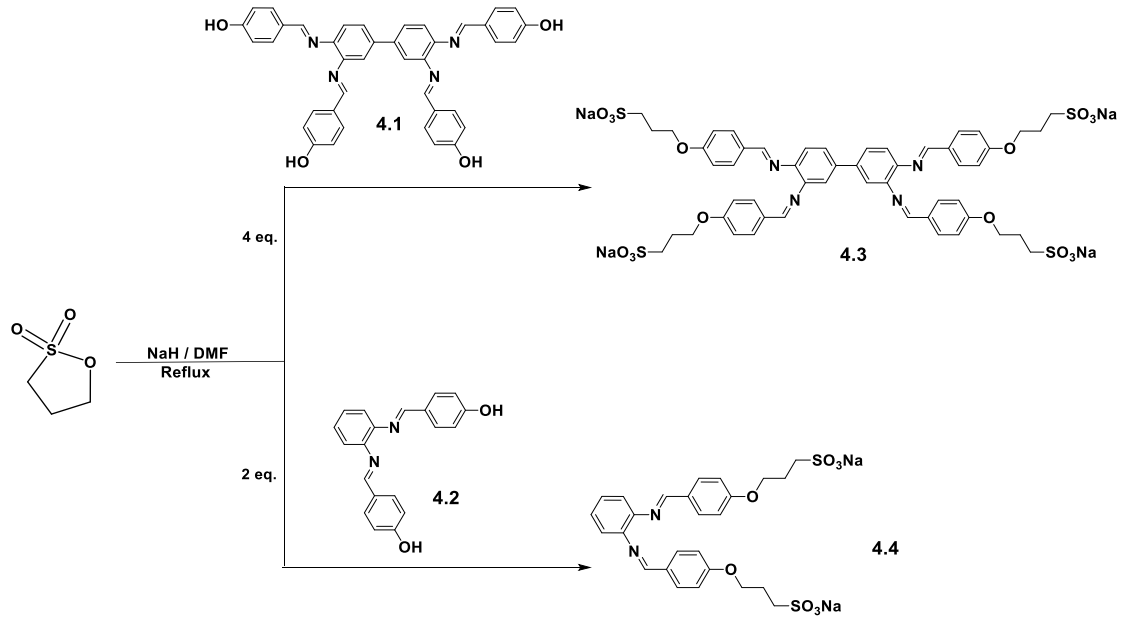


**Scheme 4.2** Synthesis of tetrasulfonated tetraamine ligand (**4.3**) and disulfonated diimine ligand (**4.4**).

Sodium hydride (NaH) was used as the deprotonating agent in the presence of anhydrous DMF. The ring-opening of the cyclic sulfonate by the nucleophilic attack from the phenoxide ion occurs readily to yield the desired compound **4.3** and **4.4**.[35,36] The tetrasulfonated tetraimine product **4.3** was isolated as an off-white powder in good yield of 74% and the disulfonated diimine compound **4.4** was isolated as a pale yellow powder in good yield of 86 %. Both compounds, **4.3** and **4.4** display excellent water-solubility of 127 mg/mL at room temperature.

***NMR spectroscopy***

The $^{1}$H NMR spectrum of compound **4.3** shown in Figure 4.4 displays aromatic proton signals in the region of 8.48 – 6.82 ppm. No phenolic signals at 9.96 and 9.40 ppm were observed. This is indicative of a successful deprotonation and the subsequent nucleophilic substitution. The sulfoalkylation of compound **4.3** is evident by the presence of aliphatic multiplet signals (H-3, H-1and H-2). Doubling up of the propyl proton signals were observed in the $^{1}$H NMR spectrum of compound **4.3**. This is ascribed to the alkylation of the two chemically non-equivalent phenolic hydroxyl protons H-1 and H-2 of compound **4.1**. The triplet at 4.15 and 3.98 ppm is assigned to the propyl protons H-3 or H-3* which is coupled to the neighbouring methylene protons H-2 or H-2*. Protons H-1 and H-1* appear as overlapping multiplets between 2.55 – 2.28 ppm due to coupling to the two adjacent methylene protons H-2 or H-2*. Additionally, the overlapping multiplets at 2.12 – 1.96 ppm are assigned to the H-2 or H-2* propyl protons which are adjacently coupled to H-1 or H-1* and H-3 or H-3* respectively.

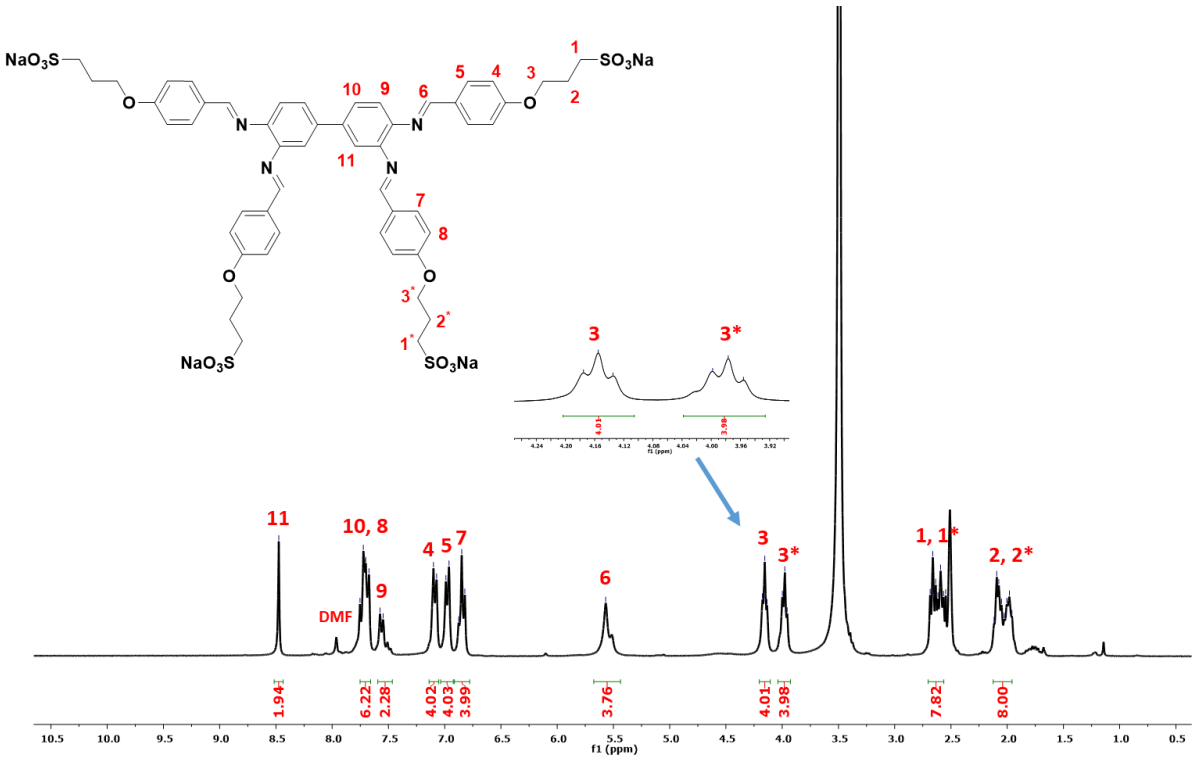


**Figure 4.4** $^{1}$H NMR spectrum of ligand **4.3** (DMSO-$d_6$), with duplicate peaks denoted by the asterisk.

The two triplet signals in the region of 4.18 – 3.96 ppm are assigned to the propyl protons H-3 which couple to the adjacent methylene protons H-2. The signals for protons H-2 appear as a multiplet at 2.12 – 1.96 ppm due to coupling to the two adjacent methylene protons H-3 and H-1. Additionally, the multiplet signals assigned to H-1 propyl protons are observed between 2.68 and 2.55 ppm.

No hydroxyl proton signals at 9.97 and 9.51 ppm were observed in the $^{1}$H NMR spectrum of ligand **4.4** as shown in Figure 4.5. This alludes to successful deprotonation and the subsequent sulfoalkylation reaction. The aromatic proton signals of ligand **4.4** appear between 7.69 and 6.84 ppm. Also, similar splitting patterns and doubling up of the propyl proton signals were observed in the $^{1}$H NMR spectrum of ligand **4.4** to that of **4.3**. The triplet at 4.14 and 3.99 ppm is assigned to the propyl proton H-10* or H-10 which is coupled to the adjacent methylene protons H-11* or H-11. The signal for proton H-11 and H-11* appear as multiplets between 2.08 – 1.92 ppm due to coupling to the two adjacent methylene protons H-10 and H-12. The

multiplets in the region of 2.61 – 2.33 ppm are assigned to the H-12* or H-12 propyl protons which are adjacently coupled to H-11 or H-11*.

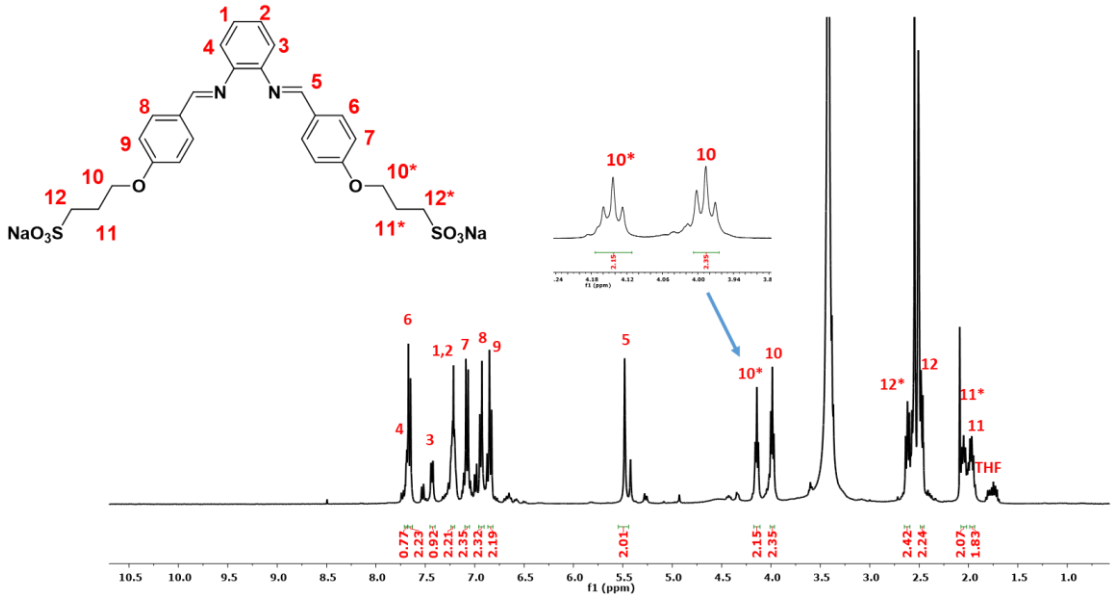


**Figure 4.5** $^{1}$H NMR spectrum of ligand **4.4** (DMSO-$d_6$), with duplicate peaks denoted by the asterisk.

The $^{13}C\{^{1}H\}$ NMR spectra of the sulfonated ligands show signals corresponding to the propyl carbon atoms, thus confirming the formation of the proposed compounds**.** The propyl carbon signals for compound **4.3** resonates at 69.57, 48.33 and 25.49 ppm while the propyl carbon signals for compound **4.4** are observed at 69.53, 48.30 and 29.16 ppm.

### *Infrared spectroscopy* and *Mass spectrometry*

IR spectroscopy was used to confirm the functional groups indicative of a successful alkylation reaction. The typical stretching frequencies for the sulfonate S=O functionality occur as an absorption band of medium intensity at 1175 $cm^{-1}$ and 1170 $cm^{-1}$ for compounds **4.3** and **4.4** respectively. Additionally, no hydroxy stretching vibration at the region of 3022 $cm^{-1}$ and 2936 $cm^{-1}$ were observed. The ESI–MS spectra of the water-soluble ligands show a fragment for $[M+H+Na]^{2+}$ in the positive ion-mode at *m/z* = 615.0889 (calcd 615.0832) for **4.3**, while a fragment for $[M+H]^{+}$ is observed in the positive ion-mode at *m/z* = 605.1008 (calcd 615.0972) for **4.4**.

### 4.2.3 Synthesis and characterization of water-soluble Rh(I) complexes 4.5 and 4.6

The synthesis of the water-soluble binuclear and mononuclear rhodium 1,5-cyclooctadiene (COD) complexes involved two reactions. First, the preparation of the $[Rh(COD)(MeCN)_2]BF_4$ metal precursor *via* successive bridge-splitting of $[(Rh(COD)Cl)_2]$ using $AgBF_4$ in acetonitrile at room temperature.[37] The by-product (AgCl) was removed using a syringe filter (PTFE, 0.25 μm) and the resulting solution was reduced under vacuum to afford $[Rh(COD)(MeCN)_2]BF_4$. This was followed by the reaction of compound **4.3** or **4.4** with $[Rh(COD)(MeCN)_2]BF_4$ in DMSO as illustrated in Scheme 4.3. The complexes **4.5** and **4.6** were isolated as pale green powders in yields of 63% and 58% respectively. The complexes, **4.5** and **4.6** display good water-solubility of 108 mg/mL and 103 mg/mL respectively at room temperature.

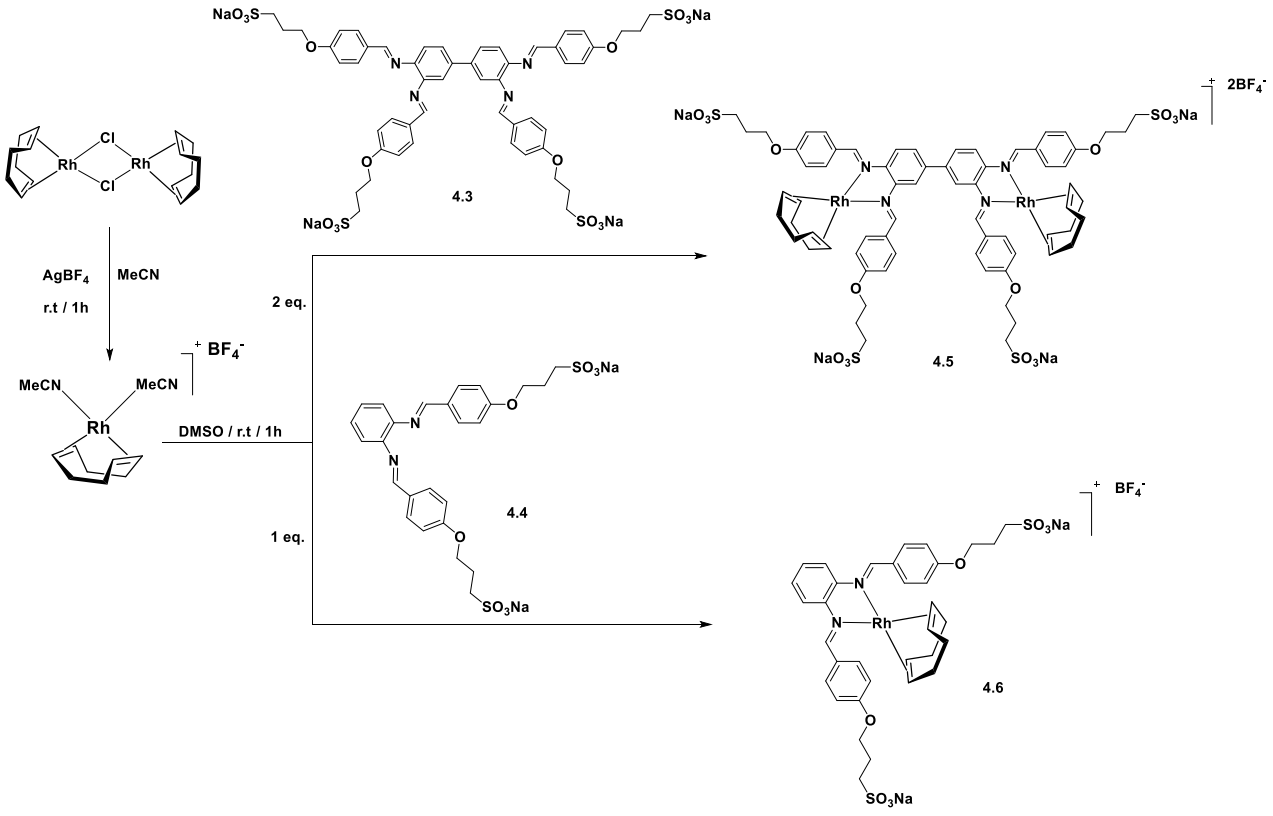


**Scheme 4.3** Synthesis of water-soluble binuclear and mononuclear rhodium complexes **4.5** and **4.6**

***NMR spectroscopy***

Comparing the $^1H$ NMR spectra of ligand **4.3** and complex **4.5** (Figure 4.6), evidence of successful coordination is the presence of the olefinic (H-12) and methylene (H-13 and H-14) proton signals of the COD ligand between 4.22 and 1.73 ppm. The olefinic COD proton H-12

appear as an overlapping broad signal with the methylene proton H-3. The methylene proton of the COD moiety H-13 and H-14 also appear as broad signals each integrating for eight protons. Additionally, a downfield shift was observed for protons H-10 and H-4 from 7.67 ppm to 8.07 ppm and from 7.09 ppm to 7.22 ppm respectively. This could be attributed to the deshielding effects of the Rh metal.

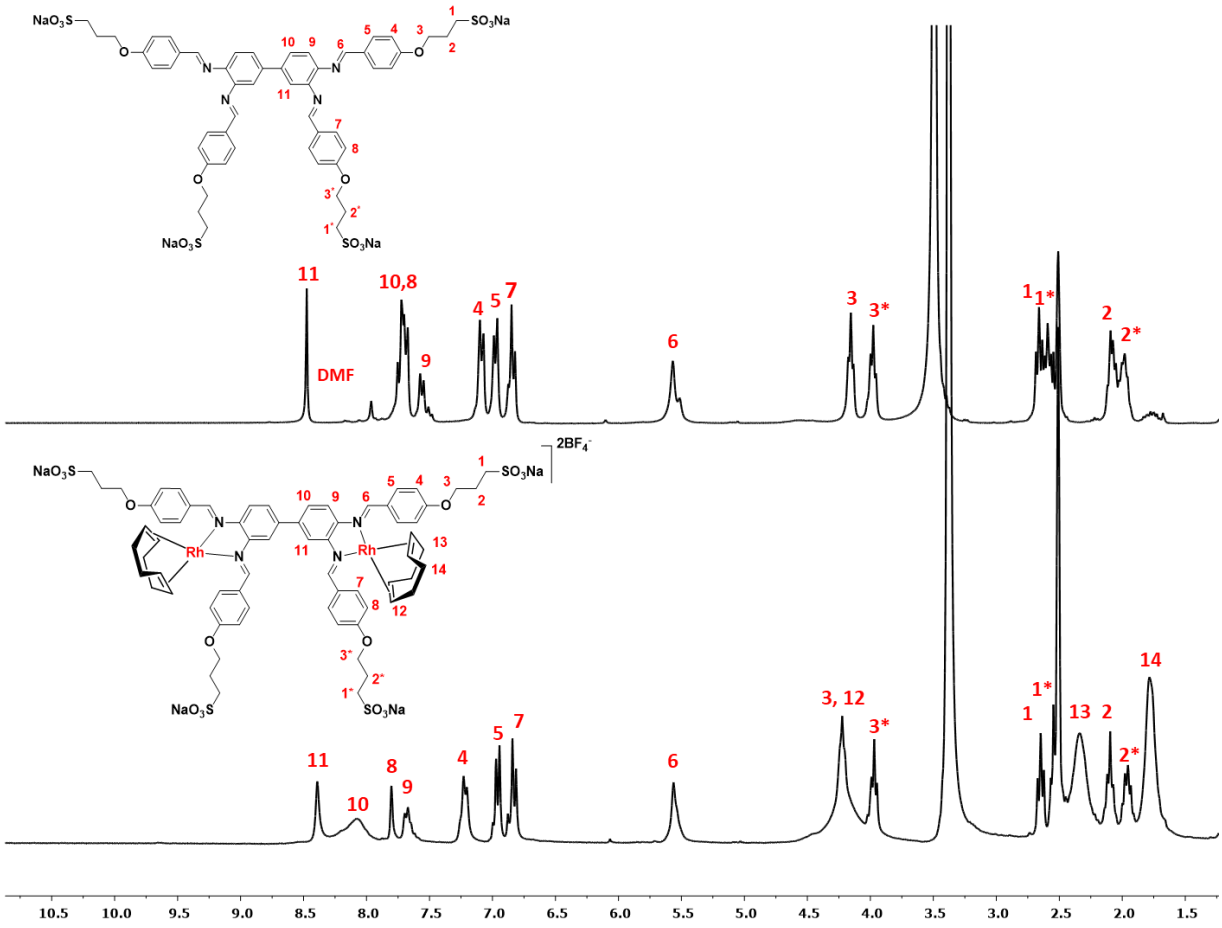


**Figure 4.6** Stacked $^{1}$H NMR spectra (DMSO-$d_6$) of ligand **4.3** and complex **4.5.**

The $^{1}$H NMR spectrum for complex **4.6** (Figure 4.7) displays similar signals to those observed in the $^{1}$H NMR spectrum of complex **4.5** (Figure 4.6). For instance, the signals of the cyclooctadiene ligand are observed as broad signals at 4.35, 2.33 and 1.80 ppm. Comparing the $^{1}$H NMR spectrum of ligand **4.4** and complex **4.6**, a significant coordination-induced downfield shift was observed for proton H-4 and H-6 from 7.69 – 7.84 ppm to 8.28 – 8.17 ppm (overlapping broad signal). This may be attributed to the deshielding effects of the Rh metal centre.[38,39]

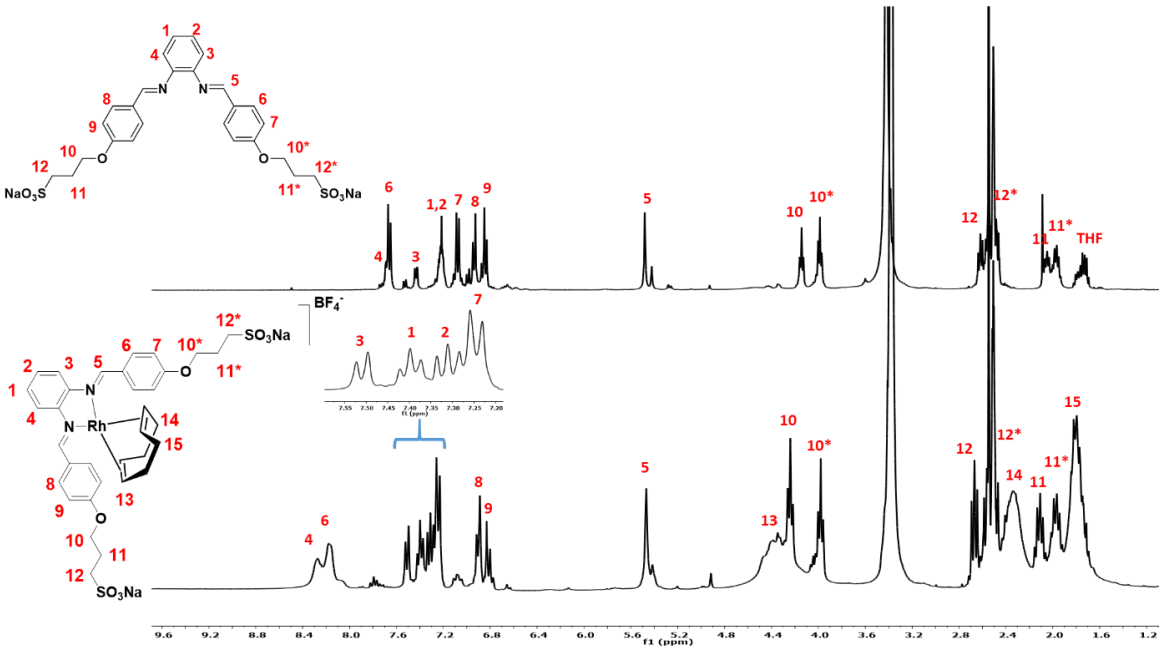


**Figure 4.7** Stacked $^{1}$H NMR spectra of ligand **4.4** and complex **4.6** in (DMSO-$d_6$).

The $^{13}$C{$^{1}$H} NMR spectra of the complexes reveal COD signals at 85.10 and 30.77 ppm for **4.5** and 86.31 and 30.73 ppm for **4.6**. This is further evidence of coordination of ligand **4.3** and **4.4** to the Rh metal centre.

***Infrared spectroscopy and Mass spectrometry***

Further evidence in support of the successful complexation of **4.3** and **4.4** is provided by Fourier-transform infrared (FT-IR) spectroscopy. The infrared spectra of the rhodium complexes show a shift of the imine absorption band to a lower wavenumber, from ν(C=N) = 1619 cm$^{-1}$ to 1608 cm$^{-1}$ for **4.5** and from ν(C=N) = 1628 cm$^{-1}$ to 1613 cm$^{-1}$ for compound **4.6**. This is attributed to the weakening of the imine functionality as a result of back-donation of electrons from the rhodium metal centre through synergic effects.[40] The mass spectrum of complex **4.5** (Figure 4.8) reveal a peak corresponding to the molecular ion adduct $[M+H+2Na]^{3+}$ at *m/z* = 558.1189 (calcd. 558.4861), while a peak for $[M]^{+}$ is observed at *m/z* =815.0464 (calcd. 815.0900) for **4.6** in the positive ion-mode.

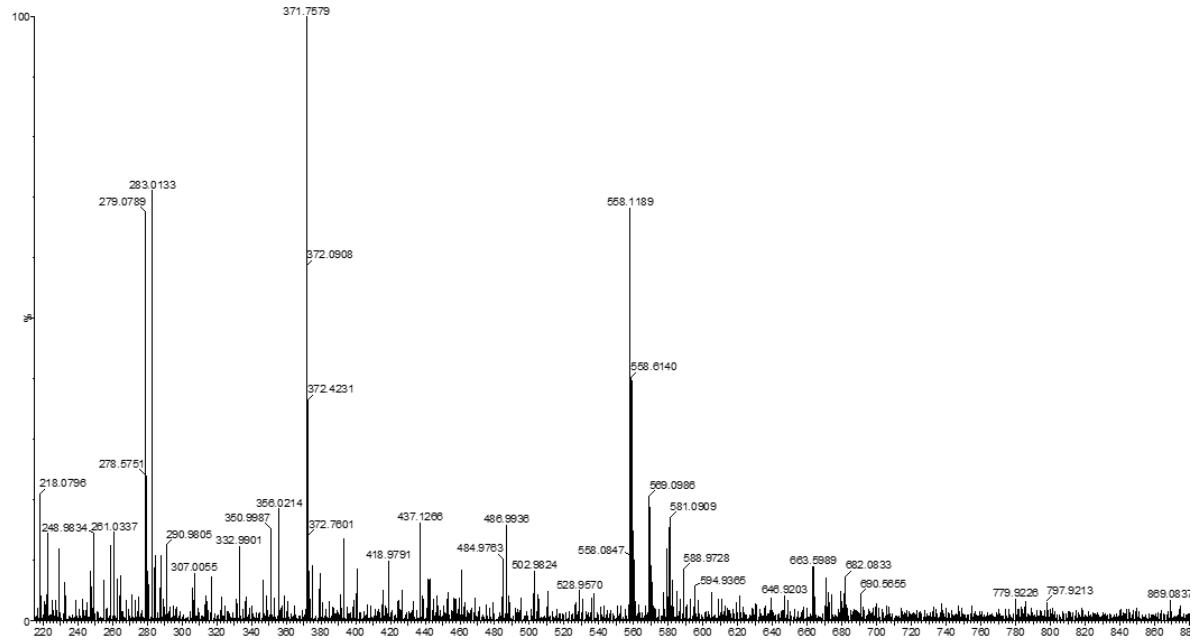


**Figure 4.8** Mass spectrum (positive mode) of complex **4.5**.

### 4.2.4 Aqueous biphasic hydroformylation studies

With the emergence of Green Chemistry, the type of reaction media used in a catalytic process is crucial for the recycling and isolation of the resulting product. The unique properties of water together with its non-toxicity has made it the solvent of choice for catalytic reactions.[41–43] In addition, the aqueous biphasic technique has been proven to be a successful tool for the separation and recycling of hydroformylation catalysts without additional energy demand.[44–46] Therefore, the continual development of this approach is integral to the economic and environmental viability of the chemical industry.

The water-soluble tetrasulfonated tetraimine Rh(I) complex **4.5** and its mononuclear analogue **4.6** were successfully evaluated as catalyst precursors in the aqueous biphasic hydroformylation of 1-octene using previously optimized conditions (75 °C and 40 bar)[47] for similar diimine systems (Section 2.3.1, Chapter 2 of this thesis).

#### 4.2.4.1 Catalytic evaluation of catalyst precursors 4.5 and 4.6

In order to obtain comparative results, the complexes, irrespective of the number of metal centres in their structures, were tested at the same catalyst loading. Additionally, the catalytic performance of catalyst precursor **4.5** was investigated in the presence of mercury and at reduced catalyst loading. The results are summarized in Table 4.1.

**Table 4.1** Hydroformylation of 1-octene using catalyst precursor **4.5** and **4.6**[a].

| Entry | Pre-catalyst | Conversion (%) | Aldehydes (%) | Linear Aldehydes (%) | Branched Aldehydes (%) | Iso-octenes (%) | TOF ($h^{-1}$) [b] |
|---|---|---|---|---|---|---|---|
| 1 | **4.5** | >99 | 94 | 59 | 41 | 6 | 581 |
| 2 | **4.6** | 96 | 87 | 57 | 43 | 13 | 525 |
| 3 | **4.5**[c] | 95 | 87 | 56 | 44 | 13 | 516 |
| 4 | **4.5**[d] | >98 | 94 | 60 | 40 | 6 | 579 |

[a]Reaction conditions: The reactor (90 mL) was loaded with $H_2O$ (5 mL), 1-octene (7.175 mmol), internal standard n-decane (1.435 mmol) and 2.87 $\times 10^{-3}$ mmol of catalyst (**4.5** and **4.6**). The reactor was purged with nitrogen three times, followed by purging three times with syngas. The reactions were carried out for 4 h at $75^0$C/40 bar and the data was analysed using GC-FID. [b]TOF = (mmol of aldehydes/mmol of catalyst)/time. [c] 1.44 $\times 10^{-3}$ mmol of Rh catalyst (**4.5**). [d]The reactions were conducted in the presence of mercury.

The binuclear precatalyst **4.5** shows good conversion (>99%, entry 1) of 1-octene at 4 h of the catalytic transformation, as well as good aldehyde selectivity (94%) and activity (581 $h^{-1}$). The mononuclear complex **4.6** shows 96% conversion of 1-octene with TOF values of 525 $h^{-1}$ and aldehyde selectivity of 87% (Table 4.1, entry 2) (Figure 4.9). The observed superior activity of precatalyst **4.5** can be ascribed to the presence of an extra metal centre. Similar trends in catalyst performance were observed by Smith and co-workers[2,48] and October *et al.*[49] in their investigation into the use of multinuclear rhodium complexes for hydroformylation reactions. In these cases, an overall increase catalyst activity is observed with increasing nuclearity from a single metal centre to multiple metal centres.

A comprehensive understanding of the observed catalytic performance is depicted in the substrate and product-distribution-time profiles of catalyst precursors **4.5** (Figure 4.10) and **4.6** (Figure 4.11), conducted over time under optimum conditions (75 °C and 40 bar). The catalyst precursors show progressive transformation of the substrate over time with substantial conversion after 4 h.

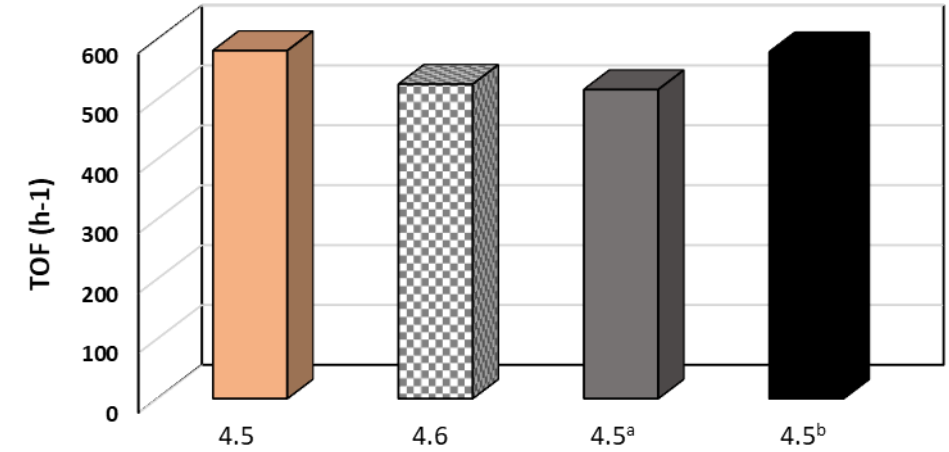


[a]Half catalyst loading
[b]In the presence of mercury

**Figure 4.9** Activity of catalyst precursor **4.5** and **4.6.**

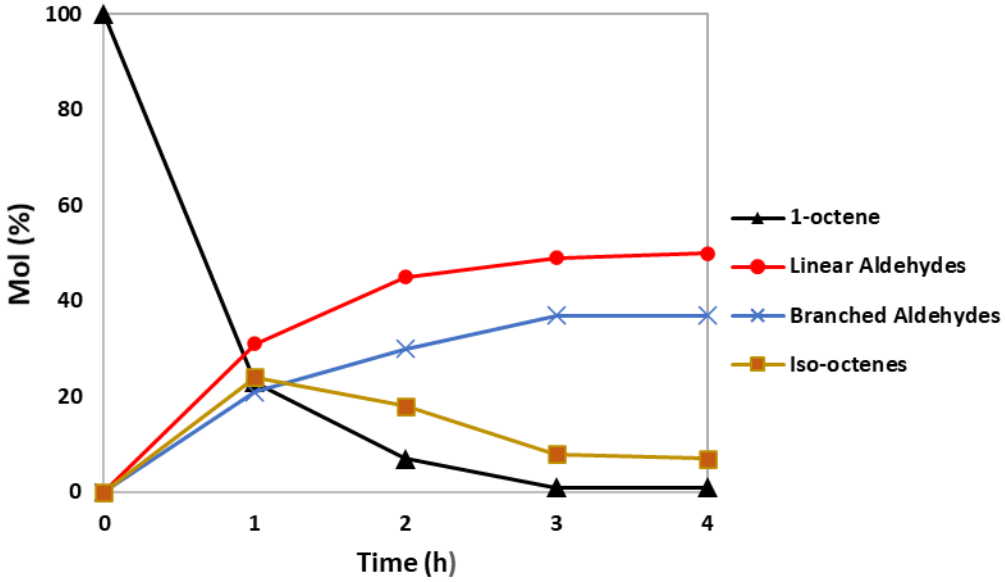


**Figure 4.10** Substrate and product-distribution-time profile of catalyst precursor **4.5**.

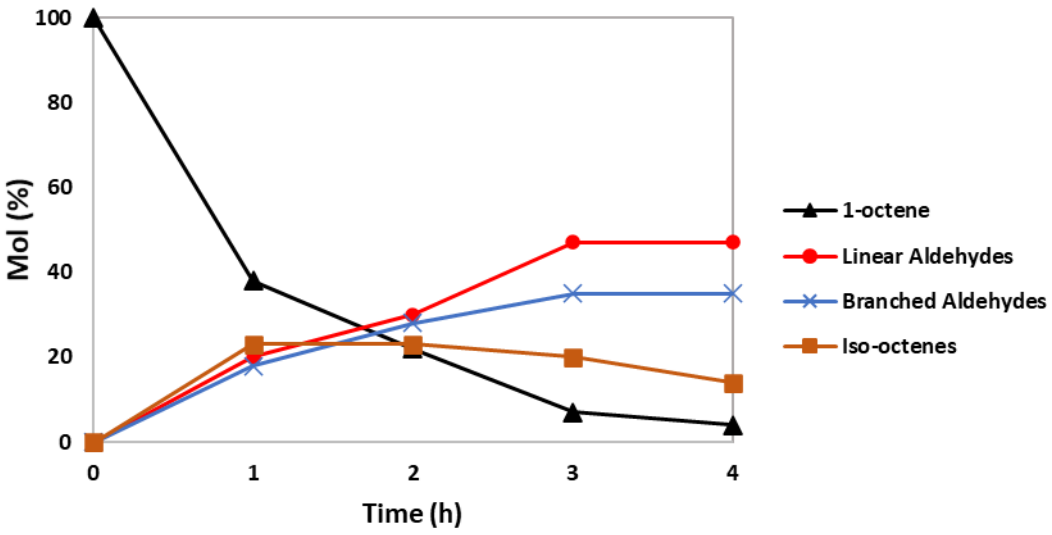


**Figure 4.11** Substrate and product-distribution-time profile of catalyst precursor **4.6**.

The superior performance of catalyst precursor **4.5** over the mononuclear complex **4.6** is observed in the first 1 h of the reaction. The product-distribution-time profile of the catalyst precursor **4.5** in the first stages of the reaction shows ca.23 mol% of 1-octene present in the system compared to ca. 38 mol% for the mononuclear complex **4.6**. Further consumption of 1-octene is noted at 2 h of the catalytic reaction giving ca. 7 mol% for catalyst precursor **4.5**. This depletes to a near quantitative conversion of 1-octene in 3 h. For the mononuclear complex **4.6**, a near quantitative catalytic transformation of 1-octene is attained at the 4 h reaction time.

With respect to chemo- and regioselectivity, the accumulation of iso-octenes is observed at 1 h of the catalytic reaction for both catalyst precursors, with comparable iso-octene quantities at this stage. An increase in the formation of branched aldehyde in the system is noted with an associated decrease in the formation of iso-octenes. This is ascribed to the ease of hydroformylation of the iso-octenes to yield branched aldehydes. It is therefore tenable to suggest that at this stage (after 1 h), the competitive isomerization of the substrate is gradually suppressed as a result of an increase in the formation of the regio-isomeric Rh-alkyl intermediates responsible for hydroformylation. Additionally, the regioselectivity towards linear aldehyde remains predominant at all stages of the reaction. This indicates that the anti-Markovnikov addition pathway is the major reaction route for the hydroformylation of 1-octene in this study.

Comparable regioselectivities are observed at 4 h with both catalyst precursors (*n/iso* = 59:41 and 57:43 (**4.5** and **4.6** respectively). This suggests that the regioselectivity was not impacted

directly by the presence of the second metal centre. This may be due to the non-closely associated metal centres (no synergistic effect). A bimetallic cooperative effect demonstrating increased regioselectivity has been reported in the literature wherein the spatial constrain of the two catalytic centres in close proximity is suggested to be a perquisite for sufficient ligand-exchange process between the two metal centres thus, leading to high regioselectivity in the hydroformylation.[50–52]

The effect of catalyst loading on the efficiency of **4.5** was examined. Reducing the catalyst loading from 2.87 $\times 10^{-3}$ mmol to 1.44 $\times 10^{-3}$ mmol (taking into consideration the presence of the two metal centres). The activity and selectivity of the precatalyst **4.5** gave results comparable to those of **4.6** as shown in Table 4.1, entries 2 and 3.

To gain insights into the homogeneity of the catalytic reaction,[53–55] mercury drop tests were conducted by adding a drop of mercury into a reactor containing catalyst precursor **4.5**, 1-octene and internal standard at conditions of 75 °C, 40 bar for 4 h. The activity, chemoselectivity and regioselectivity of the catalyst were similar to the reaction done in the absence of the mercury. This indicates that the catalytic reaction proceeds solely *via* a homogeneous species. (Table 4.1, entry 4).

#### 4.2.4.2 Recyclability of precatalyst 4.5 and 4.6

The recyclability of the water-soluble complexes **4.5** and **4.6** were evaluated as catalyst precursors in the aqueous biphasic hydroformylation of 1-octene at the same metal loading at optimum conditions of 75 °C and 40 bar. The resulting products of the reaction were extracted by adding a minimum amount of toluene and immediately decanted. The aqueous layer containing the catalyst is reused by adding fresh internal standard and substrate, this is repeated for the next catalytic cycle with assessment of the catalytic performance at each cycle. Analysis of the results obtained from the gas chromatography data is discussed in the following sections.

***The effect of catalyst recycling on conversion and activity***

The catalyst precursors were successfully recycled for at least 4 times, with a decline in conversion with each cycle (Figure 4.12). The binuclear precatalyst **4.5** shows decreased conversion of 83% in the second cycle, 45% in the third cycle and 18% in the fourth cycle. Similar decline in conversion was also observed with the mononuclear precatalyst **4.6**. The observed decrease in conversion with recycling of the catalysts could be attributed to low concentration of the active metal species in the aqueous layer after each cycle. This inevitable

decrease in active metal species may be attributed to the gradual metal degradation often observed with the continuous usage of the catalyst containing phase.[45,56–58]

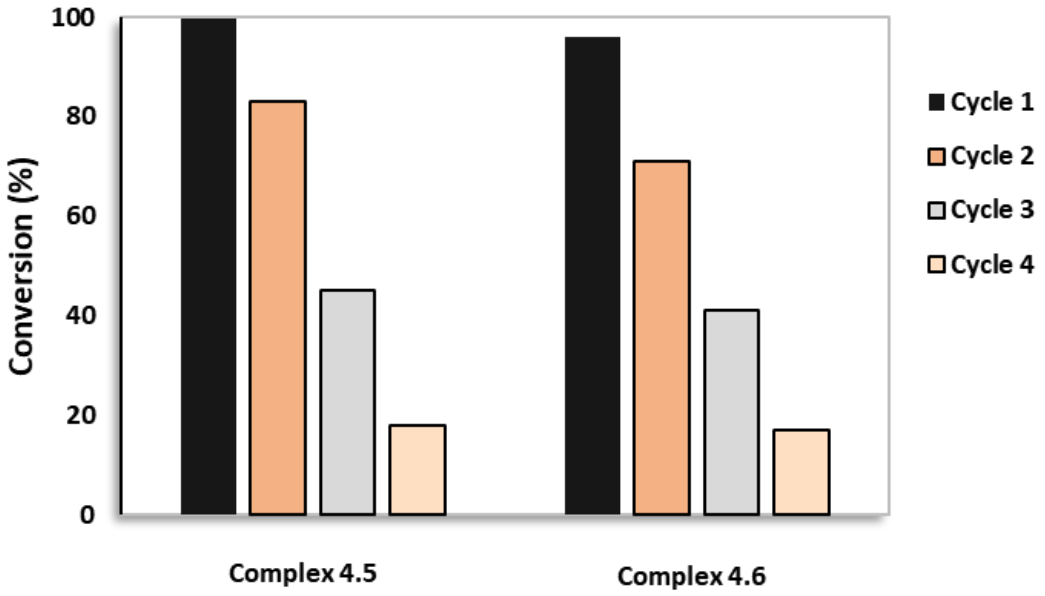


**Figure 4.12** Percentage conversion of 1-octene during the course of recycling.

Likewise, a decrease in the activity from the 1st cycle to the 2nd cycle (581 $h^{-1}$ to 284 $h^{-1}$ (**4.5**); and 526 $h^{-1}$ to 226 $h^{-1}$ (**4.6**) (Figure 4.13) is observed. The third and fourth cycle gave activities of 108 $h^{-1}$ and 32 $h^{-1}$ respectively for complex **4.5** and 67 $h^{-1}$ and 25 $h^{-1}$ respectively for complex **4.6**. It is important to note that the activities reported in the recyclability studies were calculated in reference to the initial catalyst loading.

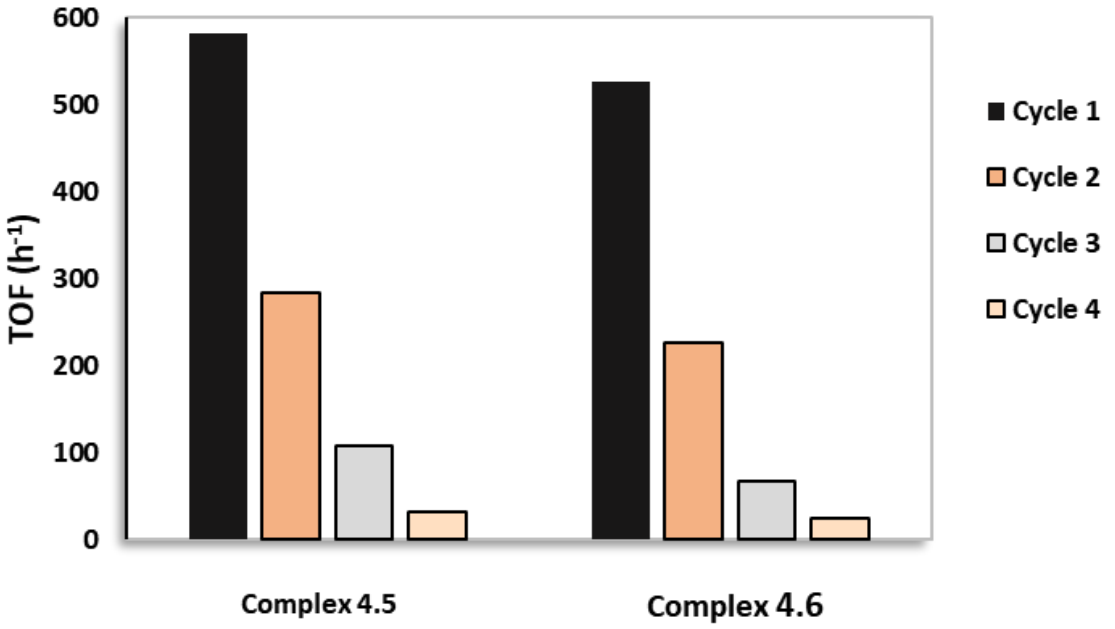


**Figure 4.13** Catalytic activity during the course of recycling.

*The effect of catalyst recycling on selectivity*

A drop in the formation of aldehyde from 94% to 55% for **4.5** and from 87% to 51% for **4.6** was observed after the second cycle, with an increase in the formation of iso-octenes from 6% to 45% for **4.5** and 13% to 49% for **4.6** as shown in Figure 4.14. The decrease in chemoselectivity is consistent in the third and fourth cycle forming predominantly isomerized products. Also, noticeable catalyst decomposition was observed by the darkened colouration of the aqueous phase. The decrease in chemoselectivity is consistent with the observed decrease in activity, as activity calculated herein is relative to the chemoselectivity for total aldehydes formed against the total conversion of the substrate.

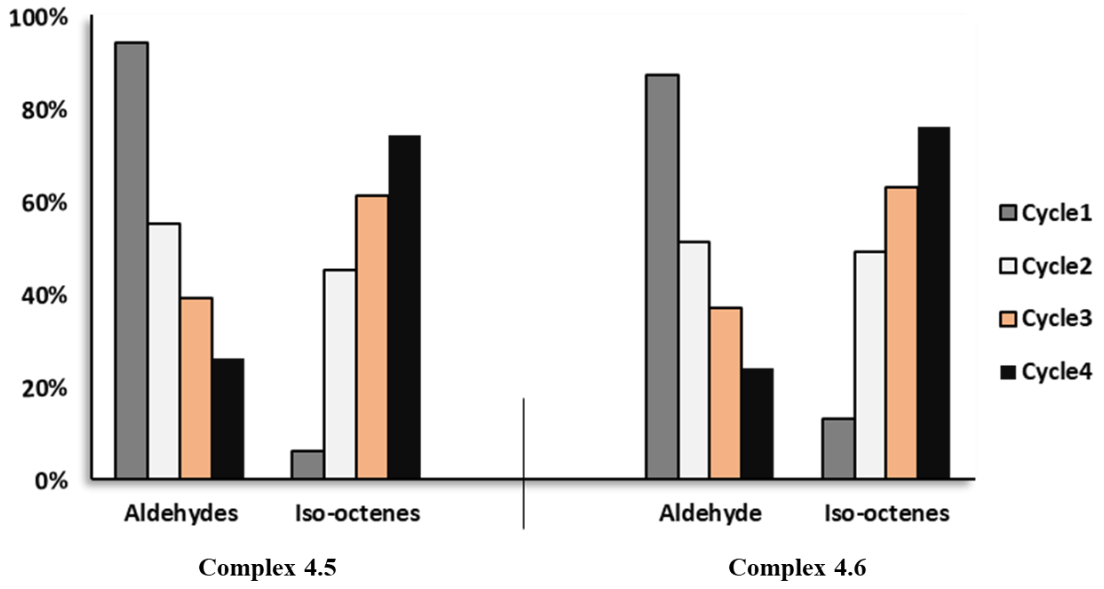


**Figure 4.14** Chemoselectivity of the complex **4.5** and **4.6** during recyclability

The regioselectivity of each catalyst varied upon recycling as shown in Figure 4.15. The predominant formation of the linear aldehyde was observed in the first two cycles while the formation of branched aldehydes appreciated in subsequent cycles. This may be attributed to changes in the structure of the active Rh-catalyst under hydroformylation conditions as it is recycled.

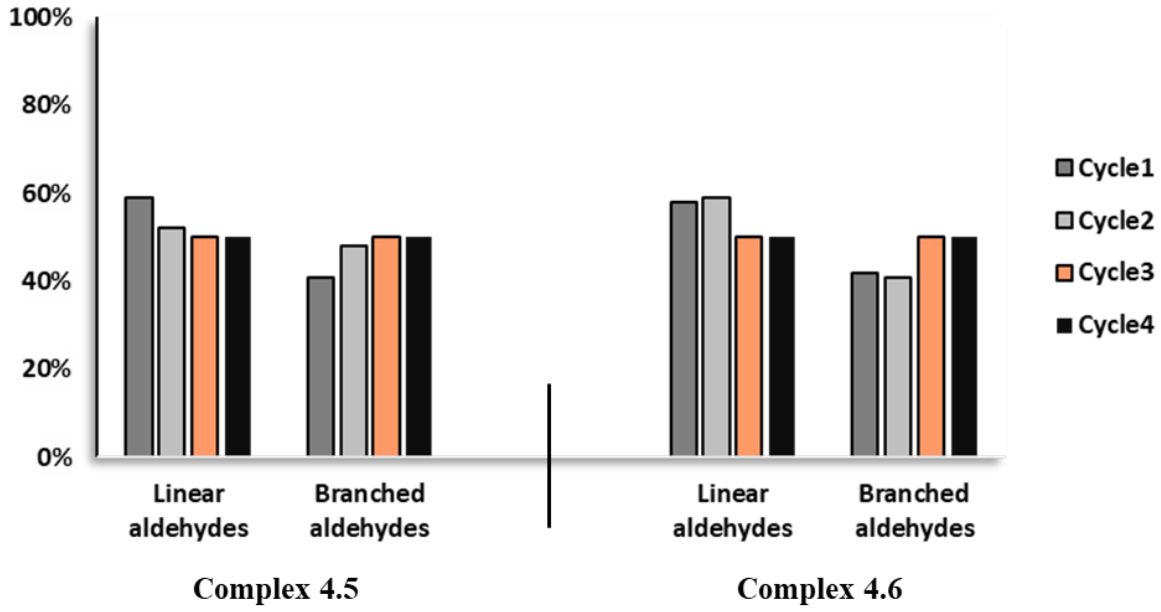


**Figure 4.15** Regioselectivity of the complex **4.5** and **4.6** during recyclability

It is also important to note that no hydrogenation products (alkanes or alcohols) were observed during the course of catalysts recycling. This is an indication of the excellent selectivity for aldehydes and iso-octenes only.

## 4.3 Summary

In this chapter, tetraimine and diimine Schiff-base compounds (**4.1** and **4.2**), and tetrasulfonated tetraimine and disulfonated diimine ligands (**4.3** and **4.4**) were successfully synthesized and isolated in good yields. The compounds (**4.1** – **4.4**) were characterised using an array of spectroscopic and analytical techniques. The sulfonated ligands (**4.3** and **4.4**) were complexed with the rhodium precursor ($[Rh(COD)(MeCN)_2]BF_4$) to form the respective sulfonated mononuclear and binuclear Rh(I) Schiff-base complexes (**4.5** and **4.6**). The complexes display excellent solubility in water and are stable at room temperature. $^{1}H$, $^{13}C\{^{1}H\}$ NMR spectroscopy, infrared spectroscopy, mass spectrometry (positive-ion mode) was used to confirm the structural integrity of the complexes. The efficiency of the water-soluble binuclear complex was evaluated as a catalyst precursor in the aqueous hydroformylation of 1-octene and compared to the hydroformylation efficiency of the water-soluble mononuclear complex.

The complexes (**4.5** and **4.6**) were active in the conversion of 1-octene to aldehydes, with TOF values over 500 $h^{-1}$. The binuclear Rh(I) catalyst precursor **4.5** gave relatively higher activities compared to catalyst precursor **4.6**. The recyclability of the active metal species was successfully conducted for over 4 cycles. Decreased catalytic activity were observed for **4.5** and **4.6** after each cycle. In addition, mercury poisoning experiment using catalyst precursor **4.5** showed that the hydroformylation reactions were catalysed by homogeneous species, a phenomenon that has been previously observed when using related catalyst precursors.[47]

## 4.4 References

1 S. Pal and C. Uyeda, *J. Am. Chem. Soc.*, 2015, **137**, 8042–8045.

2 N. C. Antonels, J. R. Moss and G. S. Smith, *J. Organomet. Chem.*, 2011, **696**, 2003–2007.

3 B. C. E. Makhubela, A. M. Jardine, G. Westman and G. S. Smith, *Dalton Trans.*, 2012, **41**, 10715.

4 S. Siangwata, N. C. C. Breckwoldt, N. J. Goosen and G. S. Smith, *Appl. Catal. A Gen.*,

2019, **585**, 117–179.

5 N. Krittametaporn, T. Chantarojsiri, A. Virachotikul, K. Phomphrai, N. Kuwamura, T. Kojima, T. Konno and P. Sangtrirutnugul, *Dalton Trans.*, 2020, **49**, 682–689.

6 D. R. Pye and N. P. Mankad, *Chem. Sci.*, 2017, **8**, 1705–1718.

7 M. Sankar, N. Dimitratos, P. J. Miedziak, P. P. Wells, C. J. Kiely and G. J. Hutchings, *Chem. Soc. Rev.*, 2012, **41**, 8099–8139.

8 F. Yu, V. M. Cangelosi, M. L. Zastrow, M. Tegoni, J. S. Plegaria, A. G. Tebo, C. S. Mocny, L. Ruckthong, H. Qayyum and V. L. Pecoraro, *Chem. Rev.*, 2014, **114**, 3495–3578.

9 C. E. Valdez, Q. A. Smith, M. R. Nechay and A. N. Alexandrova, *Acc. Chem. Res.*, 2014, **47**, 3110–3117.

10 J. J.Villafranca and F. M.Raushel, *Adv. Catal.*, 1979, **28**, 323–369.

11 S. De Doncker, A. Casimiro, I. A. Kotze, S. Ngubane and G. S. Smith, *Inorg. Chem.*, 2020, **59**, 12928–12940.

12 J. P. McInnis, M. Delferro and T. J. Marks, *Acc. Chem. Res.*, 2014, **47**, 2545–2557.

13 T. J. Mazzacano and N. P. Mankad, *J. Am. Chem. Soc.*, 2013, **135**, 17258–17261.

14 S. W. S. Choy, M. J. Page, M. Bhadbhade and B. A. Messerle, *Organometallics*, 2013, **32**, 4726–4729.

15 Y. Zhang, Z. N. Chen, X. Zhang, X. Deng, W. Zhuang and W. Su, *Commun. Chem.*, 2020, **3**, 1–9.

16 M. Shibasaki, M. Kanai, S. Matsunaca and N. Kumagai, *Acc. Chem. Res.*, 2009, **42**, 1117–1127.

17 N. Xiong, G. Zhang, X. Sun and R. Zeng, *Chinese J. Chem.*, 2020, **38**, 185–201.

18 A. B. Kremer, K. M. Osten, I. Yu, T. Ebrahimi, D. C. Aluthge and P. Mehrkhodavandi, *Inorg. Chem.*, 2016, **55**, 5365–5374.

19 A. J. Pardey, J. D. Suárez, M. C. Ortega, C. Longo, J. J. Pérez-Torrente and L. A. Oro, *Open Catal. J.*, 2010, **4**, 44–49.

20 M. G. Timerbulatova, M. R. D. Gatus, K. Q. Vuong, M. Bhadbhade, A. G. Algarra, S. A. Macgregor and B. A. Messerle, *Organometallics*, 2013, **32**, 5071–5081.

21 P. Buchwalter, J. Rosé and P. Braunstein, *Chem. Rev.*, 2015, **115**, 28–126.

22 H. W. Bohnen and B. Cornils, *Adv. Catal.*, 2002, **47**, 1–64.

23 J. Park and S. Hong, *Chem. Soc. Rev.*, 2012, **41**, 6931–6943.

24 E. K. Van Den Beuken and B. L. Feringa, *Tetrahedron*, 1998, **54**, 12985–13011.

25 D. G. H. Hetterscheid, S. H. Chikkali, B. DeBruin and J. N. H. Reek, *ChemCatChem*, 2013, **5**, 2785–2793.

26 I. Bratko and M. Gómez, *Dalton Trans.*, 2013, **42**, 10664–10681.

27 H. Li and T. J. Marks, *Proc. Natl. Acad. Sci. U. S. A.*, 2006, **42**, 15295–15302.

28 S. L. Suib, *New and Future Developments in Catalysis*, 2013.

29 M. Valencia, H. Müller-Bunz, R. A. Gossage and M. Albrecht, *Chem. Commun.*, 2016, **52**, 3344–3347.

30 S. C. Van Wyk, M. O. Onani and N. Ebbe, *Chem. Pap.*, 2016, **70**, 523–531.

31 C. Van Leeuwen, Piet W.N.M., Claver, *Rhodium Catalyzed Hydroformylation: Introduction to hydroformylation*, Kluwer Academic Publishers, Dordrecht, 2000.

32 R. Peters, *Cooperative Catalysis: Designing Efficient Catalysts for Synthesis*, John Wiley & Sons, Inc., 2015.

33 M. Gao, S. Han, Y. Hu and L. Zhang, *J. Phys. Chem. C*, 2016, **120**, 9299–9307.

34 S. Smanmoo, S. Kawasaki, P. Tangboriboonrat, T. Shibata, T. Kabashima and M. Kai, *J. Fluoresc.*, 2013, **23**, 853–857.

35 A. Natrajan and D. Wen, *Green Chem. Lett. Rev.*, 2013, **6**, 237–248.

36 M. Zhou, Y. Chen, J. Zou and J. Bu, *J. Surfactants Deterg.*, 2018, **21**, 443–453.

37 B. Oelkers and J. Sundermeyer, *Dalton Trans.*, 2011, **40**, 12727–12741.

38 J. Novotný, J. Vícha, P. L. Bora, M. Repisky, M. Straka, S. Komorovsky and R. Marek, *J. Chem. Theory Comput.*, 2017, **13**, 3586–3601.

39 W. Von Philipsborn, *Chem. Soc. Rev.*, 1999, **58**, 613–628.

40 G. Frenking and N. Fröhlich, *Chem. Rev.*, 2000, **100**, 717–774.

41 T. Kitanosono, K. Masuda, P. Xu and S. Kobayashi, *Chem. Rev.*, 2018, **118**, 679–746.

42 Y. Jung and R. A. Marcus, *J. Am. Chem. Soc.*, 2007, **129**, 5492–5502.

43 T. Lorenzetto, G. Berton, F. Fabris and A. Scarsoa, *Catal. Sci. Technol.*, 2020, **10**, 4492–4502.

44 L. C. Matsinha, S. Siangwata, G. S. Smith and B. C. E. Makhubela, *Catal. Rev. Sci. Eng.*, 2019, **61**, 111–133.

45 R. Franke, D. Selent and A. Börner, *Chem. Rev.*, 2012, **112**, 5675–5732.

46 A. Cocq, H. Bricout, F. Djedaïni-Pilard, S. Tilloy and E. Monflier, *Catalysts*, 2020, **10**, 56.

47 N. N. Omosun and G. S. Smith, *Eur. J. Inorg. Chem.*, 2019, 2558–2564.

48 D. S. Ramarou, B. C. E. Makhubela and G. S. Smith, *J. Organomet. Chem.*, 2018, **870**, 23–31.

49 J. October and S. F. Mapolie, *J. Organomet. Chem.*, 2017, **840**, 1–10.

50 M. E. Broussard, B. Juma, S. G. Train, W. J. Peng, S. A. Laneman and G. G. Stanley, *Science*, 1993, **260**, 1784–1788.

51 P. Kalck, *Homo- and Heterobimetallic Complexes in Catalysis*, Springer International Publishing, 2016.

52 A. Börner and R. Franke, *Hydroformylations: Fundamentals, Processes and Applications in Organic Synthesis*, Wiley-VCH, Weinheim, 2016.

53 O. N. Gorunova, I. M. Novitskiy, Y. K. Grishin, I. P. Gloriozov, V. A. Roznyatovsky, V. N. Khrustalev, K. A. Kochetkov and V. V. Dunina, *Organometallics*, 2018, **37**, 2842–2858.

54 J. K. Dunleavy, *Platin. Met. Rev.*, 2006, **50**, 156.

55 Y. Fonseca, B. Fontal, M. Reyes, T. Suárez, F. Bellandi, J. C. Diaz and P. Cancines, *React. Kinet. Mech. Catal.*, 2012, **7**, 27–33.

56 D. Cantillo and C. O. Kappe, *ChemCatChem*, 2015, **6**, 3286–3305.

57 S. Hanf, L. A. Rupflin, R. Gläser and S. A. Schunk, *Catalysts*, 2020, **10**, 510–546.

58 J. Pospech, I. Fleischer, R. Franke, S. Buchholz and M. Beller, *Angew. Chem. Int. Ed.*, 2013, **52**, 2852–2872.

# Chapter 5

## Summary, Conclusions and Future Outlook

### 5.1 Overall summary and conclusions

The overall aim of this project was to synthesize and characterise new water-soluble disulfonated α-diimine Rh(I) complexes, three generations of core-functionalised alpha-diimine poly(aryl ether) Rh(I) metallodendrimers, a water-soluble tetrasulfonated tetraimine binuclear Rh(I) complex and to evaluate these complexes as catalyst precursors in the hydroformylation of 1-octene. Recyclability studies of the water-soluble disulfonated α-diimine Rh(I) complexes and the water-soluble tetrasulfonated tetraimine binuclear Rh(I) complex were performed using the aqueous-biphasic strategy. The effect of increasing dendritic scaffold on catalyst performance was assessed. Also, preliminary homogeneity tests were carried out to gain insights into the nature of the catalysts. To the best of our knowledge, this is the first report on the synthesis of these complexes and their assessment as catalyst precursors for the hydroformylation reaction.

#### 5.1.1 Synthesis and catalytic evaluation of disulfonated alpha-diimine Rh(I) complexes

Alpha-diimine (1, 4-diazabutadiene) ligands bearing either ethyl or acenaphthene backbone (**2.1** and **2.2**) were synthesised *via* the Schiff condensation reaction of 4-aminophenol with carbonyl compounds (1,2-ethanedione or acenapthenequinone). The alpha-diimine ligands were reacted with $[Rh(COD)(MeCN)_2]BF_4$ to yield new alpha-diimine rhodium(I) complexes **2.5** and **2.6**. Sulfopropylation reactions of **2.1** and **2.2** with 1,3 propanesultone afforded water-soluble disulfonated α-diimine ligands (**2.3** and **2.4**). Ligands **2.3** and **2.4** display excellent water-solubility at room temperature of 123 mg/mL and 128 mg/mL respectively. New water-soluble disulfonated α-diimine Rh(I) complexes (**2.7** and **2.8**) bearing either H or $C_{10}H_8$ backbone were synthesized by reacting ligands **2.3** or **2.4** with $[Rh(COD)(MeCN)_2]BF_4$. The complexes (**2.7** and **2.8**) display good water-solubility of 102 mg/mL and 106 mg/mL respectively at room temperature.

The complexes (**2.7** and **2.8**) were evaluated as catalyst precursors in the hydroformylation of 1-octene and compared to their non-water-soluble analogues (**2.5** and **2.6)**. Preliminary studies

using catalyst precursor **2.5** identified 75 °C and 40 bar as the optimum condition with respect to activity and selectivity under mild conditions. All catalyst precursors **2.5** – **2.8** display good activity in the hydroformylation of 1-octene. In the aqueous biphasic hydroformylation of 1-octene, higher turnover frequencies and chemo/regioselectivities was observed using water-soluble catalysis precursor **2.7** and **2.8**. The recyclability experiments revealed that the catalysts can be used up to four reaction runs with a loss in catalytic activity observed after the third cycle. The decrease in catalytic performance of **2.7** and **2.8** was attributed to catalyst decomposition and not to the leaching of rhodium to the organic layer as this was confirmed by ICP-MS analysis. In addition, the mercury drop test confirmed that the water-soluble catalysts (**2.7** and **2.8**) were molecularly dispersed in the reaction media.

The advantages of the disulfonated α-diimine Rh(I) complexes include:

(a) A facile synthesis in good yields; this makes it scalable and feasible for industrial use.
(b) Facilitates hydroformylation reactions in a nontoxic and inexpensive reaction medium.
(c) Good catalytic activity and chemoselectivity for aldehydes under mild reaction conditions.
(d) The ease of catalyst/product separation through non-destructive and less energy intensive method.
(e) Reusable over multiple cycles with sustained catalytic performance.
(f) Negligible catalyst leaching into the product phase (no purification steps are required).

### 5.1.2 Synthesis and catalytic evaluation of Rh(I) alpha-diimine-cored poly aryl ether (PAE) metallodendrimers

Two generations of Fréchet-type dendrons (**3.1** – **3.4**) were successfully synthesised and characterised. New poly(aryl ether) dendrimers (**3.5** – **3.10**) based on an α-diimine-*N*,*N* core were synthesized using the convergent-growth route method by reacting methyl 4-(bromomethyl) benzoate or the Fréchet dendrons (**3.2** and **3.4**) with either α-diimine (1, 4-diazabutadiene) compounds **2.1** or **2.2**. Rh(I) alpha-diimine-cored aryl ether metallodendrimers bearing either an ethyl or acenaphthene backbone were synthesised by reacting compounds **3.5** – **3.10** with $[Rh(COD)(MeCN)_2]BF_4$ metal precursor.

The electron-donating character of the dendritic rhodium complexes was established by means of cyclic voltammetry. The complexes show irreversible oxidation, affording new species that does not revert to the starting complex upon reduction.

The efficiency of the complexes as catalyst precursors in the hydroformylation of 1-octene and styrene were evaluated using optimized conditions (75 °C and 40 bar) for 4 h. The catalyst precursors (**3.11** – **3.16**) display good activity and excellent chemoselectivity in the hydroformylation of 1-octene. Higher generation dendrimers (**3.15** – **3.16**) display better regioselectivity in the hydroformylation of 1-octene compared to the lower generation analogues as a result of increased steric interactions. However, with the exception of the $G_0$ dendrimers, a decrease in activity is observed due to mass transfer limitations. The substrate and product-distribution-time study using the representative catalyst precursor **3.16** revealed an increase in catalyst performance at extended reaction time. In the hydroformylation of styrene, the catalyst precursors (**3.11** – **3.16**) display good activity and regioselectivity towards branched aldehydes. The regioselectivity of the low generation metallodendrimers is similar to that shown by the larger dendritic analogues These observations suggest that there is no cooperativity with respect to sterics around the metal centre in the hydroformylation of styrene.

Mercury poisoning experiments performed on the complexes (**3.11**, **3.13** and **3.16**) showed significant loss in activity in the presence of mercury. This suggests a combination of homogeneous and heterogeneous catalysis. In addition, high pressure NMR (HP-NMR) spectroscopy data confirmed the formation of the catalytically active hydride specie.

The advantages of the metallodendrimers as catalyst precursors include:

(a) Mild operating conditions that give good catalytic activity and chemoselectivity for aldehydes in the hydroformylation of 1-octene.
(b) Potential candidates as separable and recyclable catalysts through nano-filtration techniques as a result of their high molecular weight.
(c) Can be used for the hydroformylation of substituted aryl olefinic substrates and the plausible application for more challenging internal olefins.

### 5.1.3 Synthesis and catalytic evaluation of water-soluble mononuclear diimine and binuclear tetraimine Rh(I) complexes

Tetraimine and diimine compounds **4.1** and **4.2** were synthesised *via* the Schiff condensation reaction of 3,3'-diaminobenzidine or *O*-phenylenediamine with 4-hydroxybenzaldehyde. Sulfopropylation reaction of **4.1** and **4.2** with 1,3 propanesultone afforded water-soluble tetrasulfonated tetraamine ligand (**4.3**) and disulfonated diimine ligand (**4.4**). New water-

soluble Rh(I) complexes (**4.5** and **4.6**) were synthesized by reacting ligands **4.3** or **4.4** with $[Rh(COD)(MeCN)_2]BF_4$. Also, the complexes display good water-solubility at room temperature (108 mg/mL and 103 mg/mL for **4.5** and **4.6** respectively).

The water-soluble tetraimine binuclear complex **4.5** and diimine mononuclear complex **4.6** were evaluated as catalyst precursors in the aqueous biphasic hydroformylation of 1-octene. The catalysts display good activity and chemoselectivity at 40 bar syngas pressure and 75 °C hydroformylation conditions. Using the same metal loading, the conversion of 1-octene is above 99% for precatalyst **4.5** and 96% for precatalyst **4.6**. This overall catalytic performance can attest to the good interaction of the substrate with the bulk catalyst–containing aqueous phase under hydroformylation conditions. The presence of an extra metal centre in complex **4.5** led to an increase in catalyst performance compared to the mononuclear analogue **4.6**. However, no significant effect on the regioselectivity was observed which is presumed to be due to the non-spatial proximity of the two metal centres. Studies of the catalyst precursors over time showed that the presence of an extra metal centre led to faster substrate conversion compared to the mononuclear analogue **4.6**. Reducing the catalyst loading by half for catalyst precursor **4.5** gave similar performance to catalyst **4.6**. In the recycling experiments, the catalysts could easily be recovered and recycled up to 4 times. However, a significant drop in catalyst performance is observed for both catalyst precursor **4.5** and **4.6** after each cycle. The decline in catalyst performance may be attributed to catalyst degradation as a consequence of persistent heating and applied pressure over the cycles. The mercury poisoning experiments conducted suggest that the catalyst precursors behave entirely as homogeneous species in the biphasic hydroformylation of 1-octene.

### 5.1.4 Comparative analyses of water-soluble complexes and metallodendrimers

This study demonstrates that the aqueous biphasic hydroformylation strategy (two-phase catalysis) is a favourable catalytic system that facilitates the separation of catalyst without any energy intensive procedures. Also, the separation method is simple, fast and no purification step is required. The incorporation of dendritic ligands to metal centres complements the focus on the designing of sterically encumbered ligands as a means of improving catalyst regioselectivity towards linear aldehydes. The water-soluble complexes display slightly superior catalytic performance in comparison to the high generation metallodendrimers. However, this dendritic strategy is suitable and more efficient for nanofiltration techniques either by batch wise processes or continuous-flow reactor systems. Although dendritic catalysts

have been used in several reactions, more experiments are required to provide deeper insight into dendritic effects in catalysis and catalyst recycling.

**Table 5.1** Comparison of catalyst performance synthesised in this study.

| Catalyst | Substrate | Conversion | Ald[a] (L:b) (%) |
|---|---|---|---|
| **2.5** | 1-Octene | 95 | 72 (69:31) |
| **2.6** | 1-Octene | 97 | 70 (70:30) |
| **2.7** | 1-Octene | 98 | 86 (66:34) |
| **2.8** | 1-Octene | 99 | 88 (73:27) |
| **3.11** | 1-Octene | 99 | 99 (51:49) |
| **3.12** | 1-Octene | 99 | 98 (49:51) |
| **3.13** | 1-Octene | 92 | 95 (54:46) |
| **3.14** | 1-Octene | 90 | 95 (59:41) |
| **3.15** | 1-Octene | 81 | 85 (67:33) |
| **3.16** | 1-Octene | 82 | 83 (67:33) |
| **3.11** | Styrene | 99 | 99 (67:33) |
| **3.14** | Styrene | 97 | 97 (67:33) |
| **3.16** | Styrene | 84 | 84 (67:33) |
| **4.5** | 1-Octene | 99 | 94 (59:41) |
| **4.6** | 1-Octene | 96 | 87 (57:43) |

[a] percentage total aldehyde, substrate (7.175 mmol) and catalyst ($2.87 \times 10^{-3}$ mmol).

## 5.2 Future outlook

The diimine Schiff-base complexes studied herein exhibit promising catalytic properties. However, in order to broaden the application of these complexes, an important question to be addressed is 'if the complexes retain their structural integrity and stability after each hydroformylation reaction cycle'. These concerns can be investigated by *in situ* temperature-programmed decomposition (TPD) studies together with operando high-pressure (HP) NMR and IR studies under hydroformylation conditions.[1,2] The operando spectroscopy technique allows for continuous spectra collection under catalytic operating conditions, therefore, the simultaneous evaluation of the structure and stability of a catalyst can be determined. In addition, for optimal efficiency, molecular-level computational investigation (quantum mechanics/molecular mechanics (QM/MM)) and in-depth kinetic studies are paramount in identifying, the resting state, the rate-determining step and the effective barriers of these class of diimine catalyts.[3–5]

Based on the outcomes of this study, structural modifications can be made to the diimine Rh(I) catalyst precursors in order to improve their catalytic efficiency. The proposed structural modifications to the diimine Rh(I) catalyst precursor are depicted in Figure 5.1. Introducing electron-donating and electron-withdrawing substituents to the Rh(I) catalyst precursors may impose favourable electronic effects which could improve the catalyst performance. Precedence of this has been reported in the literature.[6,7] Additionally, improved regioselectivity towards linear aldehyde can be achieved by incorporating bulky tertiary-butyl groups close to the metal centre.

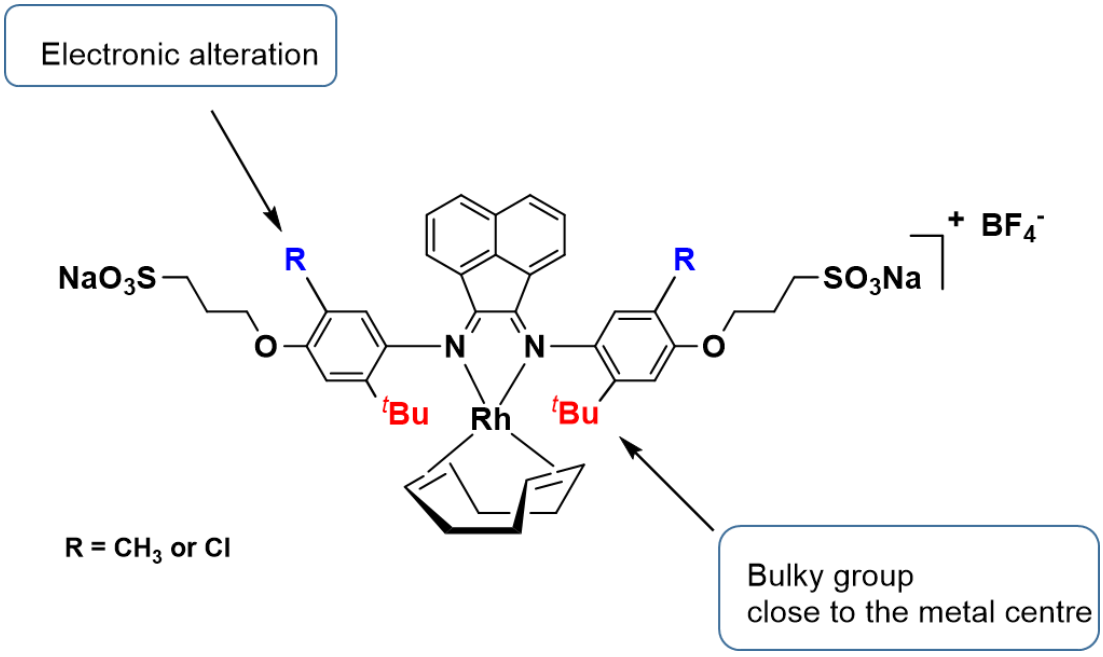


Figure 5.1 Proposed structural modification towards diimine Rh(I) catalysts improvement.

For future work, the recyclability of the metallodendrimers synthesised in this study can be touted through nanofiltration techniques. This is because, the metallodendrimers ($G_2$) attain the molecular weight cut-offs (MWCO) of commercially available nanofiltration membranes and continuous-flow membrane reactors.[8,9] Furthermore, metallodendrimers based on water-soluble Fréchet-type poly(aryl ether) (PAE) dendritic architectures can be explored for aqueous biphasic catalytic reactions. This can be achieved by converting the methyl-esters at the periphery to carboxylate salts, thus conferring hydrophilic properties.[10]

It is noteworthy to mention that utilizing environmentally viable hydroformylation catalysts that offers quantitative yields, good selectivity under mild conditions together with the

possibility of recycling the catalyst with very minimal post-reaction processing, all in a single package, is key in strengthening sustainable chemical catalysis.

## 5.3 References


1 J. M. Dreimann, E. Kohls, H. F. W. Warmeling, M. Stein, L. F. Guo, M. Garland, T. N. Dinh and A. J. Vorholt, *ACS Catal.*, 2019, **9**, 4308–4319.

2 J. B. Claridge, R. E. Douthwaite, M. L. H. Green, R. M. Lago, S. C. Tsang and A. P. E. York, *J. Mol. Catal.*, 1994, **89**, 113–120.

3 S. Aguado-Ullate, J. A. Baker, V. González-González, C. Müller, J. D. Hirst and J. J. Carbó, *Catal. Sci. Technol.*, 2014, **4**, 979–987.

4 S. A. Decker and T. R. Cundari, *New J. Chem.*, 2002, **26**, 129–135.

5 T. Kégl, *RSC Adv.*, 2015, **5**, 4304–4327.

6 L. C. Matsinha, S. F. Mapolie and G. S. Smith, *Dalton Trans.*, 2015, **3**, 1240–1248.

7 S. Kloß, D. Selent, A. Spannenberg, R. Franke, A. Börner and M. Sharif, *Catalysts*, 2019, **9**, 1036.

8 J. Shen, K. Beale, I. Amura and E. A. C. Emanuelsson, *Front. Chem.*, 2020, **8**, 375–385.

9 K. Boussu, B. Van der Bruggen, A. Volodin, C. Van Haesendonck, J. A. Delcour, P. Van der Meeren and C. Vandecasteele, *Desalination*, 2006, **191**, 245–253.

10 A. Momotake and T. Arai, *Tetrahedron Lett.*, 2004, **45**, 4131–4134.

# Chapter 6

## Experimental

### 6.1 General Considerations

All solvents and reagents were purchased from commercial suppliers (KIMIX, Sigma-Aldrich, Merck and Combi-blocks) and used without further purification unless otherwise stated. Rhodium(III) trichloride trihydrate was purchased from Heraeus South Africa. The rhodium chloro-1,5-cyclooctadiene dimer ($[Rh(COD)Cl]_2$) was prepared following a published method.[1] The compounds 4,4′-(1,2-ethanediylidenedinitrilo)bisphenol (**2.1**)[2]**,** 4,4′-(1,2-acenaphthenediylidenedinitrilo)bisphenol (**2.2**)[3], $G_1$-COOMe-OH dendron (**3.1**)[4], $G_1$-COOMe-Br dendron (**3.2**)[5], tetraylnitrilomethylidyne−hexaphenyl (**4.1**)[6] and 4,4′-[1,2-Phenylenebis(nitrilomethylidene)]bisphenol (**4.2**)[7] were synthesised according to previously reported literature procedures. All reactions were carried out under an argon atmosphere using standard Schlenk line techniques. Reaction progress was monitored using thin-layer chromatography (TLC) on pre-coated silica-gel F254 plates in a suitable solvent system and viewed under a Spectroline CM UV-viewing cabinet. Column chromatography was conducted using 60 Å silica gel (70 – 230 mesh ASTM). All compounds synthesized in this study were dried under vacuum using the E2M28 Edwards vacuum pump.

Nuclear magnetic resonance (NMR) spectra were recorded on either a Bruker 400 Biospin GmbH ($^1$H at 400.22 MHz, $^{13}C\{^1H\}$ at 100.65 MHz) or a Varian Mercury XR300 ($^1$H: 300.08 MHz, $^{13}C\{^1H\}$:75.46 MHz) spectrometer. Chemical shifts for $^1$H and $^{13}C\{^1H\}$ NMR were referenced to the tetramethylsilane (TMS) internal standard. Infrared (IR) absorptions were measured on a Perkin-Elmer Spectrum 100 FT-IR spectrometer using Attenuated Total Reflectance (ATR). Mass spectrometry determinations were carried out using Electron Impact (EI) on a JEOL GC Matell instrument or Electrospray Ionisation (ESI) on a Waters API Quattro Micro triple quadrupole mass spectrometer with data recorded in the positive ionization mode for all compounds. Inductive coupled plasma-mass spectrometry (ICP-MS) was obtained using a PerkinElmer Elan 600 quadrupole with a Cetax LSX-200 UV laser module.

Electrochemical studies were carried out on a BASi Epsilon Eclipse EF-1031 Potentiostat/Galvanostat. Melting points were determined using a Büchi Melting Point Apparatus B-540. Hydroformylation samples were analysed using a PerkinElmer Clarus 580

GC equipped with a flame-ionisation detector and a capillary column of (30 m x 0.32 mm x 0.25 μm).

## 6.2 Synthesis and characterization of alpha-diimine Schiff base ligands

### 6.2.1 Synthesis of 4,4′-(1,2-ethanediylidenedinitrilo)bisphenol (2.1)

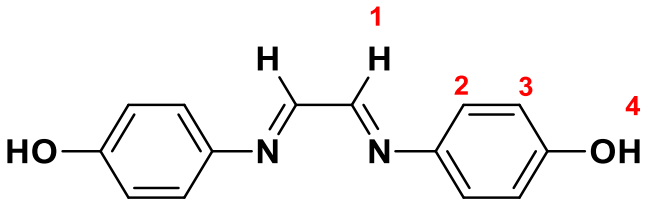


Glyoxal solution 40 % (0.0600 g, 1.09 mmol) was added to a stirring solution of 4-aminophenol (0.240 g, 2.19 mmol) in methanol (20 mL). A catalytic amount (5 drops) of acetic acid was added to the mixture. The clear solution was stirred for 24 h at 40 °C under nitrogen. Thereafter, the mixture was cooled to room temperature and the precipitate was collected by suction filtration. The resulting product was washed with cold methanol (20 mL) and diethyl ether (20 mL). The product was purified by precipitation from hot methanol (50 mL) and dried *in vacuo*. Product: Bright yellow powder. Yield: 0.058 g, 22 %. **M.P.** 207 – 209 °C. **$^{1}$H NMR (300 MHz, DMSO-*d*$_6$):** δ (ppm) = 9.78 (br s, 2H, H-4), 8.42 (s, 2H, H-1), 7.32 (d, 4H, $^{3}J$ = 12.0 Hz, H-2), 6.82 (d, 4H, $^{3}J$ = 10.0 Hz, H-3. **$^{13}$C{$^{1}$H} NMR (151 MHz, DMSO-*d*$_6$):** δ (ppm) = 158.52 (C$_{imine}$), 156.94, 141.72, 123.70, 116.65. **FT-IR (ATR, cm$^{-1}$):** $\nu$ = 3075.23 (O-H), 1603.44 (C=N), 157.11 (C=C). **ESI-MS (+):** Calculated for $C_{14}H_{12}N_2O_2$ (*m/z*): $[M+H]^+$, 241.0977; found 241.0996.

### 6.2.2 Synthesis of 4,4′-(1,2-acenaphthenediylidenedinitrilo)bisphenol (2.2)

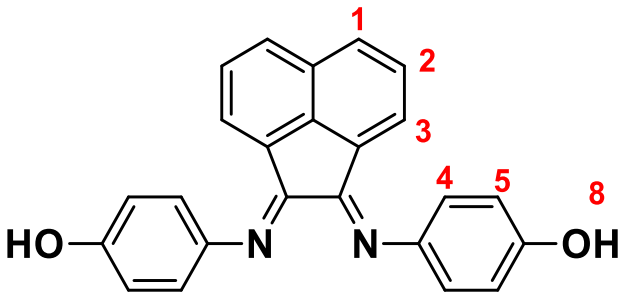


Acenapthenequinone (0.106 g, 0.58 mmol) was added to a stirring solution of 4-aminophenol (0.206 g, 1.89 mmol) in methanol (25 mL). Catalytic amount (5 drops) of acetic acid was add to the mixture. The yellow solution was stirred for 24 h at room temperature. The resulting orange precipitate was collected by suction filtration and washed with cold methanol and diethyl ether (20 mL). The product was purified by precipitation from hot methanol (50 mL). The product was filtered and dried *in vacuo*. Product: Orange powder. Yield: 0.163 g, 77%. **M.P.** 256 – 258 °C. **$^{1}$H NMR (300 MHz, DMSO-*d*$_6$):** δ (ppm) = 9.40 (br s, 2H, H-8), 8.06 (d, 2H, $^{3}J$ = 8.2 Hz, H-1), 7.53 (t, 2H, H-2), 7.00 (d, 2H, $^{3}J$ = 7.2 Hz, H-3), 6.92 (s, 8H, H-4, H-5). **$^{13}$C{$^{1}$H} NMR (151 MHz, DMSO):** δ (ppm) = 160.55 ($C_{imine}$), 155.38, 143.91, 141.02, 131.87, 129.62, 128.72, 128.30, 123.61, 119.74, 116.95. **FT-IR (ATR, cm$^{-1}$):** *v* = 3289.25 (O-H), 1636.18 (C=N). **ESI-MS (+):** Calculated for $C_{24}H_{16}N_2O_2$ (*m/z*): $[M+H]^+$, 365.1290; found 365.0854.

## 6.3 Synthesis and characterization of sulfonated *N, N*-alpha-diimine ligands

### 6.3.1 Synthesis of sodium 3,3'-(1,2 ethanediylidenedinitrilo)bis(4,1 phenoxy propane-sulfonate) (2.3)

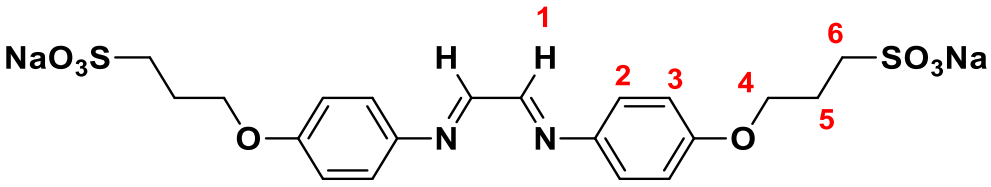


Sodium hydride (0.033 g, 1.37 mmol) dispersed in mineral oil was suspended in anhydrous THF (10 mL) under argon in a two-necked flask. A solution of **2.1** (0.100 g, 0.420 mmol)

dissolved in anhydrous THF (2 mL) was added. The mixture was allowed to stir under argon for one h at room temperature and then 1,3-propanesultone (0.15 g, 1.23 mmol) in anhydrous THF (2 mL) was added and allowed to stir for 8 h under reflux at 50 °C. After cooling to room temperature, the precipitate was collected by suction filtration, washed with THF (20 mL) and acetone (20 mL) to remove the unreacted sultone. The product was purified by precipitation from DMSO / acetone (1:1) and dried *in vacuo*. Product: Yellow powder. Yield: 0.180 g, 82 %. **M.P.** 229 – 230 °C. **$^1$H NMR (300 MHz, DMSO-*d*$_6$):** δ (ppm) = 8.41 (s, 2H, H-1), 7.41 (d, 4H, $^3J$ = 8.80 Hz, H-2), 6.98 (d, 4H, $^3J$ = 7.20 Hz, H-3), 4.11 (t, 4 H, $^3J$ = 8.30 Hz, H-4), 2.59 (t, 4H, $^3J$ = 7.40 Hz, H-6), 2.09 – 2.05 (m, 4 H, H-5). **$^{13}$C{$^1$H} NMR (151 MHz, DMSO-*d*$_6$):** δ (ppm) = 159.25 ($C_{imine}$), 157.93, 143.09, 123.56, 115.73, 67.69, 48.39, 25.80. **FT-IR (ATR, cm$^{-1}$):** *v* = 1185.22 and 1054.41 (O=S=O). **ESI-MS (+):** Calculated for $C_{20}H_{22}N_2Na_2O_8S_2$ (*m/z*): $[M+H]^+$, 526.0691; found 526.9700.

### 6.3.2 Synthesis of sodium 3,3'-(1,2-acenaphthenediylidenedinitrilo)bis(4,1 phenoxy propane-sulfonate) (2.4)

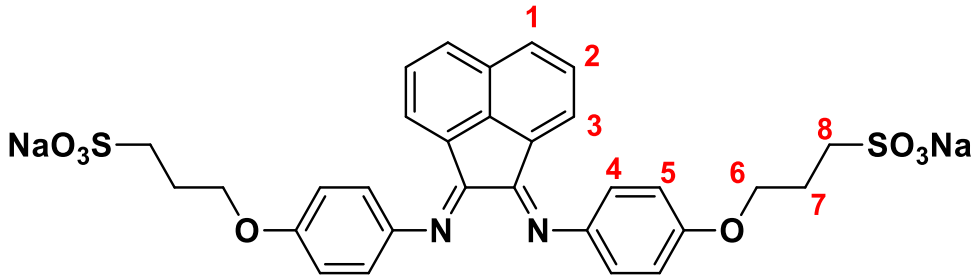


Sodium hydride (0.015 g, 0.700 mmol) dispersed in mineral oil was suspended in anhydrous THF (10 mL) under argon in a two-necked flask. A solution of **2.2** (0.100 g, 0.270 mmol) dissolved in anhydrous THF (2 mL) was added. The mixture was allowed to stir under argon for one h at room temperature and then 1, 3-propanesultone (0.08 g, 0.65 mmol) in anhydrous THF (2 mL) was added and allowed to stir for 8 h under reflux at 40 °C. Thereafter, the reaction mixture was cooled to room temperature and the precipitate was collected by suction filtration, washed with THF (20 mL) and acetone (20 mL) to remove the unreacted sultone. The product was purified by precipitation from water-ethanol mixture (1:2) and dried *in vacuo*. Product: Orange powder. Yield: 0.122 g, 67 %. **M.P.** 154 – 156 °C. **$^1$H NMR (300 MHz, DMSO-*d*$_6$):** δ (ppm) = 8.08 (d, 2H, $^3J$ = 7.9 Hz, H-1), 7.57 (t, 2H, H-2), 7.05 (dd, 8H, H-4, H-5), 6.96 (d, 2H,

$^{3}J$ = 7.2 Hz, H-3), 4.15 (t, 4 H, $^{3}J$ = 6.5 Hz, H-6), 2.63 (t, 4H, H-8), 2.07 – 2.00 (m, 4 H, H-7). **$^{13}$C{$^{1}$H} NMR (151 MHz, DMSO-*d*$_6$):** δ (ppm) = 179.32, 161.60 ($C_{imine}$), 157.26, 124.29, 120.60, 116.88, 68.35, 49.46. **FT-IR (ATR, cm$^{-1}$):** *v* = 1181.01 and 1036.58 (O=S=O). **ESI-MS (+):** Calculated for $C_{30}H_{26}N_2Na_2O_8S_2$ (*m/z*): $[M+H]^+$, 653.1004; found 653.0217.

## 6.4 Synthesis and characterization of *N, N*-alpha-diimine Rh(I) complexes

### 6.4.1 Synthesis of *N, N*-alpha-diimine Rh (COD) complex (2.5)

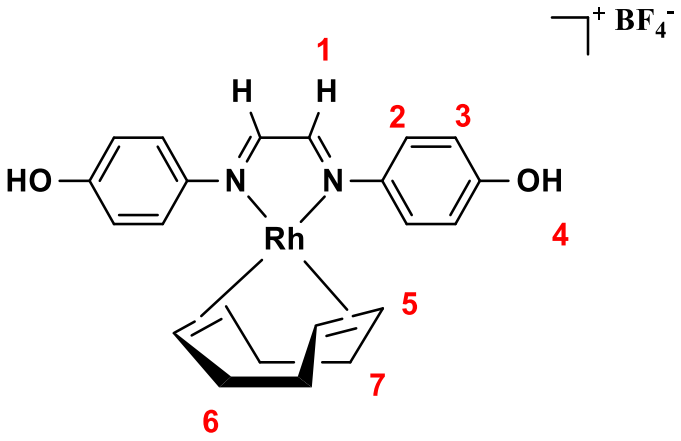


Silver tetrafluoroborate (0.243g, 1.25 mmol) and $[Rh(COD)Cl]_2$ (0.308 g, 0.624 mmol) were stirred in acetonitrile (10 mL) for one h at room temperature. The resulting silver chloride precipitate was removed using a syringe filter (PTFE, 0.45 mm) and the solution was added to a solution of ligand **2.1** (0.300 g, 1.25 mmol) in acetonitrile (10 mL). The mixture was stirred for one h at room temperature. The resulting precipitate was isolated by filtration, washed with acetonitrile and dried under vacuum. Product: Red powder. Yield: 0.134 g, 59%. **M.P.** 242 – 246 °C. **$^{1}$H NMR (300 MHz, DMSO-*d6*):** δ (ppm) = 10.20 (br s, 2H, H-4), 8.62 (s, 2H, H-1), 7.90 (d, 4H, $^{3}J$ = 6.3 Hz, H-2), 6.99 (d, 4H, $^{3}J$ = 8.8 Hz, H-3 ), 3.90 (br s, 4H, H-5), 2.35 (m, 4H, H-7), 1.86 (m, 4H, H-6). **$^{13}$C{$^{1}$H} NMR (151 MHz, DMSO-*d*$_6$):** δ (ppm) = 158.34, 157.00 ($C_{imine}$), 141.65, 123.89, 116.36 (s), 86.82 ($C_{COD}$), 30.68 ($C_{COD}$). **FT-IR (ATR, cm$^{-1}$):** *v* = 3424.25 (O–H), 1607.35 (C=N), 1581.41 (C=C). **ESI-MS (+):** Calculated for $C_{22}H_{24}N_2O_2Rh$ (*m/z*): $[M+MeCN+Na]^+$, 515.1050; found 515.1010.

### 6.4.2 Synthesis of *N, N*-alpha-diimine Rh (COD) complex (2.6)

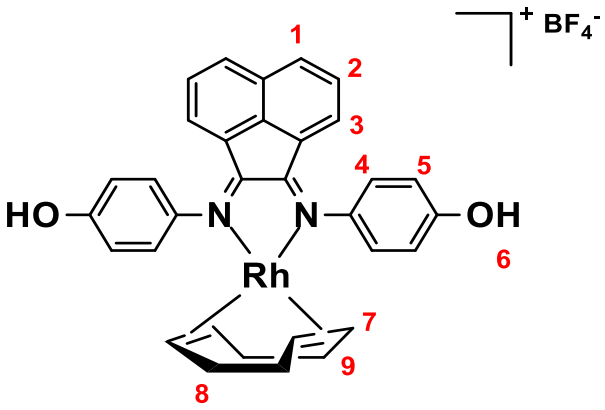


Silver tetrafluoroborate (0.160 g, 0.823 mmol) and $[Rh(COD)Cl]_2$ (0.203 g, 0.411 mmol) were stirred in acetonitrile (10 mL) for one h at room temperature. The resulting silver chloride precipitate was removed from the solution using a syringe filter (PTFE, 0.45 mm). Thereafter, the solution was added to a solution of ligand **2.2** (0.300 g, 0.823 mmol) in acetonitrile (10 mL). The mixture was stirred for one h at room temperature. Thereafter, the product was isolated by filtration, washed with acetonitrile to remove the unreacted complex precursor and dried under vacuum. Product: Red powder. Yield: 0.214 g, 61%. **M.P.** 225 – 230 °C. **$^1$H NMR (300 MHz, DMSO-*d*$_6$):** δ (ppm) = 9.99 (br s, 2H, H-6), 8.28 (d, 2H, *J* = 8.2 Hz, H-1), 7.65 (t, 2H, H-2), 7.24 (d, 4H, $^3J$ = 6.7 Hz, H-4), 7.01 (d, 4H, $^3J$ = 7.0 Hz, H-5), 6.64 (d, 2H, *J* = 1.5 Hz, H-3), 3.98 (br s, 4H, H-7), 2.43 (m, 4H, H-9), 1.87 (m, 4H, H-8). **$^{13}$C{$^1$H} NMR (151 MHz, DMSO-*d*$_6$):** δ (ppm) =161.3, 157.90, 145.50 ($C_{imine}$), 141.80, 127.50, 122.75, 117.21 (s), 85.52 ($C_{COD}$), 31.63 ($C_{COD}$). **FT-IR (ATR, cm$^{-1}$):** *v* = 3325.22 (O–H), 1623.15 (C=N), 1593.58 (C=C). **ESI-MS (+):** Calculated for $C_{32}H_{28}N_2O_2Rh$ (*m/z*): $[M]^+$, 575.1205; found 575.1060.

## 6.5 Synthesis and characterization of sulfonated water-soluble alpha-diimine Rh(I) complexes

### 6.5.1 Synthesis of sulfonated *N, N*-alpha-diimine Rh (COD) complex (2.7)

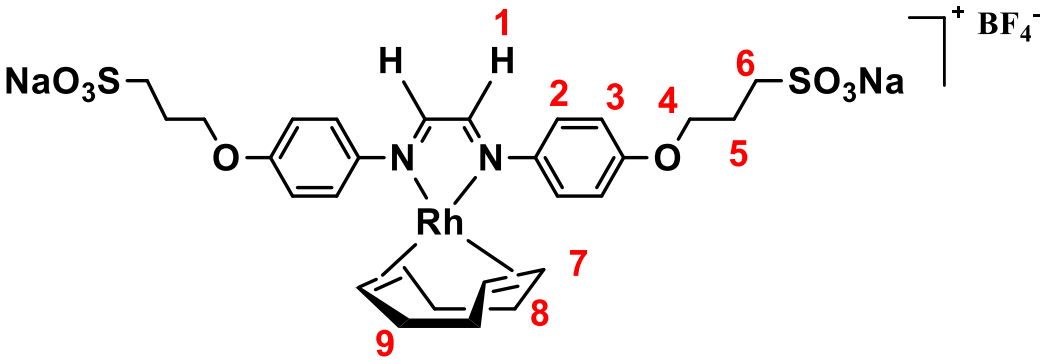


Silver tetrafluoroborate (0.0250 g, 0.128 mmol, 1.0 eq.) and $[RhCl(COD)]_2$ (0.0300 g, 0.0607 mmol, 0.5 eq.) were stirred in acetonitrile (10 mL) for one h at room temperature. The resulting silver chloride precipitate was removed from the solution using a syringe filter (PTFE, 0.25 µm). The solution was reduced under vacuum and added to a solution of ligand **2.3** (0.0600 g, 0.113 mmol) in DMSO (10 mL). The mixture was stirred for 30 minutes at room temperature. Thereafter, the reaction mixture was poured into acetone and the resulting precipitate formed was filtered and washed with acetone (10 mL). The product was purified by precipitation from DMSO and acetone mixture (1:1) and dried *in vacuo*. Product: Red powder. Yield: 0.0530 g, 56 %. **M.P.** 221 – 237 °C. **$^1$H NMR (300 MHz, DMSO-*d*$_6$):** δ (ppm) = 8.68 (s, 2H, H-1), 7.97 (d, $^3J$ = 8.4 Hz, 4H, H-2), 7.17 (d, $^3J$ = 9.0 Hz, 4H, H-3), 4.20 (t, $^3J$ = 6.5 Hz, 4H, H-4), 3.92 (br s, 4H, H-7), 2.63 – 2.56 (m, 4H, H-6), 2.36 (s, 4H, H-8), 2.09 – 2.01 (m, 4H, H-5), 1.77 (d, $^3J$ = 5.9 Hz, 4H, H-9). **$^{13}$C{$^1$H} NMR (151 MHz, DMSO-*d*$_6$):** δ (ppm) =157.90, 147.80 ($C_{imine}$), 140.65, 128.70, 122.76 (s), 86.82 ($C_{COD}$) 32.61 ($C_{COD}$). **FT-IR (ATR, cm$^{-1}$):** $\nu$ = 1185.11 and 1054.28 (O=S=O), 1599.27 (C=N), 1571.17 (C=C). **ESI-MS (+):** Calculated for $C_{28}H_{34}N_2Na_2O_8S_2Rh$ (*m/z*): $[M]^+$, 739.0607; found 739.2161 and $[M+H]^+$, 740.0685; found 740.2184.

### 6.5.2 Synthesis of sulfonated *N, N*-alpha-diimine Rh (COD) complex (2.8)

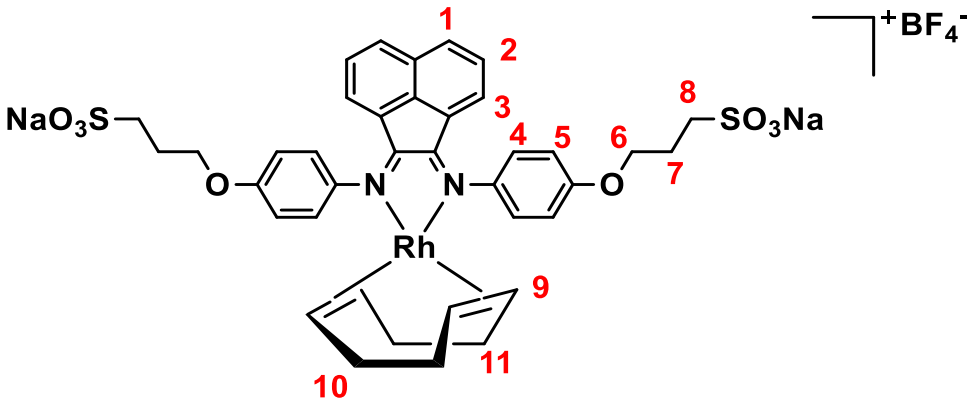


Silver tetrafluoroborate (0.0240 g, 0.123 mmol, 1.0 eq.) and $[RhCl(COD)]_2$ (0.0300 g, 0.0607 mmol, 0.5 eq.) were stirred in acetonitrile (10 mL) for one h at room temperature. The precipitated silver chloride was removed using a syringe filter (PTFE, 0.25 μm). The resulting solution was evaporated to dryness under reduced pressure. Ligand **2.4** (0.0793 g, 0.122 mmol) dissolved in DMSO (10 mL) was added to the resulting $[Rh(COD)(MeCN)_2]BF_4$ residue and stirred for 30 minutes at room temperature. The reaction mixture was poured into acetone and the precipitate formed was washed with acetone (10 mL). The resulting product was purified by precipitation from DMSO and acetone mixture (1:1) and dried *in vacuo*. Product: Red powder. Yield: 0.0520 g, 62%. **M.P.** 215 – 222 °C. **$^1$H NMR (300 MHz, DMSO-*d*$_6$):** δ (ppm) = 8.26 (d, $^3J$ = 8.3 Hz, 2H, H-1), 7.67 (t, $^3J$ = 7.8 Hz, 2H, H-2), 7.35 (d, $^3J$ = 8.6 Hz, 4H, H-3), 7.18 (d, $^3J$ = 8.7 Hz, 4H, H-5), 6.60 (d, $^3J$ = 7.2 Hz, 4H, H-5), 4.19 (t, $^3J$ = 6.3 Hz, 4H, H-6), 3.97 (br s, 4H, H-9), 2.62 (d, $^3J$ = 7.1 Hz, 4H, H-8), 2.43 (m, 4H, H-11), 2.10 – 2.03 (m, 4H, H-7), 1.86 (m, 4H, H-10). **$^{13}$C{$^1$H} NMR (151 MHz, DMSO-*d*$_6$):** δ (ppm) = 160.82, 157.50 ($C_{imine}$), 144.85, 128.09, 115.76 (s), 86.80 ($C_{COD}$) 32.60 ($C_{COD}$). **FT-IR (ATR, cm$^{-1}$):** $\nu$ = 1181.27 and 1036.77 (O=S=O), 1601.29 (C=N), 1571.17 (C=C). **ESI-MS (+):** Calculated for $C_{38}H_{38}N_2Na_2O_8S_2Rh$ (*m/z*): $[M+H]^+$, 864.0998; found 864.0600.

## 6.6 Synthesis and characterization of Fréchet-type dendritic wedges

### 6.6.1 Synthesis of $G_1$-COOMe-OH dendron (3.1)

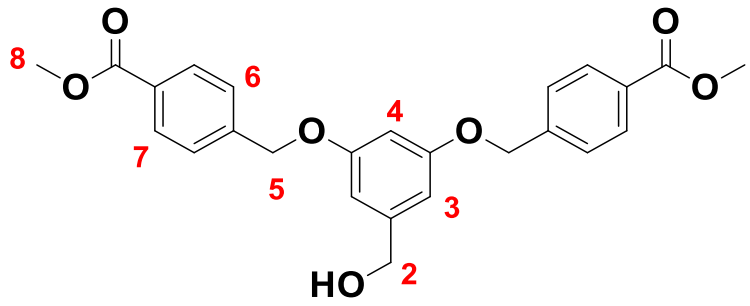


A mixture of 3,5-dihydroxy benzyl alcohol (0.500 g, 3.560 mmol), potassium carbonate (0.340 g, 1.92 mmol) and 18-crown-6 (0.01 g, 0.04 mmol) in anhydrous acetone (50 mL) were stirred for 1 h at room temperature. Thereafter, methyl 4-(bromomethyl) benzoate (1.634 g, 7.133 mmol) was added and refluxed for 24 h under argon. The mixture was cooled to room temperature and evaporated to dryness under reduced pressure. The residue was partitioned between water (100 mL) and dichloromethane (100 mL). The aqueous layer was extracted with dichloromethane (3 x 50 mL). The combined organic extracts were washed with brine solution (100 mL) and dried using anhydrous magnesium sulfate. The drying agent was removed by filtration and the filtrate was collected and evaporated to dryness under reduced pressure. The resulting crude material (brown oil) was purified by column chromatography (silica gel) using dichloromethane and increasing portions of petroleum ether (1:9, *v/v*). Thereafter, the solvent was reduced under pressure and the resulting residue was triturated in pentane. The precipitate formed was filtered and dried *in vacuo*. Product: White powder. Yield: 1.22 g, 78%. **M.P.** 82.55 –85.0 °C. **$^1$H NMR (300 MHz, $CDCl_3$):** δ (ppm) = 7.96 (d, $^3J$ = 8.3 Hz, 4H, H-7), 7.39 (d, $^3J$ = 8.2 Hz, 4H, H-6), 6.54 (d, $^4J$ = 2.1 Hz, 2H, H-3), 6.43 (t, $^4J$ = 2.2 Hz, 1H, H-4), 5.01 (s, 4H, H-5), 4.55 (s, 2H, H-2), 3.84 (s, 6H, H-8). **$^{13}$C{$^1$H} NMR (151 MHz, $CDCl_3$):** δ (ppm) = 166.77 ($C{=}O_{ester}$), 141.76, 130.32, 126.98, 108.43, 102.32, 33.15. **FT-IR (ATR, cm$^{-1}$):** *v* = 3520.25 (O-H), 1720.17 (C=O).

### 6.6.2 Synthesis of $G_1$-COOMe-Br dendron (3.2)

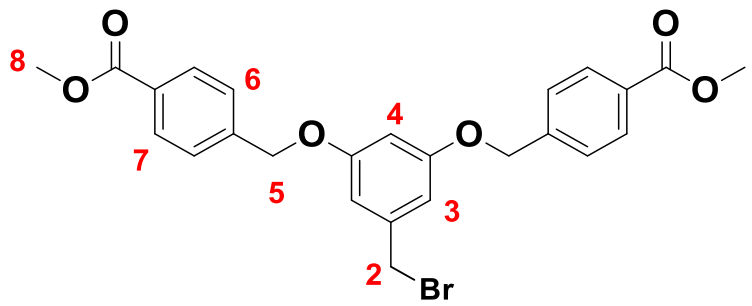


Compound **3.1** (0.500 g, 1.15 mmol), triphenylphosphine (2.95 g, 11.23 mmol) and carbon tetrabromide (3.81 g, 11.23 mmol) were dissolved in anhydrous THF. The mixture was stirred under argon for 2 h at room temperature. Additional triphenylphosphine and carbon tetrabromide (0.25 eq.) were added and reacted further for another 2 h. Thereafter, the reaction mixture was evaporated to dryness under reduced pressure and residue was partitioned between water (100 mL) and dichloromethane (100 mL), and the aqueous layer was extracted with dichloromethane (3 x 50 mL). The combined organic extracts were washed with brine solution (100 mL) and dried using anhydrous magnesium sulfate. The drying agent was removed by filtration and the filtrate was collected and evaporated to dryness. The resulting crude material was purified by column chromatography (silica gel) using hexane: dichloromethane (1:1) and increasing portions of dichloromethane (100%). Subsequent trituration in pentane afforded the desired product which was collected by suction filtration and dried *in vacuo*. Product: white powder. Yield: 0.410 g, 82%. **M.P.** 119.5 – 121.8 °C. **$^1$H NMR (300 MHz, $CDCl_3$):** δ (ppm) = 7.98 (d, $^3J$ = 8.3 Hz, 4H, H-7), 7.41 (d, $^3J$ = 8.3 Hz, 4H, H-8), 6.57 (d, $^4J$ = 2.2 Hz, 2H, H-3), 6.45 (t, $^4J$ = 2.2 Hz, 1H, H-4), 5.02 (s, 4H, H-5), 4.33 (s, 2H, H-2), 3.85 (s, 6H, H-8). **$^{13}$C{$^1$H} NMR (151 MHz, $CDCl_3$):** δ (ppm) = 166.90 ($C{=}O_{ester}$), 159.93, 141.88, 140.17, 130.04, 129.97, 127.12, 108.51, 102.39, 33.42. **FT-IR (ATR, cm$^{-1}$):** $\nu$ = 1712.25 (C=O).

### 6.6.3 Synthesis of $G_2$-COOMe-OH dendron (3.3)

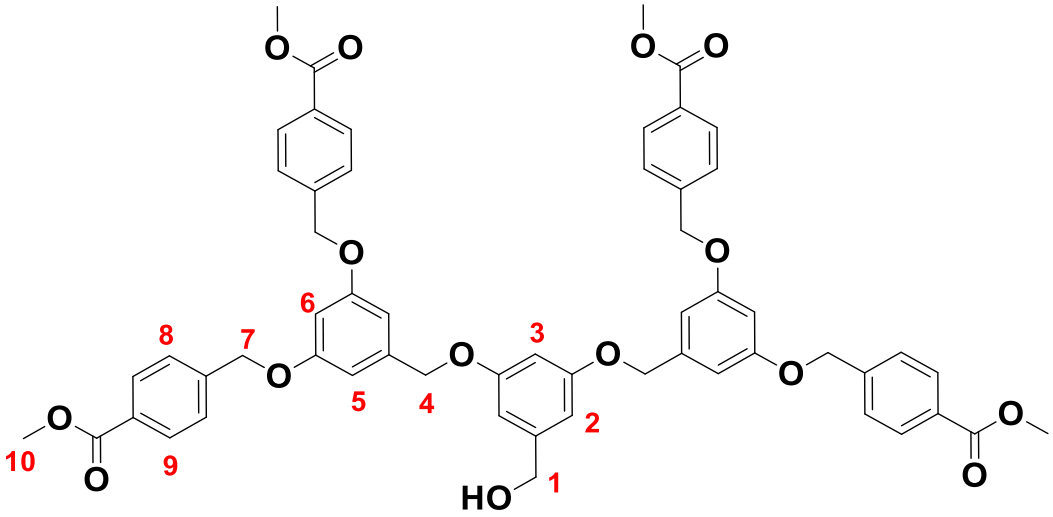


A mixture of 3,5-dihydroxy benzyl alcohol (0.100 g, 0.416 mmol), potassium carbonate (0.340 g, 1.92 mmol) and 18-crown-6 (0.01 g, 0.04 mmol) in anhydrous acetone (50 mL) were stirred at room temperature for 1 h. Thereafter, compound **3.2** (0.750 g, 1.502 mmol) was added and refluxed for 24 h under argon. When the reaction was deemed complete, the mixture was cooled to room temperature and evaporated to dryness under reduced pressure. The residue was partitioned between water (100 mL) and dichloromethane (100 mL), and the aqueous layer was extracted with dichloromethane (3 x 50 mL). The combined organic extracts were washed with brine solution (100 mL) and dried using anhydrous magnesium sulfate. The drying agent was removed by filtration and the filtrate was collected and evaporated to dryness under reduced pressure. The resulting crude material (brown oil) was purified by column chromatography (silica gel) using dichloromethane and increasing portions of petroleum ether (1:9, *v/v*). The mixture was reduced under pressure and the resulting residue was triturated in pentane. The precipitate formed was filtered and dried *in vacuo*. Product: White powder. Yield: 0.08 g, 62%. **M.P.** 119.4 – 120.1 °C. **$^1$H NMR (300 MHz, $CDCl_3$):** δ (ppm) = 7.95 (d, $^3J$ = 8.3 Hz, 8H, H-9), 7.38 (d, $^3J$ = 8.2 Hz, 8H, H-8), 6.57 (d, $^4J$ = 2.1 Hz, 4H, H-5), 6.48 (d, $^4J$ = 2.0 Hz, 2H, H-2), 6.45 (t, $^4J$ = 2.1 Hz, 2H, H-6), 6.38 (t, $^4J$ = 2.0 Hz, 1H, H-3), 5.01 (s, 8H, H-7), 4.88 (s, 4H, H-4), 4.53 (s, 2H, H-1), 3.84 (s, 12H, H-10). **$^{13}$C{$^1$H} NMR (151 MHz, $CDCl_3$):** δ (ppm) = 166.92 ($C{=}O_{ester}$), 160.15, 160.04, 143.70, 142.09, 139.77, 130.04, 129.07, 127.15, 106.57,105.92, 101.87, 101.33, 69.91. **FT-IR (ATR, cm$^{-1}$):** *v* = 1712.74 (C=O), 3511.38 (O-H).

### 6.6.4 Synthesis of $G_2$-COOMe-Br dendron (3.4)

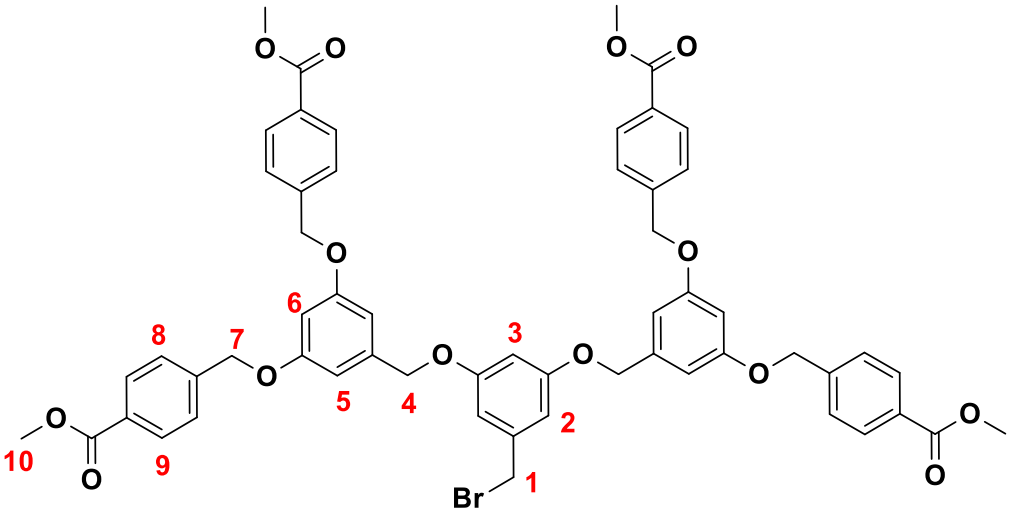


Compound **3.3** (0.500 g, 0.512 mmol), triphenylphosphine (1.95 g, 11.23 mmol) and carbon tetrabromide (1.81 g, 11.23 mmol) were dissolved in anhydrous THF. The mixture was stirred under argon for 2 h. Additional triphenylphosphine and carbon tetrabromide (0.25 eq.) were added and reacted further for another 2 h. Thereafter, the reaction mixture was evaporated to dryness under reduced pressure. The residue was partitioned between water (100 mL) and dichloromethane (100 mL), and the aqueous layer was extracted with dichloromethane (3 x 50 mL). The combined organic extracts were washed with brine solution (100 mL) and dried using anhydrous magnesium sulfate. The drying agent was removed by filtration and the filtrate was collected and evaporated to dryness. The resulting crude material was purified by column chromatography (silica gel) using hexane:dichloromethane (1:1) and increasing portions of dichloromethane (100%). Subsequent trituration in pentane afforded the desired product which was collected by suction filtration and dried *in vacuo*. Product: White powder. Yield: 0.32 g, 68%. **M.P.** 120.4 – 123.1 °C. **$^1$H NMR (300 MHz, $CDCl_3$):** δ (ppm) = 7.96 (d, $^3J$ = 8.4 Hz, 8H, H-9), 7.40 (d, $^3J$ = 8.5 Hz, 8H, H-8), 6.58 (d, $^4J$ = 2.2 Hz, 4H, H-5), 6.53 (d, $^4J$ = 2.2 Hz, 2H, H-2), 6.47 (t, $^4J$ = 2.2 Hz, 2H, H-6), 6.40 (t, $^4J$ = 2.2 Hz, 1H, H-3), 5.03 (s, 8H, H-7), 4.89 (s, 4H, H-4), 4.32 (s, 2H, H-1), 3.85 (s, 12H, H-10). **$^{13}$C{$^1$H} NMR (151 MHz, $CDCl_3$):** δ (ppm) = 166.74 ($C{=}O_{ester}$), 159.91, 159.94, 141.90, 139.83, 139.37, 129.91, 129.79, 126.98, 108.22, 106.55, 102.22, 101.72, 69.91. **FT-IR (ATR, cm$^{-1}$):** *ν* = 1712.34 (C=O).

## 6.7 Synthesis and characterization of alpha-diimine poly(aryl ether)dendrimers

### General procedure for the preparation of dendrimers

Alpha-diimine ligands **2.1** or **2.2** (1 eq.), potassium carbonate (2 eq.) and a catalytic amount of 18-crown-6 were dissolved in anhydrous acetone (30 mL) and refluxed for 1 h. A solution of methyl 4-(bromomethyl) benzoate, compound **3.2** or **3.4** (2 – 2.5 eq.) in anhydrous acetone (20 mL) were added and refluxed for 24 h. Thereafter, the reaction mixture was cooled to room temperature and the volatiles were reduced under vacuum. The residue was partitioned between water (100 mL) and dichloromethane (100 mL). The aqueous layer was extracted with dichloromethane (3 x 50 mL). The combined organic extracts were partitioned with brine solution (100 mL) and dried using anhydrous magnesium sulfate. The drying agent was removed by filtration and the resulting filtrate was reduced under pressure. The resulting residue is purified by trituration in hexane and dichloromethane (1:1). The resulting precipitate was collected by suction filtration washed with hexane and methanol to afford the respective ligands **3.5** – **3.10**.

### 6.7.1 Synthesis of $G_0$-COOMe-*N,N*-alpha-diimine ligand (3.5)

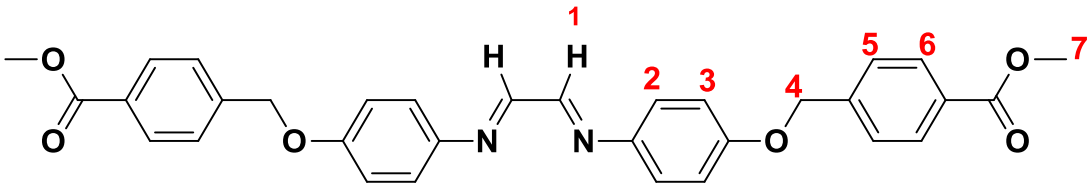


The title compound was prepared with compound **2.1** (0.200 g, 0.823 mmol), $K_2CO_3$ (0.230 g, 1.66 mmol), methyl 4-(bromomethyl) benzoate (0.400 g, 1.75 mmol) and catalytic amount of 18-crown-6. Product: Yellow powder. Yield: 0.295 g, 66%. **M.P.** 158 − 165 °C. **$^1$H NMR (300 MHz, $CDCl_3$):** δ (ppm) = 8.33 (s, 2H, H-1), 8.00 (d, $^3J$ = 8.4 Hz, 4H, H-6), 7.44 (d, $^3J$ = 8.5 Hz, 4H, H-5), 7.26 (d, $^3J$ = 8.9 Hz, 4H, H-2), 6.94 (d, $^3J$ = 9.0 Hz, 4H, H-3), 5.09 (s, 4H, H-4), 3.86 (s, 6H, H-7). **$^{13}$C{$^1$H} NMR (151 MHz, $CDCl_3$):** δ (ppm) = 166.77 ($C{=}O_{ester}$), 158.61, 154.89 ($C_{imine}$), 143.57, 141.87, 129.94, 126.96, 123.06, 115.60, 69.67, 52.10. **FT-IR (ATR, cm$^{-1}$):** $\nu$ = 1768.59 (C=O), 1691.54 (C=N). **ESI-MS (+):** Calculated for $C_{32}H_{28}N_2O_6$ **(***m/z***)**: $[M+H]^+$, 537.2025; found 537.2008.

### 6.7.2 Synthesis of $G_0$-COOMe-*N*,*N*-alpha-diimine ligand (3.6)

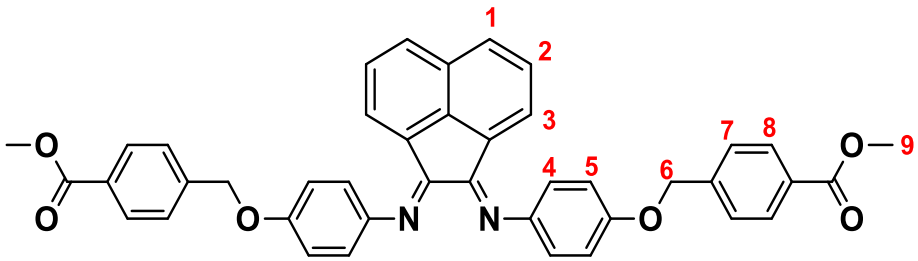

The title compound was prepared with compound **2.2** (0.500 g, 1.37 mmol), $K_2CO_3$ (0.380 g, 2.75 mmol), catalytic amount of 18-crown-6 and methyl 4-(bromomethyl)benzoate (0.700 g, 3.06 mmol). Product: Orange powder. Yield: 0.571 g, 63%. **M.P.** 146 − 155 °C. **$^1$H NMR (300 MHz, $CDCl_3$):** δ (ppm) = 8.02 (d, $^3J$ = 8.3 Hz, 4H, H-8), 7.82 (d, $^3J$ = 8.2 Hz, 2H, H-1), 7.50 (d, $^3J$ = 8.3 Hz, 4H, H-7), 7.38 – 7.25 (t, 2H, H-2), 7.02 (s, 8H, H-4 and H-5), 6.93 (d, $^3J$ = 7.2 Hz, 2H, H-3), 5.13 (s, 4H, H-6), 3.86 (s, 6H, H-9). **$^{13}$C{$^1$H} NMR (151 MHz, $CDCl_3$):** δ (ppm) = 166.84 ($C{=}O_{ester}$), 161.65 ($C_{imine}$), 155.88, 145.47, 142.31, 129.91, 126.94, 120.04, 115.98, 52.10, 30.85. **FT-IR (ATR, cm$^{-1}$):** *ν* = 1726.43 (C=O), 1661.10 (C=N). **ESI-MS (+)**: calculated for $C_{42}H_{32}N_2O_6$ (*m/z*): $[M+H]^+$, 661.2338; found 661.2320.

### 6.7.3 Synthesis of $G_1$-COOMe-*N*,*N*-alpha-diimine ligand (3.7)

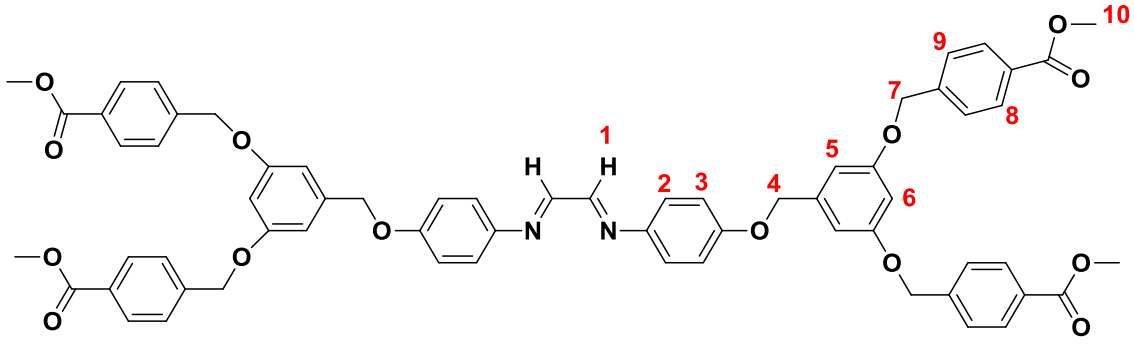

The title compound was prepared with compound **2.1** (0.100 g, 0.416 mmol), $K_2CO_3$ (0.340 g, 1.92 mmol) catalytic amount of 18-crown-6 and compound **3.2** (0.416 g, 0.832 mmol). Product: Yellow powder. Yield: (0.300 g, 67%). **M.P.** 166 − 172 °C. **$^1$H NMR (300 MHz, $CDCl_3$):** δ (ppm) = 8.39 (s, 2H, H-1), 7.97 (d, $^3J$ = 8.3 Hz, 8H, H-9), 7.41

(d, $^{3}J$ = 8.3 Hz, 8H, H-8), 7.28 (d, $^{3}J$ = 8.9 Hz, 4H, H-2), 6.92 (d, $^{3}J$ = 9.0 Hz, 4H, H-3), 6.61 (d, $^{4}J$ = 2.2 Hz, 4H, H-5), 6.48 (t, $^{4}J$ = 2.2 Hz, 2H, H-6), 5.04 (s, 8H, H-7), 4.97 (s, 4H, H-4), 3.85 (s, 12H, H-10). **$^{13}C\{^{1}H\}$ NMR (151 MHz, $CDCl_3$):** δ (ppm) = 166.76 ($C{=}O_{ester}$), 159.86 (s), 156.41 ($C_{imine}$), 141.96, 140.42, 129.88, 126.97, 123.07, 116.29, 106.50, 101.65, 69.48, 30.84. **FT-IR (ATR, $cm^{-1}$):** $\nu$ = 1714.53 (C=O), 1611.45 (C=N). **ESI-MS (+):** Calculated for $C_{64}H_{56}N_2O_{14}$ **(***m/z***)**: $[M+H]^+$, 1077.3809; found 1077.3798.

### 6.7.4 Synthesis of $G_1$-COOMe-*N,N*-alpha-diimine ligand (3.8)

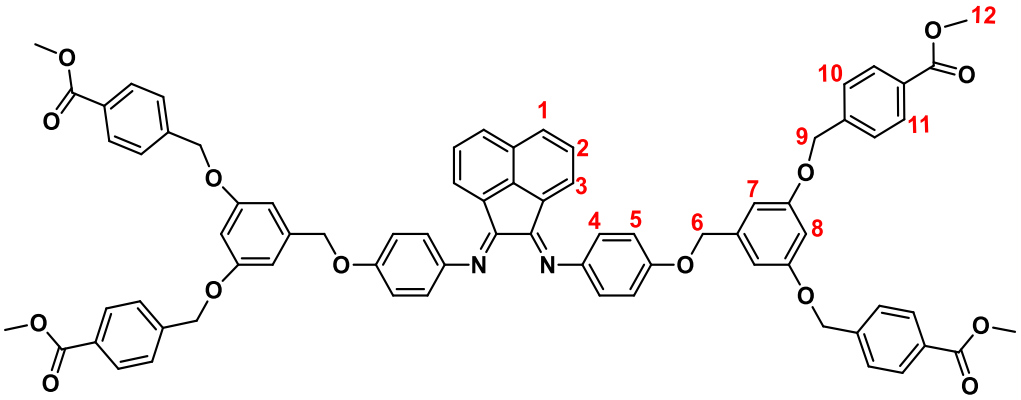


The title compound was prepared with compound **2.2** (0.100 g, 0.274 mmol), $K_2CO_3$ (0.0800 g, 0.549 mmol), catalytic amount of 18-crown-6 and compound **3.2** (0.350 g, 0.701 mmol). Product: Orange powder. Yield: 0.237 g, 72%. **M.P.** 163 − 170 °C. **$^{1}H$ NMR (300 MHz, $CDCl_3$):** δ (ppm) = 7.99 (d, $^{3}J$ = 8.2 Hz, 8H, H-10), 7.80 (d, $^{3}J$ = 8.2 Hz, 2H, H-1), 7.43 (d, $^{3}J$ = 8.2 Hz, 8H, H-11), 7.37 – 7.24 (t, 2H, H-2), 7.00 (s, 8H, H-4 and H-5), 6.93 (d, $^{3}J$ = 7.2 Hz, 2H, H-3), 6.68 (d, $^{4}J$ = 2.1 Hz, 4H, H-7), 6.51 (t, $^{4}J$ = 2.1 Hz, 2H, H-8), 5.07 (s, 8H, H-9), 5.01 (s, 4H, H-6), 3.85 (s, 12H, H-12). **$^{13}C\{^{1}H\}$ NMR (151 MHz, $CDCl_3$):** δ (ppm) = ($C_{imine}$), 159.93 ($C{=}O_{ester}$), 141.95 132.56, 129.91, 127.11, 123.80, 120.23, 116.02, 106.60, 101.73, 70.31, 69.50, 52.11. **FT-IR (ATR, $cm^{-1}$):** $\nu$ = 1715.14 (C=O), 1651.10 (C=N). **ESI-MS (+):** Calculated for $C_{74}H_{60}N_2O_{14}$ **(***m/z***)**: $[M+H]^+$, 1201.4122; found 1201.4121.

### 6.7.5 Synthesis of $G_2$-COOMe-*N*,*N*-alpha-diimine ligand (3.9)

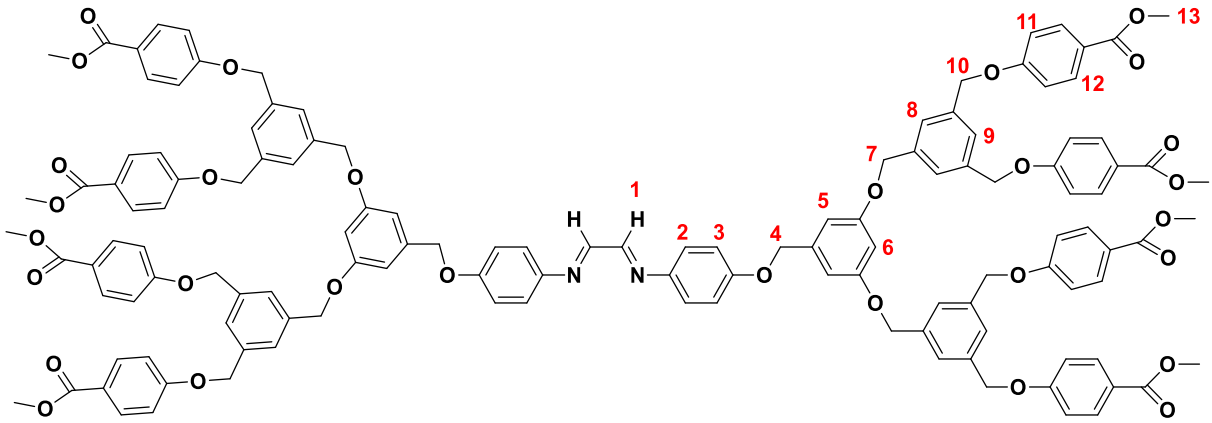

The title compound was prepared with compound **2.1** (0.0300 g, 0.125 mmol), $K_2CO_3$ (0.0400 g, 0289 mmol), catalytic amount of 18-crown-6 and compound **3.4** (0.259 g, 0.249 mmol). Product: Yellow powder. Yield: 0.143 g, 53%. **M.P.** 142 − 148 °C. **$^1$H NMR (300 MHz, $CDCl_3$):** δ (ppm) = 8.30 (s, 2H, H-1), 7.96 (d, $^3J$ = 8.2 Hz, 16H, H-12), 7.39 (d, $^3J$ = 8.1 Hz, 16H, H-11), 7.23 (d, $^3J$ = 8.9 Hz, 4H, H-2), 6.91 (d, $^3J$ = 8.8 Hz, 4H, H-3), 6.52 – 6.30 (overlapping br, 18H, H-5, H-8, H-6 and H-9), 5.02 – 4.90 (overlapping br, 28H, H-10, H-7 and H-4 ), 3.83 (s, 24H, H-13). **$^{13}$C{$^1$H} NMR (151 MHz, $CDCl_3$):** δ (ppm) 166.75 ($C{=}O_{ester}$), 154.95 ($C_{imine}$), 141.91, 139.40, 129.87, 126.96, 106.56, 101.71, 70.03, 68.42, 52.08. **FT-IR (ATR, cm$^{-1}$):** $\nu$ = 1716.51 (C=O), 1657.58 (C=N). **ESI-MS (+):** Calculated for $C_{128}H_{112}N_2O_{30}$ **(*m/z*)**: $[M+2H]^{2+}$, 1079.3722; found 1079.3376.

### 6.7.6 Synthesis of $G_2$-COOMe-*N,N*-alpha-diimine ligand (3.10)

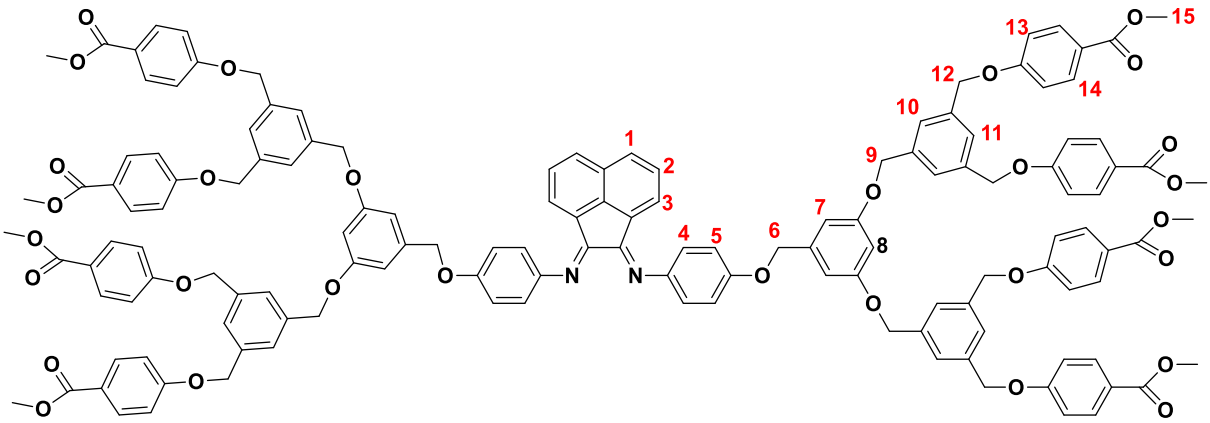

The title compound was prepared with compound **2.2** (0.0300 g, 0.0823 mmol), $K_2CO_3$ (0.0200 g, 0.145 mmol), catalytic amount of 18-crown-6 and compound **3.4** (0.200 g, 0.192 mmol). Product: Orange powder. Yield: 0.109 g, 58%. **M.P.** 155 − 162 °C. **$^1$H NMR (300 MHz, $CDCl_3$):** δ (ppm) = 7.95 (d, $^3J$ = 8.2 Hz, 16H, H-14), 7.77 (d, $^3J$ = 8.2 Hz, 2H, H-1), 7.39 (d, $^3J$ = 8.1 Hz, 16H, H-13), 7.33 – 7.22 (m, 2H, H-2), 7.00 (s, 8H, H-4 and H-5), 6.91 (d, $^3J$ = 7.1 Hz, 2H, H-3), 6.69 – 6.36 (overlapping s, 18H, H-7, H-10, H-8 and H-11), 5.11 – 4.60 (overlapping s, 28H, H-12, H-9, H-6), 3.83 (s, 24H, H-15). **$^{13}$C{$^1$H} NMR (151 MHz, $CDCl_3$):** δ (ppm) = 166.75 ($C{=}O_{ester}$), 159.95 ($C_{imine}$), 141.94, 139.60, 132.03, 129.88, 126.96, 120.23, 115.82, 106.72, 101.75, 70.11, 69.13, 52.08. **FT-IR (ATR, cm$^{-1}$):** $\nu$ = 1715.11 (C=O), 1662.99 (C=N). **ESI-MS (+):** calculated for $C_{138}H_{116}N_2O_{30}$ (*m/z*): $[M+H]^+$, 2281.7691; found 2281.6196.

## 6.8 Synthesis and characterization of Rh(I) *N,N*-alpha-diimine poly(aryl ether) metallodendrimers

**General procedure for the metalation of dendrimers**

$[Rh(COD)(MeCN)_2]BF_4$ (1 eq.), dissolved in dichloromethane (20 mL) was added to a stirring solution of the dendritic ligands (**3.5** – **3.10**) (1 eq.), in dichloromethane (10 mL). The mixture was stirred for 2 h at room temperature. After the reaction was deemed complete, the reaction mixture was reduced under vacuum and precipitates were formed by trituration using diethyl ether and dichloromethane. The resulting precipitate was collected by suction filtration and washed with diethyl ether and dried *in vacuo*.

### 6.8.1 Synthesis of G0-COOMe-*N*,*N*-alpha-diimine Rh(COD) complex (3.11)

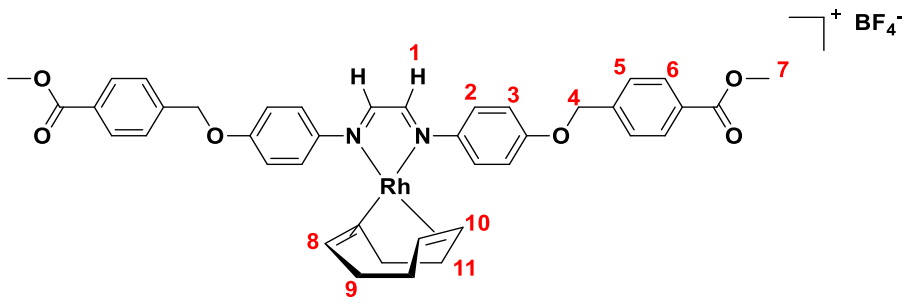


The title complex was prepared with compound **3.5** (0.200 g, 0.373 mmol) and (0.142 g, 0.373 mmol) of $[Rh(COD)(MeCN)_2]BF_4$. Product: Red powder. Yield: 0.187 g, 60%. **M.P.** 215 − 221 °C. **$^1$H NMR (300 MHz, $CDCl_3$):** δ (ppm) = 8.15 (s, 2H, H-1), 7.99 (d, $^3J$ = 8.3 Hz, 4H, H-6), 7.42 (d, $^3J$ = 8.3 Hz, 4H, H-5), 7.21 (d, $^3J$ = 9.3 Hz, 4H, H-2), 6.93 (d, $^3J$ = 8.9 Hz, 4H, H-3), 5.06 (s, 4H, H-4), 4.32 (br s, 2H, H-8), 4.02 (br s, 2H, H-10), 3.86 (s, 6H, H-7), 2.39 (m, 4H, H-4), 1.82 (m, 4H, H-11). **$^{13}$C{$^1$H} NMR (151 MHz, $CDCl_3$):** δ (ppm) = 166.77 ($C{=}O_{ester}$), 158.61, 157.89 ($C_{imine}$), 143.57 141.87, 129.94, 126.96, 123.06, 115.60, 82.98 ($C_{COD}$), 69.67, 52.10, 28.17 ($C_{COD}$). **FT-IR (ATR, cm$^{-1}$):** $\nu$ = 1718.50 (C=O), 1675.77 (C=N). **ESI-MS (+):** calculated for $C_{40}H_{40}N_2O_6Rh$ (*m/z*): $[M+NH_4]^+$, 765.2279; found 765.1935.

### 6.8.2 Synthesis of G0-COOMe-*N*,*N*-alpha-diimine Rh(COD) complex (3.12)

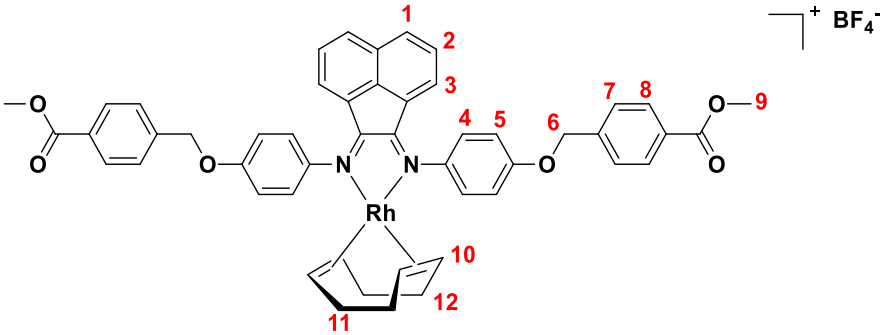


The title complex was prepared with compound **3.6** (0.200 g, 0.303 mmol) and (0.115 g, 0.303 mmol) of $[Rh(COD)(MeCN)_2]BF_4$. Product: Red powder. Yield: 0.183 g, 63%. **M.P.** 238 − 242 °C. **$^1$H NMR (300 MHz, $CDCl_3$):** δ (ppm) = 8.02 (d, $^3J$ = 8.3 Hz, 4H, H-8),

7.95 (d, $^3J$ = 8.3 Hz, 2H, H-1), 7.49 (d, $^3J$ = 8.3 Hz, 4H, H-7), 7.37 (d, $^3J$ = 7.6 Hz, 2H, H-2), 7.31 (d, $^3J$ = 9.1 Hz, 4H, H-4), 7.11 (d, $^3J$ = 8.8 Hz, 4H, H-5), 6.52 (d, $^3J$ = 7.3 Hz, 2H, H-3), 5.14 (s, 4H, H-6), 4.00 (br s, 4H, H-10), 3.87 (s, 6H, H-9), 2.46 (m, 4H, H-11), 1.79 (m, 4H, H-12). **$^{13}$C{$^1$H} NMR (151 MHz, CDCl$_3$):** δ (ppm) 166.84 (C=O$_{ester}$), 161.65 (C$_{imine}$), 155.88, 145.47, 142.31, 129.91, 126.94, 120.04, 115.98, 82.55 (C$_{COD}$), 52.10, 30.85 (C$_{COD}$). **FT-IR (ATR, cm$^{-1}$):** $v$ = 1766.19 (C=O), 1643.21 (C=N). **ESI-MS (+):** Calculated for $C_{50}H_{44}N_2O_6Rh$ (*m/z*): $[M+H]^+$, 871.2254; found 871.2234.

### 6.8.3 Synthesis of G$_1$-COOMe-*N,N*-alpha-diimine Rh(COD) complex (3.13)

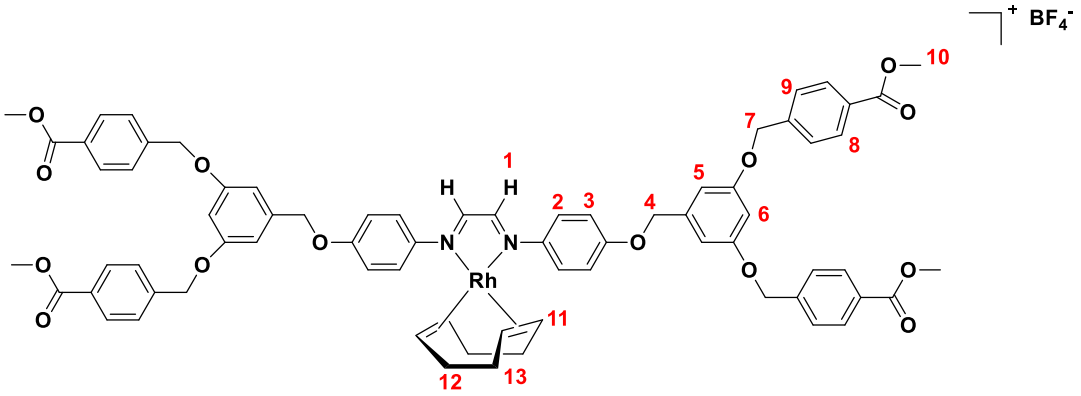


The title complex was prepared with compound **3.7** (0.201 g, 0.186 mmol) and (0.0705 g, 0.186 mmol) of [Rh(COD)(MeCN)$_2$]BF$_4$ under reflux condition for 1h. Product: Red powder. Yield: 0.133 g, 52%. **M.P.** 258 − 263 °C. **$^1$H NMR (300 MHz, CDCl$_3$):** δ (ppm) = 8.39 (s, 2H, H-1), 7.96 (d, $^3J$ = 8.3 Hz, 8H, H-9), 7.40 (d, $^3J$ = 8.3 Hz, 8H, H-8), 7.18 (d, $^3J$ = 8.9 Hz, 4H, H-2), 6.90 (d,$^3$ $^3J$ = 8.9 Hz, 4H, H-3), 6.58 (d, $^4J$ = 2.2 Hz, 4H, H-5), 6.48 (t, $^4J$ = 2.2 Hz, 2H, H-6), 5.03 (s, 8H, H-7), 4.92 (s, 4H, H-4), 4.16 (s, 2H, H-11), 3.85 (s, 12H, H-10). 2.40 (m, 4H, H-12), 1.79 (d, $J$ = 8.3 Hz, 4H, H-13). **$^{13}$C{$^1$H} NMR (151 MHz, CDCl$_3$):** δ (ppm) 166.76 (C=O$_{ester}$), 159.86, 156.41 (C$_{imine}$), 141.96, 140.42, 129.88, 126.97, 123.07, 116.29, 106.50, 101.65 , 85.97 (C$_{COD}$), 69.48, 30.84 (C$_{COD}$). **FT-IR (ATR, cm$^{-1}$):** $v$ = 1711.23 (C=O), 1601.14 (C=N). **ESI-MS (+):** Calculated for $C_{72}H_{68}N_2O_{14}Rh$ (*m/z*): $[M+NH_4]^+$, 1305.4063; found 1305.3751.

### 6.8.4 Synthesis of $G_1$-COOMe-*N,N*-alpha-diimine Rh(COD) complex (3.14)

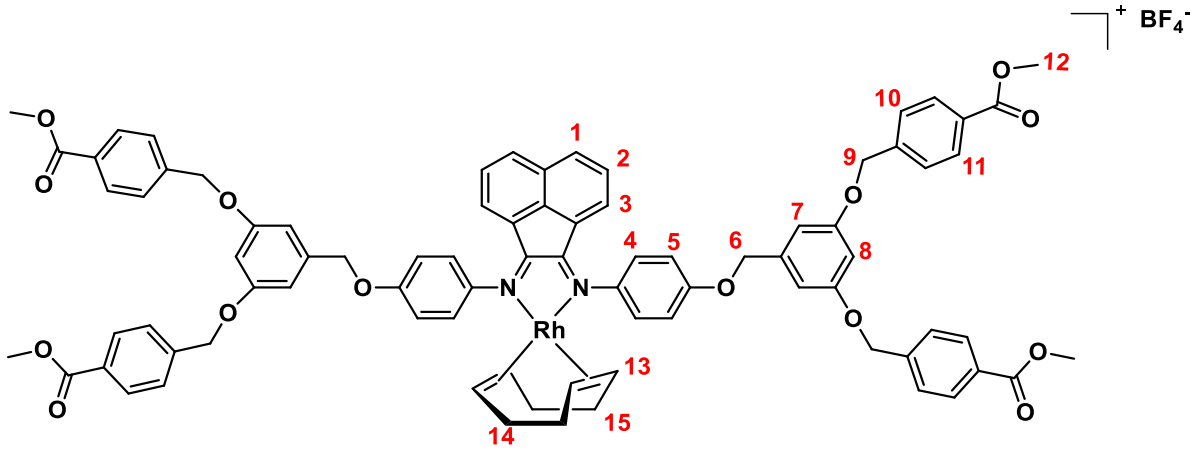


The title complex was prepared with compound **3.8** (0.201 g, 0.166 mmol) and (0.0632 g, 0.166 mmol) of $[Rh(COD)(MeCN)_2]BF_4$. Product: Red powder. Yield: 0.168 g, 67%. **M.P.** 244 – 253 °C. **$^1$H NMR (300 MHz, $CDCl_3$):** δ (ppm) = 7.98 (d, $^3J$ = 8.3 Hz, 8H, H-10), 7.91 (d, $^3J$ = 8.3 Hz, 2H, H-1), 7.43 (d, $^3J$ = 8.3 Hz, 8H, H-11), 7.36 – 7.26 (overlapping m, 6H, H-2 and H-4 ), 7.08 (d, $^3J$ = 8.8 Hz, 4H, H-5), 6.66 (d, $^4J$ = 2.1 Hz, 4H, H-7), 6.54 – 6.48 (overlapping m, 4H, H-8 and H-3), 5.06 (s, 8H, H-9), 5.02 (s, 4H, H-6), 4.01 (s, 4H, H-13), 3.85 (s, 12H, H-12), 2.46 (m, 4H, H-14), 1.78 (m, 4H, H-15). **$^{13}$C{$^1$H} NMR (151 MHz, $CDCl_3$):** δ (ppm) = 159.93 ($C{=}O_{ester}$), 141.95 ($C_{imine}$), 132.56, 129.91, 127.11, 123.80, 120.23, 116.02, 106.60, 101.73, 83.45 ($C_{COD}$) 70.31, 69.50, 52.11, 26.75 ($C_{COD}$). **FT-IR (ATR, cm$^{-1}$):** $\nu$ = 1713.14 (C=O), 1624.18 (C=N). **ESI-MS (+):** calculated for $C_{82}H_{72}N_2O_{14}Rh$ **(*m/z*)**: $[M+K]^+$, 1450.3670; found 1450.5105.

### 6.8.5 Synthesis of $G_2$-COOMe-*N,N*-alpha-diimine Rh(COD) complex (3.15)

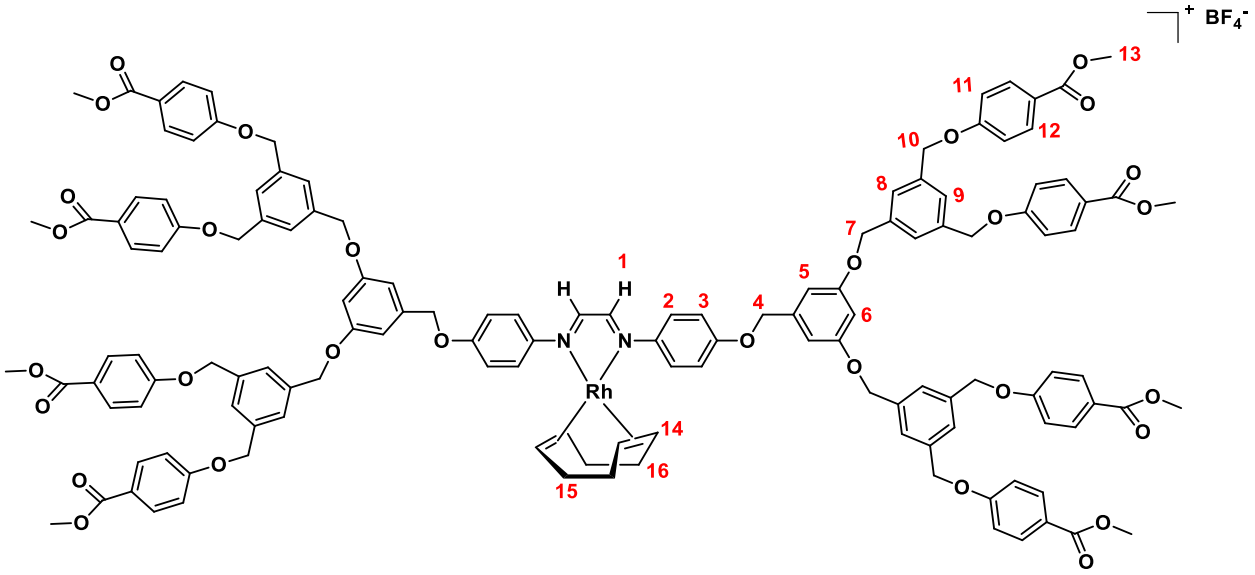


The title complex was prepared with compound **3.9** (0.200 g, 0.093 mmol) and (0.0352 g, 0.093 mmol) of $[Rh(COD)(MeCN)_2]BF_4$. Product: Red powder. Yield: 0.134 g, 59%. **M.P.** 242 − 247 °C. **$^1$H NMR (300 MHz, $CDCl_3$):** δ (ppm) 8.35 – 7.96 (overlapping s, 18H, H-1 and H-12), 7.39 (d, $^3J$ = 8.0 Hz, 16H, H-11), 7.23 (d, $^3J$ = 8.9 Hz, 4H, H-2), 6.92 (br d, $^3J$ = 8.6 Hz, 4H, H-3), 6.59 – 6.47 (overlapping br, 18H, H-5, H-8, H-6 and H-9), 5.02 – 4.90 (br, 28H, H-10, H-7 and H-4), 4.15 (br s, 4H, H-14), 3.83 (s, 24H, H-13). 2.43 (m, 4H, H-15), 1.69 (m, 4H, H-16), **$^{13}$C{$^1$H} NMR (151 MHz, $CDCl_3$):** δ (ppm) = 166.85 ($C{=}O_{ester}$), 158.43, 154.82 ($C_{imine}$)141.91, 139.44, 129.87, 126.96, 106.56, 101.71, 83.36 ($C_{COD}$), 70.01, 68.23, 52.08, 26.25. **FT-IR (ATR, cm$^{-1}$):** $\nu$ = 1714.51 (C=O), 1644.42 (C=N). **ESI-MS (+):** Calculated for $C_{136}H_{124}N_2O_{30}Rh$ **(***m/z***)**: $[M+MeCN+Na]^{2+}$ 1216.1047; found 1216.4147.

### 6.8.6 Synthesis of $G_2$-COOMe-*N,N*-alpha-diimine Rh(COD) complex (3.16)

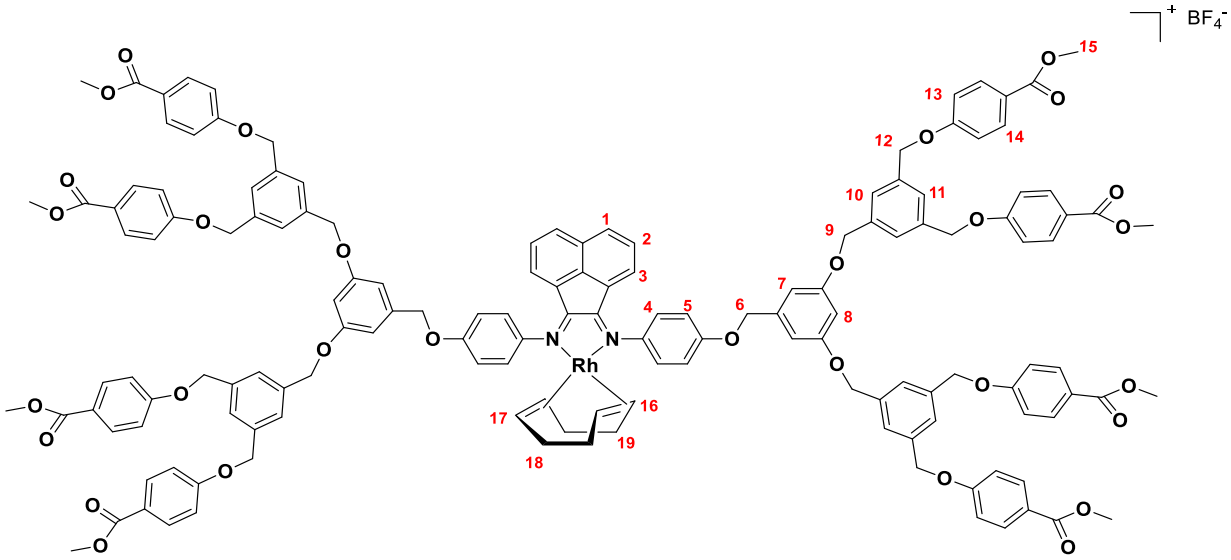


The title complex was prepared with compound **3.10** (0.150 g, 0.066 mmol) and (0.0245 g, 0.066 mmol) of $[Rh(COD)(MeCN)_2]BF_4$. Product: Red powder. Yield: 0.0848 g, 50%. **M.P.** 248 − 254 °C. **$^1$H NMR (300 MHz, $CDCl_3$):** δ (ppm) = 7.94 (d, $^3J$ = 7.9 Hz, 16H, H-14), 7.82 (br d, $^3J$ = 8.2 Hz, 2H, H-1), 7.34 – 7.19 (overlapping br, 22H, H-2, H-4 and H-13), 7.02 (br d, $^3J$ = 8.2 Hz, 4H, H-5), 6.61 – 6.21 (overlapping br, 20H, H-7, H-10, H-3, H-8 and H-11), 5.13 – 4.57 (overlapping br, 28H, H-9, H-12 and H-6), 4.14 (br s, 2H, H-16), 3.95 (s, 2H, H-17), 3.70 (s, 24H, H-15), 2.14 (m, 4H, H-18), 1.67 (m, 4H, H-19). **$^{13}$C{$^1$H} NMR (151 MHz, $CDCl_3$):** δ (ppm) = 168.15 ($C{=}O_{ester}$), 155.35 ($C_{imine}$), 141.44, 137.63, 132.73, 129.84, 126.75, 121.23, 115.82, 106.54, 101.75, 83.44 ($C_{COD}$), 52.08, 26.14. **FT-IR (ATR, cm$^{-1}$):** $\nu$ = 1708.31 (C=O), 1632.15 (C=N). **ESI-MS (+):** Calculated for $C_{146}H_{128}N_2O_{30}Rh$ (*m/z*): $[M+H+NH_4]^{2+}$, 1255.4009; found 1255.3978.

## 6.9 Synthesis and characterization of tetraamine and diimine Schiff base ligands

### 6.9.1 Synthesis of tetraylnitrilomethylidyne−hexaphenyl (4.1)

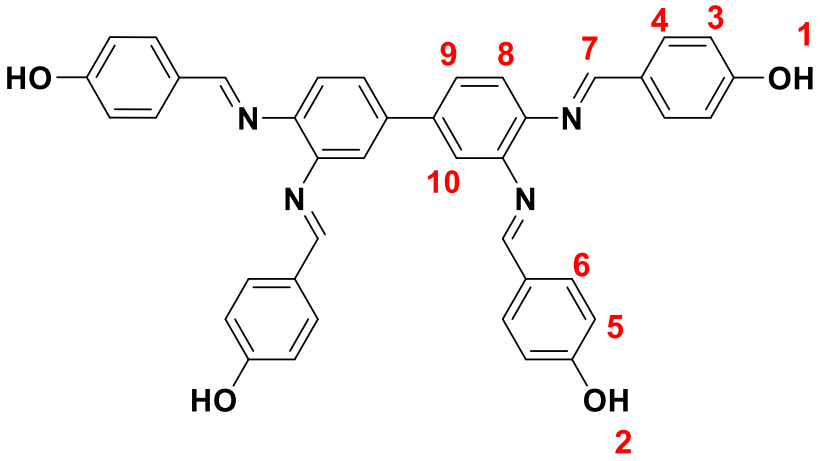


3,3'-Diaminobenzidine (0.100 g, 0.467 mmol) was added to a stirring solution of 4-hydroxybenzaldehyde (0.228 g, 1.87 mmol) in methanol (25 mL). A catalytic amount of acetic acid (5 drops) was added to the stirring solution. The resulting yellow solution was stirred for 24 h under reflux conditions. The white precipitate that formed was collected by suction filtration and washed with cold methanol and diethyl ether (20 mL). The product was purified by precipitation from hot methanol (20 mL). The resulting precipitate was filtered and dried *in vacuo*. Product: Off-white powder. Yield: 0.244 g, 83%. **M.P.** 143 – 152 °C. **$^{1}$H NMR (300 MHz, DMSO-*d*$_6$):** δ (ppm) = 9.96 (br s, 2H, H-1), 9.40 (br s, 2H, H-2), 7.72 (s, 4H, H-10 and H-9), 7.70 – 7.53 (overlapping m, 6H, H-5 and H-8), 6.93 – 6.88 (m, 8H, H-3 and H-4), 6.69 – 6.67 (m, 4H, H-6), 5.51 (s, 4H, H-7). **$^{13}$C{$^{1}$H} NMR (151 MHz, DMSO-*d*$_6$):** δ (ppm) =159.35, 157.17, 154.64 ($C_{imine}$), 143.81, 142.52, 137.11, 136.11, 135.89, 135.61, 130.84, 127.60, 122.40, 121.29, 119.50, 117.42, 116.03, 111.67, 109.56. 142.54, 137.10, 135.92, 131.05, 128.04, 122.05, 121.34, 119.51, 116.00. **FT-IR (ATR, cm$^{-1}$):** *v* = 3022.78 (O-H), 1619.14 (C=N).

### 6.9.2 Synthesis of 4,4′-[1,2-Phenylenebis(nitrilomethylidene)]bisphenol (4.2)

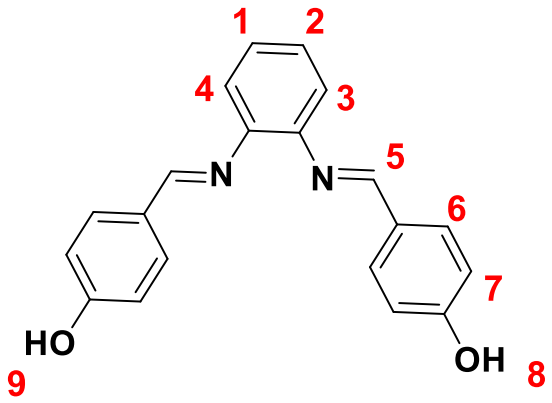


*O*-phenylenediamine (1.00 g, 9.25 mmol) was added to a stirring solution of 4-hydroxybenzaldehyde (2.26 g, 18.5 mmol) in methanol (25 mL). A catalytic amount of acetic acid (5 drops) was added to the stirring solution. The solution was stirred for 24 h under reflux conditions. Thereafter, the precipitate that formed was collected by suction filtration and washed with cold methanol and diethyl ether (20 mL). The product was purified by precipitation from hot ethanol (20 mL) and the resulting precipitate was filtered and dried *in vacuo*. Product: White powder. Yield: 2.34 g, 80%. **M.P.** 116 – 121 °C. **$^{1}$H NMR (300 MHz, DMSO-*d*$_6$):** δ (ppm) = 9.97 (br s, 1H, H-8), 9.51 (br s, 1H, H-9), 7.66 (d, $^{3}J$ = 8.8 Hz, 1H, H-4), 7.56 (d, $^{3}J$ = 8.7 Hz, 2H, H-6), 7.40 (d, $^{3}J$ = 9.6 Hz, 1H, H-3), 7.26 – 7.14 (m, 2H, H-1, H-2), 6.91 (d, $^{3}J$ = 8.7 Hz, 2H, H-7), 6.84 (d, $^{3}J$ = 8.5 Hz, 2H, H-11), 6.66 (d, $^{3}J$ = 11.4 Hz, 2H, H-10), 5.42 (s, 2H, H-5). **$^{13}$C{$^{1}$H} NMR (151 MHz, DMSO-*d*$_6$):** δ (ppm) = 159.32, 157.14, 154.06 ($C_{imine}$), 143.19, 136.33, 131.06, 127.96, 127.59, 122.57, 122.32, 121.28, 119.30. **FT-IR (ATR, cm$^{-1}$):** *v* = 2936.70 (O-H), 1628.20 (C=N).

## 6.10 Synthesis and characterization of water-soluble tetraimine ligands

### 6.10.1 Synthesis of tetrasulfonated tetraamine ligand (4.3)

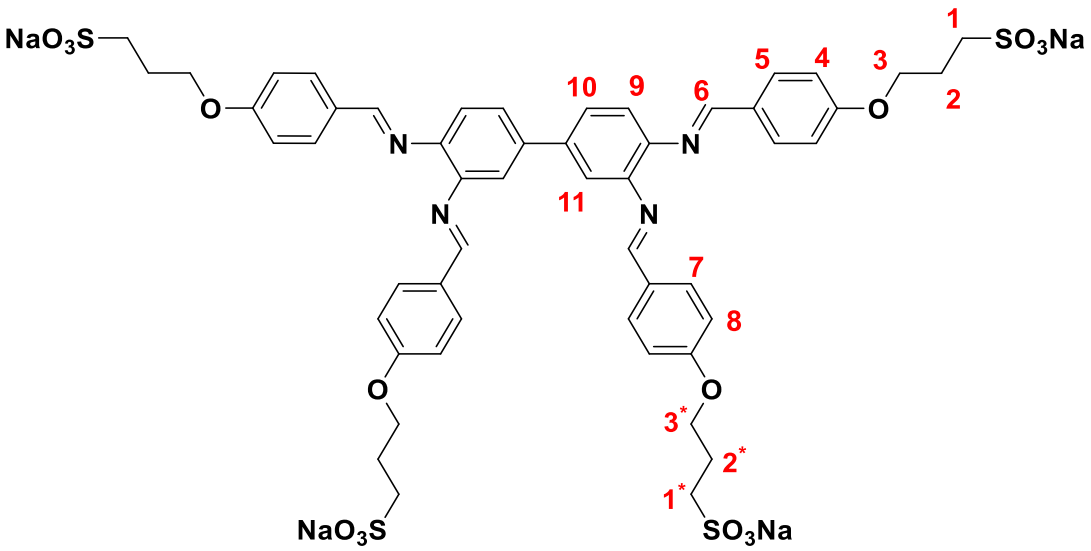


Sodium hydride (0.0171 g, 0.713 mmol) dispersed in mineral oil was suspended in anhydrous DMF (5 mL) under argon in a two-necked flask. A solution of **4.1** (0.100 g, 0.159 mmol) dissolved in anhydrous DMF (2 mL) was added. The mixture was allowed to stir for one h at room temperature. Thereafter, 1,3-propanesultone (0.0871 g, 0.713 mmol) was added and allowed to stir for 8 h at 50 °C. When the reaction was considered complete, the reaction mixture was cooled to room temperature and the precipitate was collected by suction filtration. The precipitate was washed with acetone (20 mL) to remove the unreacted sultone. The product was purified by precipitation from DMSO/acetone (1:1) and dried *in vacuo*. Product: White powder. Yield: 0.142 g, 74 %. **M.P.** 119 – 131 °C. **$^{1}$H NMR (300 MHz, DMSO-*d*$_6$):** δ (ppm) = 8.48 (s, 2H, H-11), 7.72 – 7.67 (overlapping m, 6H, H-10 and H-8), 7.56 (d, $^{3}J$ = 8.2 Hz, 2H, H-9), 7.09 (d, $^{3}J$ = 8.5 Hz, 4H, H-4), 6.98 (d, $^{3}J$ = 8.3 Hz, 4H, H-5), 6.83 (d, $^{3}J$ = 8.4 Hz, 4H, H-7), 5.57 (br s, 4H, H-6), 4.15 (t, $^{3}J$ = 6.1 Hz, 4H, H-3), 3.98 (t, $^{3}J$ = 6.4 Hz, 4H, H-3$^{*}$), 2.55 – 2.28 (overlapping m, 8H, H-1 and H-1$^{*}$), 2.12 – 1.96 (overlapping m, 8H, H-2 and H-2$^{*}$). **$^{13}$C{$^{1}$H} NMR (151 MHz, DMSO-*d*$_6$):** δ (ppm) = 160.30, 158.40, 154.19 ($C_{imine}$), 142.51, 137.15, 136.04, 130.95, 129.25, 127.90, 122.65, 122.04, 119.65, 115.21, 109.61, 69.57, 67.36, 48.33, 25.49. **FT-IR (ATR, cm$^{-1}$):** *ν* = 1175.84 (O=S=O), 1619.14 (C=N). **ESI-MS (+):** Calculated for $C_{52}H_{50}N_4Na_4O_{16}S_4$ **(***m/z***)**: $[M+H+Na]^{2+}$, 615.0832; found 615.0889.

### 6.10.2 Synthesis of disulfonated diimine ligand (4.4)

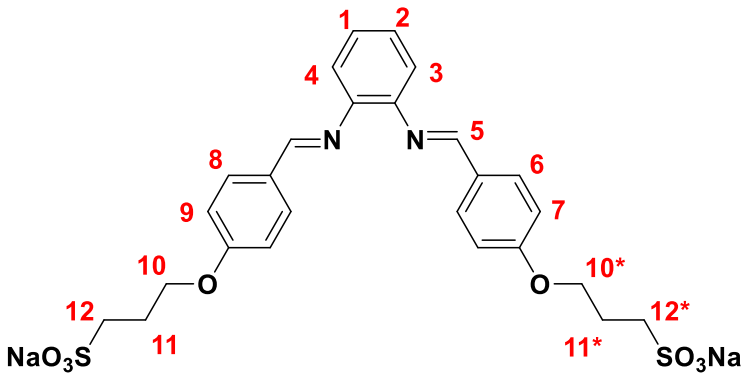


Sodium hydride (0.948 g, 3.951 mmol) dispersed in mineral oil was suspended in anhydrous THF (20 mL) under argon in a two-necked flask. A solution of **4.2** (0.500 g, 1.58 mmol) dissolved in anhydrous THF (2 mL) was added. The mixture was allowed to stir for one h at room temperature. 1,3-propanesultone (0.386 g, 3.16 mmol) in dry THF (2 mL) was added and allowed to stir for 24 h at 55 °C. The reaction mixture was cooled to room temperature and the resulting precipitate was collected by suction filtration and washed with acetone (20 mL) to remove the unreacted sultone. The product was purified by precipitation from DMSO/acetone (1:1) and dried *in vacuo*. Product: White powder. Yield: 0.822 g, 86 %. **M.P.** 114 – 120 °C. **$^{1}$H NMR (300 MHz, DMSO-*d*$_6$):** δ (ppm) = 7.69 – 7.64 (overlapping m,3H, H-4, H-6), 7.44 (d, $^{3}J$ = 6.4 Hz, 1H, H-3), 7.33 – 7.16 (m, 2H, H-1, H-2), 7.08 (d, $^{3}J$ = 8.8 Hz, 2H, H-7), 6.94 (d, $^{3}J$ = 8.7 Hz, 2H, H-8), 6.84 (d, $^{3}J$ = 8.8 Hz, 2H, H-9), 5.48 (s, 2H, H-5), 4.14 (t, $^{3}J$ = 6.5 Hz, 2H, H-10$^{*}$), 3.99 (t, $^{3}J$ = 6.3 Hz, 2H, H-10), 2.61 – 2.58 (m, 2H, H-12$^{*}$), 2.47 – 2.33 (m, *2*H, H-12), 2.08 – 2.01 (m, 2H, H-11$^{*}$), 2.01 – 1.92 (m, 2H, H-11). **$^{13}$C{$^{1}$H} NMR (151 MHz, DMSO-*d*$_6$):** δ (ppm) = 160.24, 158.19, 153.39 ($C_{imine}$), 143.20, 136.15, 131.18, 129.12, 127.86, 122.47, 119.41, 116.01, 115.16, 111.47, 69.53, 67.32, 60.82, 48.30, 29.16, 25.63. **FT-IR (ATR, cm$^{-1}$):** *ν* = 1170.78 (O=S=O), 1628.20 (C=N). **ESI-MS (+):** Calculated for $C_{26}H_{26}N_2Na_2O_8S_2$ **(***m/z***)**: $[M+H]^+$, 605.0972; found 605.1008.

## 6.11 Synthesis and characterization of water-soluble tetrasulfonated and disulfonated Rh(COD) complexes

### 6.11.1 Synthesis of water-soluble binuclear Rh(COD) complex (4.5)

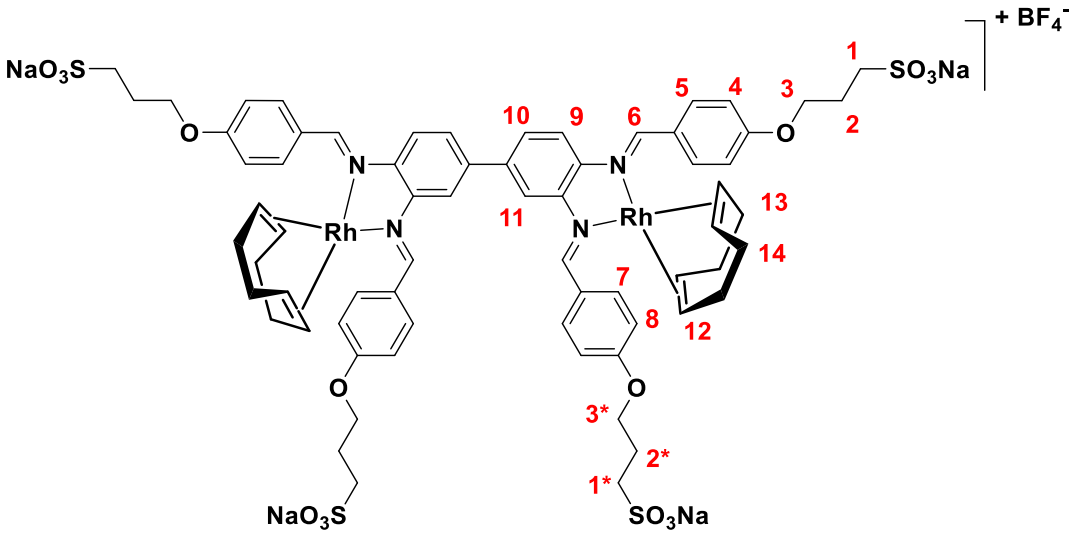


Silver tetrafluoroborate (0.020 g, 0.102 mmol, 1.0 eq.) and $[RhCl(COD)]_2$ (0.025 g, 0.0507 mmol, 0.5 eq.) were stirred in acetonitrile (10 mL) for one h at room temperature. The precipitated silver chloride was removed using a syringe filter (PTFE, 0.25 µm). The resulting solution was evaporated to dryness under reduced pressure. Ligand **4.3** (0.05 g, 0.414 mmol) dissolved in DMSO (3 mL) was added to a stirring solution of the previously synthesised $[Rh(COD)(MeCN)_2]BF_4$ (0.015 g, 0.0414 mmol) in DMSO (5 mL) for one h at room temperature. The reaction mixture was poured into acetone and the precipitate that formed was washed with acetone (10 mL). The product was purified by precipitation from DMSO and acetone mixture (1:1) and dried *in vacuo*. Product: Pale green. Yield: 0.0392 g, 63%. **M.P.** 215 – 220 °C. **$^1$H NMR (300 MHz, DMSO-$d_6$):** δ (ppm) = 8.39 (s, 2H, H-11), 8.07 (br s, 2H, H-10), 7.80 (s, 4H, H-8), 7.68 (d, $^3J$ = 7.5 Hz, 2H, H-9), 7.22 (d, $^3J$ = 7.6 Hz, 4H, H-4), 6.96 (d, $^3J$ = 8.1 Hz, 4H, H-5), 6.83 (d, $^3J$ = 8.5 Hz, 4H, H-7), 5.56 (br s, 4H, H-6), 4.15 (overlapping m, 8H, H-3, H-12), 3.97 (t, $^3J$ = 6.4 Hz, 4H, H-3*), 2.67 – 2.55 (overlapping m, 8H, H-1 and H-1*), 2.34 (br s, 8H, H-13), 2.12 – 1.96 (overlapping m, 8H, H-2 and H-2*), 1.78 (br s, 8H, H-14). **$^{13}$C{$^1$H} NMR (151 MHz, DMSO-$d_6$):** δ (ppm) =160.65, 158.75 ($C_{imine}$), 153.91, 136.35, 131.77, 129.09, 128.07, 115.14, 109.76, 102.49, 85.10 ($C_{COD}$), 69.52, 67.09, 48.32, 30.77 ($C_{COD}$), 27.97, 25.67. **FT-IR (ATR, cm$^{-1}$):** $\nu$ = 1175.84 (O=S=O), 1608.67 (C=N). **ESI-MS (+):** Calculated for $C_{60}H_{62}N_4Na_4O_{16}S_4Rh$ (*m/z*): $[M+H+2Na]^{3+}$, 558.4861; found 558.1189.

### 6.11.2 Synthesis of water-soluble mononuclear Rh(COD) complex (4.6)

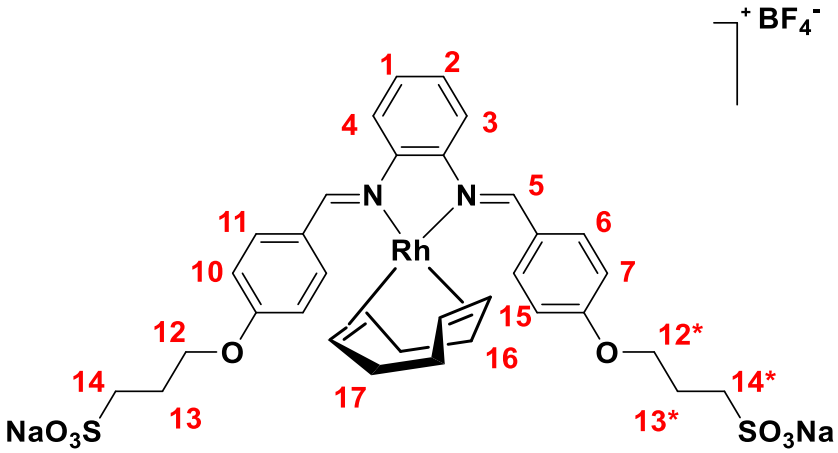


Silver tetrafluoroborate (0.020 g, 0.102 mmol, 1.0 eq.) and $[RhCl(COD)]_2$ (0.025 g, 0.0507 mmol, 0.5 eq.) were stirred in acetonitrile (10 mL) for one h at room temperature. The precipitated silver chloride was removed using a syringe filter (PTFE, 0.25 μm). The resulting solution was evaporated to dryness under reduced pressure. Ligand **4.4** (0.05 g, 0.083 mmol) dissolved in DMSO (3 mL) was added to a stirring solution of the previously synthesised $[Rh(COD)(MeCN)_2]BF_4$ (0.031 g, 0.083 mmol) in DMSO (5 mL) and stirred for one h at room temperature. The reaction mixture was poured into acetone, the precipitate formed was isolated by filtration and washed with acetone (10 mL). The product was purified by precipitation from DMSO and acetone mixture (1:1) and dried *in vacuo*. Product: Pale green. Yield: 0.0433 g, 58%. **M.P.** 209 – 212 °C. **$^1$H NMR (300 MHz, DMSO-*d*$_6$):** δ (ppm) = 8.28 – 8.17 (overlapping br s, 3H, H-4, H-6), 7.51 (d, $^3J$ = 8.0 Hz, 1H, H-3), 7.41 (t, 1H, H-1), 7.31 (t, 1H, H-2), 7.26 (d, $^3J$ = 8.8 Hz, 2H, H-7), 6.92 (d, $^3J$ = 8.7 Hz, 2H, H-8), 6.83 (d, $^3J$ = 8.8 Hz, 2H, H-9), 5.47 (s, 2H, H-5), 4.35 (br s, 4H, H-13), 4.22 (t, $^3J$ = 6.5 Hz, 2H, H-10*), 3.96 (t, $^3J$ = 6.3 Hz, 2H, H-10), 2.69 – 2.59 (m, 2H, H-11*), 2.49 – 2.47 (m, *2*H, H-11), 2.33 (br s, 4H, H-14), 2.13 – 2.08 (m, 2H, H-12*), 1.99 – 1.94 (m, 2H, H-12). 1.80 (br s, 4H, H-15). **$^{13}$C{$^1$H} NMR (151 MHz, DMSO-*d*$_6$): δ (ppm) =** 161.01, 158.53 ($C_{imine}$), 152.75, 140.90, 134.77, 132.19, 129.84, 128.10, 123.59, 120.87, 119.67, 115.97, 115.16, 112.22, 86.31 ($C_{COD}$), 69.49, 67.55, 67.05, 60.77, 48.29, 30.73 ($C_{COD}$), 29.09, 27.98, 25.56. **FT-IR (ATR, cm$^{-1}$):** *ν* = 1170.78 (O=S=O), 1613.48 (C=N). **ESI-MS (+):** Calculated for $C_{34}H_{38}N_2Na_2O_8S_2Rh$ (*m/z*): $[M]^+$, 815.0900.0972; found 815.0464.

## 6.12 General cyclic voltammetric procedure

Electrochemical studies were carried out on a BASi Epsilon Eclipse Potentiostat/Galvanostat connected to a C-3 cell stand, using a three-electrode cell unit. The cell was charged with a glassy carbon working electrode disc (3.0 mm diameter), platinum wire counter electrode and a Ag/AgCl (Sat'd NaCl) reference electrode. For all measurements, $[NBu_4][BF_4]$ (0.10 M in anhydrous $CH_2Cl_2$) was used as the supporting electrolyte with an analyte concentration of approximately 1.0 mM. The cell was deoxygenated by purging with $N_2$ for 10 minutes while stirring. After this, the solution was protected from air by allowing $N_2$ to flow over the solution. Ferrocene/ferrocenium (II/III) oxidation potential, measured at 0.54 V was used as internal standard and measurements were performed at 100 mV $s^{-1}$ scan rate.

## 6.13 General hydroformylation procedure

The hydroformylation reactions were performed in a 90 mL stainless steel pipe reactor equipped with a Teflon-coated magnetic stirrer bar. The reactor was charged with toluene (5 mL) or water (5 mL), substrate (1-octene or styrene ) (7.175 mmol) and the catalyst precursor ($2.87 \times 10^{-3}$ mmol) resulting in a substrate to rhodium molar ratio of (2500 : 1). The reactor was sealed and flushed with nitrogen three times and then with syngas ($CO:H_2$ = 1:1). After purging, the reactor was pressurised to the appropriate syngas ($CO:H_2$ = 1:1) pressure and then heated to the required temperature by submerging the reactor into a container filled with preheated silicon fluid which was heated by means of a heating plate. The reaction was stirred vigorously at a stirring speed of 500 rpm. After the desired reaction time, the gas was slowly vented off and the reactor was allowed to cool to room temperature prior to opening.

All reactions were performed in triplicate and were recorded as an average of three identical experiments. Authentic standards of internal octenes and isomers of nonanal were used to confirm the products.

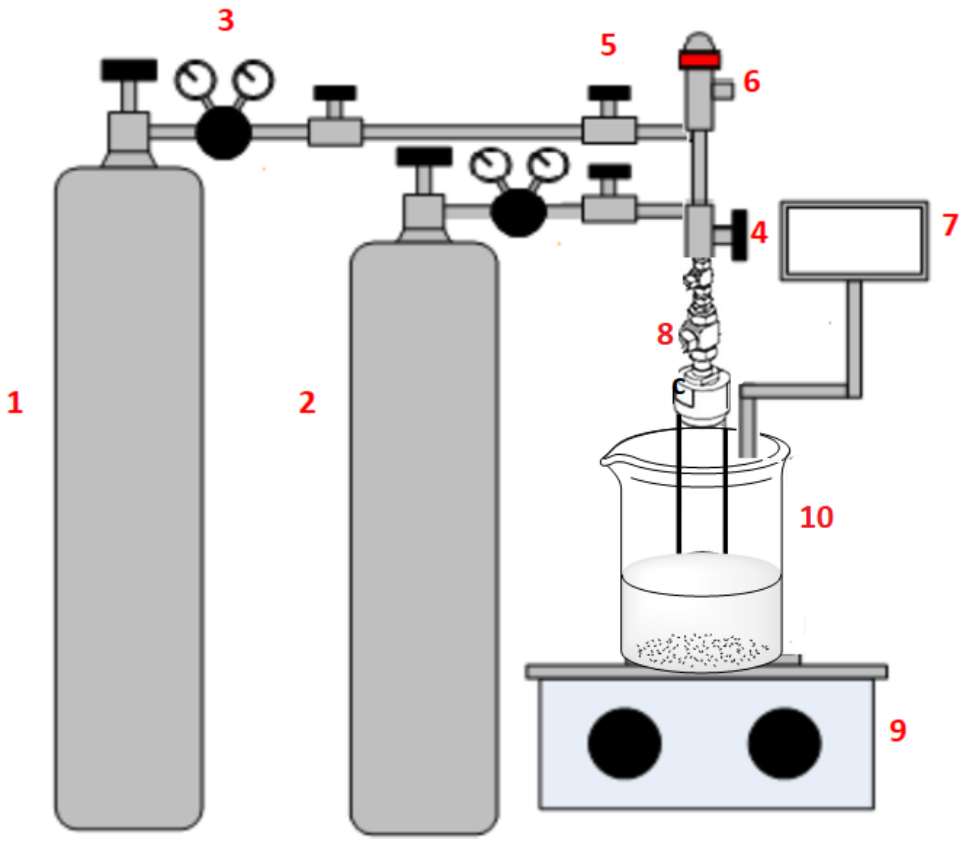


**(1)** $N_2$ cylinder (2) Syngas ($CO:H_2$ = 1:1) **(3)** Pressure gauge (bar) **(4)** Reactor pressure release valve **(5)** Cylinder pressure relief valve (**6)** Vent line **(7)** Temperature indicator **(8)** Stainless steel pipe reactor **(9)** Magnetic stirrer **(10)** Silicon fluid container.

**Figure 6.1**: Schematic representation of hydroformylation experimental setup used in this study.

In a typical recyclability assessment presented in Section 2.3.5 of Chapter 2 and Section 4.2.3.2 of Chapter 4 of this thesis, the organic phase (product) was extracted by adding a small amount of toluene to the reaction mixture and decanted from the catalyst-containing aqueous-phase. The resulting product was analysed by gas chromatography against standards. Fresh substrate (1-octene) and internal standard (*n*-decane) was added to the same catalyst-containing aqueous layer. This procedure was repeated for each successive catalytic cycle.

## 6.14 References

1 B. Oelkers and J. Sundermeyer, *Dalton Trans.*, 2011, **40**, 12727–12741.

2 L. Biancalana, L. K. Batchelor, T. Funaioli, S. Zacchini, M. Bortoluzzi, G. Pampaloni, P. J. Dyson and F. Marchetti, *Inorg. Chem.*, 2018, **57**, 6669–6685.

3 E. C. I. Matei, T. Lixandru, *Bul. Institutului Politeh. din Iasi*, 1960, **6**, 171–176.

4 C. Williams, M. Ferreira, E. Monflier, S. Mapolie and G. S. Smith, *Dalton Trans.*, 2018, **47**, 9418–9429.

5 P. E. Berget, J. M. Teixeira, J. L. Jacobsen and N. E. Schore, *Tetrahedron Lett.*, 2007, **48**, 8101–8103.

6 M. Gao, S. Han, Y. Hu and L. Zhang, *J. Phys. Chem. C*, 2016, **120**, 9299–9307.

7 S. Smanmoo, S. Kawasaki, P. Tangboriboonrat, T. Shibata, T. Kabashima and M. Kai, *J. Fluoresc.*, 2013, **23**, 853–857.